ON THE PROGRESSION OF BARRETT'S OESOPHAGUS TO BARRETT'S ADENOCARCINOMA

Thesis submitted for the degree of Doctor of

Medicine (Research) at the University of London

by

Shabuddin Khan

M.B.B.S., M.R.C.S.,

Submitted 15th April 2016

Primary supervisor – Dr. Stuart McDonald

Secondary supervisor – Professor Sir Nicholas Wright

Centre for Tumour Biology

Barts Cancer Institute

Barts and the London School of Medicine and Dentistry,

Queen Mary, University of London

Charterhouse Square, London EC1M 6BQ

Statement of originality

I, Shabuddin khan, confirm that the research included within this thesis is my own work and that where it has been carried out in collaboration with, or supported by others, that this is duly acknowledged below and my contribution indicated. Previously published material is also acknowledged below.

I attest that I have exercised reasonable care to ensure that the work is original, and does not to the best of my knowledge break any UK law, infringe any third party's copyright or other Intellectual Property Right, or contain any confidential material.

I accept that the College has the right to use plagiarism detection software to check the electronic version of the thesis.

I confirm that this thesis has not been previously submitted for the award of a degree to this or any other university.

Signature: Shabuddin khan

Date: 15/04/2016

Details of collaboration and publications:

This work was supported by Barts and the London Charity grant.

Grant number – DDCG1B6R, 2010.

Collaborations:

- Statistical support for methylation analysis was designed by Trevor Graham, Barts Cancer Institute, UK.
- Tissue sections were cut by Emma Nye (London Research Institute, Cancer Research UK, London) and George Elia (Department of Tumour Biology, Barts Cancer Institute, London)
- Dr Sebastian Zeki (Department of Tumour Biology, Barts Cancer Institute, London) provided some assistance for sequencing in Crypt dysplasia chapter.
- Neo-Barrett's specimens originated from the Northern Oesophago-gastric Unit, Newcastle and the work was carried out in collaboration with Prof. Michael Griffins and Dr Lorna Dunn.

The research work has led to the following original publication:

1) Khan S, McDonald SA, Wright NA, Graham TA, Odze RD, Rodriquez-Justo M, Zeki S. Crypt dysplasia in Barrett's oesophagus shows clonal identity between crypt and surface cells. J Pathol. 2013 Sep; 231(1):98-104. doi: 10.1002/path.4211.

Abstract

Barrett's oesophagus(BO) is the major precursor of oesophageal adenocarcinoma (OA) and we do not understand the dynamics of the evolution of BO in order to identify patients at high risk of cancer. Studies have proposed that BO is a monoclonal lesion, however recent work has shown that there are multiple independent clones present. *Project 1:* Determines the evolution of polyclonal dysplasia through sequencing and mapping clones onto tissue sections. I show that several cases are polyclonal but in each case only one clone progresses to cancer, suggesting oesophageal cancers are monoclonal outgrows from polyclonal Barrett's dysplasia. *Project 2:* Aims to understand the clonal relationship between cells in glands displaying basal crypt dysplasia-like atypia (BCDA), as it is unclear whether those cells in the upper part of the gland arise from the same stem cell that generates the gland bases. Glands displaying BCDA show a common mutation between the dysplastic base and non-dysplastic surface suggesting a common cell of origin. *Project 3:* 50% of patients who undergo oesophagectomy for OA develop post-oesophagectomy Barrett's (neo-BO) within 3-5 years possibly due to a field effect, wherein pre-neoplastic cells remain post-resection in histologically normal areas of epithelium predisposing the patient to cancer recurrence. Here I show that no genetic link between the neo-BO and the cancer is present. Immunohistochemical analysis shows that neo-Barrett's glands are gastric in nature. *Project 4:* The stem cell dynamics and clonal expansion rates of BO are unknown. Here I employed diversity analysis of methylation patterns of CpG islands in the promoter regions of non-expressed

genes as a molecular clock. My data suggests that 3-4 stem cells are found in each Barrett's gland. Methylation patterns within a gland were less diverse compared to adjacent and distant glands, suggesting BO is characterized by long periods of stasis followed by bursts of clonal expansions.

Acknowledgements

I would take this opportunity to thank my research supervisor, family and friends for their support and guidance without which this research would not have been possible.

I would like to thank my supervisor Dr Stuart McDonald, who has been a constant support throughout my hardship. You have been an excellent mentor and would like to call you as a sculptor who never gives up until the final sculpture has been shaped. Your constant guidance and encouragement have helped me build my career.

My sincere thanks to Professor Sir Nicholas Wright, who has been and will remain inspirational for the rest of my life. He is an institution by himself with great ideas, motivation and professionalism.

Thanks to my colleagues who made my stay enjoyable and motivated me to work even over the weekends. Special thanks to Bianca, who is my troubleshooter and to whom I could ask any stupid question. Thanks to Noor, Laura, Sebastian, Lorna, Tania, Jonny, Rosemary, Richard, Nadine and, of course, Chung. It's been a pleasure working with you all. Trevor, thank you for your expertise and putting up with my schoolboy scientific knowledge. Thanks to Manuel, Marco and Hugh for providing specimens and support. Lakshmi and Graham for helping with thousands of sequencing.

This thesis is dedicated to my wife Nousheen who was next to me like my shadow throughout this journey.

List of contents

List of figures

List of tables

List of abbreviations

In alphabetical order:

ACS - adenoma-carcinoma-sequence

APC – Adenomatous polyposis coli

BO - Barrett's oesophagus

BCDA - Basal crypt dysplasia-like atypia

CCO – Cytochrome c oxidase

CDK – Cyclin dependenant kinase

CK - Cytokeratin

CLO - Columnar lined oesophagus

COSMIC - Catalogue of Somatic Mutations In Cancer

CRC - Colorectal cancer

EGF – Epidermal growth factor

EMRs - Endoscopic mucosal resection (EMRs)

ERK – Extrcellular signal regulated kinases

FAP – Familial adenomatous polyposis

GOJ – Gastro-oesophageal junction

GORD - Gastro-oesophageal reflex disease

HCL – Hydrochloric acid

HGD – High-grade dysplasia

IM - intestinal metaplasia

ISCs – Intestinal stem cells

KRAS - Kirsten-RAS

LCM - Laser capture microscopy

LGD – Low-grade dysplasia

LGR5 – Leucine-rich repeat-containing G protein-coupled receptor

LOH - Loss of heterozygosity

MAPK – Mitogen-activated protein kinase

mtDNA - mitochondrial DNA

MDC - metaplasia-dysplasia-carcinoma sequence

MDM2 - mouse double minute 2 gene

MLE – Multilayered epithelium

MREC - Multicentre research ethics committee

MSI - Microsatellite instability

MtDNA – mitochondrial DNA

NSE - neosquamous islands

OA - Oesopahgeal adenocarcinoma

OR – Odds ratio

p53 – *TP53* protein

PCR - Polymerase chain reaction

PI3K – Phosphoinositol-3 kinase

PPI – Proton pump inhibitor

Rb - Retinoblastoma

SCJ – Squamo-columnar junction

SDH – Succinate dehydrogenase

TFF – Trefoil family factor

WT – Wild type

Chapter 1: Introduction

Chapter 1: Introduction

1.1 Background:

Barrett's oesophagus is a common metaplastic premalignant condition in which the normal squamous epithelium of the human distal oesophagus is replaced by a columnar epithelium (Fitzgerald 2014). It is thought to be an acquired condition developed as a consequence of chronic exposure to gastro-oesophageal reflux disease (GORD) (Reid et al., 2015). Barrett's is highly prevalent in populations who suffer from chronic GORD and seen typically in the overweight, middle-aged Caucasian male (Wong and Fitzgerald, 2005). Around 5-10% of patients with GORD subsequently, develop Barrett's metaplasia (Voutilainen et al., 2000, Westhoff et al., 2005). The known incidence of Barrett's in western populations varies from 0.5-2% (Powell and McConkey, 1992) and prevalence varies from 1.3-1.6% (Zagari et al., 2008, Ronkainen et al., 2005). Autopsy studies have shown that the incidence rate of Barrett's could be as high as 30%, indicating that Barrett's may be vastly underdiagnosed (Cameron, 2002).

In a large population-based study, the incidence of malignant progression in males and females is low; 0.28% and 0.13% per year respectively (Bhat et al., 2011). Considering the number of Barrett's patients diagnosed each year, this represents a significant number of patients who will develop OA. The incidence of OA in Western countries has increased by six-fold over the last three decades (Pohl and Welch, 2005). A systematic review of the impact of OA has shown that the average incidence was 6.1 cases per 1000 person-years (0.61%/year or 1 in

164 person-years) (Yousef et al., 2008). Furthermore, the incidence of OA has been particularly rising in the UK; in 2013, OA was diagnosed in 8,161 patients resulting in 7,610 deaths within 1 year of diagnosis (http://info.cancerresearchuk.org/cancerstats). The 5-year survival rate of OA is around 15% ('Oesophageal cancer survival statistics". Cancer Research UK) and, therefore, understanding the progression of Barrett's into cancer has become a research priority and Cancer Research UK has termed OA as a cancer of unmet need and therefore is a research priority.

1.2 Macroscopic features of Barrett's oesophagus:

Barrett's oesophagus is endoscopically identified by the presence of salmon-pink mucosa (Figure 1). Barrett's can present in a circumferential manner or a tongue-like projection at the gastro-oesophageal junction (GOJ). During endoscopy, islands of squamous epithelium are sometimes seen within a Barrett's segment, especially in patients who were treated with proton pump inhibitors (PPIs) (Gore et al., 1993) and in patients who underwent photodynamic therapy for Barrett's dysplasia (Barr et al., 1996). These observations suggest, there may be multipotent stem cells within Barrett's, which have the capacity to regenerate squamous epithelium (Berenson et al., 1993). However, histology of these squamous islands indicates they may originate from the deep submucosal ducts (Biddlestone et al., 1998), a characteristic of the human oesophagus (Shepherd, 2000). These submucosal ducts drain mucous produced by the submucosal gland into the oesophageal lumen.

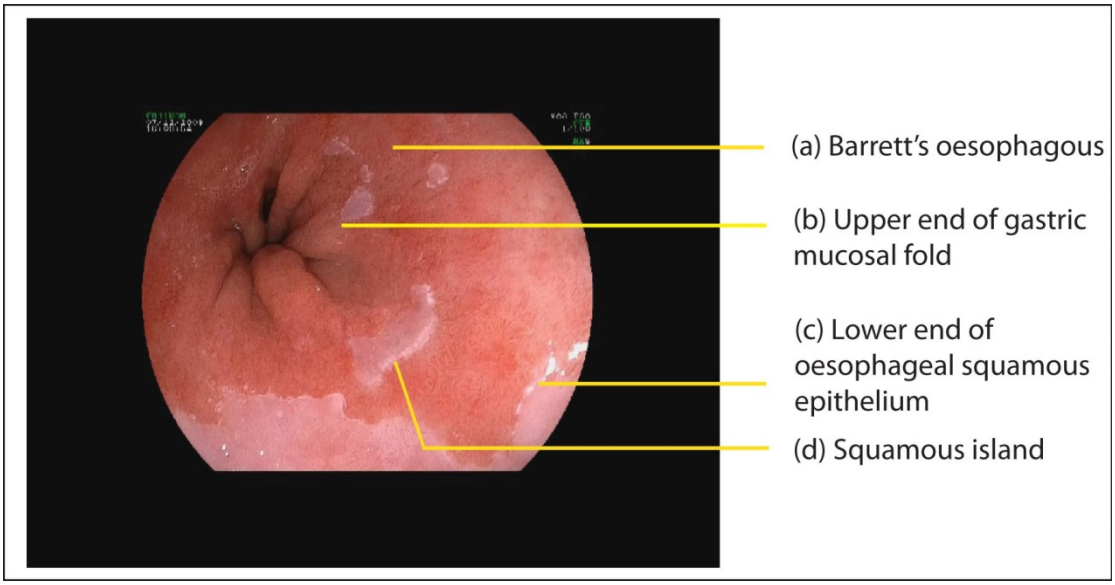

Figure 1: The endoscopic appearance of Barrett's oesophagus.
(a) Barrett's appears as a salmon-pink patch in-between (b) the upper end of the gastric mucosal fold and (c) the lower end of the oesophageal squamous epithelium. (d) Occasionally there are areas of white squamous epithelium within Barrett's segment called squamous islands, which may originate from underlying submucosal ducts. (Courtesy Ms Lorna Dunn, Newcastle Royal Infirmary, Newcastle, United Kingdom).

1.3 The Histology of Barrett's glands:

Barrett's is referred to as an intestinal metaplasia (IM), defined by the presence of mucin secreting goblet cells usually seen in the bowel (Sampliner et al., 1996, Going et al., 2004). However, according to the British Society of Gastroenterology (BSG), BO is defined as "an endoscopically apparent area above the oesophagogastric junction that is suggestive of Barrett's which is supported by the finding of columnar lined oesophagus on histology. The presence of areas of intestinal metaplasia (IM), although often present, is *not* a requirement for diagnosis". Typically, Barrett glands show the presence of both intestinal goblet cells and gastric foveolar cells (figure 2). Barrett glands that are entirely

composed of goblet cells (sometimes with Paneth cells) or entirely consisting of gastric type cells can also be detected.

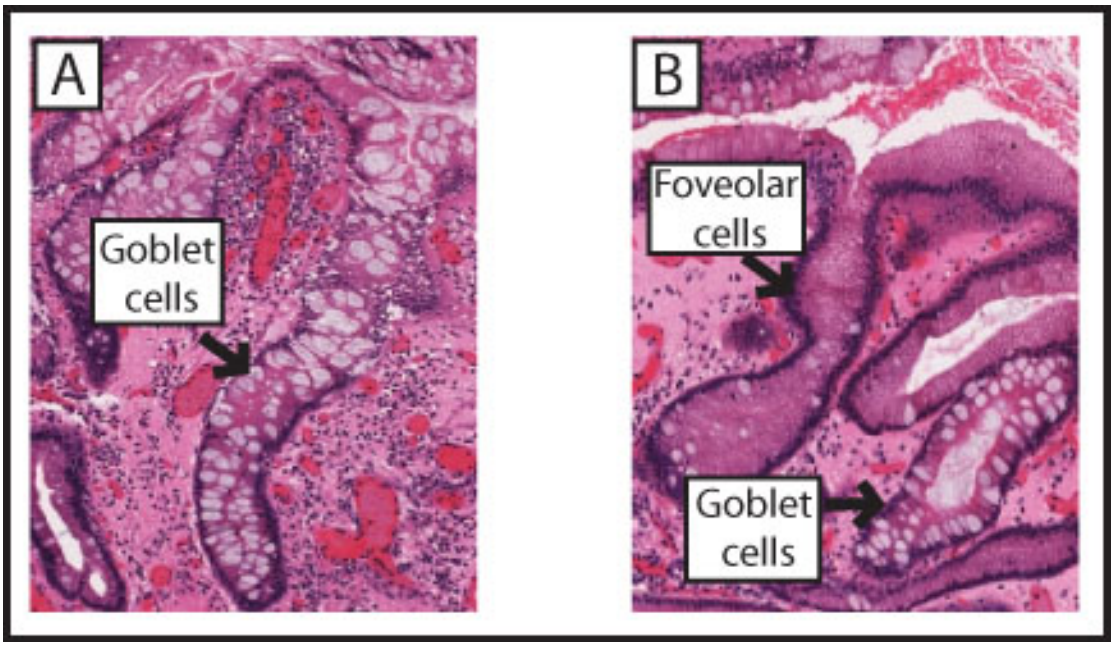

Figure 2: Histology of Barrett's oesophagus.
(A) Haematoxylin and eosin stain showing typical Barrett's gland with goblet cell (black arrow) metaplasia. (B) Barrett's gland exhibiting foveolar cells (top black arrow).

There is some evidence that Barrett's glands can evolve from a gastric to an intestinal phenotype (Going et al., 2004). Therefore Barrett's glands display phenotypic heterogeneity and can be defined as (i) complete intestinal metaplasia (IM) consisting of goblet cells and Paneth cells (Chandrasoma et al., 2010), (ii) incomplete IM, consisting of both gastric and intestinal differentiation and (iii) cardia-type epithelium consisting of mucinous glands without parietal cells or goblet cells (Chandrasoma et al., 2000). Barrett glands contain both gastric and intestinal lineages expressing markers of gastric epithelium (MUC1, MUC5AC and MUC6) and intestinal epithelium (MUC2 and MUC3) (Glickman et al., 2006, Reis et al., 1999). Barrett's exhibits cellular compartmentalization; and the

upper zone of the gland mainly consists of columnar foveolar cells which are positive for MUC5AC and TFF1 and goblet cells (expressing MUC2), the middle zone or neck is the stem cell zone and the basal region mainly consists of mucous secreting cells which are positive for MUC6 and TFF2 (Figure 3). Recently, Lavery et al., (2014), have demonstrated that foveolar cells and goblet cells within the same gland are clonally related showing they originate from a common stem cell (Lavery et al., 2014b).

1.4 Stem cells in Barrett's oesophagus:

Stem cells are long-lived cells, which have the capacity to self-renew (maintaining their progeny) and are multipotent, having the ability to produce the entire repertoire of differentiated cells from their niche (Blanpain and Fuchs, 2009). Stem cells can be classified as embryonic stem cells that are derived from early blastocyst and somatic stem cells that are found in adult tissue (Potten and Loeffler, 1990). To maintain the organ homoeostasis and to repair during injury, stem cells divide to replace cells which are lost. When the stem cell divides it can produce either a stem cell or a progenitor cell. The progenitor cell then further proliferates and differentiates as it progresses towards the oesophageal lumen (Daniely et al., 2004).

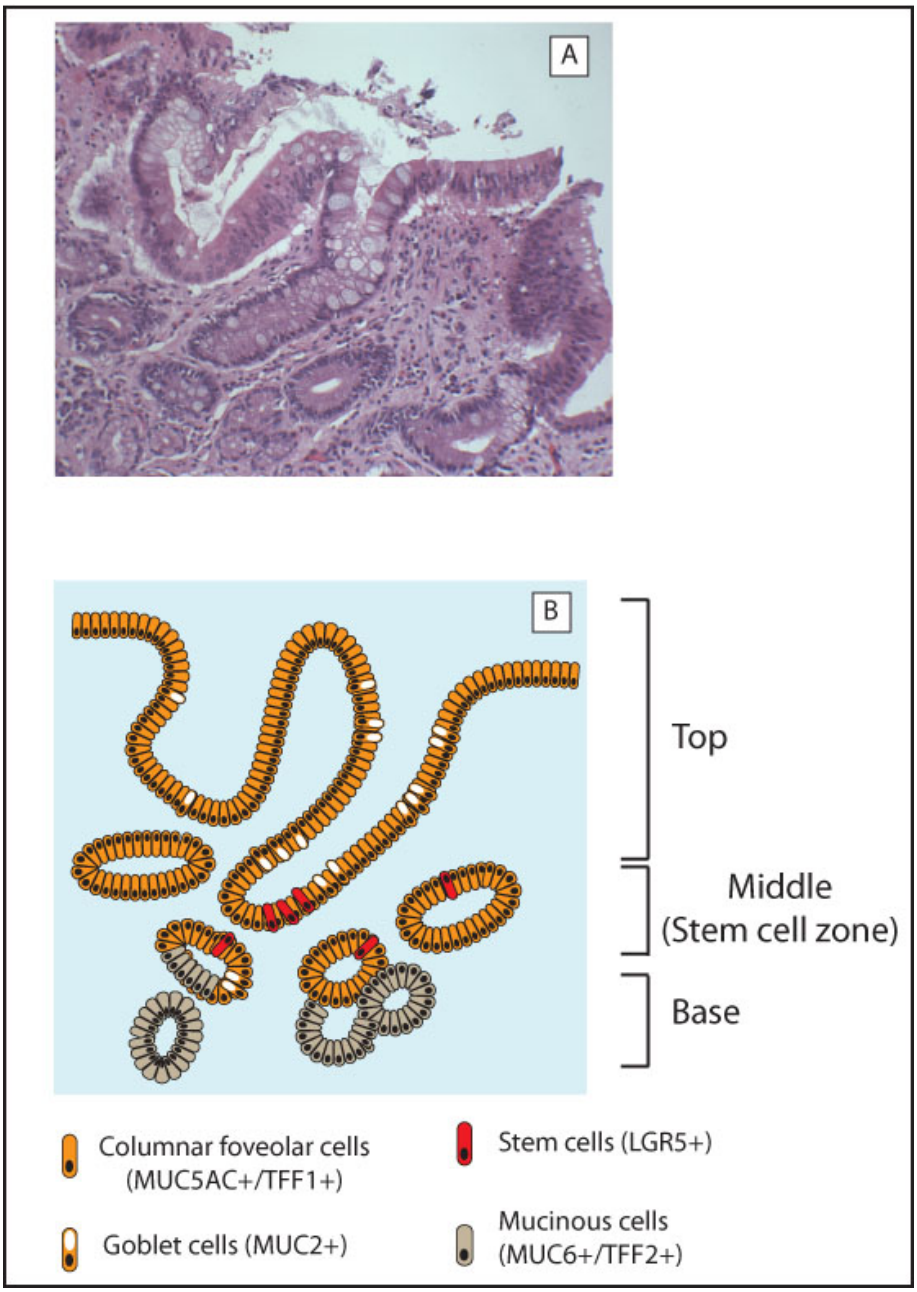

Figure 3: The cellular distribution in a typical Barrett's gland.
(A) Haematoxylin and Eosin stain of Barrett's glands. (B) Barrett's glands exhibit cellular distribution, such as; the upper zone consists of columnar foveolar cells (MUC5AC+/TFF1+), the middle zone mainly consists of stem cells (LGR5+) and the basal region composed of mucinous cells (MUC6+/TFF2+).

The Barrett's gland stem cell is capable of producing all metaplastic cell lineages (Glickman et al., 2006, Reis et al., 1999) and can be identified by the expression of Leucine-rich repeat-containing G-protein-coupled receptor 5 (LGR5). LGR5 is a part of the Wnt signalling pathway and is a known intestinal stem cell marker with self-renewal and multi-lineage capacity (Barker et al., 2007, Barker et al., 2009). Lavery et al., (2014) have shown by *in situ* hybridization that *LGR5* mRNA is expressed in the isthmus or neck region of the Barrett's gland. A similar distribution is seen in gastric pylorus glands, suggesting a common architecture between Barrett and gastric glands. In the same study, Lavery and colleagues injected patients, who were scheduled to have an oesophagectomy for Barrett's adenocarcinoma, with low level radiolabelled iododeoxyuridine (a thymidine analogue that is incorporated into proliferating cells) permitting analysis of cellular migration over time (the time between injection and operation). They showed that Barrett's glands displayed bidirectional migration from the stem cell zone in the neck, up to the surface and down to the gland base (Lavery et al., 2014b). This is similar to earlier observations made in the stomach (Karam et al., 2003). Furthermore, the expression of the proliferation marker Ki67 in Barrett's glands is most concentrated in the neck region (Nicholson et al., 2012). Nicholson et al., used cytochrome *c* oxidase (CCO) staining and mitochondrial DNA mutation analysis to show that all cell lineages within Barrett's metaplasia arise from a single stem cell and are therefore clonal (Nicholson et al., 2012).

1.5 The origins of Barrett's oesophagus:

The current dogma on the origins of Barrett's is that it evolves from the native squamous epithelium (Souza et al., 2008). However, there are alternative sources, such as proximal migration of gastric glands and submucosal oesophageal glands (Figure 4) and residual embryonic-like cells at the gastroesophageal junction. It is important to understand the origin of Barrett's to understand its evolution. Here I discuss the putative sources of Barrett's epithelium to put into context the evolution to cancer I propose later in the thesis.

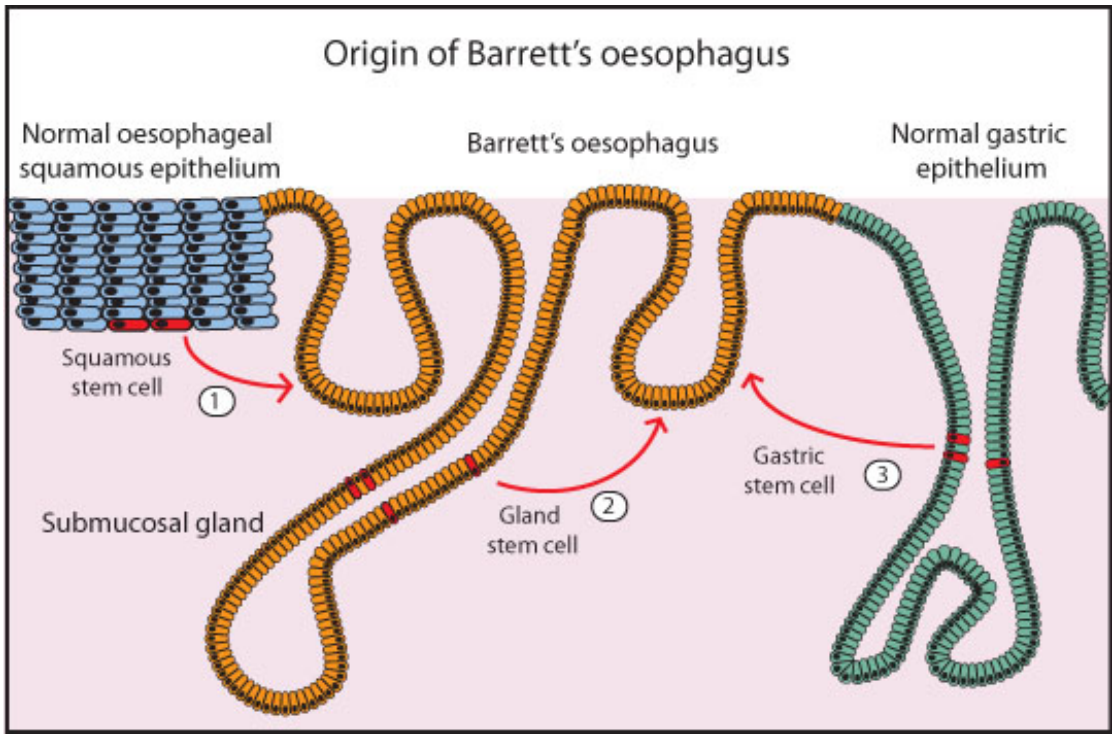

Figure 4: Origin of Barrett's oesophagus.
The source of Barrett's epithelium could be; (1) Native squamous epithelium (2) Submucosal oesophageal gland/ducts and (3) Gastric epithelium. Modified from (McDonald et al., 2015).

1.5.1 The squamous oesophagus:

Gastro-oesophageal reflux consisting of acid and bile leads to ulceration of the lower end of the oesophagus, lined by the normal squamous epithelium. In the majority of cases squamous epithelium regenerates, however in a small proportion of patients with chronic GORD, the squamous epithelium is replaced by columnar metaplasia (Spechler, 2002). Over the last few decades, the most accepted hypothesis is that bile and acid reflux over the GOJ stimulates abnormal differentiation of stem cells present in the basal layers of squamous epithelium at the lower end of oesophagus resulting in Barrett's metaplasia (Jankowski et al., 1999, Seery, 2002). Furthermore, during the 17th week of gestation the ciliated columnar lined oesophagus is replaced by squamous epithelium and some have proposed that Barrett's is a reversal back to the embryonic state (Johns, 1952). However, the transition between these two phenotypes secondary to GORD is yet to be seen *in vivo* (Riddell, 2005).

The multilayered epithelium (MLE) is a pathological feature of the transition zone between squamous and columnar epithelium which displays ultrastructural features of both squamous epithelium at the base and columnar epithelium superficially under certain conditions (Riddell, 2005) including Barrett's, in which it is strongly associated with goblet cell metaplasia (Shields et al., 2001, Upton et al., 2006). MLE has been shown to be a histological marker of GORD (Glickman et al., 2009). Glickman et al., have shown that MLE expresses mucins such as sialomucin (in 100% of cases), neutral mucin (88%) and sulfomucin (71%) along with expression of specific cytokeratins (CK13 and 19 in basal squamous epithelium and CK 7, 8/18, 19 and 20 in the superficial columnar

epithelium), these characteristics are similar to the cytokeratin profile of Barrett's. In a single patient they observed a mucosal gland duct in continuity with MLE suggesting a common cell of origin and that MLE maybe an early transitioning stage to Barrett's, but this is unconfirmed and could be artefactual (Glickman et al., 2009). In a recent prospective Central European Multicenter (histoGERD trial) cross-sectional study, MLE was seen either within or adjacent to an oesophageal gland duct in 1 in 10 individuals undergoing OGD. MLE was seen to be associated with increasing age, obesity, hiatus hernia, oesophagitis and Barrett's ($p=0.001$, 0.026, 0.001, 0.002 and 0.001 respectively) indicating GORD (Langner et al., 2014). Its association with cardiac mucosa ($p<0.001$) and Barrett's suggest MLE to be an intermediate step in the development of Barrett's (Langner et al., 2014).

After endoscopic ablation therapy for Barrett's, some areas of Barrett's are replaced by squamous epithelium (Biddlestone et al., 1998), MLE may play a role in bringing this change in phenotype. However, regenerated squamous epithelium does not exhibit MLE. MLE is most commonly seen towards the area of high inflammation (Shields et al., 2001) and is not seen along the entire length of the Barrett's segment (Upton et al., 2006), suggesting that inflammation may not be the driving force behind the origin of MLE. It may well be that a high degree of inflammation at the squamocolumnar junction promotes the development of MLE, which may transition into Barrett's epithelium. However, clonality studies on MLE, suggesting that the basal squamous and superficial columnar epithelium sharing common ancestry have not been performed.

1.5.2 Submucosal glands and ducts:

The submucosal gland is a tubule-acinar structure with stratified squamous epithelium lining the duct (Al Yassin and Toner, 1977) (Figure 5). There is evidence suggesting that cells lying in deep submucosal glands or ducts could be the source of Barrett's (Badreddine and Wang, 2010, Souza et al., 2008). Coad et al., (2005) carried out serial sections through 46 Barrett's specimens, 21 specimens displayed oesophageal gland ducts in continuity with surface Barrett's epithelium. 17 out of 21 specimens had a clear demarcation between two different phenotypes. However, four specimens showed continuity with gradual morphological changes between Barrett's and ductal epithelium, suggesting that the surface Barrett's epithelium is arising from deep mucosal glands. In the same study, 15/15 squamous islands in Barrett's were found to be in continuity with the underlying oesophageal gland ducts, suggesting that they are arising from deep mucosal glands (Coad et al., 2005). It has also been shown that the submucosal gland duct contains clonal patches of CCO-deficient cells (Nicholson et al., 2012) and therefore maybe a potential site of a stem cell niche (Fellous et al., 2009a). Leedham et al., have presented a case that showed an oesophageal gland duct sharing a common p16 point mutation with an area of Barrett's contiguous to the duct indicating that both had a common cell of origin. The same mutation was also seen in oesophageal gland acini (Leedham et al., 2008), suggesting a bi-directional spread of mutation similar to that observed in the Brunner's gland (Ahnen et al., 1994). There is also evidence showing that the oesophageal gland duct is a source of oesophageal adenomas (Rouse et al., 1995), adenocarcinomas (Endoh et al., 1999) and squamous cell carcinomas (Takubo et

al., 1993), suggesting the presence of a multipotent stem cell niche in the oesophageal gland duct.

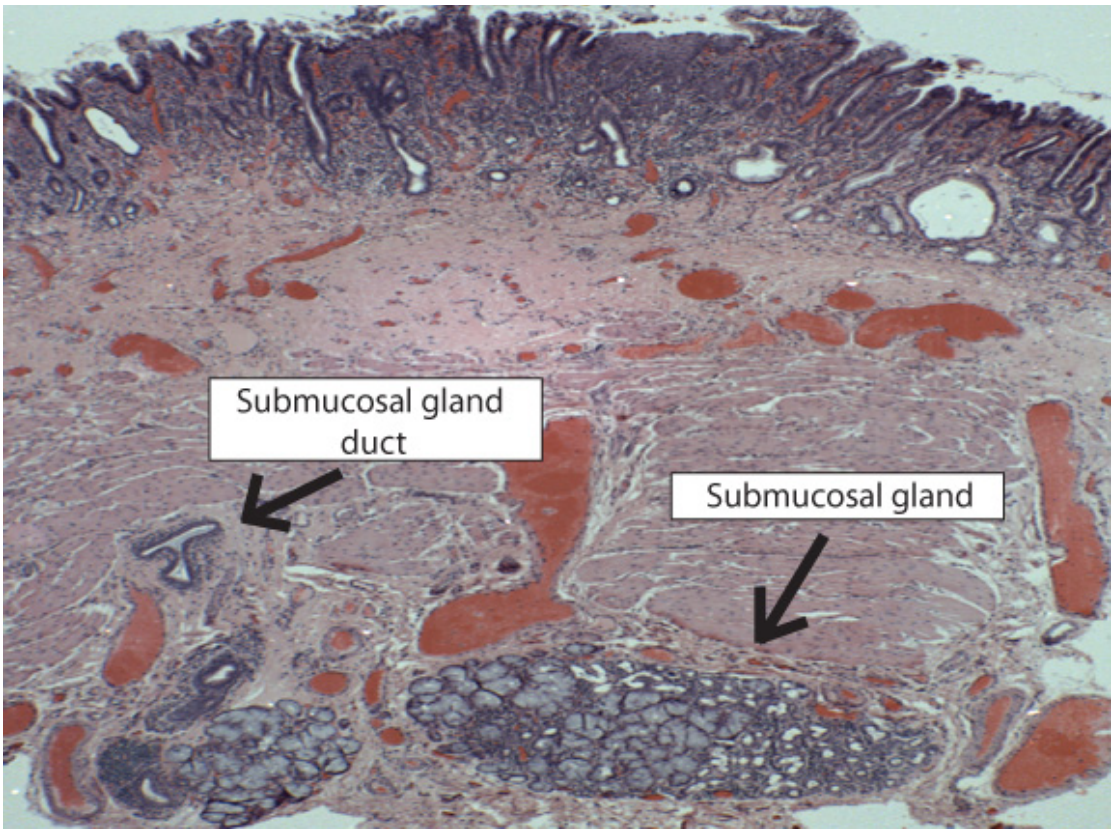

Figure 5: H & E of Barrett's showing a submucosal gland duct and submucosal glands.

Neosquamous islands (NSE) are patches of squamous epithelium that develop in Barrett's lesions after acid suppression or ablation therapy (Biddlestone et al., 1998). Sometimes they arise spontaneously (Sampliner et al., 1988). Biddlestone et al., have shown that NSEs can be seen in continuity with the neck of the Barrett's gland (Biddlestone et al., 1998). Paulson et al., have shown that NSEs, do not typically share common somatic mutations with adjacent Barrett's epithelium (19 out of 20 patients). However in a single patient there was a clonal relationship and it is possible that 19 patients that did not show a somatic

relationship possessed common mutations in genes that were not targeted in this experiment. Leedham et al., have identified Barrett's epithelium in continuity with a squamous island and have shown that the squamous island wild type compared to the adjacent *TP53* mutated Barrett's epithelium, suggesting that NSE originated from a different clone to the adjacent Barrett's epithelium (Leedham et al., 2008). The same criticism of not targeting sufficient numbers of genes can also be levelled at this study, therefore the relationship of NSE with Barrett's is still a matter of debate.

Recent observations have shown that sub-mucosal glands were more concentrated underneath NSE compared to the columnar-lined Barrett's epithelium and that sub-mucosal glands are more concentrated at the squamocolumnar junctions compared to the columnar and squamous-lined oesophageal epithelium. These observations suggest that both NSE and Barrett's epithelium can originate from stem cells present in the submucosal glands (Lorinc and Oberg, 2012).

1.5.3 Proximal migration of gastric glands:

Another potential source of Barrett's oesophagus is the migration of gastric glands into an area denuded by acid/bile reflux that undergo intestinal metaplasia (Bremner et al., 1970, Barrett, 1950). However, the presence of goblet cells is not necessary for the diagnosis of Barrett's (Riddell and Odze, 2009). It may well be that the cardiac mucosa at the squamocolumnar junction creeps up proximally and gradually increases its length in response to chronic acid reflux (DeMeester and DeMeester, 2000, Chandrasoma et al., 2003).

Several studies in patients who have undergone oesophagectomies have shown the development of columnar epithelium at the oesophago-gastric anastomotic junction (Lord et al., 2004, Oberg et al., 2002, Meyer et al., 1979). Columnar epithelium found at the anastomotic junction is similar to the cardiac-type epithelium and shows progression towards intestinal metaplasia (Lord et al., 2004). In a study looking at biopsy specimens at different levels of Barrett's segment, Going et al., have shown that gastric cardia-like epithelium is present throughout the length of the Barrett's segment. However, it was observed more frequently at the distal end of the Barrett's segment. Gastric oxyntic-like epithelium was often found in the distal segment of Barrett's. Lavery et al., (2014) have shown that Barrett's glands consisting of gastric (MUC5AC and MUC6) and intestinal (MUC2 and MUC3) cell lineages are clonal. The stem cell zone is located at the neck of the Barrett's gland similar to pyloric-type glands which are capable of giving rise to all cell lineages (Nicholson et al., 2011). Lgr5 is a known stem cell marker for small intestine and colon, however in Barrett's its expression mimics that of the gastric pylorus and antrum (Lavery et al., 2014b, Barker et al., 2010). Quante et al., shown in a transgenic model of Barrett's that in response to inflammation secondary to acid reflux, Lgr5+ gastric cardiac progenitor cells migrate into the oesophagus, suggesting that Barrett's may originate from gastric cardia progenitor cells located at the squamocolumnar junction (Quante et al., 2012).

1.5.4 Barrett's arises from an embryonic precursor cell present at the squamocolumnar junction:

An alternative hypothesis for the origins of Barrett's is that a remaining embryonic stem cell population with columnar potential remains at the squamocolumnar junction and may be the source of Barrett's epithelium (Wang et al., 2011). P63 is a p53 homolog and is required for self-renewal of stratified squamous epithelial stem cells (Senoo et al., 2007). In p63 null embryos, a lack of self-renewal capacity results in loss or ulceration of stratified squamous epithelium ((Yang et al., 1998), (Yang et al., 1999), (Senoo et al., 2007). Recently Wang et al., have shown that p63 knockout mice develope intestinal metaplasia similar to Barrett's (Wang et al., 2011). They also tried to track its source and suggested Car4+/CK7+ (carbonic anhydrase/cytokeratin 7) cells present at the squamocolumnar junction (SCJ) are the source of origin of Barrett's metaplasia. Usually, these cells were undermined and replaced by p63 expressing cells (Wang et al., 2011). However, the authors did not demonstrate any lineage tracing and also did not explain as to how Barrett's develops at the anastomotic site in patients who have undergone oesophagectomy or gastrectomy, wherein, the SCJ is excised during the operation.

1.6 The evolution of Barrett's oesophagus to oesophageal adenocarcinoma:

Long-term follow-up of patients who were diagnosed with columnar-lined oesophagus (CLO) either with or without IM has shown that there is no significant difference in the rate of progression to dysplasia or OA amongst those two groups (Gatenby et al., 2008). Recent evidence suggests that goblet cells containing complete IM carry a higher risk of developing OA (Desai et al., 2012), but Chandrasoma et al., have shown that CLO without evidence of goblet cells did not carry any risk of developing OA (Chandrasoma et al., 2012). However, recently, Lavery et al., have shown that non-goblet containing metaplastic columnar epithelium has malignant potential (Lavery et al., 2015), and the frequency of DNA abnormalities in goblet and non-goblet containing metaplastic epithelium remains the same.

Barrett's oesophagus progresses through different histological stages before progressing to OA, such as (a) Barrett's metaplasia (b) Barrett's dysplasia which can be low-grade dysplasia (LGD) or high-grade dysplasia (HGD) and (c) oesophageal adenocarcinoma (Figure 6). Dysplasia can be defined as "neoplastic epithelium confined to the basement membrane which can give rise to intraepithelial neoplasia" (Skinner et al., 1983). The dysplastic cells in Barrett's show evidence of high nuclear to cytoplasmic ratio, cellular atypia and nuclear hyperchromasia without stratification (Skinner et al., 1983). Barrett's dysplasia can be histologically graded as low-grade and high-grade depending on the

degree of cellular atypia. Barrett's biopsies are reported as either negative for dysplasia, indefinite for dysplasia, containing LGD or HGD or adenocarcinoma.

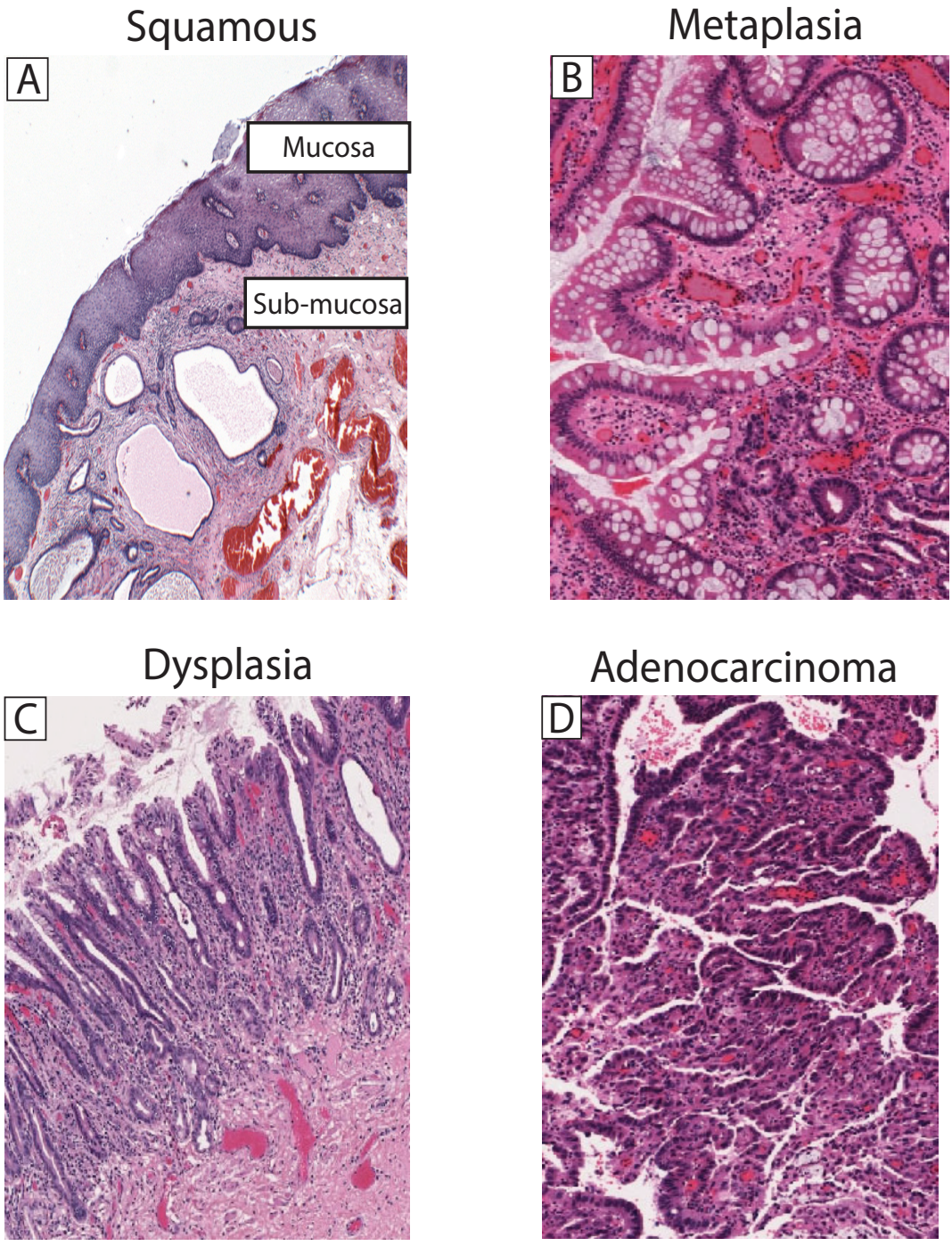

Figure 6: The histological sequence of progression from Barrett's to OA.
(A) H&E of lower end of the oesophagus showing normal squamous epithelium. (B) Barrett's metaplasia showing the presence of mucous secreting goblet cells. (C) Barrett's dysplasia with the absence of goblet cell, nuclear prominence and increased in the nuclear:cytoplasmic ratio. (D) Oesophageal adenocarcinoma.

In LGD, the architecture of Barrett's glands is maintained but cellular atypia and nuclear hyperchromasia is present in the gland base and occasionally goblet cells are present. In HGD, there is an increase in glandular branching, dysplastic cells show prominent nuclei with an increase in the nuclear to cytoplasmic ratio. Indefinite for Dysplasia is the term used when the diagnosis of dysplasia is ambiguous. It means that there are some histological abnormalities seen but dysplasia can't be ruled out. A study from Netherlands has shown that the incidence rate of HGD or OA in patients diagnosed with indefinite for dysplasia was 1.4 per 100 person-years, suggesting the need for their surveillance (Kestens et al., 2014). In low-grade dysplasia, 10-15% may progress to high-grade dysplasia and adenocarcinoma over 2-5years (Heading et al., 2005– BGS guidelines 2005, http://www.bsg.org.uk). The incidence of OA in LGD was reported as 1.4% per year versus 0.17% in patients with no dysplasia ($p<0.001$) (Bhat et al., 2011). In high-grade dysplasia, 34% will develop adenocarcinoma over 5yrs (Heading et al., 2005– BGS guidelines 2005, http://www.bsg.org.uk).

1.7 Genetic events during the metaplasia: dysplasia: carcinoma (MDC) sequence:

In 1953, Carl Nordling suggested that cancer develops from the accumulation of multiple mutations in critical genes over a period of time (Nordling, 1953). Subsequently, in 1976, Nowell et al. proposed the "somatic mutation theory". According to the somatic mutation theory of cancer development, mutations occur in long-lived, dividing cell populations such as stem cells and accumulate

mutations over time, some of which provide a growth advantage over neighbouring cells. Eventually sufficient mutations are acquired resulting in the transformation into a neoplasm (Nowell, 1976).

Barrett's oesophagus is a risk factor for the development of oesophageal adenocarcinoma (Wang et al., 2008), therefore patients with Barrett's are kept under regular surveillance to detect any evidence of malignancy. Since this lesion is left *in situ*, it provides a serendipitous means to study the progression to cancer over time. Barrett's progresses to cancer in a stepwise manner from metaplasia to dysplasia and then carcinoma (Stein et al., 2003). The MDC is characterised by the acquisition of multiple genetic alterations, such as chromosomal instability (Chaves et al., 2007), *TP53* mutations (Prevo et al., 1999), *CDKN2A* mutations (Paulson et al., 2008), loss of heterozygosity (LOH) of *TP53* and *CDKN2A*, loss of p16 via methylation and aneuploidy, suggesting that clonal evolution during the MDC sequence seems to follow a more complex pathway rather than a linear pathway.

The advent of next generation sequencing has permitted a much deeper understanding of the genetic and clonal events that occur as Barrett's progresses to OA. Agarwal et al., have used exome sequencing and shown that the mutation rate in Barrett's mucosa lying adjacent to OA is up to 80% (Agrawal et al., 2012). However, it is important to identify the extent of identical mutation, which may be present in pre-dysplastic Barrett's patients who do not progress to OA. A recent study that employed whole genome sequencing to investigate mutation events along the MDC sequence has shown that the majority of somatic mutations

(including *CDNK2A*) present in OA were also present in matched non-dysplastic Barrett's, whereas *TP53* and *SMAD4* mutations were seen mainly in high-grade dysplasia and OA respectively (Weaver et al., 2014). However, Stachler et al., (2015), using similar techniques demonstrated that *TP53* mutations were frequent in non-dysplastic Barrett's (Stachler et al., 2015). These observations suggest, mutations identified in early non-dysplastic Barrett's can be used to predict patients who are at risk of progressing to OA. Interestingly, some mutations found in pre-dysplastic Barrett's were in cancer-associated genes such as ARID1A and SMARCA4, suggesting that even pre-dysplastic Barrett's is characterised by the presence of a complex genetically mutated landscape. The importance of these genes in the early stages of MDC is unknown. However, these somatic mutations may provide increase fitness for clonal expansions in pre-dysplastic Barrett's (Weaver et al., 2014), similar to PTEN mutation found in 35% of normal endometrial tissue but the risk of endometrial cancer is around 2-3% (Mutter et al., 2001).

These observations suggest that multiple genetic and epigenetic alterations occur during the MDC sequence and by placing these genetic events in chronological order gives a better understanding of stepwise progression from Barrett's to OA. During MDC sequence; Barrett et al., 1999, have suggested that LOH of *CDKN2A* and *TP53* is seen early, whereas, aneuploidy was a late event (Barrett et al., 1999). Maley et al., have shown that clonal size consisting of *TP53* LOH or aneuploidy carries a higher risk of progression to OA compared to *CDKN2A* clone size (Maley et al., 2004a), and have further shown that genetic diversity predicts the progression from Barrett's to OA (Maley et al., 2006). Recently, Andor et al., 2016,

using exome sequencing across twelve cancer types, have shown that 86% of 12 different tumours had more than one clone and have suggested that tumours with more than four clones within a sample had increased mortality risk. These observations suggest genetic diversity could be used as a useful tool to identify patients at high-risk of cancer (Andor et al., 2016).

Recently, a Genome-Wide study has found that there is a high genetic correlation with significant polygenic overlap between BO and OA, suggesting that shared multiple genetic alterations are involved in the progression of BO to OA (Ek et al., 2013). Similar genetic diversity was seen in a case-cohort follow-up study by Li et al., SNP arrays technique was used to investigate genetic alteration in Barrett's patients who progressed to OA (progressors) and patients who did not progress to OA (non-progressors). They have shown that the genomes in non-progressors remained stable and showed very little genetic diversity such as, genomic deletions, *CDKN2A* loss/LOH), whereas progressors showed significant genetic diversity such as chromosomal alterations in the form of gains/losses and genome doublings up to 48 months prior to the development of cancer (Li et al., 2014). Recently, a large population-based study using fluorescence *in situ* hybridization have also suggested that identifying genetic diversity within a specimen helps to identify high-risk patients. An abnormal marker count of genetic alterations in *CDKN2A*, MYC and aneusomy (a genetic imbalance within a pair of chromosomes due to deletion or duplication of the allelic segment) could be used to identify high-risk patients with non-dysplastic Barrett's. Patients with high genetic diversity identified by an abnormal marker count had a 8.7-fold higher risk of progression towards OA compared to the low-risk group. These

data along with the clinical scoring of age and length of BO may help to identify low-risk patients who may not need a regular invasive endoscopic procedure (Timmer et al., 2015).

Study involving whole exome sequencing from BO, OA, and specimens from BO and OA from same patients were analysed. It revealed that *TP53* mutations occurred during early stages of MDC sequence, and 62.5% of OA developed after genome doubling (Stachler et al., 2015). In tumours that show genome doublings, oncogenic amplifications (such as *TP53*) are seen more often than inactivation of tumour suppressor genes (such as *CDKN2A*) (Stachler et al., 2015). This suggests that OA occurs as a consequence of change in copy number rather than a stepwise accumulation of gene alterations (Stachler et al., 2015). However, it is likely that both mutations and copy number alterations occur together throughout the progression to cancer.

Intra-tumour genetic heterogeneity has been seen in various cancers (Marusyk et al., 2012). Gerlinger et al., have used whole exome multi-region spatial sequencing on metastatic renal cell carcinomas. They have shown that around 65% of mutations detected were heterogeneous and spatially separated within the tumour. These mutations were not seen in every spatially separated sample analysed, suggesting genetic heterogeneity within a single tumour (Gerlinger et al., 2012). Genomic analysis of a biopsy sample from a tumour may not detect the heterogeneity present within the tumour, which carries significant clinical implication during validation of biomarkers for any cancer. These observations suggest that cancer progression follows a branching pattern rather than a linear

pathway and in order to provide robust biomarkers we need to understand the clonal architecture of the tumour (Gerlinger et al., 2012).

Genomic sequencing studies have identified a high mutational burden in OA and have identified various mutational gene signatures (Chong et al., 2013, Agrawal et al., 2012, Weaver et al., 2014, Dulak et al., 2013). Ross-Innes et al., have used whole-genome sequencing to analyse paired samples taken at the same time from OA and the adjacent Barrett's. The average number of single nucleotide variants (SNVs) in Barrett's was much higher (6.7/Mb) compared to other cancers, such as colorectal, breast, liver and multiple myelomas (5.9 SNVs/Mb, 1.1 SNVs/Mb, 3.6 SNVs/Mb and 2.9 SNVs/Mb respectively). There was a 20% overlap between SNVs in Barrett's and OA and *TP53* genomic mutations were the most common recurrent mutations was seen in almost 82% of OA compared to 39% in Barrett's metaplasia. They also found that *TP53* mutations found in adjacent Barret's mucosa were not found in paired samples of OA. EYS, ARIDIA and ABCB1, which were previously reported as driver genes for OA. The genetic heterogeneity seen within Barrett's tissue suggests polyclonality and interestingly very little genetic commonality between Barrett's and OA (Ross-Innes et al., 2015). To further investigate the genetic landscape and genetic diversity, they sequenced samples from a single patient who presented with a 10cm Barrett's segment over a period of 3 years and had undergone five endoscopies with 78 biopsy samples. This patient was diagnosed with various stages of Barrett's metaplasia, dysplasia and adenocarcinoma. In his follow-up specimens, six distinct clonal mutations were identified in the non-dysplastic Barrett's, of which four clones progressed to LGD, and three clones were

identified in HGD. Only four clones spread across the whole length of the Barrett's segment. These data support the polyclonal evolution model in Barrett's proposed by Leedham et al., (2008). Interestingly, there were three common mutations (non-coding) present in all Barrett's samples supporting common ancestor model from Reid et al., group (Maley et al., 2004b) and presence of multiple clones of which two clones were not able to selectively sweep across the whole length of Barrett's segment supporting the polyclonal model of clonal evolution proposed by Leedham et al., (2008). These observations suggest genetic heterogeneity in Barrett's oesophagus, which was further supported by evidence of multiple clones within the same sample on deep sequencing (Ross-Innes et al., 2015).

1.8 Assessment of clonality in Barrett's oesophagus:

Determining the clonal architecture of an epithelial unit (of which the Barrett's gland can be considered as one) and comparing it with other units in the same tissue allows for analysis of the evolution of premalignant disease to cancer. Clonal populations are groups of cells arising from a single progenitor. A mutation that gets passed onto a cell's progeny can be detected and used to lineage trace its ancestry, which helps to distinguish those cells that are clonal from other unrelated cells. Various techniques have been used to assess tissue clonality. Here I introduce the basic techniques to perform clonal analysis in order to give context for my methodological approaches I use in this thesis.

1.8.1 Point mutations as a marker of clonality:

Identification of genetic alterations, such as genomic or mitochondrial point mutation can be used as markers of clonality: the likelihood that two cells sharing the same mutation originating from independent progenitor cells are low. Regardless if such common mutations affect amino acid coding or protein function or not, their strength as clonal markers depends on the variation of mutations within each gene in the population. In this thesis I have used Sanger sequencing to identify mutations in specific exons of *TP53*, *CDKN2A* and *KRAS* that are known to be frequently mutated in Barrett's (Maley et al., 2004b).

1.8.2 Mitochondrial DNA mutations:

Mitochondria are organelles in the cell cytoplasm whose function is to produce energy via the production of adenosine triphosphate-ATP. Mitochondrial DNA (mtDNA) is double-stranded, 16,600 base pairs in size and encodes 13 proteins, 2 trRNAs and 22 tRNAs (Taanman, 1999). MtDNA is susceptible to somatic mutations due to poor DNA repair mechanisms (Taylor and Turnbull, 2005), a lack of protective histones and reside in an oxidative environment. This results in a higher mutation rate of mtDNA compared with genomic DNA and furthermore mutant cells can be readily identified in tissue sections by enzyme histochemistry for deficiency of cytochrome *c* oxidase (CCO) which has been shown to be frequently mutated in aged human cells (Fellous et al., 2009b). Tracing common mutations in CCO-deficient cells permits clonal analysis in tissues. MtDNA mutations have been used as a marker of clonality in the brain (Kirches et al., 2003), small intestine (Gutierrez-Gonzalez et al., 2009), normal colon (Taylor et

al., 2003) and colonic adenomas (Humphries et al., 2013). Studies in Barrett's, using mtDNA mutations associated with CCO deficiency as the clonal marker, have shown that Barrett's glands are clonal and are maintained by multiple stem cells (Nicholson et al., 2011).

1.8.3 Microsatellite markers and loss of heterozygosity (LOH):

DNA Microsatellites (MS) are simple sequence repeats consisting of 2-5 base pairs (Bidichandani et al., 1998) and loss of heterozygosity (LOH) is a genetic event wherein a particular locus is lost in a single allele and the remaining allele is all that is left. Any mutation of this remaining allele can have a major impact on the cell.

The progenitor of a particular cell can be identified using MS, as the number of nucleotide repeats varies within a population but is inherited. LOH has been used as a tool to determine clonality in various carcinomas, such as bladder (Hartmann et al., 2000), pituitary (Clayton et al., 2000) and liver (Ng et al., 2003) (Lin et al., 2005). In Barrett's; LOH was assessed, by amplifying the genomic DNA using PCR followed by genotyping (Galipeau et al., 1999, Barrett et al., 1999). The amplified microsatellite markers, from metaplasia-dysplasia-carcinoma MDC areas can be compared with non-epithelial tissue from the same patient (which acts as a control or constitutional DNA). The healthy tissue usually shows two allelic peaks; rarely we may see only one allelic peak indicating that the sample is non-informative (and we are unable to detect loss of one of the alleles) and therefore this cannot be used to compare with the tumour samples. LOH is

considered to be present if the area under one allelic peak was less than 0.5 times or more than two times the area of the corresponding allele in the constitutional DNA (i.e. microdissected areas of muscle/squamous tissue) from the same patient (Figure 7).

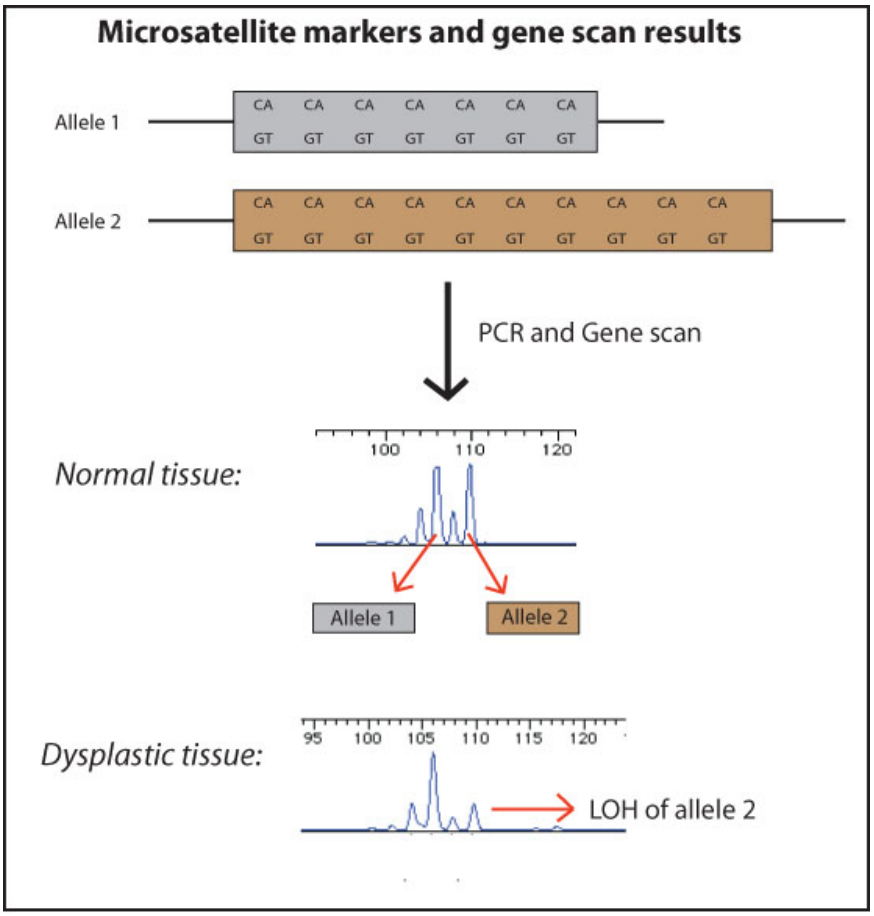

Figure 7: Microsatellite markers and gene scan.
Microsatellite markers are areas of repetitive sequence of DNA within an allele. Variation in these repeats occurs naturally and allows distinction between alleles. Loss of heterozygosity (LOH) is confirmed by comparing two alleles from the metaplastic/dysplastic DNA against the standard DNA (muscle).

1.9 Clonal ordering:

Individual clones are classified according to their mutation status/profile. Gastrointestinal crypts and glands are known to be clonal. Therefore, we assume that each cell within crypts and glands contain the same mutation. Over time, an individual clone will acquire more mutations, expanding through the tissue as it does so by crypt division (otherwise known as fission, discussed later in this chapter). Hence, we can use these genetic events to infer the sequence of events leading to cancer.. Genetic dependency analysis, or clonal ordering, is a valuable tool for studying clonal evolution in neoplasms (Maley et al., 2004b, Merlo et al., 2006). This technique uses the spatial distribution and frequency of shared mutations to infer information about the order in which mutations arise. Figure 8 shows, in a hypothetical tissue, that mutation A must occur first because if A is absent, then the sample is wild type. Mutation B must have been acquired after mutation A because B is only found together with A and mutation C must have come after B as C is only found together with A and B. The relative order of mutation D and E cannot be inferred since they are found in different samples at the same frequency (Figure 8).

.

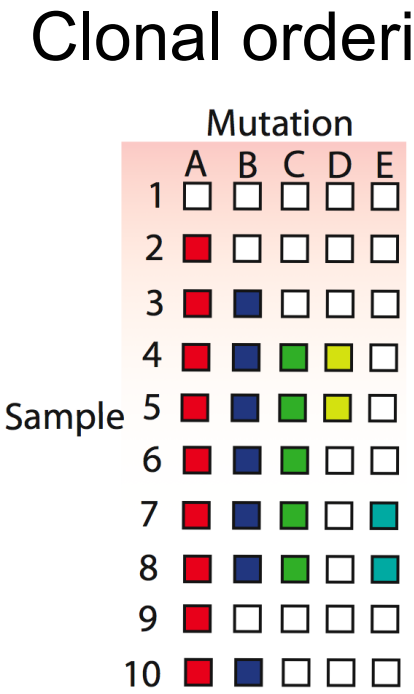

Figure 8: The concept of clonal ordering
Here mutation A must have occurred before mutation B as only a subset of the samples that contained mutation A have mutation B. Mutation B must have arisen before mutation C which preceded mutations D and E. Mutations D and E cannot be ordered due to the fact they appear to arise at the same time.

1.10 Field cancerization:

In 1953 Slaughter et al., proposed the concept of field cancerization in head and neck squamous cell carcinomas (Slaughter et al., 1953). They suggested "a regional carcinogenic activity of some kind, in which a preconditioned epithelium has been activated over an area in which multiple cell groups undergo a process of irreversible change towards cancer". This concept was subsequently modified by (Braakhuis et al., 2003), suggesting that carcinomas and their surrounding histologically normal epithelium share a common genetic alteration, such as, a point mutation, suggesting that field cancerization is due to the proliferation of

clonally related cells with a susceptibility to cancer formation (Braakhuis et al., 2003) This carries an important clinical implication: apparently morphologically normal epithelium surrounding a resection margin may possess genetic abnormalities that when left *in situ*, may result in the recurrence of cancer.

Evidence of field cancerization has been shown in various tissues, such as lung; LOH of chromosome 2q and 12p was seen in non-small cell lung cancer tissue and the surrounding normal bronchial epithelium (Grepmeier et al., 2005). Franklin et al., showed in the bronchial epithelium from the autopsy specimen of a smoker, that the same somactic *TP53* mutation identified from the cancer occurred in multiple sites in both lungs showing squamous metaplasia. A single clone had therefore spread across a long distance, suggesting field cancerization in the lung (Franklin et al., 1997). In the colon; Mutations in *TP53* and *KRAS* found in colitis-associated cancer were also found in surrounding non-dysplastic crypts, suggesting clonality and field concretization (Leedham et al., 2009). Pancreas; Identical *KRAS* mutation was seen in intraductal papillary mucinous tumour and the surrounding normal tissue (Kitago et al., 2004), skin (Hafner et al., 2010) and breast (Deng et al., 1996). Field cancerization might play a significant role in assessing patients who are at risk of developing future carcinomas (Franklin et al., 1997).

1.10.1 Mechanisms of field cancerization in the gastrointestinal tract:

Crypts and glands themselves can divide by fission (Wong et al., 2002) whereby the gland begins to bifurcate from the stem cell zone, splitting the gland into two (Figure 9). This process is repeated and therefore permits the expansion of their progeny giving rise to a patch of clonally related glands. Fission seems to be the primary mechanism by which adenomas expand in familial adenomatous polyposis (FAP) (Wasan et al., 1998). Gland fission also appears to be the primary mechanism by which clones spread in the stomach (McDonald et al., 2008) and colon (Greaves et al., 2006). In Barrett's, Nicholson et al., have shown large patches of CCO-deficient glands sharing the same non-pathogenic mtDNA mutation, suggesting an expansion of a single Barrett's gland by gland fission (Nicholson et al., 2012).

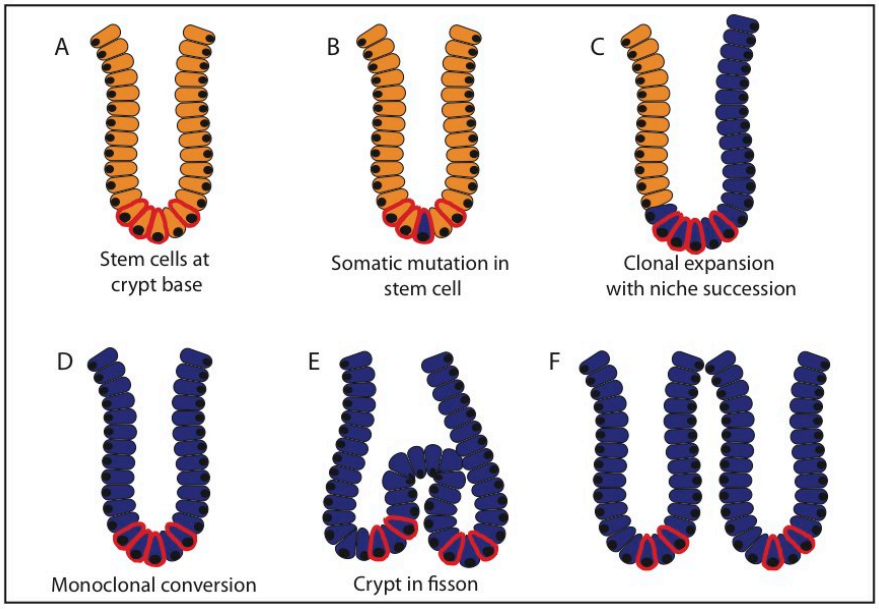

Figure 9: Crypt expansion by niche succession, monoclonal conversion and crypt fission.
Stem cells present at the base of a crypt (A) acquire somatic mutation (B). Mutated cells clonally expand through the entire crypt leading to monoclonal conversion (C, D). Monoclonal crypt then undergoes fission resulting in crypt expansion (E, F). Modified from (Graham et al., 2011b).

Barrett et al., have shown that pre-tumour clones (mutated for *CDKN2A* or *TP53*) can be present throughout large segments (17cm) of Barrett's oesophagus, suggesting that Barrett's is the product of field cancerization, and these clones can be detected 6 years before the development of cancer (Barrett et al., 1999). Further studies have shown genetic alterations in *CDKN2A* and *TP53* are present in premalignant Barrett's, years before the development of OA (Galipeau et al., 1999, Maley et al., 2004b), suggesting that Barrett's metaplasia be defined as a field cancerization. It has been shown that histological clear margins following oesophagectomy for BO-related OA have a better prognosis (Dexter et al., 2001). However, Kim et al., 2006, have shown that KRAS mutation seen in 53% of histologically clear resection margins following pancreatectomy for pancreatic adenocarcinoma had a poorer prognosis compared to *KRAS* -ve resection margins (Kim et al., 2006a). This raises the possibility that neo-Barrett's following oesophagectomy could develop as a consequence of field cancerization effect. At least 10% of gastric carcinoma patients have synchronous or metachronous tumours (Marrano et al., 1987), however, the clonal relationship between these cancers was not established. These studies suggest that field cancerization may be the underlying mechanism of further cancer development, and, therefore, synchronous tumours should have a founder mutation (Galipeau et al., 1999, Maley et al., 2004b). Leedham et al., have shown, in ulcerative colitis, that adenocarcinoma and the adjacent non-dysplastic tissue share the same *TP53* or *KRAS* mutation, suggesting field cancerization in the preneoplastic tissue (Leedham et al., 2009). Recent work in Crohn's disease by Galandiuk et al., has shown that cancers can recur throughout the colon and terminal small bowel over many years, each containing the same founder mutation as its predecessors

(Galandiuk et al., 2012). These observations demonstrate that field cancerization can encompass extensive areas of the colon and also suggests some degree of plasticity in the colon and small bowel. Salk et al., have suggested that identification of pre-tumour clonal expansion in non-dysplastic ulcerative colitis which could be used as a guide to identify patients at risk of developing ulcerative colitis-associated carcinoma (Salk et al., 2009). These clones appear before the development of carcinoma. Hence, characterization of pre-tumour clones in that field of histologically normal epithelium is essential to predict cancer development.

1.11 Neo-Barrett's oesophagus:

Around 50% of patients undergoing oesophagectomy for oesophageal carcinoma (including adenocarcinomas and squamous cell carcinomas) develop post-operative Barrett's oesophagus (Neo-Barrett's) in the remnant oesophagus over a period of 3-5 years (O'Riordan et al., 2004a). During this operation, the remnant oesophagus in joined to the gastric mucosa by the gastric pull-up. Neo-Barrett's specimens are an excellent means to study the genesis of Barrett's oesophagus and these patients undergo an increased frequency of surveillance. This serendipitously provides us with a model that is currently lacking in Barrett'. It is difficult to observe early Barrett's in the general population due to the fact that symptoms may not be present or are ignored by patients. Neo-Barrett's gives us an opportunity to understand how different gland phenotypes evolve following oesophagectomy for OA.

1.11.1 Role of acid reflux and the lower oesophageal sphincter in the development of neo-Barrett's:

Dresner et al., have shown that post-oesophagectomy patients are exposed to increase acid reflux, 35% (14 out of 40) of patients had developed grade I-III oesophagitis (Dresner et al., 2003). In a recent study; 151 patients with OA underwent oesophagectomy, 98 out of 151 underwent fundoplication (wrapping of the remnant stomach around the anastomosis, which mimics lower oesophageal sphincter and reduces acid reflux) and 53 patients did not have this procedure. Post-op follow-up endoscopy revealed neo-Barrett's in 6% of fundoplication group compared to 18% in patients without fundoplication, suggesting the role of acid reflux in the development of neo-Barrett's and lower oesophageal sphincter has some role in reducing the incidence of development of Barrett's (Tsiouris et al., 2011).

1.11.2 The endoscopic appearance of neo-Barrett's oesophagus:

Neo-Barrett's oesophagus is endoscopically identified by the presence of salmon-pink mucosa (similar to Barrett's oesophagus) above the gastro-oesophageal anastomotic line (Figure 10). Neo-Barrett's can present in a circumferential manner or a tongue-like projection at the gastro-oesophageal anastomotic junction. The anastomotic line is generally the only feature that distinguishes Neo-Barrett's from Barrett's.

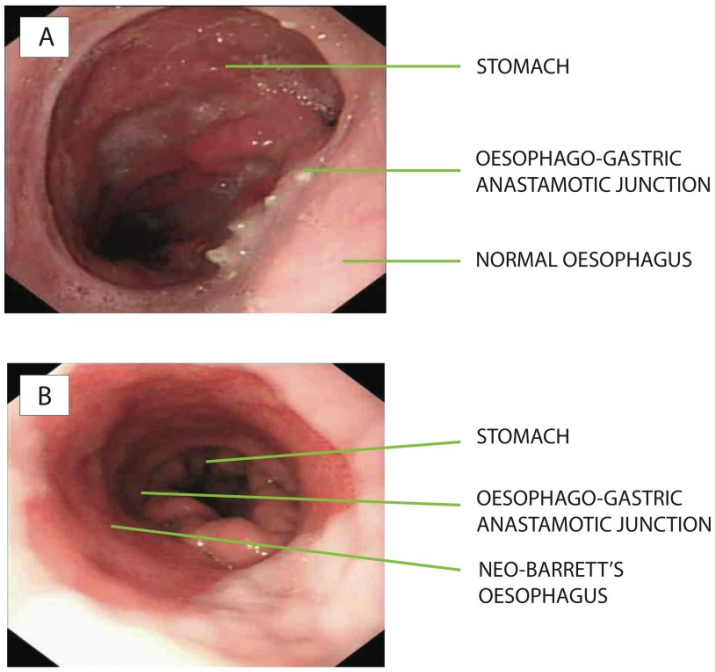

Figure 10: Endoscopic appearance of neo-Barrett's oesophagus.
A) Shows oesophagogastric anastomotic junction following oesophagectomy for OA, and the remaining normal oesophagus is seen above the new OGJ. B) Shows neo-Barrett above the oesophagogastric anastomotic junction (B). (courtesy, Lorna Dunn, Newcastle Royal Infirmary, Newcastle, United Kingdom).

1.11.3 The phenotype of neo-Barrett's glands:

Dresner et al., in their study, have shown that 48% of patients developed columnar metaplasia post-oesophagectomy, approximately half of which displayed gastric cardia-type epithelium and the remainder with IM. Upon follow up those that showed cardia-type epithelium were found to develop IM at a later date, suggesting that gastric cardiac type epithelium appears first following oesophagectomy (Dresner et al., 2003). These observations have also been confirmed by Lord et al., who has shown that the oesophageal epithelium above the anastomosis changes from normal squamous epithelium to cardiac type followed by intestinal metaplasia (Lord et al., 2004). The columnar mucosa of

neo-Barrett's stained for CK7/20 and DAS-1 showed patterns similar to the control group who had Barrett's. The cardiac mucosa was seen to develop within 1-2 years followed by intestinal metaplasia in 3-5 years (Lord et al., 2004, Dresner et al., 2003, O'Riordan et al., 2004a). In 50% of patients with neo-Barrett's, the cardiac mucosa showed Topoisomerase 2alpha protein expression indicating cellular proliferation (Lord et al., 2004).

1.12 Methylation patterns as a molecular clock to measure rates of clonal expansion:

Determining the rate of clonal expansion is difficult within tissues. Whole genome sequencing has the potential to determine this but unfortunately the technology is not sufficiently advanced in order to perform this on individual Barrett's glands from tissue sections. This limits us to temporal but not spatial analysis. The molecular clock theory suggests that the diversity between the genotypes or epigenomes of two cell types reflects the time since their common ancestry; the greater the number of replication errors the greater the number of divisions will have occurred and therefore is a measurement of time (Bromham and Penny, 2003). Gene expression can be regulated by methylation of CpG sites in its promoter. Areas of promoters rich in CpG sites are called CpG islands. At birth all DNA is unmethylated (Bird, 2002) and methylation is acquired over time, and therefore increases with age (Ahuja et al., 1998, Kim and Shibata, 2004, Issa et al., 1994, Issa, 2000). Methylation is inherited during mitosis and methylation error at mitosis is also passed on to a cell's progeny therefore as time and the number

of cell divisions increases, the methylation pattern between two daughter cells becomes dissimilar (Velicescu et al., 2002). Analysing the epigenetic distance within promoters between two cells or glands within a tissue therefore reflects the lineage relationships between them.

This project aims to use methylation patterns of CpG islands in the promoter region of non-expressed genes such as CSX (cardiac-specific homeobox) and MYOD (member of basic-helix-loop-helix family of proteins) as markers of clonal expansion. Since these genes are not expressed, there is no selection for a particular methylation signature. Adjacent glands may share a common ancestry if their parent gland has divided by fission. In the normal human colon this is a rare event (Graham et al., 2011a), though in conditions of inflammation crypt fission is increased (Cheng et al., 1986) & (Wong et al., 2002). Estimating the fission rate requires a marker of clonal expansion that changes over time at a low but measurable rate. This would allow us to estimate the growth and stem cell dynamics within glands that are related. Methylation patterns become diverse with ageing in mitotic tissues such as the colon (Yatabe et al., 2001). Since mitotic errors can mainly be accumulated in the long-term through stem cell lineages, their methylation patterns record ancestry and this can be used to understand stem cell dynamics (Shibata, 2009).

Stem cell diversity can be explained by two different scenarios. The immortal stem cell scenario, where individual Barrett's glands are maintained by a population of immortal stem cells each generating their own progeny therefore stem cell diversity remains the same over time or a niche scenario where stem

cells undergo random loss and replacement from the niche creating a series of bottlenecks where there is a point at which stem cell diversity is minimal and increases over time. Therefore analysis of methylation pattern diversity reflects the point in time since the last bottleneck and we can therefore calculate the stem cell dynamics within glands (Yatabe et al., 2001). Methylation patterns are similar in glands that share a recent common ancestry and more diverse in those with a greater period of time since fission. Unrelated glands will show no similarity in methylation patterns (Figure 11). These techniques can therefore be used for clonal analysis and to study gland dynamics in BO.

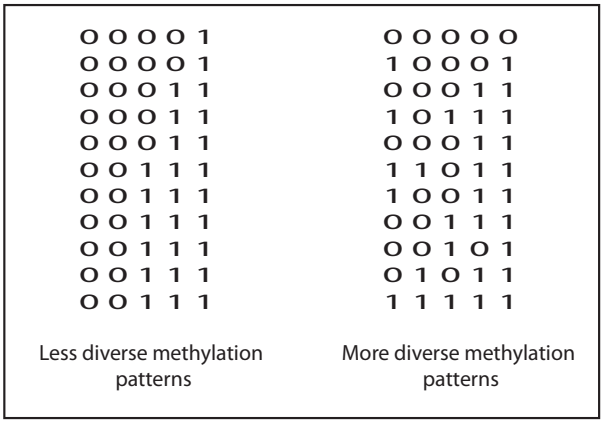

Figure 11: Binary presentation of methylation patterns from Barrett's glands.
11 methylation tags sampled from two different Barrett's glands. Each row represents methylation tags from individual cloned PCR products derived from bisulfite treated DNA extracted from a single Barrett's gland. Each column represents CpG site in a CpG island. Methylated site in a CpG island are designated as '1' and unmethylated site as '0'.

Chapter 2: Materials and methods

Chapter 2: Materials and methods

2.1 Patients and ethics:

Chapter-1: A total of 36 patient specimens (EMRs & oesophagectomies) were initially screened for *CDKN2A* (p16), *TP53* and *KRAS*: 16 patient specimens had identifiable mutations and, were therefore, informative. 10 out of 16 informative patient specimens have been used so far in this project.

Chapter-2: A total of 25 patient oesophagectomy specimens from patients with neo-Barrett's were initially screened for *CDKN2A* (p16), *TP53* and *KRAS*.

Chapter-3 and Chapter-4: Paraffin-embedded and fresh frozen endoscopic mucosal resections (EMR) specimens, were obtained from Leicester University Hospitals, Gloucestershire Hospitals NHS Trust and oesophagectomy blocks from the Royal Victoria Infirmary, Newcastle.

Ethics: Multicentre Ethics approval was obtained from (i) National Research Ethics Service, Stanmore, London (11/LO/1613) and (ii) Oxfordshire Research and Ethics Committee (MREC 07/Q1604/17). Specimens were collected as per UK Home Office regulations.

2.2 Needle macro-dissection:

Specimens were initially screened for genomic DNA mutations in genes, which are known to be mutated in Barrett's adenocarcinoma, namely *CDKN2A* (p16), *TP53* and *KRAS*. The areas of dysplasia/cancer were identified on a haematoxylin and eosin-stained section and traced onto four serial dewaxed and unstained sections. Tissue was macrodissected using a 19 gauge sterile needle and incubated in 30µl Picopure (Applied Biosystems, U.K) at 65^{o}C overnight and then denatured at 95^{o}C for 10 minutes.

2.3 Laser capture microdissection:

2.3.1 Single glands from paraffin sections:

Six-micron serial sections of individual blocks were cut onto P.A.L.M. membrane slides (Zeiss, Munich, Germany). All sections were de-waxed in xylene and rehydrated in decreasing concentrations of ethanol (100%, 95%, 80%, 70% and 50%) and finally washed with distilled water. Sections underwent staining with 2% methylene green staining (Sigma-Aldrich, U.K) to differentiate the epithelium from the surrounding stroma. A serial haematoxylin and eosin stain were performed to act as a guide for microdissection. Individual glands were laser microdissected using a P.A.L.M. laser capture dissection microscope system into 0.5ml adhesive cap tubes (Zeiss, Munich, Germany). Each captured gland was incubated in 14µl of Picopure proteinase K solution (Applied Biosystems, U.K) and subjected to the same temperature conditions as section 2.2.

2.3.2 Single cells and glands from frozen sections:

Twenty-micron serial sections from individually frozen blocks were cut onto P.A.L.M. membrane slides (Zeiss, Munich, Germany). Sections were allowed to air dry at room temperature for 45 minutes. Sections were then either subjected to dual CCO-SDH staining (described in section 2.9). Slides were allowed to dry for 30-45minutes before microdissection. Individual cells from CCO-deficient (blue) and CCO-positive (brown) glands were laser microdissected for identifying point mutations using a P.A.L.M. laser capture dissection microscope system into 0.5ml adhesive cap tubes (Zeiss, Munich, Germany). Each captured cell was incubated in 14µl of Picopure proteinase K solution (Applied Biosystems, U.K) at 65^{o}C for a minimum period of 3 hours and then denatured at 95^{o}C for 10 minutes. In partially CCO-deficient glands, a single cell from CCO-deficient (blue) area was microdissected and then the remaining blue and brown area (CCO-proficient) areas microdissected separately for genomic and methylation analysis.

2.4 Polymerase chain reaction (PCR):

2.4.1 PCR of genomic DNA:

A nested PCR protocol was followed. Briefly, 1µl of DNA was added to a 25µl PCR reaction mixture containing 0.4pmol of first round forward and reverse gene-specific primers (Appendix, Table – 6), $MgCl_2$ (Qiagen, Crawley, UK), 0.2mM of each dNTP (Life Science, Buckinghamshire, U.K), Q solution (Qiagen, Crawley, UK) and 1unit of *Taq* polymerase (Qiagen, Crawley, UK). The precise concentrations of MgCl2 and volumes of Q solution are outlined in Table 8). The first round PCR was prepared in an Omni PCR UV hood (Bioquell, Berkshire, U.K) to reduce

contamination and then subjected to 37 cycles of denaturing, annealing and extension (Appendix, Table 9). 1µl of the first round PCR product was then subjected to a second round of PCR subjected to 37 cycles of denaturing, annealing and extension (Appendix, Table 9). Details of individual primer reactions are again detailed in Appendix, Table 9. To ensure successful amplification, 2nd round PCR products were electrophoresed through a 1.5% agarose gel (Sigma, UK).

2.4.2 PCR of the mitochondrial genome:

The entire mitochondrial genome was amplified into nine 2kb segments by a series of overlapping primers designed to amplify each segment. To achieve sufficient quantities of DNA to sequence, a nested PCR protocol was applied using 36 M13-tailed primers resulting in each 2kb fragment split into four 500bp fragments. Briefly, 1µl of DNA extracted was added to a 25µl PCR reaction mixture containing 0.6µmol of first round forward and reverse gene-specific primers (Appendix, Table 12 and 13), 1mM MgCl2 (Qiagen, Crawley, UK), 0.2mM of each dNTP (Life Science, Buckinghamshire, U.K), and 1.75units of AmpliTaq Gold polymerase (Applied Biosystems, U.K). The first round PCR was prepared in an Omni PCR UV hood (Bioquell, Berkshire, U.K) to reduce contamination and then subjected to 38 cycles of denaturing, annealing and extension. 1µl of first round PCR product was then subjected to the second round of PCR (1.3 units of AmpliTaq Gold is used for 2nd round PCR). Details of individual PCR reactions are again detailed in Appendix, Table 12, and 13). To ensure successful amplification,

2nd round PCR products were electrophoresed through a 1.5% agarose gel (Sigma, UK).

2.5 PCR clean-up (ExoSAP-IT):

The purification of PCR products was performed, by adding 2µl of ExoSAP-IT (USB Corporation, Cleveland, OH) to 5µl of second round PCR product and run on PCR machine at 37^{o}C for 15 minutes followed by 80^{o}C for 15 minutes. The treated products were then diluted with distilled water (10-20µl) depending on the intensity of DNA bands on 1.5% agarose gel.

2.6 Sequencing:

PCR products were subjected to Sanger sequencing. Sequencing reaction conditions are shown in Appendix, Table 10. Each sequencing reaction contained 4µl of diluted exosap-treated PCR product, 1µl of primer (forward or reverse), 5µl of distilled water, and 10µl of Big Dye Terminator (Applied Biosystems, U.K). Genomic primers for *TP53*, CDNK2A and *KRAS* are described in the appendix. Each sequencing reaction was run on an ABI 3100 DNA sequencer (Applied Biosystems, Foster City, California, USA). The sequences obtained were compared with the Catalogue of Somatic Mutations in Cancer (http://www.sanger.ac.uk/genetics/CGP/cosmic) database. Each mutated sample was repeated from the original DNA to confirm mutation. Polymorphisms

were eliminated by comparing their sequence against that held in the Ensembl database (http://www.ensembl.org) and by sequencing normal tissue (muscle). The same protocol was used to sequencing the mitochondrial genome with some adaptions. M13 primer sequences were added to each primer (Appendix, Table 15) permitting universal sequencing. Each sequence output was compared against the revised Cambridge reference sequence (http://www.mitomap.org/MITOMAP/HumanMitoSeq).

2.7 2D mutation/LOH maps:

To understand the clonal architecture and the spatial distribution of different clones in each EMR and oesophagectomy specimen, topographical maps indicating the mutational status or LOH of individual laser captured glands with different phenotypes and genotypes were constructed using a colour code to distinguish separate clones.

2.8 Microsatellite markers and loss of heterozygosity:

Microsatellite markers located on chromosomes 9p (*CDKN2A* - D9S932, D9S942, D9S43, D9S171, D9S1752), 17p (*TP53* - D17S1832, D17S1176, D17S1678, D17S1881), 5q (APC – D5S346, D5S2001, D5S489), 3p (FHIT – D3S1300), and 18q (SMAD4 – D18S58, D18S474F) were selected using the University of California, Santa Cruz database (http://genome.ucsc.edu). The microsatellite loci were amplified by using multiplex PCR kit (Qiagen, Crawley, U.K) and custom-made primers (Applied Biosystems), (Appendix, Table 11). The 5' ends of each of

the primers were tagged with either an FAM (tetrachloro-6-carboxyfluorescin) or HEX (hexachloro-6-carboxyfluorescin) fluorescent marker. The amplified microsatellite markers from metaplastic, dysplastic and cancerous areas were compared with constitutional DNA (muscle) from the same patient and analysed on an ABI 3100 Genetic analyser (Applied Biosystems). Results were analysed using GeneMapper software (Applied Biosystems). For each marker, loss of heterozygosity was considered to be present if the area under one allelic peak was less than 0.5 times or more than two times the area of the corresponding allele in the constitutional DNA. LOH of a single microsatellite marker is not sufficient to confirm clonality since LOH in unrelated cells can occur as a coincidence; hence, LOH of multiple microsatellite markers is a better indicator of clonality. Each sample was repeated from the original extracted DNA.

2.9 Enzyme histochemistry:

Frozen sections were air-dried for 45 minutes and dual CCO and succinate dehydrogenase (SDH, a nuclear-encoded mitochondrial-active enzyme) histochemistry was performed. Sections were first incubated in CCO medium (100mmol/litre cytochrome c, 20mg/ml catalase and 4 mmol/litre diaminobenzidine(DAB) tetrahydrochloride in 0.2 mol/litre phosphate buffer, pH 7.0, all sourced from Sigma-Aldrich, Poole, UK) for 45-60 minutes at 37°C. Crypts with normal CCO activity stain brown, sections were washed three times with PBS for 5 minutes each and CCO-deficient cells were counterstained with SDH (pH of 7.0, 1.5 mmol/L nitroblue tetrazolium in 0.2 mol/L phosphate buffer, 130 mmol/L sodium succinate, 200 mmol/L phenazine methosulfate, and 1 mmol/L

sodium azide, all sourced from Sigma-Aldrich, Poole, UK) for a maximum of 45 minutes at 37°C, or until an intense blue stain had developed in CCO-deficient cells. Sections were washed in PBS for 3x5 minutes and dehydrated in a graded ethanol series (70%, 90%, 100%, 100%). If tissue was for LCMD, sections were further air-dried for 1 hour before being used or stored at -80°C. Single CCO-deficient and normal cells were microdissected and then subjected to PCR sequencing as described earlier (Section 2.5 and 2.6).

2.10 Methylation analysis:

A schematic representation of the methylation analysis performed in this thesis is shown in Figure 12.

2.10.1 Bisulphite treatment of extracted DNA:

EpiTect Plus Bisulphite kits (Qiagen, UK) were used for bisulphite-treating extracted DNA. When sodium bisulphite is applied to DNA, unmethylated cytosines are converted to uracils yet methylated cytosines remain unchanged. Each bisulphite reaction of 140µl consists of DNA (1ng-2ng), RNase-free water (extracted DNA + RNase-free water must total 20µl), Bisulphite mix dissolved (85µl) and DNA protect buffer (35µl). The bisulphite DNA reaction was performed in a thermocycler and the conditions are shown in Appendix, Table 19.

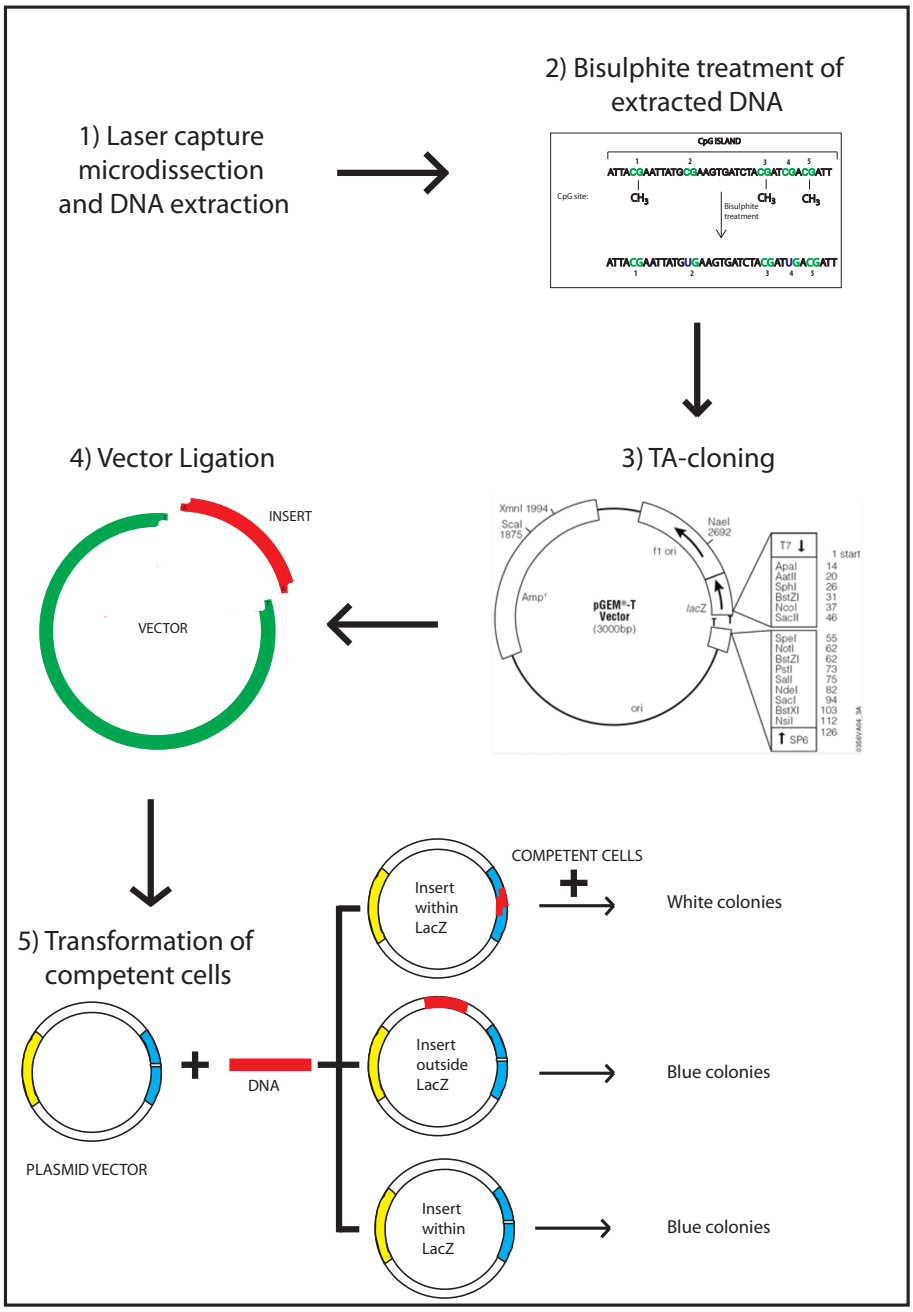

Figure 12: Schematic representation of methodology for methylation analysis:
Barrett's glands were laser-captured microdissected (1) followed by bisulphite treatment of extracted DNA (2), where-in unmethylated cytosines were converted to uracil (Thymidine). Followed by TA-cloning (3), wherein the Taq DNA polymerase adds a 3'-terminal "A" overhang on either end of the PCR product, which helps in cloning of the PCR product and Vector ligation (4). Competent JM109 cells (Promega, UK) were used for transformation of the ligation product (5). Successful cloning was identified by the presence of β-galactosidase negative colonies.

2.10.2 Bisulphite-treated DNA-clean up:

The bisulphite-treated DNA was centrifuged in a EpiTect spin column along with a buffer containing 10µg/ml of carrier RNA followed by wash buffer (provided by the manufacturer) at 12000 rpm for 1 min, and the flow-through was discarded. The desulfonation buffer was added to each spin column and incubated at 56^{o}C for 15 minutes to evaporate any remaining liquid, followed by centrifuge at 1200 rpm for 1 min. 20µl of buffer was added to spin column membrane and spun at 1200rpm for 1 minute to elute the bisulphite converted DNA. The eluate was then stored at -20^{o}C until further use. Bisulphite conversion yields very little DNA due to DNA fragmentation, hence a two-round nested PCR was used to increase the DNA yield. CpG islands of non-expressed genes MYOD1 (Myoblast determination protein 1 on chromosome 11p) and CSX (Cardiac-specific homeobox on chromosome 5q) were amplified. Primers were designed using the Primer 3 website (MIT, Cambridge, Massachusetts, USA) (for primer sequences see Appendices, Table 15 and 16). To ensure successful amplification, 2nd round PCR products were electrophoresed through a 1.5% agarose gel (Sigma, UK). PCR products with uncontaminated negative control underwent cloning.

2.10.3 TA-cloning:

pGEM®-T vector kits (Promega, UK) were used to clone PCR products. The TA-cloning pGEM®-T vector kit consists of linearized cloning vector which has a single 3'-terminal “T” (thymidine) overhangs to prevent recircularization of the vector. The Taq DNA polymerase adds a 3'-terminal “A” overhang on either end

of the PCR product, which permits cloning of the PCR product. The vector also contains a LacZ gene, which permits staining of successful cloning with X-gal (Fermentas, UK).

2.10.4 Vector Ligation:

Each 10µl ligation reaction consisted of 2µl PCR product, 5µl Rapid Ligation Buffer (Promega, UK), 1µl vector, 1µl T4 DNA Ligase and 1µl nuclease-free water. Incubate the reaction at room temperature for 1 hour or overnight at 4^{o}C to increase the yield of ligated vector.

2.10.5 Transformation of competent cells:

Competent JM109 cells (>1 x 108cfu/ mg DNA, Promega, UK) were used for transformation of the ligation product. 2µl of the ligation reaction was treated with 50µl of thawed competent cells in a 1.5ml microcentrifuge tube, and were gently swirled and then placed on ice for 20minutes. Cells were subject to heat-shock for 45s at 42^{o}C followed by placing the tube on ice for 2 minutes. 950µl of SOC medium was added at room temperature and Incubated at 37^{o}C for 90 minutes on a shaker (225rpm). 100ml of transformation product was plated onto LB-agar plate containing ampicillin, X-galactose and Isopropyl β-D-1-thiogalactopyranoside (IPTG) (Sigma, UK). Plates were incubated overnight at 37^{o}C. Cloning of PCR products into the vector interrupts the coding sequence of β-galactosidase and the successful colonies appear as white colonies and unsuccessful cloning results in blue colonies. 10-12 white colonies were picked and PCR amplified using M13 primers. To ensure successful amplification, PCR

products were electrophoresed through a 1.5% agarose gel (Sigma, UK). PCR reaction clean-up and sequencing using M13 primers (forward or reverse) was performed as explained earlier (Section 2.5 and 2.6, Appendices, Table 15). PCR products were subjected to Sanger sequencing reaction. The sequencing reaction conditions are shown in Appendix, Table 15. The colony sequence was compared against the standard CSX and MYOD sequence.

2.11 Statistical analysis of methylation patterns:

The pattern of methylated and unmethylated sites in non-expressed genes was analysed according to Yatabe and colleagues methodology (Yatabe et al., 2001). The methylation patterns observed in one CpG island/at a single locus is called a tag. To analyse methylation patterns within each gland/clone and to compare them with the adjacent gland/clone the following statistical parameters were used.

2.11.1 Number of unique tags:

Methylation patterns obtained from a single clony PCR were called tags and the number of different tags observed within a gland/clone were called as unique tags.

2.11.2 Percentage methylation (PM):

The average number of methylated CpG sites in one CpG island/single locus for colonies picked from single gland/clone.

2.11.3 Intragland or Intra-clone diversity (acd):

It is the average difference between the number of methylation tags within a gland/clone, which measures the epigenetic diversity within a gland/clone. For example, the distance between methylation pattern 1-0-0-1-1 (reflecting 6 CpG positions) and 0-0-0-0-1 is two, due to the difference in the CpG methylation site at position 1 and position 4.

2.11.4 Intergland or Inter-clone diversity (icd):

The average number of pair-wise methylation tag differences between two adjacent glands/clones.

2.11.5 Correlation between epigenetic and spatial distance:

The physical distance between glands was measured by expressing the distance in units. One unit corresponds to one average gland diameter (most glands in the given specimen were measured, averaged over at least 40 - 50 glands, all glands were measured in specimens where only a few glands were present). The epigenetic distance (icd) between adjacent and distant glands was then compared with spatial distance.

2.11.6 Statistical tests used:

1. Mann-Whitney U-test: In each descriptive statistic, the non-parametric Mann-

Whitney U-test was used to determine significance.

2. Kruskal-Wallis one-way analysis of variance: This test was used to determine the percentage of Ki67+ cells expression with-in neo-BO (Chapter 5).

3. ANOVA test: To calculate statistical significance between the number of unique tags and percentage methylation between individual patients specimen for CSX and MYOD gene (Chapter 6).

4. Spearman correlation: To calculate the correlation between the percent methylation and patient age (Chapter 6).

To analyse methylation patterns within each crypt/clone and to compare them with the adjacent crypt/clone the following statistical parameters were used.
Where $k = 1, \ldots$ M CpG sites, N is number of sequences analysed within that crypt at locus l (CSX or MYOD) in the tag j and M is number of CpG sites at locus l.
$S^l jk = 0$ denoted un-methylated site and $S^l jk = 0$ denoted methylated site.

Intra-crypt or Intra-clone diversity (A):

$$A = \frac{1}{N(N-1)} \sum_{i=1}^{N} \sum_{j=i+1}^{N} \sum_{k=1}^{M} \left| S_{ik}^{l} - S_{jk}^{l} \right|$$

Inter-crypt or Inter-clone diversity (I):

$$I = \frac{1}{N_1 N_2} \sum_{i=1}^{N_1} \sum_{j=1}^{N_2} \sum_{k=1}^{M} \left| S_{ik}^{l} - C_{jk}^{l} \right|$$

$S^l jk$ and $C^l jk$ represents methylation tags, whereas, N_1 and N_2 represents number of tags analysed and from two different crypts/clones.

2.12 Immunohistochemistry:

Sections from EMRs and oesophagectomy specimens were cut at 6mm thickness and used to study p53, Ki67, MUC2, MUC5AC, MUC6, TFF1 and TFF2 staining. Sections were dewaxed, rehydrated using decreasing dilutions of alcohol and endogenous peroxidase was blocked using 3% hydrogen peroxide in methanol for 10 minutes. Antigen retrieval was achieved by microwaving slides in 1M citrate buffer (pH6.0) for 10 minutes. Slides were incubated in rabbit serum for 15 minutes, followed by incubation in a primary antibody 1 hour, then washed 3x5 mins in PBS. The sections were then incubated with secondary antibody (shown in Table 1) for 35 minutes followed by a tertiary layer of 1:500 dilution of peroxidase-conjugated streptavidin (strep-HRP; DAKO). The slides were washed with PBS 3 times for 5 minutes each in between all three layers. Sections were then treated with 3-diaminobenzidine-tetra-hydrochloride solution (DAB; Sigma, Poole, UK) for 2-5 minutes followed by washing in phosphate buffered saline (PBS) for 5 minutes. The slides were then counterstained with light haematoxylin, dehydrated through increasing concentrations of ethanol, cleared in xylene and mounted in DPX (mixture of distyrene, a plasticizer, and xylene). The negative control slide also underwent all the steps except that incubation with primary antibody layer was replaced by incubation in PBS. Details of the protocol are shown in Table 1 below.

Antibody	Concentration	Species	Secondary Antibody	Source
p53	1:300	mouse	Rabbit anti mouse biotin	DAKO
Ki67	1:4000	Rabbit	Swine anti rabbit biotin	Epitomics 3025-1
MUC2	1:500	mouse	Horse anti mouse biotin	Leica Biosystems
MUC6	1:100	mouse	Horse anti mouse biotin	Leica Biosystems
MUC5AC	1:100	mouse	Horse anti mouse biotin	Leica Biosystems
TFF1	1:400	mouse	Horse anti mouse biotin	Abcam
TFF2	1:400	mouse	Horse anti mouse biotin	Leica Biosystems

Table 1: Antibody details for immunohistochemistry protocol for p53, Ki76, MUC2, MUC6, MUC5AC, TFF1 and TFF2 antibodies.

Chapter 3: Genetic evolution of Barrett's oesophagus to oesophageal adenocarcinoma

Chapter 3: Genetic evolution of Barrett's oesophagus to oesophageal adenocarcinoma

3.1 Introduction:

Intial studies into the genetic basis of Barrett's oesophagus (BO) proposed that BO is a clonal lesion from which a carcinoma can arise. However, recent work has indicated that there are multiple independent clones present; therefore, Barrett's appears to be a genetically heterotypic disease. Furthermore, genetic diversity increases the risk of cancer progression possibly as a result of clonal competition or interference (Maley et al., 2006) yet there have been no studies examining the spatial distribution within Barrett's. Here I examine genetic diversity in Barrett's metaplasia, dysplasia and carcinoma by combining gland-by-gland mutation analysis with mapping onto tissue sections in an attempt to show evolution to cancer.

To understand the evolutionary pathway leading to carcinoma development, several studies have tried to reconstruct phylogenetic trees within human breast (Navin and Hicks 2010) and renal (Gerlinger, Rowan et al. 2012) carcinomas. Genetic heterogeneity is seen in various stages of cancer progression (Marusyk et al., 2012). Navin et al., 1996, have shown that cancers can be either monogenomic (a single clone) or polygenomic (multiple independent clones). This raises an important question as to how cancers develop in polyclonal diseases. Thirlwell et al., have also identified multiple independent clones (as determined by the presence of crypts with distinct APC mutations) in FAP and some sporadic colonic

adenomas (Thirlwell, et al. 2010). These data suggest that glandular dysplasias in the gastrointestinal tract are polyclonal and that we perhaps have to rethink how dysplasia develops.

In BO, little is known about the spatial distribution of clones. The Reid group in Seattle have demonstrated the widespread expansion of *CDNK2A* (p16) and *TP53* mutations in flow-purified whole biopsy specimens and proposed that BO develops as a clonal lesion and each additional mutation undergoes a selective sweep through the lesion and becomes fixed i.e., no wild type glands perisist (Maley et al., 2004a). However Leedham et al., (2008) proposed that Barrett's progresses to cancer in a polyclonal fashion suggesting there are no founder mutations and not all mutations will become fixed and demonstrated this by sequencing *CDKN2A* and *TP53* mutations in individual Barrett's glands. This suggests that Barrett's adenocarcinoma may develop from interactions between independent clones – as suggested by the clonal interference model subsequently developed by Martens,et al., (2011). The polyclonal theory would readily explain why genetic diversity is present in oesophageal cancers (Merlo et al., 2006). Ross-Innes et al., (2015) have shown by whole genome sequencing that dysplasia exhibits multiple dysplastic clones but were not able to map these mutations onto tissue sections (Ross-Innes et al., 2015). While the work in this chapter was performed before the publication of whole genome sequencing studies, it set out to determine the relationship between polyclonal dysplasias and carcinomas, furthermore we do not know the geographical distribution of mutated glands within dysplasia. This will provide important information on how diversity is generated and how clones mix through the lesion.

3.2 Hypothesis:

The Barrett's metaplasia-dysplasia-carcinoma sequence (MDC) is characterised by the presence of multiple genetically diverse and spatially distributed clones but only one clone progresses to cancer.

3.3 Aims:

1) To analyse individual gland clonal architecture of lesions representing the progression of Barrett's oesophagus to oesophageal adenocarcinoma and to infer the timing of significant mutations during the metaplasia-dysplasia-carcinoma sequence.

2) To study, on a gland-by-gland basis in resected material showing all stages of the MDC, the relationship of genetic diversity with progression towards OA.

3) To map clones onto Barrett's tissue sections to visualize clonal mixing in EMR specimens.

3.4 Methods:

DNA was macro-dissected (for details, refer chapter-2. Methods-2.2) from the dysplastic regions of EMR specimens and then screened for mutations in the variable regions of p16INK4A, *TP53* and *KRAS* genes. EMRs & Oesophagectomy specimens with an identified mutation were then serially sectioned, and glands were histologically graded and then microdissected using a P.A.L.M. laser capture microscope (chapters 2.3 and 2.4). Glands were then sequenced (for sequencing details, see chapter 2.6) for the point mutation identified in the initial screen. Maps indicating the mutation burden of each gland were constructed. Multiplex PCR was performed with a panel of microsatellite markers located within *TP53* (17q) SMAD4 (18q) and *CDKN2A* gene. For each marker, loss of heterozygosity was considered to be present if the area under one allelic peak was less than 0.5 times or more than two times the area of the corresponding allele in the constitutional DNA. Results were analysed using GeneMapper software (Applied Biosystems).

3.5 Results:

3.5.1 Initial mutation screening of EMR results:

Areas of dysplasia/cancer were identified on a haematoxylin and eosin-stained section by two pathologists, and these areas were further traced onto four serial dewaxed and unstained sections. 36 EMRs/oesophagectomy specimens were macrodissected and screened for somatic gene mutations in commonly mutated genes in OA, i.e., *TP53*, *CDKN2A* and *KRAS*. 16 out of 36 specimens had identifiable mutations, 10 out of 16 informative samples have been used in this project. The mutation screening results of these ten samples are shown in Table 2 below.

EMRs/ Oesophagecto-my specimens	***TP53* - Exon5 mutation**	***TP53* - Exon6 mutation**	***TP53* - Exon7 mutation**	***TP53* - Exon8 mutation**	***CDKN2A* - (p16) mutation**	***KRAS* - mutation**
1	**c.473G>A**	WT	WT	WT	WT	WT
2	WT	WT	**c.722C>T**	WT	WT	WT
3	WT	WT		WT	**c.329G>A**	WT
4	WT	WT	WT	**c.814G>A**	WT	WT
5	**c.524G>A**	WT	WT	WT	WT	**c.35G>A**
6	**c.487T>C**	WT	WT	WT	WT	WT
7	**c.451C>T**	WT	WT	WT	WT	WT
8	WT	WT	**c.743G>A**	WT	WT	WT
9	WT	WT	WT	WT	**c.238C>T**	WT
10	WT	WT	WT	WT	**c.382C>T c.409A>G c.442G>A**	WT

Table 2: Initial screen results of specimens, which had identifiable mutations in *TP53*, *CDKN2A* and *KRAS* genes.

3.5.2 Evolution of polyclonal Barrett's to monoclonal oesophageal adenocarcinoma:

To determine the clonal evolution in my cohort of 10 EMRs and oesophagectomies, I laser-capture microdissected multiple glands from each specimen and individually sequenced them for the mutations identified in Table 2 and the results are shown in Table 3. I performed LOH analysis on each gland (also shown on Table 3). I then mapped the genotype onto an H&E of each specimen using a colour code to distinguish gland genotypes and served to delineate a clonal order of evolution with spatial resolution.

Four specimens (patient 1, 2, 5, and 10) displayed more than one clone in metaplasia and dysplasia (polyclonal), three specimens (patient 4, 6, and 9) showed monoclonal evolution of OA and two specimens (patient 7 and 8) only had dysplasia which was monoclonal. All identified adenocarcinomas were monoclonal regardless of the clonal status of the metaplasia and dysplasia. Patient 3 did not show any dysplasia or cancer and therefore we can only state that clones of mixed genotype were present and cannot infer clonal ordering based on tissue phenotype.

EMRs/OESO-PHAGECTOMY	METAPLASTIC GLANDS	DYSPLASTIC GLANDS	CANCER
1	30/31 (97%) – *TP53* WT 1/31 (3%) – *TP53* mutant (c.473G>A)	18/62 (29% - *TP53* WT 44/62 (71%) – *TP53* mutant (c.473G>A)	8/8 (100%) Monoclonal for *TP53* mutant (c.473G>A)
2	9/11(82%) – *TP53* WT 2/11(18%) – *TP53* mutant (c.722C>T) 4/8 (50%) - *TP53* LOH	3/28(11%) – *TP53* WT 25/28(89%) – *TP53* mutant (c.722C>T) 17/18 (95%) - *TP53* LOH	4/4 (100%) Monoclonal for *TP53* mutant (c.722C>T) and *TP53* LOH
3	1/18 (6%) – WT for *CDKN2A* 17/18 (94%) – *CDKN2A* mutant (c.329G>A) 16/18 (89%) - *CDKN2A* LOH	None present	None present
4	2/8 (75%) – WT 6/8 (25%) – mutated for *TP53* (c.487T>C)	10/10 (100%) - mutated for *TP53* (c.487T>C)	30/30 (100%) - mutated for *TP53* (c.487T>C)
5	9/9(100%) – *TP53* and *KRAS* WT 2/9 (22%) – *TP53* LOH	1/14 (7%) – WT 4/14(29%) – *TP53* Mutant (c.524G>A) 9/14(64%) – *TP53* (c.524G>A) and *KRAS* (c.35G>A) Mutant 8/8 (100%) - *TP53* LOH	10/10 (100%) Monoclonal for *TP53* (c.524G>A) and *KRAS* (c.35G>A) and *TP53* LOH
6	7/7 (100%) WT for *TP53* (c.743G>A)	None present	4/4 (100%) mutated for *TP53* (c.743G>A)
7	None present	7/7 (100%) mutant for *TP53* (c.451C>T)	None present
8	None present	3/29(10%) – WT for *TP53* 26/29 (90%) *TP53* mutant (c.814G>A) 11/13 (85%) - *TP53* LOH	None present
9	None present	5/5 (100%) - mutated for *CDKN2A* (c.238C>T)	5/5 (100%) mutated for *CDKN2A* (c.238C>T)
10	*CDKN2A* mutant Clone-1: c.382C>T	*CDKN2A* mutant: Clone-1: c.442G>A Clone-2: c.442G>A and c.382C>T Clone-3: c.409A>G	8/8 (100%) Monoclonal for *CDKN2A* mutant, c.442G>A)

Table 3: The distribution of genotype in 4 EMRs and 6 oesophagectomy specimens.
Data is expressed as the number and percentage of mutant glands compared with wild type along with LOH analysis (patient 2, 3, 5, and 8). Two or more clones in pre-neoplastic Barrett's lesion (specimens 1,2,5, and 10) and only one clone was detected in each oesophageal carcinoma. WT=wild type.

The results of the individual specimens clonal analysis are now described. Genotypic analysis of metaplasia from patient 1 showed the presence of *TP53* WT glands (30/31 laser captured glands) and a single mutated c.473G>A metaplastic gland (Figure 13). Both these clones were also seen in dysplasia from the same patient (Figure 14). Because the *TP53* mutation was detected in metaplasia, the presence of wild type and mutated dysplasia must suggest a polyclonal dysplasia. It is interesting that the two different clones were geographically mixed within the dysplasia, suggesting that the rates of clonal expansion were similar. Spatially distinct areas from the patient's cancer were also laser captured (eight areas in total). All areas of cancer had the same *TP53* mutation detected in the metaplasia and dysplasia. No *TP53* wild type areas were detected and all areas were positive for the c.473G>A mutation (Figure 15). This suggests that the *TP53* mutant clone outcompeted the wild type (in so far that it did not express the *TP53* mutation) clone to cancer.

Areas of metaplasia in the sections from patient 2 showed at least three clones; *TP53* WT (9/11 glands), *TP53* mutated c.722C>T (2/11 glands) and *TP53* mutated with LOH (4 out of 8) (Figure 16). All three clones were also identified in dysplasia (Figure 17) from the same patient suggesting that multiple metaplastic clones have formed dysplasia independently. All areas of the neighbouring cancer showed only one clone (*TP53* mutated with LOH, Figure 17). The genetic diversity seen in metaplasia and dysplasia was not seen in OA, suggesting cancer from this patient was monoclonal, whereas, metaplasia and dysplasia were polyclonal.

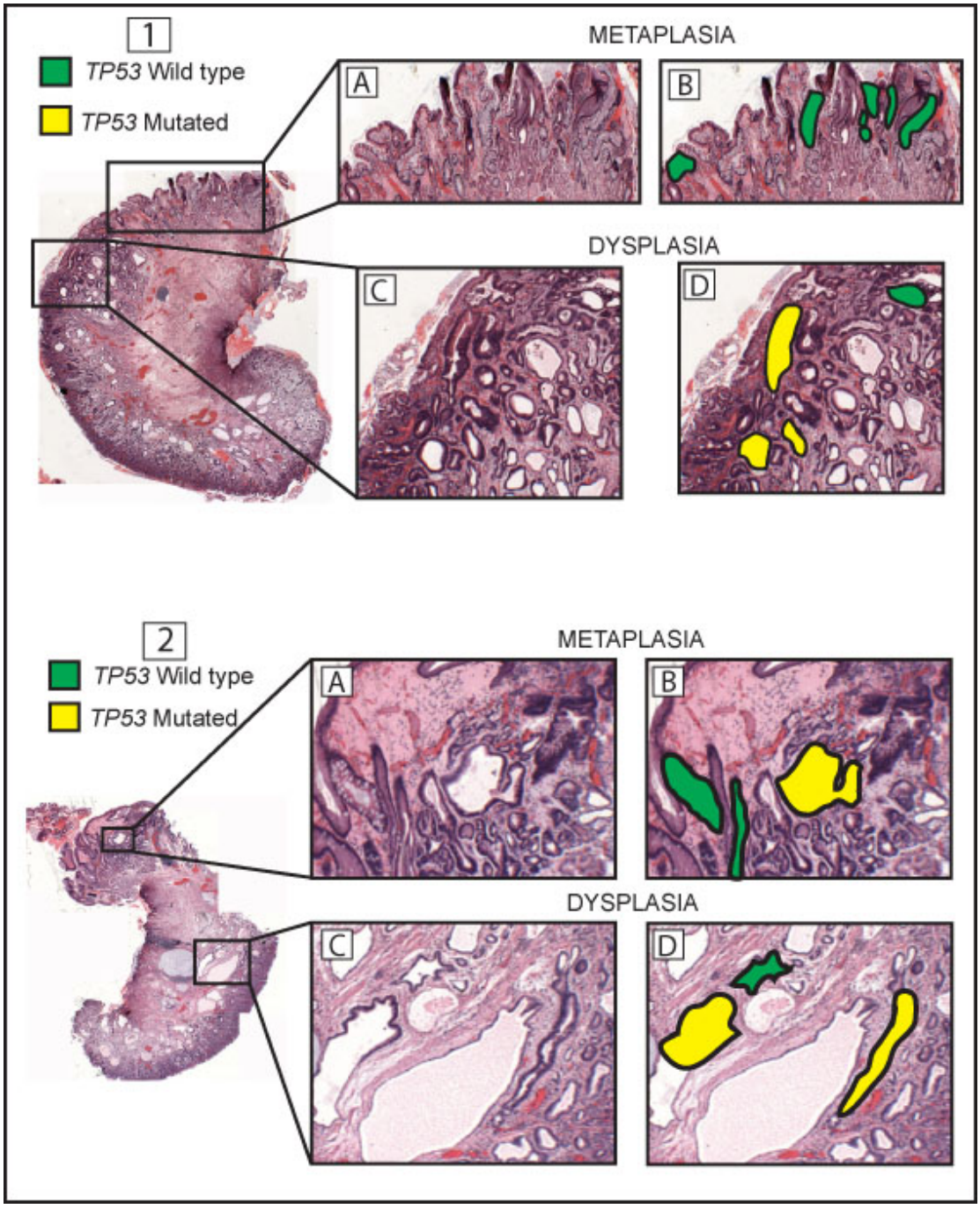

Figure 13: Spatial distribution of different phenotypes and genotypes in two separate sections from patient 1.
(1) & (2) are H&E slides from 2 separate tissues (patient 1), show enlarged areas of metaplasia (A) and dysplasia (C). Mutational status of individual glands, indicating heterogeneity in Barrett's metaplasia and dysplasia (B and D respectively). Wild type glands are coloured green, mutated (*TP53* c.473G>A) glands are stained yellow respectively.

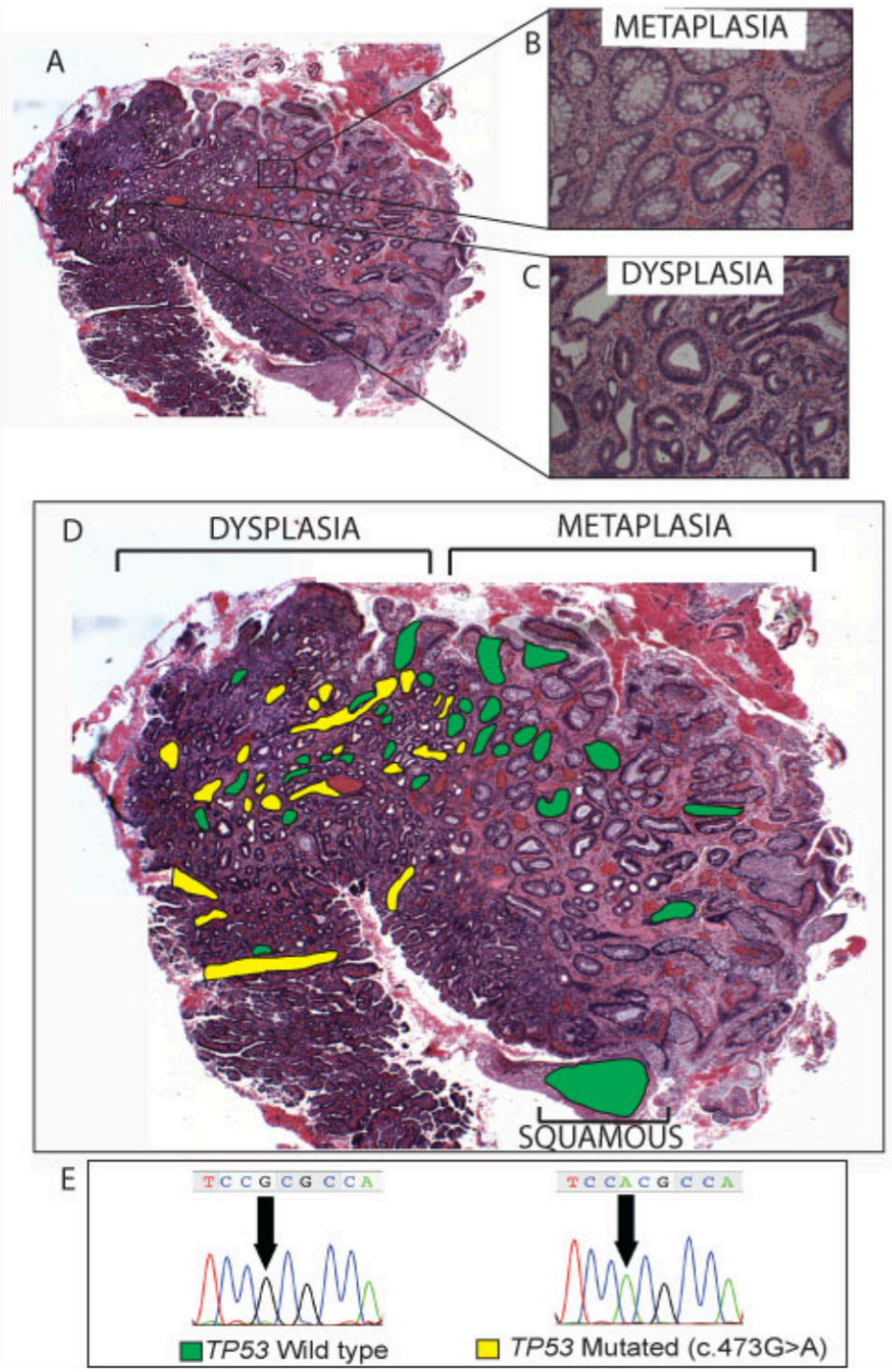

Figure 14: Spatial distribution of metaplastic and dysplastic gland genotypes in the second EMR specimen from patient 1.
(A) H&E of the EMR from patient 1 with high powered images of metaplastic glands (B) and dysplastic glands (C). The mutational status of individual glands (TP53 mutated = yellow, WT=green) (D). Sanger sequencing tracing demonstrating the *TP53* c.473G>A muations (E). Overall most dysplastic glands were clonal for the TP53 mutation identified in the metaplasia, however some were also WT suggesting a polycloncal origin of the dysplasia.

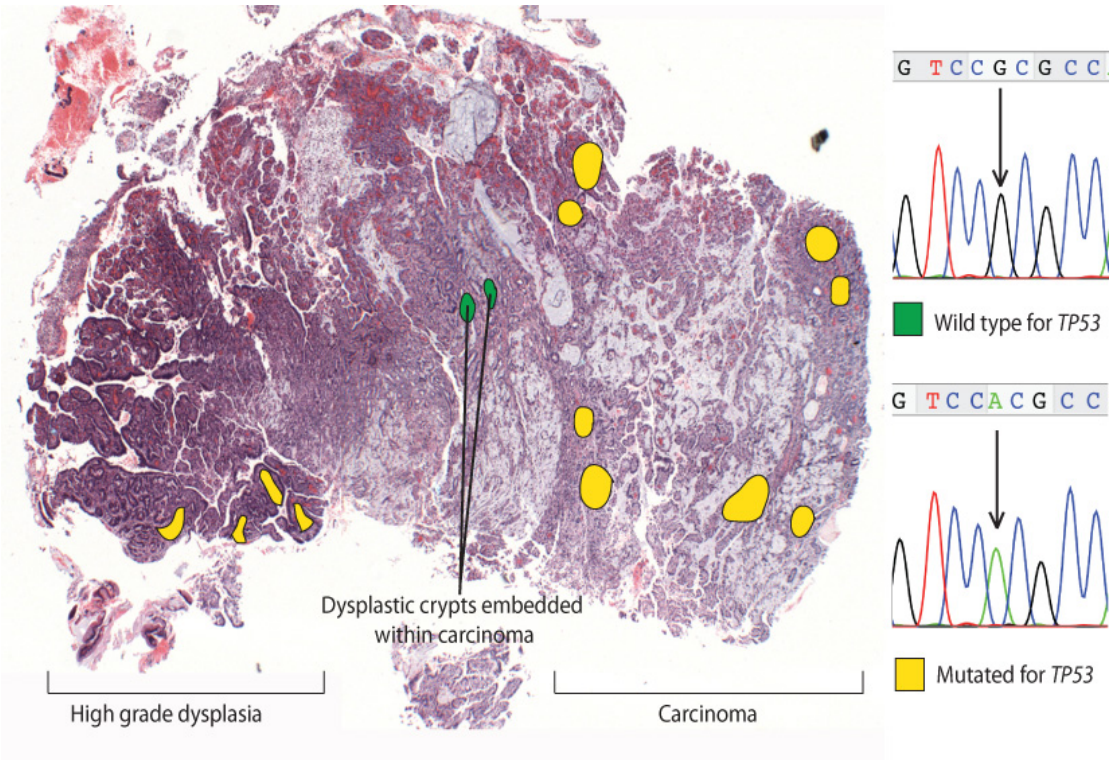

Figure 15: Adenocarcinoma from patient 1 is monoclonal.
In a separate section from patient1, there is identifiable dysplasia and adenocarcinoma present. The genotype of each microdissected gland has been shown. Wild-type glands are coloured green, mutated (*TP53* c.473G>A) glands are coloured yellow. Barrett's adenocarcinoma from the same patient seems to be monoclonal for the same mutation identified in the dysplasia.

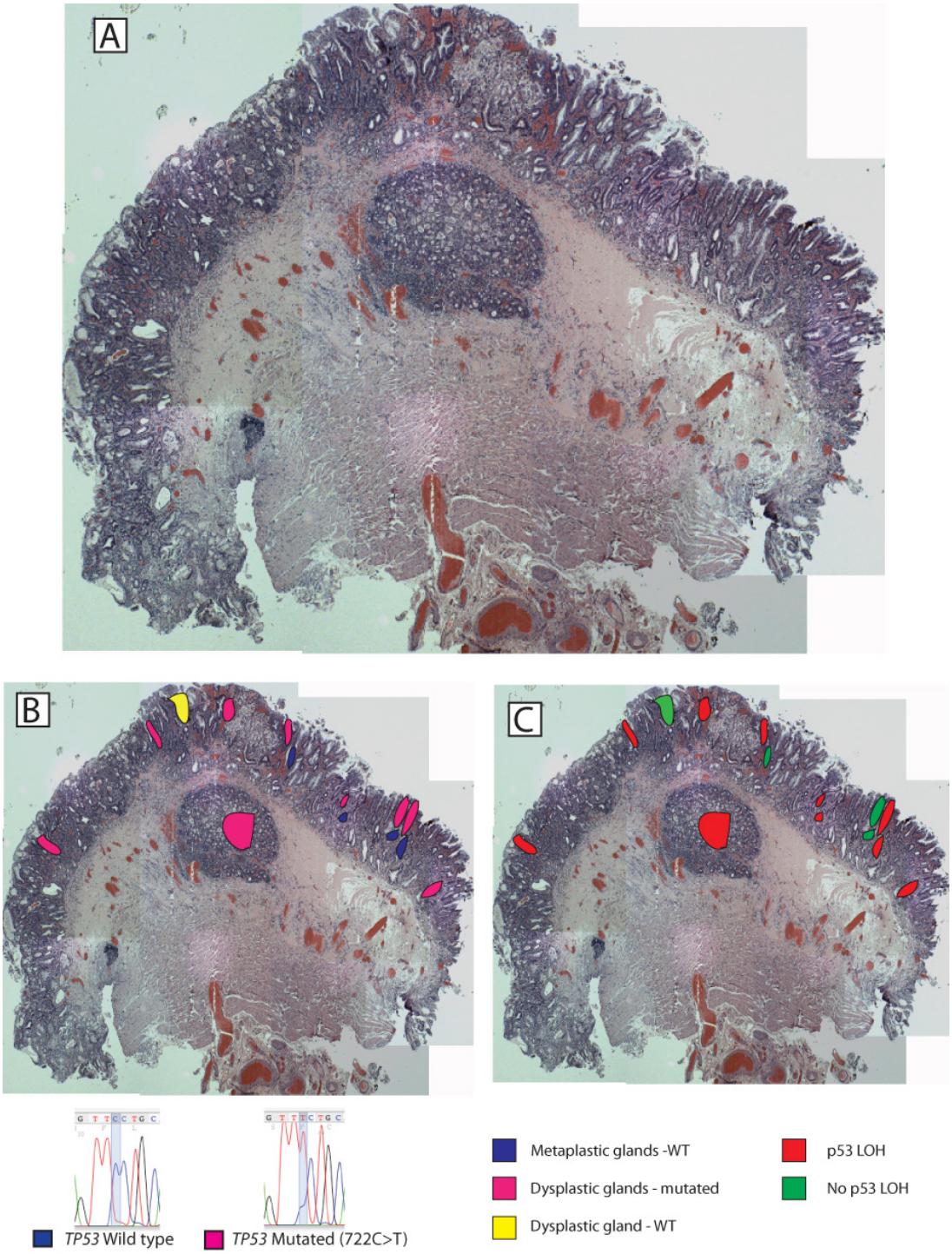

Figure 16: Topographical map illustrating spatial distribution of different gland phenotypes and genotypes from patient 2 with Barrett's high grade dysplasia.

H&E micrograph of the EMR from patient 2 illustrating different phenotypes (A). The spatial distribution of metaplastic glands that are wild type (blue) and one wild type dysplastic gland (yellow) or mutated (pink) for *TP53* (722C>T) (B). Microdissected individual glands with LOH (red) and glands without LOH (green).

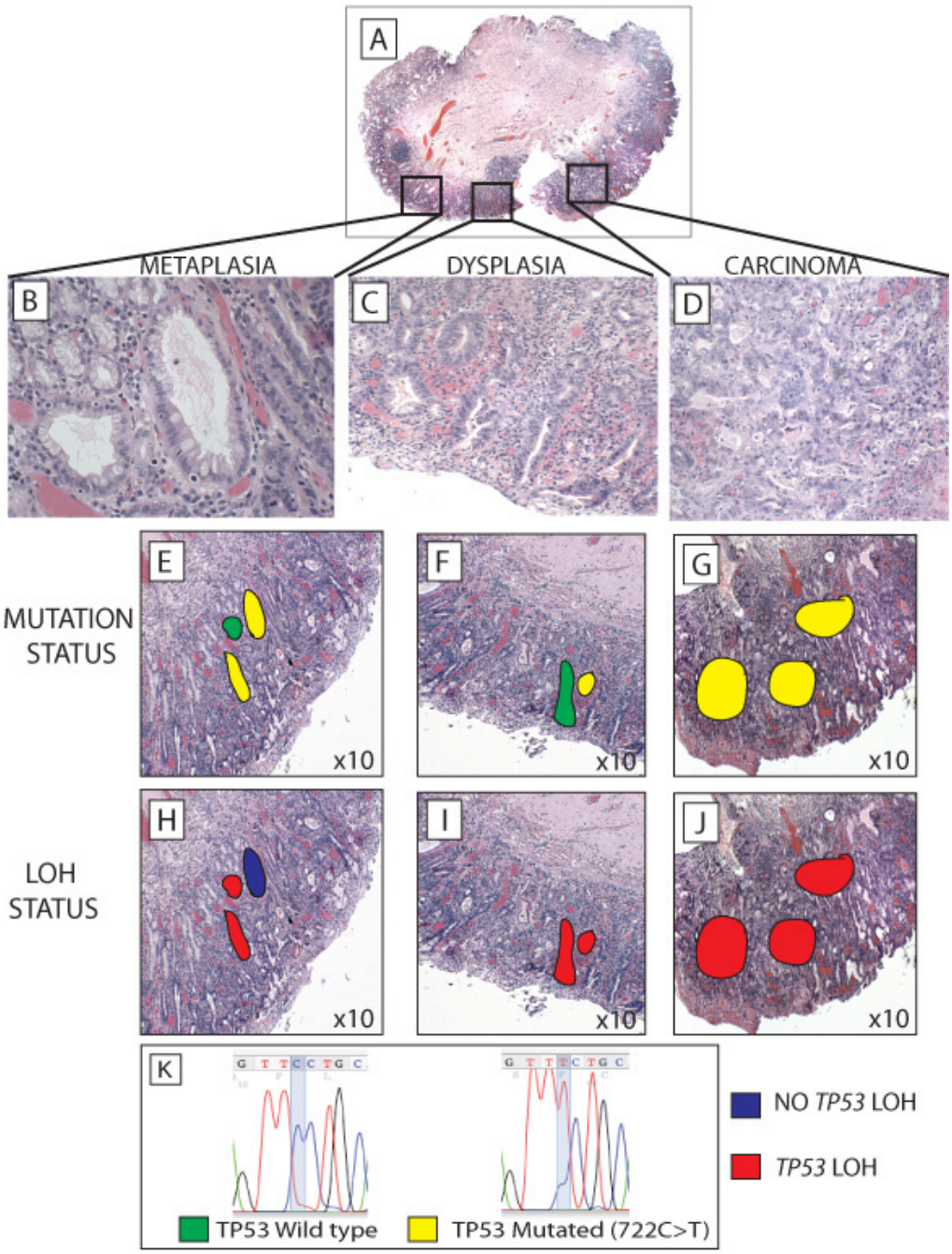

Figure 17: 2-dimensional map illustrating spatial distribution of mutant glands in dysplasia and metaplasia from patient 2.
H&E of an EMR with Barrett's high-grade dysplasia (A). Magnified images of Barrett's metaplasia, dysplasia and carcinoma (B, C and D respectively). The majority of glands were mutated for *TP53* (722C>T), some metaplastic and dysplastic glands were wild type for *TP53* (E and F respectively) suggesting polyclonality. The carcinoma was monoclonal for *TP53* (722C>T) (G). Most metaplastic and dysplastic gland showed LOH for *TP53* at two microsatellite markers (D17S1176 and D17S1881) (Red, H, I and J), All areas of the carcinoma showed LOH for *TP53* (J). The wild type and mutated *TP53* sequencing has been shown in (K).

Metaplasia specimen from patient 5 showed at least 2 clones. Most metaplastic glands were *TP53* WT (7/9) however a minority showed *TP53* LOH (2/9). Dysplastic areas from patient 5 also showed the presence of two clones. A single glands was *TP53* WT (1/14), a proportion of dysplastic glands were mutated for *TP53* (4 /14, c.524G>A) but the remained also expressed a *KRAS* mutation (9/14, c.35 G>A) mutation. All mutated glands displayed *TP53* LOH. This suggests that both clones identified in the metaplasia progressed to dysplasia and the *TP53* LOH clone acquired additional *TP53* and *KRAS* mutations with time. All 8 areas of the cancer section were also mutated for *TP53* & *KRAS* mutation with *TP53* LOH (Figure 18), suggesting that dysplasia was polyclonal but the cancer was monoclonal.

Patient 10 was first identified by Leedham et al., (2008) who found one clone in metaplasia Clone-1: *CDKN2A* mutant c.382C>T) and three clones in dysplasia (Clone-1: c.442G>A Clone-2: c.442G>A and c.382C>T, Clone-3: c.409A>G). My work involved screening the cancer specimen from the same patient. Eight out of 8 cancer areas were monoclonal for *CDKN2A* mutant, c.442G>A. (Figure 19).

These observations show genetic diversity within Barrett's metaplasia and dysplasia and suggest that Barrett's is a polyclonal lesion. However, Barrett's-related oesophageal adenocarcinoma is monoclonal.

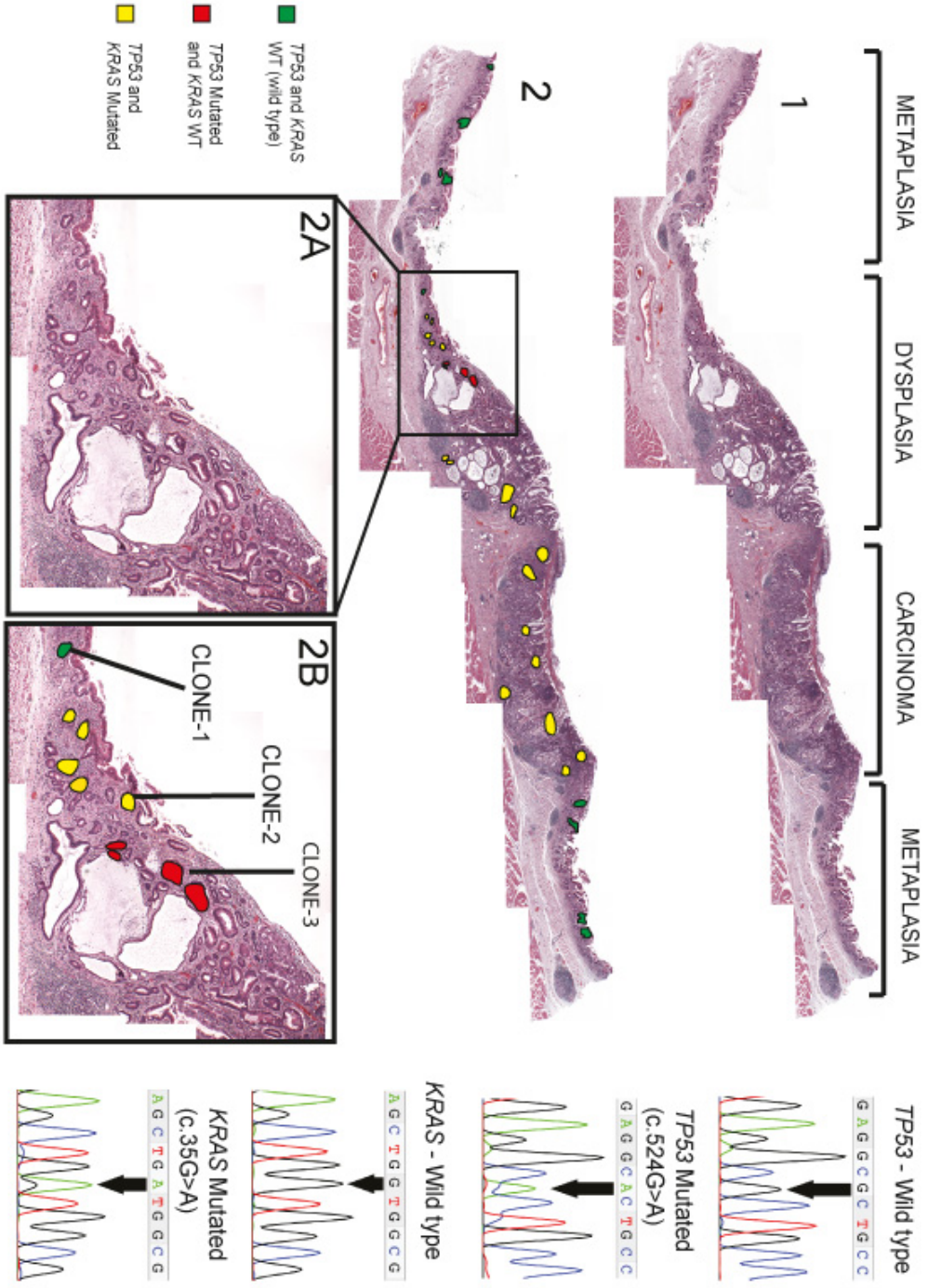

Figure 18: Monoclonal outgrowth of Barrett's oesophageal carcinoma from polyclonal dysplasia from patient 5.

H&E of from the EMR from patient 5 showing different gland phenotypes (1). Distinct clones were identified by colour (WT=green, TP53 mutant= red, TP53/KRAS= Yellow) (2). Dysplasia (2A) displayed two independent clones (2B) whereas the carcinoma (middle right) was a monoclonal (*TP53* & *KRAS* mutated).

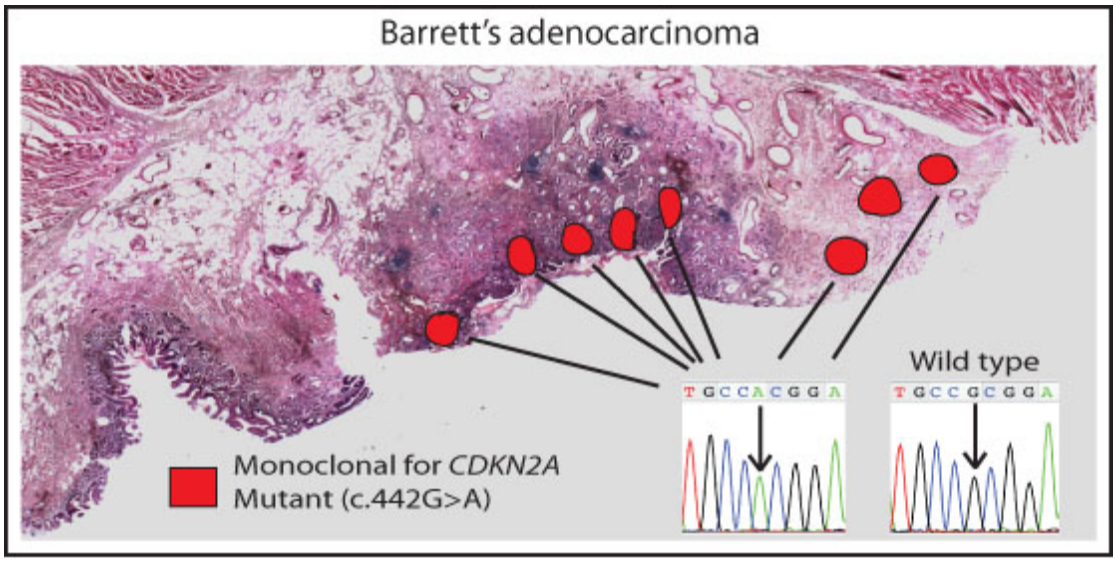

Figure 19: A monoclonal outgrowth of Barrett's oesophageal carcinoma from polyclonal dysplasia from patient 10.
Dysplasia specimen from patient 10 had more than two clones, however, multiple areas laser captured from cancer area were mutated for *CDKN2A* mutation (c.442G>A), suggesting monoclonal Barrett's adenocarcinoma from polyclonal dysplasia.

3.5.3 Evolution of monoclonal Barrett's to oesophageal adenocarcinoma:

Three specimens (patient 4, 6, and 9) showed monoclonal evolution of OA and two specimens (patient 7 and 8) only had dysplasia which was monoclonal. In patient 4, the EMR displayed metaplasia, dysplasia and carcinoma. Individual glands were laser-captured and the sequenced for *TP53* mutation. Four out of eight metaplastic glands were WT and remaining four metaplastic glands were mutated for *TP53* (c.487T>C) (Figure 20), suggesting at least two clones in metaplasia. Ten out of ten dysplastic glands were mutated for *TP53* (c.487T>C), suggesting that only mutated clone progressed to dysplasia (Figure 21). Thirty small areas of cancer were laser-captured to check heterogeneity in cancer. However, all 30 laser-captured areas were mutated for *TP53* (c.487T>C, see

Figure 22), suggesting monoclonal cancer and *TP53* mutated clone progressed from metaplasia, dysplasia and cancer.

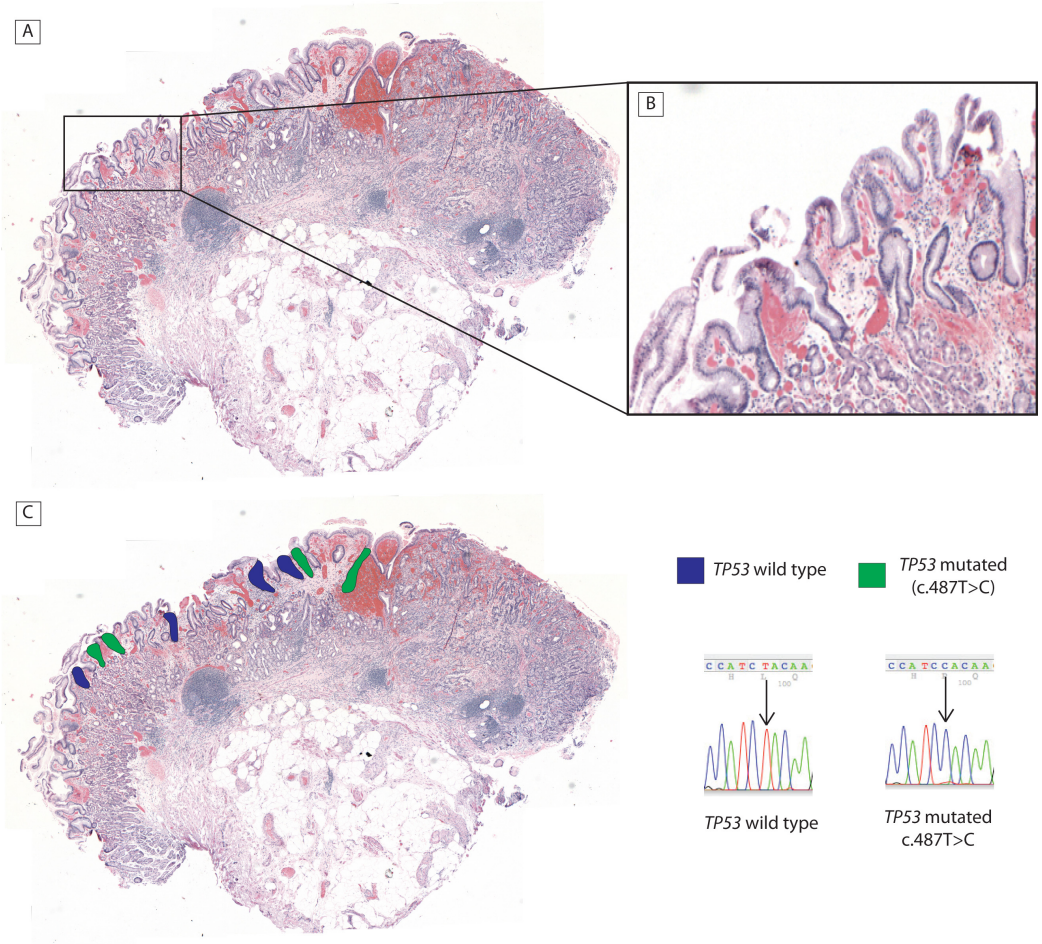

Figure 20: Spatial distribution of metaplastic gland genotypes in the first EMR specimen from patient 4.
(A) Haematoxylin and Eosin staining of metaplasia tissue from patient 4. (B) Magnified H&E image from patient 4 specimen, showing metaplastic glands. (C) Multiple metaplastic glands laser captured, some were WT for *TP53* mutation and some were mutated for *TP53* (c.487T>C), indicating at least two clones in the metaplastic areas within this specimen.

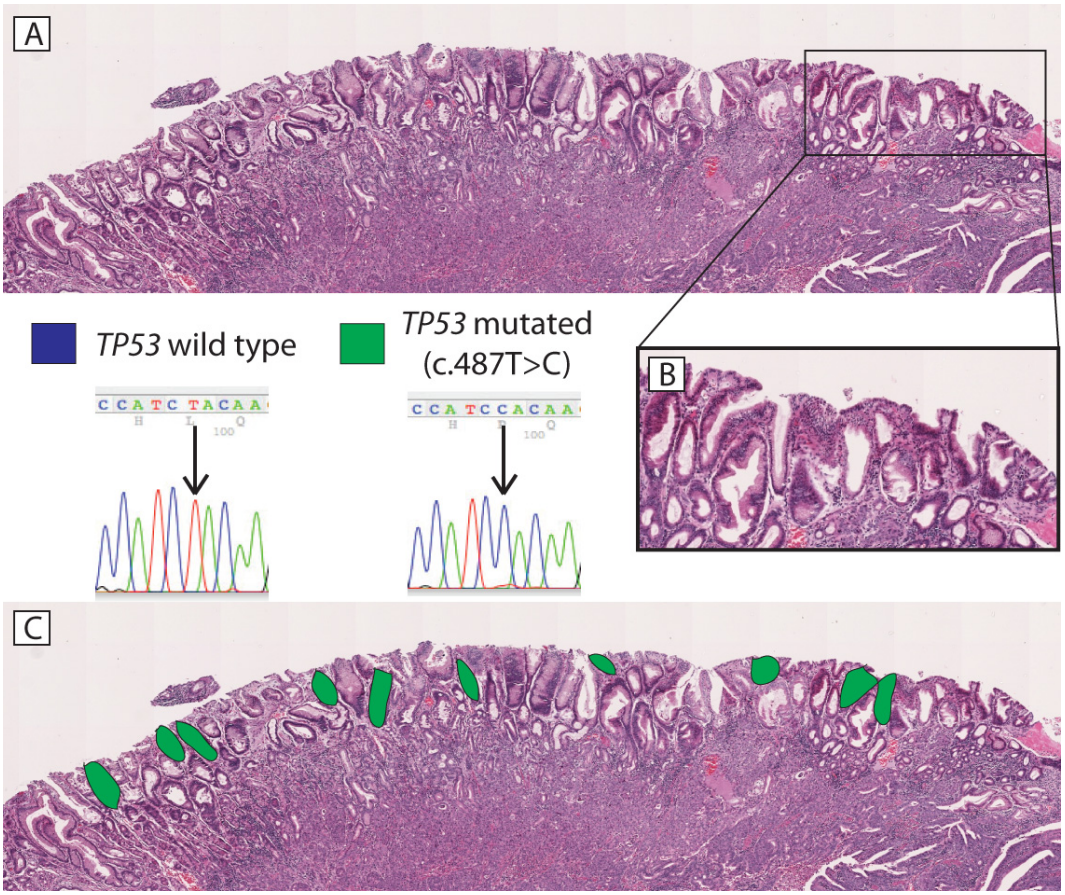

Figure 21: Spatial distribution of dysplastic gland genotypes in the second EMR specimen from patient 4.
(A) Haematoxylin and Eosin staining of dysplasia tissue from patient 4. (B) Magnified H&E image from patient 4 specimen, showing dysplastic glands (C) Multiple dysplastic glands were laser captured and all were mutated for *TP53* (c.487T>C), indicating that only one metplastic clone progressed to dysplasia.

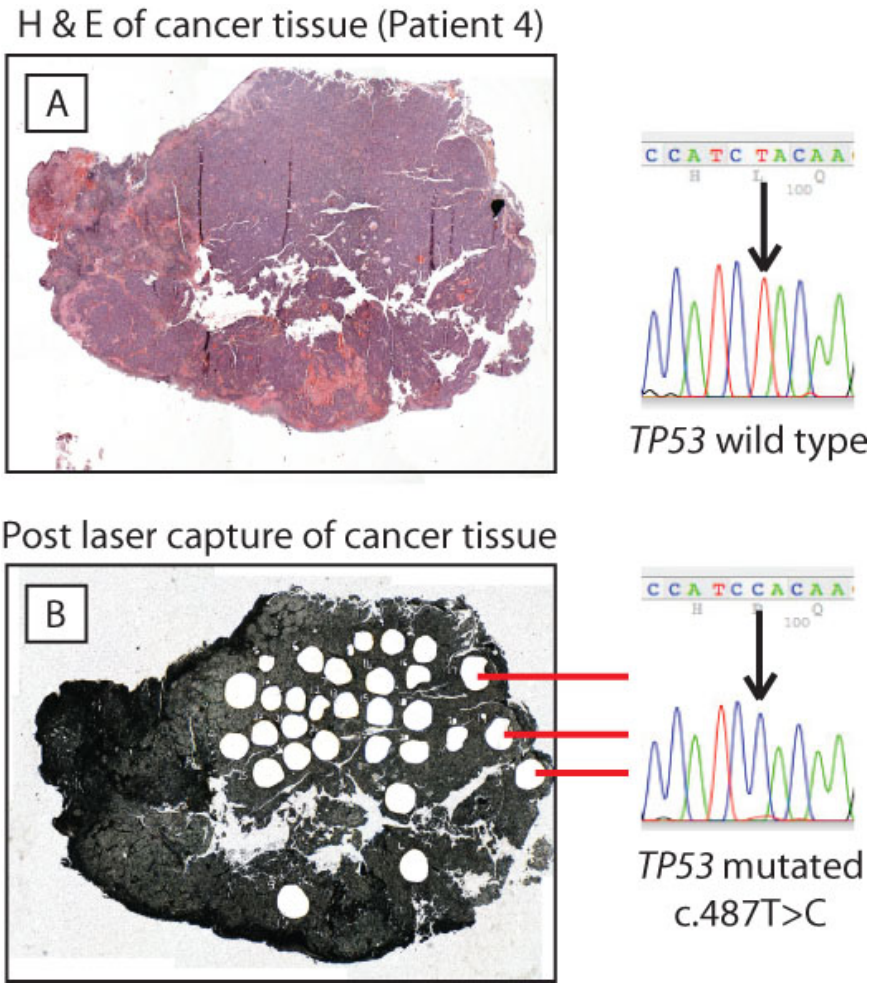

Figure 22: Monoclonal cancer tissue from patient 4.
(A) Haematoxylin and Eosin staining of cancer tissue from patient 4. (B) Multiple cancer areas laser captured were mutated for *TP53* (c.487T>C), indicating monoclonal oesophageal adenocarcinoma.

The EMR specimen from patient 9 showed areas of dysplasia and cancer. Five individual glands were laser captured from the dysplastic area and all 5 dysplastic glands were mutated for *CDKN2A* (c.238C>T). Five areas of cancer were also mutated for *CDKN2A* (c.238C>T), suggesting monoclonal cancer. Three squamous areas laser-captured were WT for *CDKN2A* (Table 3).

3.5.4 Clonal ordering of all the mutation and LOH data shown in all patients in this study:

The clonal ordering technique (chapter 1) was used to determine the timeline of the acquisition of genetic abnormalities detected in microdissected metaplastic, dysplastic and cancer glands shown in Figure 23. These demonstrate the presence of multiple clones identified in Barrett's metaplasia and dysplasia, however, Barrett's adenocarcinoma was uniformly monoclonal (Figure 23).

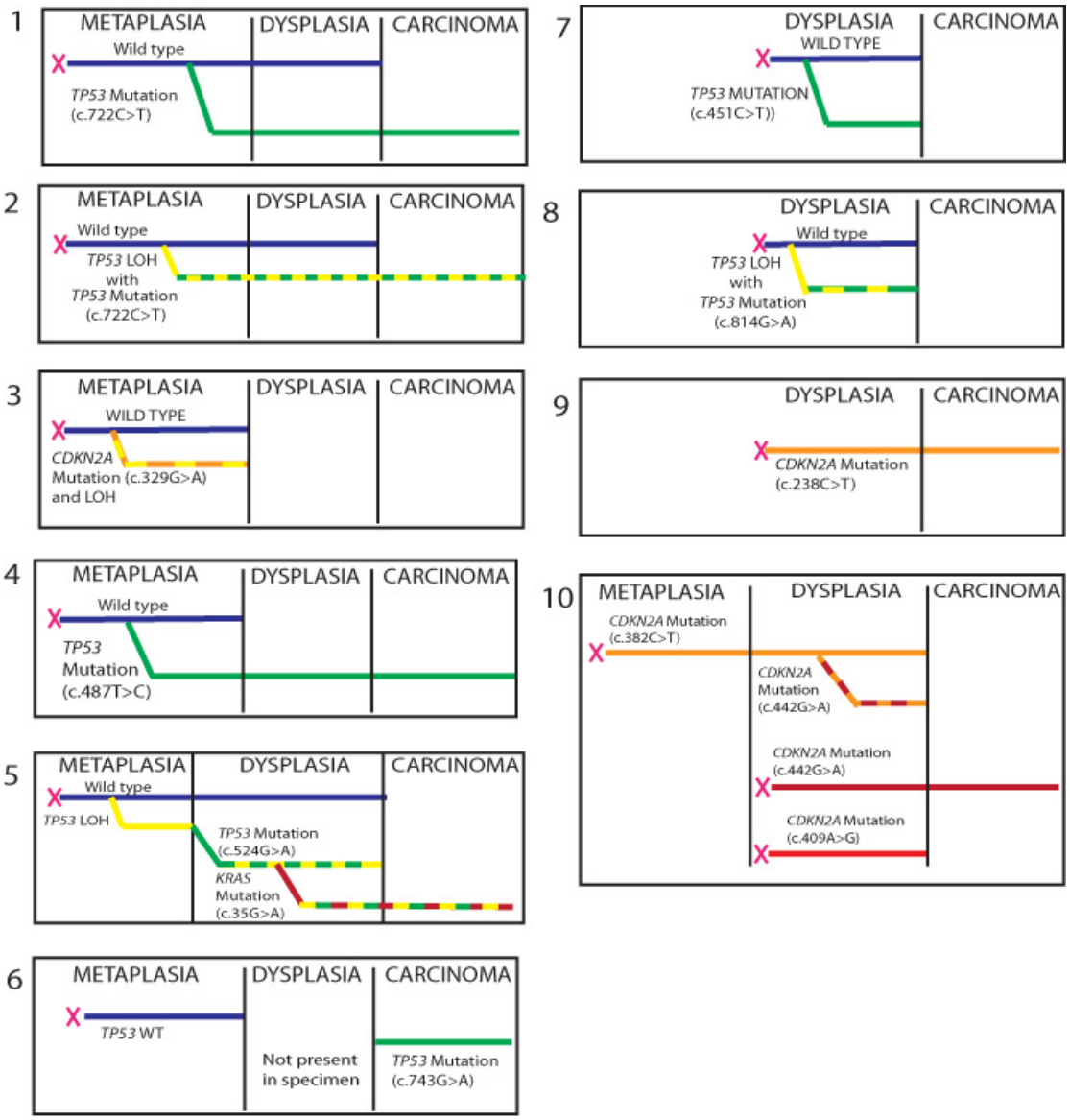

Figure 23: Clonal ordering trees constructed from the genetic analysis of all patients in Table 3.
Multiple clones were identified in Barrett's metaplasia and dysplasia, whereas, only one clone progressed to carcinoma, suggesting monoclonal Barrett's adenocarcinoma from polyclonal Barrett's metaplasia and dysplasia in some of the cohort studied here.

3.5.5 Heterogeneity at the protein level: Correlation between *TP53* mutational status and p53 protein expression:

Numerous studies have evaluated the expression pattern of p53 and its correlation with the grade of dysplasia and the risk of progression to OA. *TP53* mutations are found in all stages of MDC associated with p53 expression (Hamelin et al., 1994). Interestingly, the results of numerous immunohistochemical studies have demonstrated a strong p53 protein overexpression in more than 50% of OA (Hamelin et al., 1994, Younes et al., 1993, Neshat et al., 1994). Younes et al., (1993), have demonstrated that p53 protein accumulation increases with severity of histology, such as from low-grade to high-grade dysplasia (Younes et al., 1993). Increased expression of p53 has been correlated with increased proliferation in the progression of Barrett's to OA in some studies (Hritz et al., 2009, Binato et al., 2009). A positive predictive value for neoplastic progression is seen in patients with LGD (15% progression) and LGD with positive p53 expression (33% progression) (Kastelein et al., 2013). Potentially this could be used as a valuable biomarker in the prediction of an increased risk of disease progression in patients with Barrett's.

Identifying *TP53* mutated glands is a time consuming process. To simplify this procedure, I attempted to correlate *TP53* mutations with p53 immunohistochemistry. It has been shown that some oesophageal

adenocarcinomas express p53. Normally, p53 has a short half-life and is quickly degraded within the cell, but often when the *TP53* gene is mutated then p53 can become stabilised and accumulates within the cell. This can be detected by immunohistochemistry. Here I investigate if mutation status is correlated with protein expression of microdissected Barrett's glands. *TP53* mutated EMRs and oesophagectomy specimens (n=4) showing all stages of MDC were immunostained for p53 expression. Three out of four specimens expressed variable levels of p53 and the remaining specimen did not express p53. P53 was not expressed in areas of metaplasia (Figure 24); dysplastic glands fully expressed p53 or, at least, showed partial expression (Table 4). The areas of cancer fully expressed p53. In Metaplasia; a few glands were mutated for *TP53* – Exon 7 (Figure 24D), but none expressed p53 (Figure 24E). In dysplasia; mutated and wild type dysplastic glands both expressed p53 (Figure 25D and 25E), suggesting there is no absolute correlation between mutational status and gene expression.

Specimen	Identified mutation	p53 expressed	Mutation/Protein expression correlation?
1-EMR	*TP53* – Exon5 (c.473G>A)	No	No
2-EMR	*TP53* – Exon7 (c.722C>T)	Yes	No
3-EMR	*TP53* – Exon8 (c.814G>A)	Yes	No
4-Oesophagectomy for OA	*TP53* – Exon5 (c.442G>A)	Yes	Yes

Table 4: Comparing the mutational status of different Barrett's gland phenotypes and genotypes with p53 expression.
Only patient 4 showed 100% correlation between p53 expression and the mutational status of glands.

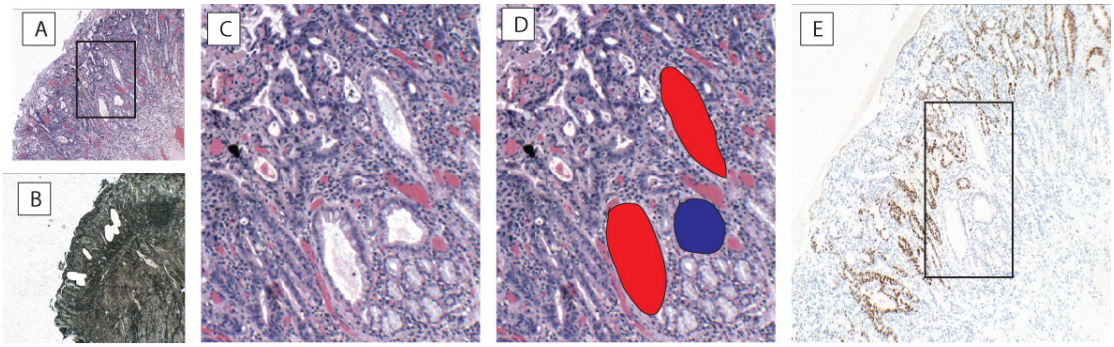

Figure 24: Correlation between mutational status and protein expression in Barrett's metaplasia.
H&E from patient 2(A). Post laser captured image (B). Enlarged image of an area with metaplastic glands (C). Two out of those three glands were mutated for *TP53* (c.722C>T) (Red) and 1 was wild type (blue)(D), but none expressed p53 (E). Mutated metaplastic glands did not express p53 (highlighted area - E).

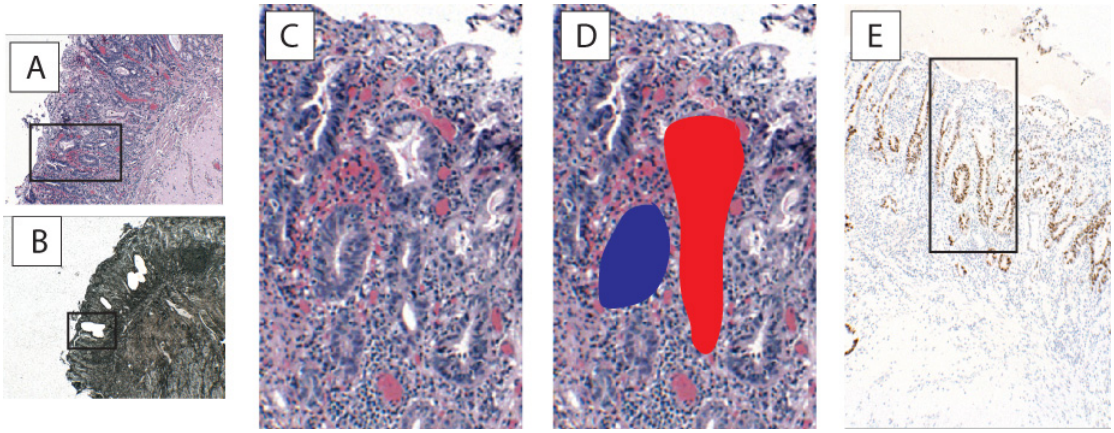

Figure 25: Correlation between mutational status and protein expression in Barrett's dysplasia.
(A)– H&E from the EMR from patient 3. (B) Post laser-captured image. (C) Dysplastic glands from highlighted area. (D) Mutational status of two dysplastic glands- wild type gland (blue) and mutated gland for *TP53* (c.722C>T) (red). (E) Immunostaining for p53. Mutated and wild type dysplastic glands both expressed p53.

These studies failed to demonstrate any significant relationship between protein expression and mutation status (Figure 24 and 25 and Table 4). p53 expression is variable: not all *TP53* mutations stabilise the protein

intracellular leading to expression. Hence, p53 immunostaining does not reflect the underlying mutational status of the individual gland.

3.6 Conclusions:

1) Wild type dysplastic glands were seen mixed with mutant dysplastic glands indicating that mutations in *TP53* and *CDKN2A* genes may not be the dysplasia-causing event.

2) Barrett's oesophagus exhibits genetic diversity, as multiple clones were seen in metaplasia and dysplasia.

3) The presence of a *TP53*, *CDKN2A* (p16) and *KRAS* mutation in associated cancer suggests that the mutated clone but not the wild type dysplastic clone progressed to cancer.

4) Oesophageal carcinomas are monoclonal outgrowths from polyclonal dysplasia.

3.7 Discussion:

Earlier studies into the genetic evolution of BO have lead to the theory that BO is a genetically clonal lesion from which cancer can arise (Galipeau, Prevo et al. 1999). However, Leedham et al., (2008) has shown that there are multiple independent clones present in Barrett's dysplasia; therefore, BO is a genetically heterotypic disease. Furthermore, Maley et al. have shown that genetic diversity increases the risk of cancer progression (Maley et al., 2006). In this study, I have shown that oesophageal adenocarcinomas can develop as a result of monoclonal outgrowths from polyclonal Barrett's dysplasia. Phenotypic and genotypic heterogeneity is detected between glands mixed through each EMR/oesophagectomy specimen. Gland-by-gland sequencing analysis has identified the presence of multiple clones within Barrett's dysplasia that may have been missed even by next generation sequencing due insufficient depth. Nevertheless, data that has been obtained from whole genome and whole exome sequencing studies have confirmed that Barrett's dysplasia is a heterogenous lesion and displays polyclones (Weaver et al., 2014, Timmer et al., 2015). My data has also shown that invasive oesophageal adenocarcinomas appear as clonal outgrowths from the surrounding polyclonal Barrett's dysplasia suggesting that 'winner' clones can now be identified using histological sections. This suggests that there may be a cellular interaction between different dysplastic clones that may contribute to the evolution of Barrett's adenocarcinoma. These multiple clones were present in close contact with each other, as a mosaic, raising the possibility of clonal interference (wherein, two or more clones compete with each other in the same genetic background).

In some cases, I detected some wild type dysplastic glands mixed with mutant dysplastic glands indicating that mutations in *TP53* and *CDKN2A* genes may not be the dysplasia-causing event. This is important because it reveals that *CDKN2A* and *TP53* mutations, while present in cancers, do not necessarily contribute to the change of pathology from metapasia to dysplasia and dysplasia to cancer. The change in pathology is likely to be due to either other genomic defects, such as mutations in SMAD4, ARID1A and SMARCA4, copy number changes or a combinations of genetic events that occur simultaneously (Weaver et al., 2014).

Recently, a case-cohort follow-up study by Li et al., have used SNP arrays to investigate genetic alterations in Barrett's patients who progressed to OA (progressors) and patients who did not progress to OA (non-progressors) over time. They have shown that the genomes in non-progressors remained genetically stable and showed very little genetic diversity whereas progressors showed significant genetic diversity such as chromosomal alterations in the form of gains/losses and genome doublings up to 48 months prior to the development of cancer (Li et al., 2014). Similar results were shown by Timmer et al, 2015, suggesting that genetic diversity, defined by an abnormal marker count of alterations in *CDKN2A*, MYC and aneusomy could be used to identify high-risk patients with non-dysplastic Barrett's (Timmer et al., 2015). *TP53* and *CDKN2A* commonly mutated in OA, http://www.sanger.ac.uk/cosmic and a limitation of this study is that the whole genome was not sequenced. Ross-Innes et al., (2015) have shown by whole genome sequencing that dysplasia exhibits multiple dysplastic clones BO demonstrates various mutations suggesting polyclonality

even in the absence of dysplasia within the specimens. They have also demonstrated that OA shows genetic heterogeneity with very few common mutations between OA and the adjacent BO, but were not able to map these mutations onto tissue sections (Ross-Innes et al., 2015). However, current technology does not permit such next generation sequencing techniques on laser capture microdissected glands and a strength of this study is being able to map clones onto tissue sections. Thus, although this study has high spatial resolution, the genomic resolution is low. These observations support my findings that mutations in *TP53* and *CDKN2A* may not be the only dysplasia causing genetic alterations.

Detecting mutations or genetic heterogeneity in a tissue sample involves considerable use of time and resources: hence, it is important to use easier and reliable methods such as p53 immunostaining in an attempt to reflect the underlying mutational status of a sample. Around 72% of OA express p53 (Binato et al., 2009). However, not all *TP53* mutations stabilise the protein, leading to accumulation in the cell (Hamelin et al., 1994). The recent case-control study, to evaluate the p53 protein expression in the progression of BO to OA has shown that p53 expression is associated with an increased risk of neoplastic progression in Barrett's MDC. The positive predictive value of aberrant p53 expression when compared to the histological diagnosis of LGD 15% and 33% respectively, suggesting that aberrant p53 expression is a better predictor of neoplastic progression (Kastelein et al., 2013). In my study, both non-mutated and mutated dysplastic glands expressed p53, indicating that other mechanisms (other than mutations) may be involved. Murine double minute-2 gene (mdm-2) negatively

regulates p53: its expression results in stabilization of the wild type p53 protein and losses its tumour suppressor activity. Soslow et al., (1999) have shown in OA, that mdm-2 is differentially expressed in wild-type *TP53* cancers compared to *TP53* mutated cancers (Soslow et al., 1999). This Indicates that mdm-2 expression may be responsible for p53 stabilization and loss of *TP53* function. Data presented here shows that immunostaining for p53 does not reflect the underlying mutational status of the individual gland. Future work on immunostaining for regulators of p53 expression such as mdm-2 expression in BO and OA may better identify mutant versus wild type clones.

Darwinian selection states that the fittest organism survives to dominate (positive selection) and the weaker organisms get eliminated (negative selection). In BO, mutant clones may interact with each other competing for fixation (clonal interference), and thus, a winning clone would acquire sufficient growth advantage to become carcinoma. According to the somatic mutation theory of carcinogenesis, a single founder mutation arising from the progeny of a single stem cell acquires a selective growth advantage over its predecessors and neighbouring cells as it acquires more driver mutations (Maley et al., 2004a). However, Leedham et al., have shown that multiple independent clones exist within Barrett's (Leedham et al., 2008). Here, I have shown that polyclonal premalignant tissue is common in patients with dysplasia but only a single clone from the dysplasia progresses to carcinoma, and, therefore Barrett's adenocarcinomas are monoclonal in origin. This has now been confirmed through whole genome sequencing (Ross Innes et al., 2015).

There are three possible factors which may dictate why Barrett's OA demonstrates a monoclonal origin and not a polyclonal origin as shown in dysplasia. First, given enough time in a slow growing cancer, each dysplastic clone may have the potential to become malignant but the rate of progression to cancer is such that the first clone to do so ends up killing the patient before other dysplastic clones can evolve. Second, the selective advantage of the winner dysplastic clone is such that it outcompetes the loser clone essentially preventing it becoming malignant. This raises the possibility that clones interact and compete or cooperate to form a cancer. This has been demonstrated by Miller et al., who isolated several tumour cells from a single breast tumour from BALB/cfC3H chimeric mice and established sublines *in vitro*. When neoplastic cells from the same or different sublines were injected into opposite flanks of mice, each inhibited the others growth (Miller et al., 1980). Conversely, Wu et al., have shown that mutant clones can cooperate to form a cancer. Using mutant Drosophila as a model, $Scrib^{-/-}$ cells promote the neoplastic development of Ras^{v12} cells and produce larger tumours when compared to flies that only possess one of these mutations. JNK crosstalk between both mutant cell populations mediates this cooperation (Wu et al., 2010).

Cellular and genetic heterogeneity is a feature of some human tumours (Heppner, 1984). By understanding the genetic characteristics of dominant clones and where they fit into the fitness landscape in premalignant disease, the evolution of the neoplasm may be predicted. Identification of differential expression of tumour suppressor genes or differences between such dominant clones may allow the prediction of the behaviour of the clone which progresses ultimately to

malignancy and help to identify a high-risk group patient for developing carcinoma. Fundamental to this is the mechanism of clonal expansion of mutant clones in BO. Clones expand via crypt fission in the colon (Greaves et al., 2006), in the small intestine (Gutierrez-Gonzalez et al., 2009) and in the gastric mucosa (McDonald et al., 2008). In gastric intestinal metaplasia (Gutierrez-Gonzalez et al., 2009) patches of clonally identical glands are seen, suggesting that gland fission is the process underlying this expansion. Recently, patches of Barrett's glands have been shown to be clonal populations, and Barrett's mucosa contains large groups of clonally identical glands (Nicholson et al., 2011). It appears probable that mutant clones involved in the development of Barrett's dysplasia also clonally expand via gland fission, probably with a growth advantage conferred by the p16 or *TP53* mutation. On the other hand, immediately adjacent glands may not be derived from the same clone (Rhiner and Moreno, 2009). There is no evidence that Barrett's segments increase in length with time (Gatenby et al., 2007).

Martens and colleagues (Martens et al., 2011, Martens and Hallatschek, 2011) have drawn attention to the fact that many pre-cancerous tissues have a distinct spatial structure, which will impinge in the manner in which clones expand. Such spatial structure, coupled with the possibility that clones can interfere or compete, can lead to lower adaptation speeds in comparison to non-structured or well-mixed populations. This will increase the time to acquire a given number of driver mutations; which may well explain the long prodromal period seen before invasion occurs in pre-invasive lesions such as Barrett's (Spechler, 2003), inflammatory bowel disease (Jess et al., 2006) and most colorectal adenomas

(Hofstad et al., 1996). The present work shows the existence of multiple contiguous but genotypically different clones. According to Martens et al., clones which are smaller in size, grow in a linear pattern with time until they reach a particular size, beyond which they start interacting with their neighbouring clones with variable outcomes of selection. Which would appear to underline the potential for clonal competition in BO, with a winning clone eventually acquiring sufficient growth advantage to become carcinoma (Martens et al., 2011).

Studying clonal evolution and genetic diversity may lead towards the development of genetic biomarkers for the prediction of neoplastic progression in patients with BO (Andor et al., 2016). To interpret the genetic diversity as a clinical predictor of the disease progression, it is important to determine which diversity measures to use (mean pairwise genetic divergence (Maley et al., 2006), the number of clones (richness) or the frequency of clones). However, the type of genetic alterations, which should be used to predict the risk of progression from BO to OA, is also equally important. A single genetic diversity measurement may not accurately predict the likelihood of cancer progression (Merlo et al., 2006). Maley et al., in their prospective study of cancer as an outcome, have shown that a combination of genetic instability (mutations, LOH, aneuploidy and tetraploidy) and clone size is a better predictor of cancer outcome (Maley et al., 2004a).

Chapter 4: The genetic origins of Barrett's dysplasia – phenotype:genotype correlations in the development of epithelial atypia in BO

Chapter 4: The genetic origins of Barrett's dysplasia – Phenotype:Genotype correlations in the development of epithelial atypia in BO

4.1 Introduction:

Dysplasia is the only clinical risk factor, which predicts progression to OA. It represents pre-invasive disease which requiring intervention. Dysplasia can be morphologically described: nuclear hyperchromatism with or without pleomorphism increased mitosis, loss of polarity and differentiation (Bignold, 2003). It has also been suggested that definition of dysplasia should also include morphological changes involving the entire length of gland/crypt and also the surface epithelium (Reid et al., 1988, Riddell et al., 1983). Glands/crypts with 'surface maturation' are often termed as 'reactive' and are dismissed for dysplasia. This could be on the basis that such neoplasia with clonal alterations in genes cannot be affected by environmental signals, which increases differentiation and reduces proliferation as the cell migrates towards the surface.

However, genetic changes, which are responsible for this change in phenotype, are unknown. There is enough evidence to suggest that Barrett's dysplasia is irreversible: in basal crypt dysplasia-like atypia (BCDA), obvious dysplastic changes occur in Barrett's glands and other gastrointestinal pre-malignant lesions; however, the upper gland/crypts associated with these dysplastic glands show a well-differentiated epithelium (Lomo et al., 2006). The genetic

relationship between these two phenotypes within a single gland is not very clear (Daniely et al., 2004).

In BCDA; cellular atypia is restricted to the base of gland or crypt, without the involvement of upper half of the gland or crypt and the surface epithelium. Recently, Odze and Maley et al., have shown the significance of BCDA in BO but also in stomach, inflammatory bowel disease and colonic adenomas (Odze and Maley, 2010). Lomo et al., have shown that BCDA in BO is associated with LGD or HGD or even OA elsewhere in the oesophagus. They have also shown that BO associated with BCDA showed increased incidence of *TP53* LOH, aneuploidy and proliferation (indicated by Ki67 staining and p53 immunohistochemistry) compared to control group (Lomo et al., 2006).

Recently, combined efforts from 6 gastrointestinal pathologists to evaluate the criteria and reproducibility in the diagnosis of BCDA showed that there was moderate interobserver agreement. BCDA may be of low-grade or high-grade depending on the degree of cellular atypia and crypt branching. The basal cells are mucin depleted, however, the surface epithelium consist of mucous secreting cells with regenerative changes (Coco et al., 2011). Two years follow-up of patients with BCDA showed that 87% of BO patients with BCDA had either synchronous or metachronous dysplasia or OA elsewhere in the oesophagus (Lomo et al., 2006). It was also suggested that dysplasia in BO begins at the bases of the glands, which further, in time progresses to involve the entire gland and surface epithelium (Coco et al., 2011). However, what is not clear is; whether dysplastic cells at the base of the gland share the same genetic alterations with cells present in the upper portion of the gland. The technical problem lies in

identifying these glands, as Barrett's glands are often very complex and determining which surface epithelium is associated with which gland could be a challenge.

My aim is to identify BCDA glands in BO, laser capture basal dysplastic cells and non-dysplastic surface cells separately, analyse their mutational burden and to see if these two phenotypes are clonally related. This will allow me to determine what is the mutational status of a gland before it becomes overtly dysplastic and whether dysplastic cells still retain differentiation capacity as they move up the gland.

4.2 Methods:

Patients: A total of 17 patient specimens (Formalin-fixed, paraffin-embedded-FFPE) were obtained from patients undergoing biopsy for monitoring of BO. H&E staining was carried out for histological assessment (by two expert pathologists; Prof. Sir Nicholas Wright (Queen Mary, University of London) and Prof. Robert Odze (Harvard University). Areas of basal crypt dysplasia-like atypia were identified. Specimens were initially screened for *CDKN2A* (p16), *TP53* and *KRAS*: only five specimens had identifiable mutations and, therefore, informative (Table 5), of which three specimens were inconclusive either due to lack of crypts with BDCA or not able to extract the DNA. Two patient samples were analyzed in detail.

Biopsy specimens with an identified mutation in *CDKN2A*, *TP53* and *KRAS* genes were then serially sectioned, and two independent pathologists histologically graded glands. The dysplastic gland bases and the associated maturing upper glands and surface epithelium were differentially microdissected using a laser capture microscope (for LCM and PCR details, refer chapter-2, Methods-2.3 and 2.4). Glands were sequenced (for sequencing details, refer chapter-2. Methods-2.6) for the point mutation identified in the initial screen. The mutation burden of each gland is indicated using a self-explanatory colour system.

4.3 Results:

Studies were limited to areas where the BDCA could be seen in direct continuity with the differentiating surface epithelium so that it could be reasonably proposed that the glands displaying BCDA were supplying cells to the maturing surface epithelium. Below is a magnified H &E of Barrett's gland; the basal cells are characterized by nuclear hyperchromatism with pleomorphism, increased mitosis, loss of polarity and differentiation, whereas, cells present in upper half of the gland and surface epithelium are characterised by well-differentiated mucin containing surface maturation cells (Figure 26).

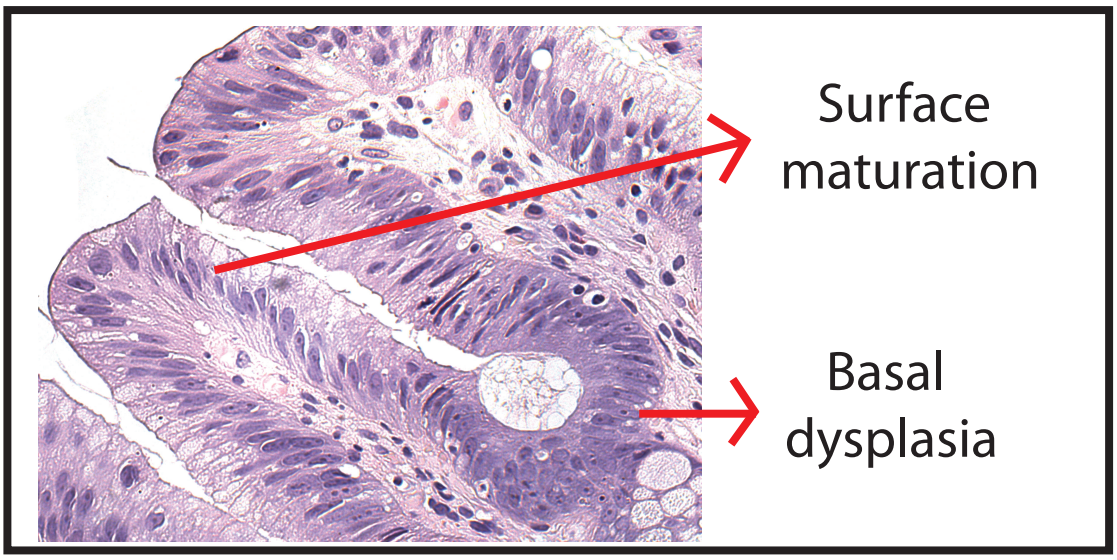

Figure 26: H & E staining, showing basal crypt dysplasia-like atypia within specialized intestinal-type Barrett's epithelium.
Evidence of maturation of the surface epithelium, which shows a distinct lack of dysplastic features (such as nuclear hyperchromatism with pleomorphism, increased mitosis, loss of polarity and differentiation).

4.3.1 Mutation screening of specimens with BCDA:

In a cohort of 45 Barrett's specimen's, 17 had identifiable glands with BCDA. Glandular tissue was macrodissected from these cases and screened for somatic gene mutations in *TP53*, *CDKN2A* and *KRAS*. The screening results of these samples have been shown in Table 5 below. 5 out of 17 specimens had identifiable mutations. It was frequently found that the complexity of the architecture in Barrett's mucosa meant that only 2 patients showed glands where their bases were in direct continuity with the surface epithelium could not be visualized. Therefore only 2 patients were taken forward for detailed microdissection (Patients 3 and 4).

Patient	Specimen	Mutation
1	Biopsy	c.238C>T *CDKN2A*
2	Biopsy	c.238C>T *CDKN2A*
3	Biopsy	c.742C>T *TP53*
4	Biopsy	c.844C>T *TP53*
5	Biopsy	c.733G>A *TP53*

Table 5: Sequencing of whole tissue sections from showing the specimens that had identifiable mutations in *TP53*, *CDKN2A* and *KRAS* genes.

The 2 patients put forward for clonal analysis showed low-grade BCDA with maturing gland epithelium in continuity with the dysplastic glands. Patient 1 was a female aged 72 with a history of long segment Barrett's oesophagus of more than ten years. Patient 2 was a 66 male also with a long history of long segment Barrett's oesophagus. Neither patient had a history of dysplasia. In this study, both patients had *CDKN2A* mutation, which was clonal for the entire gland population; however, this may not be the only mutation present in those cells.

The *CDKN2A* mutation c.238C>T was seen in both patients (Figures 27 and 28). In patient 2, non-dysplastic epithelium without any evidence of BCDA showed the same *CDKN2A* mutation (Figure 29), and it is most likely that the *CDKN2A* mutant cells were derived from the adjacent BCDA gland which was clonal for the *CDKN2A* mutation c.238C>T. These observations suggest that dysplastic cells still retain some differentiation capacity as they move up the gland.

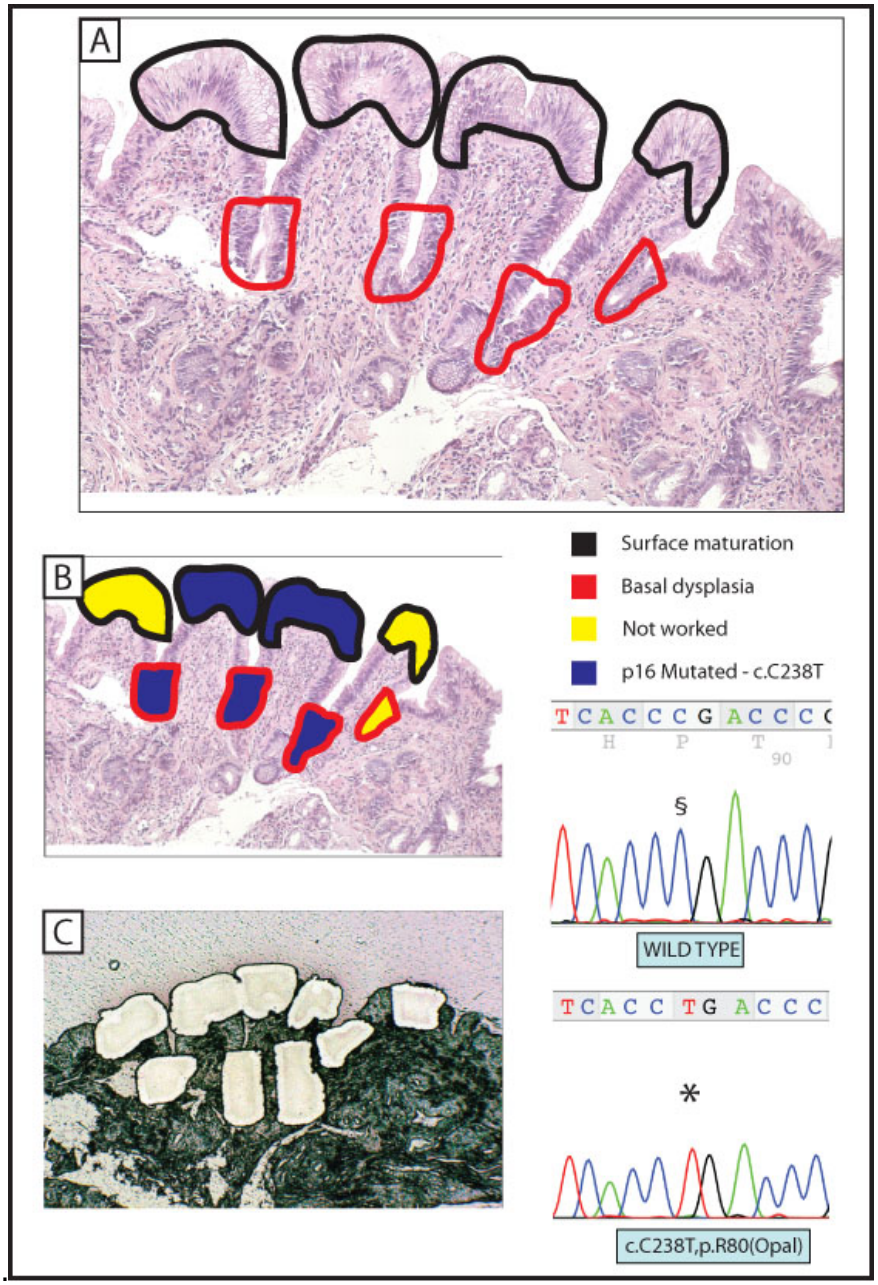

Figure 27: Assessment of genetic alterations in basal crypt dysplasia-like atypia (BCDA).
A) H & E staining of Barrett's glands with basal crypt dysplasia-like atypia, Non-dysplastic surface cells are highlighted in black and basal dysplasia is shown in red. B) Both the basal gland dysplasia and the maturing surface epithelium shares the same C238T mutation in *CDKN2A*. C) LCM areas. Thus the surface epithelium, despite its bland appearance, shares a clonal mutation with the overtly dysplastic gland epithelium beneath it.

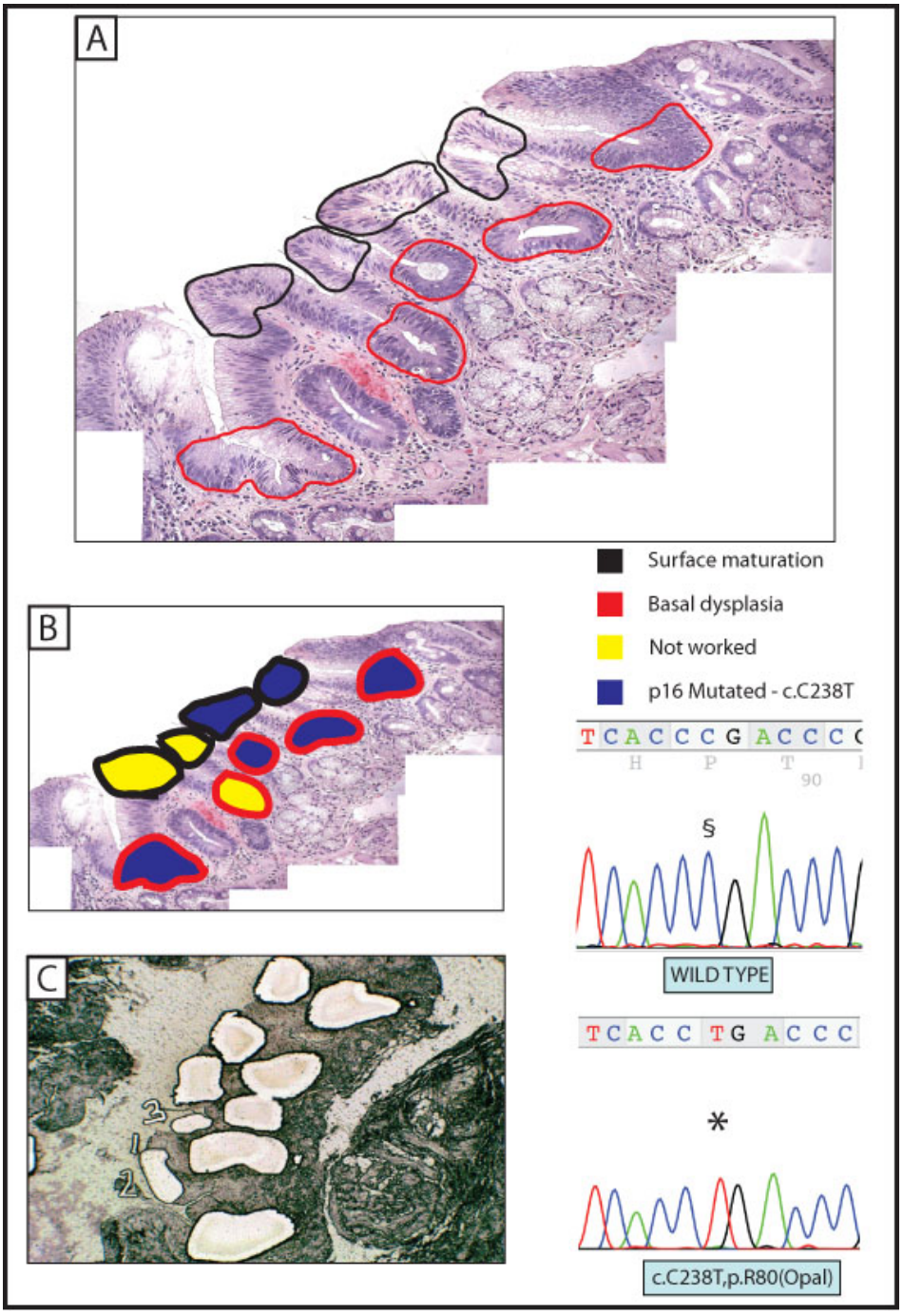

Figure 28: Assessment of genetic alterations in basal crypt dysplasia-like atypia (BCDA).
A) H & E staining of Barrett's glands with basal crypt dysplasia-like atypia, Non-dysplastic surface cells are highlighted in black and basal dysplasia is shown in red. B) Both the basal gland dysplasia and the maturing surface epithelium share the same C238T mutation in *CDKN2A*. C) LCM areas. Thus the surface epithelium, despite its bland appearance, shares a clonal mutation with the overtly dysplastic gland epithelium beneath it.

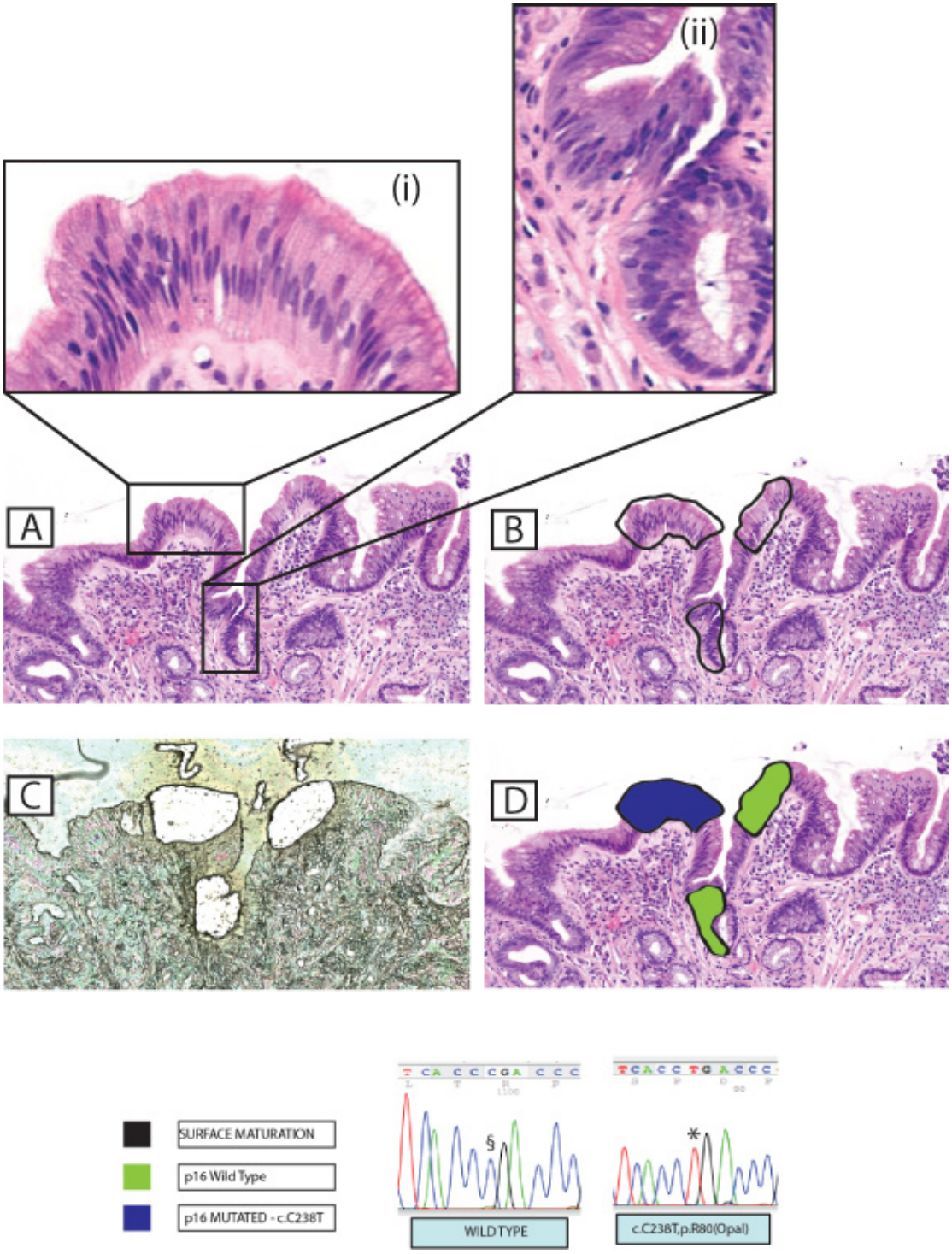

Figure 29: A second example of the clonal relationship of BCDA with surface epithelium from patient 2.

A) H & E staining. (B, C) Sections taken before and after laser microdissection. (D) While the surface epithelium (Ai) and gland epithelium at the base (Aii) are non-dysplastic, one area on the surface epithelium shows a C238T mutation of *CDKN2A.*

4.4 Conclusions:

This study shows that Barrett's glands consisting of basal crypt dysplasia-like atypia, characterised by basal cells displaying features of dysplasia-like atypia and the upper half of gland with surface epithelium showing features of differentiation are clonal. The differentiated upper gland and surface epithelium share a common ancestry containing same *CDKN2A* mutation as dysplastic cells present at the base of the Barrett's gland.

This study has also shown that even after acquiring genetic alteration, such as mutation in *CDKN2A* tumour suppressor gene, the Barrett's gland retained its healthy glandular organization and certainly did not show evidence of dysplasia. Future work will help us to understand the genotypic correlation of dysplastic epithelium.

4.5 Discussion:

This study has shown that dysplastic Barrett's glands can consist of two phenotypically distinct cells, in which basal cells with dysplasia and surface maturation cells share a common somatic *CDKN2A* gene mutation, suggesting that these cells share a common ancestry and are clonal in origin. These observations confirm that basal dysplastic cells give rise to the surface maturation cells and the exact reason as to why dysplastic cells with *CDKN2A* mutation result in well-differentiated surface maturation cells in not clear.

In BO, the dysplastic cell biology and its progression within a gland is not very well understood (Odze and Maley, 2010). Recently it has been shown that multipotential stem cells in BO reside in the middle portion of Barrett's gland giving rise to their clonal progeny (Lavery et al., 2014b). In Familial Adenomatous Polyposis (FAP), a second hit on the second allele of APC gene causes a change in the phenotype of the entire colonic crypt to dysplasia (Lamlum et al., 2000). However, in the stomach; intestinal metaplasia found adjacent to dysplasia was mutated for APC gene, but did not show any evidence of dysplasia (Gutierrez-Gonzalez, Graham et al. 2011). Suggesting, that gene mutations may not necessarily lead to a change in gland phenotype, the genetic interactions within the niche may play a vital role.

It has been shown that BO with glands containing BCDA are associated with either synchronous or metachronous dysplasias or OAs elsewhere in the oesophagus (Lomo et al., 2006, Coco et al., 2011). It has also been shown that these pre-tumour clones can form large patches, expanding areas of up to 17cm of a Barrett's segment (Barrett et al., 1999, Wong et al., 2001, Maley et al., 2004a). This has also been observed in non-dysplastic tissue in ulcerative colitis which can also carry a substantial mutational burden without phenotypic changes (Leedham et al., 2009). This raises the question of the acceptability of dysplasia as a marker for cancer risk prediction, as apparently morphologically non-dysplastic cells can also carry the carcinogenic mutation. Hence, genetic profiling of pre-dysplastic epithelium can be a more suitable marker to identify high-risk patients. Saadi et al., have shown that different phenotypes, such as metaplasia, dysplasia and OA can be distinguished based on a gene expression signature from

microdissected Barrett's stromal tissue. Overexpression of any of five genes (TMEPAI, FAP, JMY, BCL6 and TSP1) indicated poor prognosis in patients with OA (Saadi et al., 2010).

This study has shown that entire gland with BCDA share a clonal mutation: suggesting that dysplasia can respond to environmental differentiation signals, indicating us to re-visit the biology of dysplasia and also to understand the correlation between gene mutations and their impact on different epithelial phenotypes.

Chapter 5: The genetic relationship between neo-Barrett's and oesophageal adenocarcinoma

Chapter 5: The genetic relationship between neo-Barrett's and oesophageal adenocarcinoma

5.1 Introduction:

Neo-Barrett's oesophagus (neo-BO) is the recurrence of BO in patients who have undergone oesophagectomy for OA (O'Riordan et al., 2004b, Hamilton and Yardley, 1977). This project investigates the clonal relationship between neo-BO and their original carcinoma. Approximately 50% of patients develop neo-Barrett's following surgery for OA of which 27% of patients displayed specialised intestinal metaplasia (O'Riordan et al., 2004b). Therefore, there is a need to investigate the origins of neo-Barrett's to assess the efficacy of the cancer surgery and the tumourigenic potential of neo-Barrett's. Most patients presenting with BO developed metaplasia many years before diagnosis. Neo-BO provides us with an opportunity to investigate the origin of a newly-developed Barrett's lesion. Here I analyse the mutational status of the original resected oesophageal carcinoma specimens and compare these to the mutational status of the neo-Barrett's lesions. Identifying the same clone in the original OA and the neo-Barrett's lesion would indicate a common ancestry and demonstrate field cancerization in the post-oesophagectomy patients.

Barrett's oesophagus exhibits a range of different gland phenotypes (Paull et al., 1976, Glickman et al., 2009). Paul et al., have shown that Barrett's segments can exhibit zonation. This has been described as gastric-fundic type epithelium with parietal and chief cells present in the distal Barrett's segment, cardia-like gland

in the mid zone and specialized IM in the proximal part of the segment (Paull et al., 1976). However, there are studies, which do not report zonation and have suggested that BO segment consists of a mosaic of phenotypes(Theodorou et al., 2012, Going et al., 2004). It has also been shown that Barrett's glands can consist of foveolar cells expressing MUC1, MUC5AC and MUC6, features characteristic of gastric epithelium (Glickman et al., 2009) and goblet cells expressing MUC2 and MUC3, features of intestinal epithelium (Reis et al., 1999). However, it is still not clear as to which phenotype progresses or increases the risk of developing OA (Chandrasoma et al., 2012, DeMeester and DeMeester, 2000). Recently, Lavery et al., have shown that the proliferative zone and stem cell niche in Barrett's gland are located in the middle portion of the gland from where cells migrate bidirectionally. These characteristics of Barrett's glands resemble pyloric glands of the stomach rather than intestinal glands. Using immunohistochemistry they have also shown that gene expression of Barrett's glands also resembles gastric gland pattern rather than intestinal glands (Lavery et al., 2014a).

Studies have shown that gastric acid and bile reflux and the duration of oesophageal exposure to these refluxate, plays an important role in the origin of columnar metaplasia (Oberg et al., 2000, Vaezi and Richter, 1996). Hence, neo-BO would be a useful *in vivo* model to study the pathogenesis of BO, as following oesophagectomy, remaining stomach is joined to the remaining cervical oesophagus, which has hardly been exposed to acid reflux. Endoscopic studies following oesophagectomies have shown that the amount of oesophagitis and columnar metaplasia is proportional to the amount of oesophageal acid exposure and at the same time exposure to bile did not seem to effect columnar metaplasia.

They have also shown that 15 out of 32 (46%) patients had developed columnar metaplasia following oesophagectomy, of which, 11 out of 15 (69%) patients had BO at the time of surgery, suggesting that development of neo-BO was more common in patients who had previous BO (Oberg et al., 2002).

5.1.1 Histology of neo-BO:

Endoscopically, neo-BO looks similar to BO (see Figure 10). Little is known about the histological features of neo-BO. Histological examination of neo-BO has shown that columnar metaplasia showed 60% gastric-cardiac type, 20% gastric-fundic type and 20% had IM consisting of goblet cells. The time taken for the appearance of IM since oesophagectomy was longer compared with those without IM (9.5 Vs 4.2 years respectively (Oberg et al., 2002) and 61 Vs 20 months (O'Riordan et al., 2004b)). These observations suggest IM may develop as a consequence of chronic exposure to acid and bile reflux. Dresner et al., have suggested that neo-BO develops as sequential events of change in the epithelium from cardiac to IM (Dresner et al., 2003). Histological characteristics of cardiac mucosa seen in neo-BO were similar to cardiac mucosa which was seen at the original GEJ (DeMeester and DeMeester, 2000). Recently, Dunn et al., have shown that 36% of neo-BO showed phenotypic changes of metaplasia, Non-goblet cell columnar epithelium was seen earlier than goblet-cell metaplasia (median of 4.8 vs 8.1 years; p=0.025) (Dunn et al., 2016). In this study majority of neo-BO specimens showed gastric type epithelium (Figure 30).

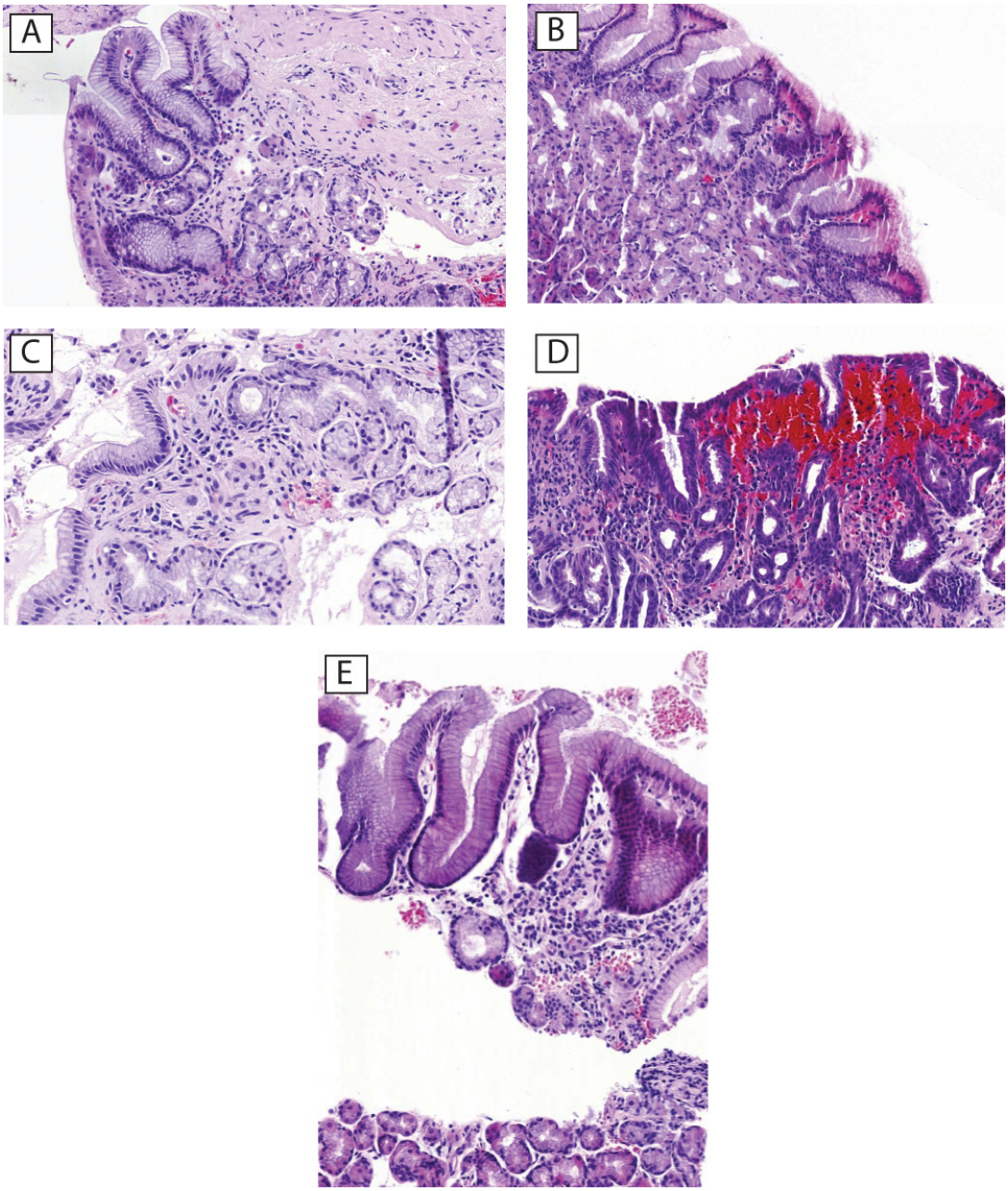

Figure 30: Histology of neo-Barrett's oesophagus.
H & E staining of neo-BO from five patients, mainly showing gastric type epithelium (A to E).

Cytokeratin (CK) is a keratin protein, present in the cytoplasm of glandular epithelium. CK7, which is a marker of ductal differentiation, is not expressed in the normal oesophagus. Ormsby et al., have shown that CK7 was expressed throughout Barrett's glands, but CK20, which is a marker of intestinal

differentiation and also foveolar epithelium in the stomach was expressed only in the superficial epithelium of BO. This pattern was not seen in biopsies from gastric-cardia and gastric resection specimen with features of IM (Ormsby et al., 1999). 100% of Barrett's oesophagus tissue sections stain positive for CK7/CK20 of which 78% contain IM at the GOJ and none for the stomach. DAS-1 is expressed in incomplete type colonic intestinal metaplasia, Lord et al., have shown that DAS-1 was significantly expressed in BO and IM at GEJ compared to the stomach (Lord et al., 2004). Immunohistochemical staining of neo-BO has shown that CK7/CK20 and DAS-1 staining pattern of the columnar mucosa was similar to that of BO. Cellular proliferation using topoisomerase 2alpha protein was seen in 50% of cardiac mucosa (Lord et al., 2004). However, clonality of neo-BO has not been established.

5.2 Hypotheses:

1) Neo-Barrett's develops as a *de novo* lesion post-oesophagectomy

2) Neo-Barrett's displays gastric architecture suggesting a gastric source of Neo-Barrett's

5.3 Aims:

1) To determine whether the neo-Barrett's lesion is a field cancerization effect of the original lesion or this is de novo Barrett's.

2) To investigate the neo-BO relationship with Gastric glands.

5.4 Methods:

Tissue was macro-dissected (for details, refer chapter-2. Methods-2.2) from the cancer regions of EMR specimens and then screened for mutations in the mutable regions of p16INK4A, *TP53* and *KRAS* genes. Neo-Barrett's biopsies from patients with identified mutations were then serially sectioned, and glands were histologically graded and then micro-dissected using a laser capture microscope (chapters 2.3 and 2.4). Glands were sequenced (chapter 2.6) for the point mutation identified in the initial screen of their OA. Cellular proliferation within neo-BO gland was assessed using Ki67. Immunohistochemistry was used to stain neo-BO glands for mucin core proteins (MUC2, MUC5 an MUC6) and trefoil family factor (TFF).

5.5 Results:

To determine whether neo-BO is a *de novo* lesion or is a result of field cancerization, 25 oesophagectomy specimens were screened (Table 6); macro-dissected tissue was screened for mutations in genes known to be mutated in OA (*TP53*, *CDKN2A* and *KRAS*). Individual glands from neo-BO were laser captured, micro-dissected and sequenced. Preliminary data reveals that mutations detected in oesophageal adenocarcinoma were not found in neo-BO tissue, indicating that neo-Barrett's is genuinely a de novo Barrett's lesion and not a recurrence of the clone that gave rise to the OA.

5.5.1 Mutation analysis of patients with neo-BO:

Biopsy specimens form neo-BO of all eleven patients who had identifiable mutations in their OA were screened for other commonly mutated genes (*TP53*, *CDKN2A* and *KRAS*). Mutations identified in OA were not present in any of neo-BO specimens (Table 6). 14 other patients did not display any mutations in the limited number of genes sequenced.

Patient	Oesophagectomy	Cancer mutation	Present in Neo Barrett's?
1	Adenocarcinoma	c.35G>A *KRAS*	No
2	Adenocarcinoma	c.743G>A *TP53*	No
3	Adenocarcinoma	c.238C>A *CDNK2A*	No
4	Adenocarcinoma	c.820G>A *TP53*	No
5	Adenocarcinoma	c.451C>T *TP53*	No
6	Adenocarcinoma	c.844C>T *TP53*	No
7	Adenocarcinoma	c.677C>T *TP53*	No
8	Adenocarcinoma	c.853G>T *TP53*	No
9	Adenocarcinoma	c.527G>C *TP53*	No
10	Adenocarcinoma	c.742C>T *TP53*	No
11	Adenocarcinoma	c.818G>A *TP53*	No

Table 6: Screening of oesophageal adenocarcinoma for mutations in *TP53, CDKN2A* and *KRAS*.
No shared mutations between the adenocarcinoma and the neo-Barrett's in all patients within this cohort.

5.5.2 Laser capture microscopic dissestion and sequencing individual neo-BO gland:

To confirm this, Individual glands from neo-BO were laser captured. DNA was PCR and sequenced to identify mutations, which were seen in their OA. None of the neo-BO glands had mutations identified in their OA (Figure 31 and 32).

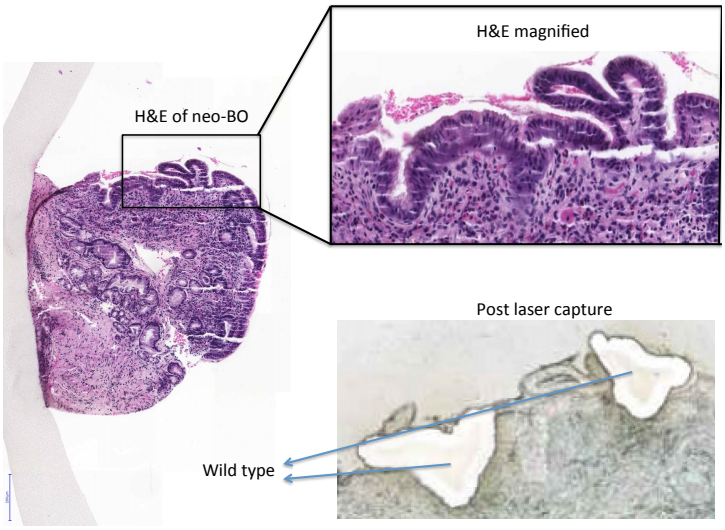

Figure 31: H&E and post laser capture from oesophageal biopsy specimen taken from patient 9 with neo-BO in table-6.

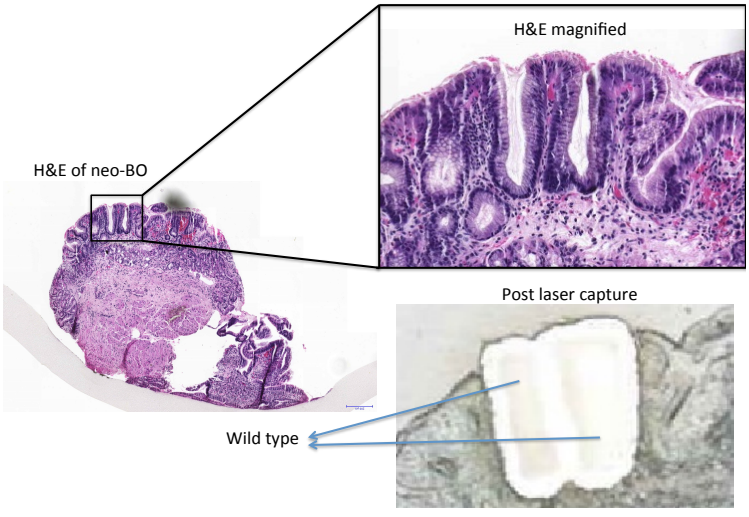

Figure 32: H&E and post laser capture from oesophageal biopsy specimen taken from patient 14 with neo-BO in table-6.

5.5.3 Comparison of the proliferative zone in neo-BO glands compared with Barrett's:

Cellular proliferation within neo-BO glands was quantified by Ki67 expression. 5 patients were selected from table 6. Ki67+ cells were predominantly present in the middle portion (or neck) of all neo-Barrett's glands compared with the gland bases and gland foveoli (Figure 33). All five specimens from neo-BO, the expression of Ki67+ cells was significantly higher in the middle region than that of the base of the gland and the gland surface (Kruskal-Wallis one-way analysis of variance, $p<0.05$). Overall 54% of Ki67+ cells were detected in the neck of neo-BO glands (Figure 34). This is similar to the levels of Ki67 expression in non-dysplastic Barrett's (Lavery et al., 2014b). Data presented here can therefore be used to suggest that Neo-Barrett's glands have a similar cellular architecture of pyloric glands.

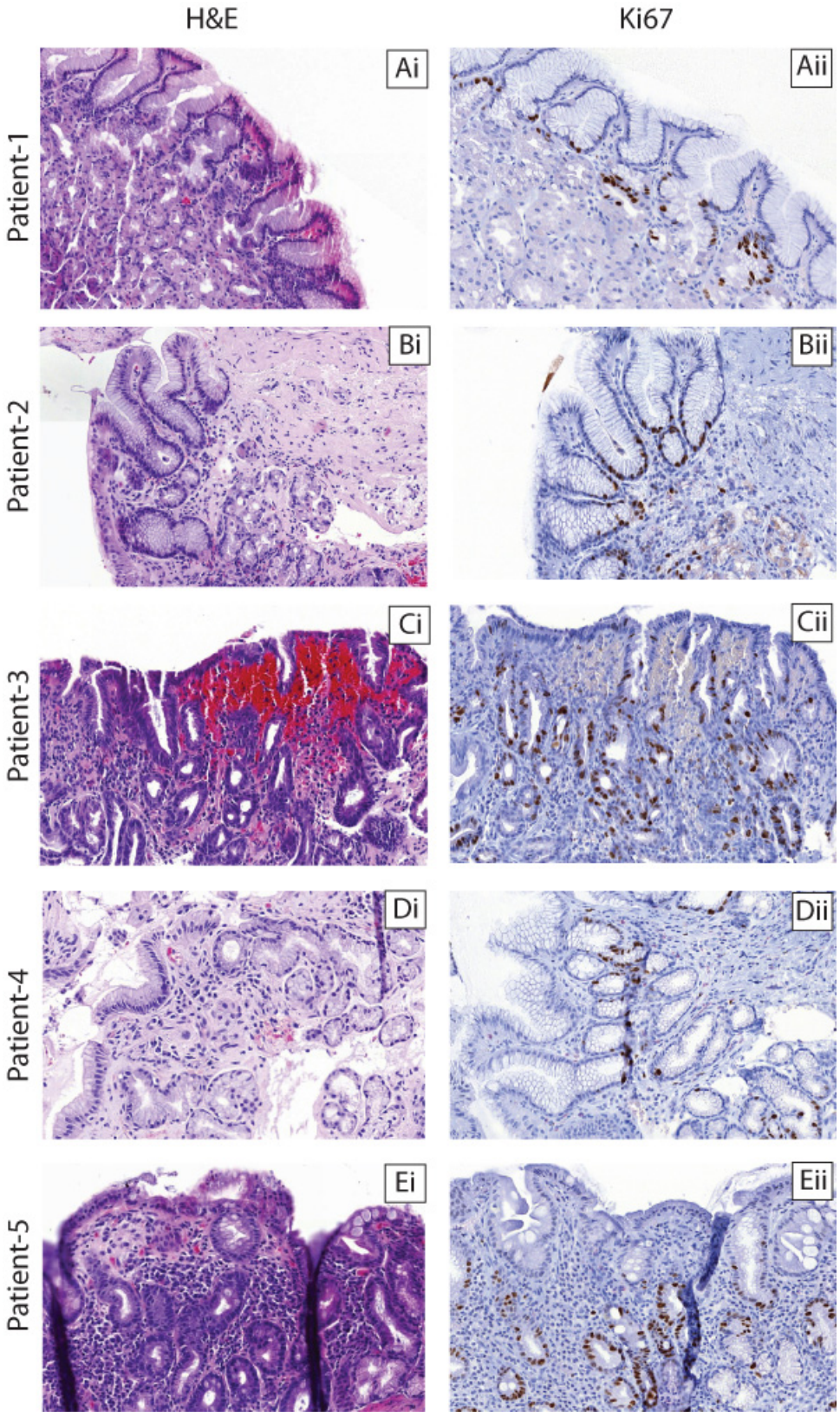

Figure 33: Ki67 expression in neo-Barrett's glands from five patients.
(i) Haematoxylin and Eosin staining of neo-Barrett's glands from 5 patients. (ii) Ki67 expression in each patient's biopsy. Ki67 positive cells are predominantly located in the central portion of the gland, similar to pyloric glands.

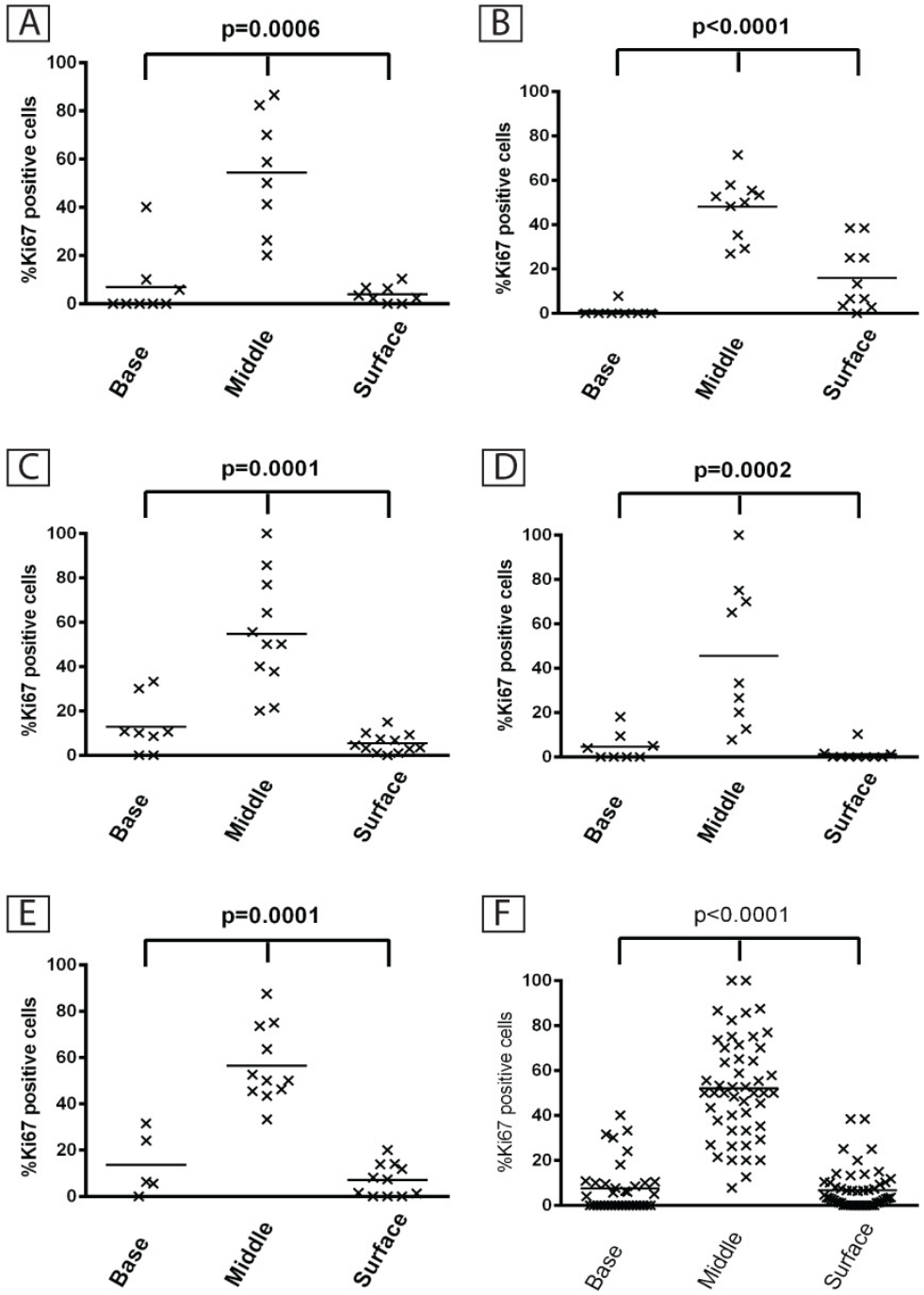

Figure 34: Quantification of the number of Ki67+ cells in each region of neo-Barrett's glands.
Significant proportion of Ki67 positive cells were present in the middle portion of the glands, similar to gastric pyloric gland (A-patient 1, B-patient 2, C-patient 3, D-patient 4, E-patient 5) (Kruskal-Wallis one-way analysis of variance, $p<0.05$). Cumulative percentage of Ki67 positive cells within neo-Barrett's glands (F).

5.5.4 Comparison of mucin and trefoil factor expression in neo-Barrett's, Barrett's oesophagus and gastric glands:

Barrett's glands show compartmentalistion of differentiated cell types. Foveolar cells express MUC5AC and Trefoil factor 1(TFF1) and mucinous secreting cells express MUC6 and TFF2. In neo-Barrett's oesophagus; expression of MUC5AC and TFF1 were seen in the upper part of the neo-BO glands with decreasing expression towards the middle region of neo-Barrett's glands (Figure 35 and 36). A similar expression was also seen in non-dysplastic Barrett's (Figure 37) and gastric-pyloric glands (Lavery et al., 2014b). Mucous cells expressing MUC6 and TFF2 were mainly seen at the base of the neo-BO glands below the Ki67+ zone (Figure 35 and 36). Goblet cells are MUC2+ and only 2/5 patients (patient 3 and 5) demonstrated positive staining. This, and analysis of the H&E section from each specimen reveals that the majority of the neo-Barrett's patients in this study displayed cardia or oxyntic epithelium. This is evidence that Barrett's originates from the gastric epithelium.

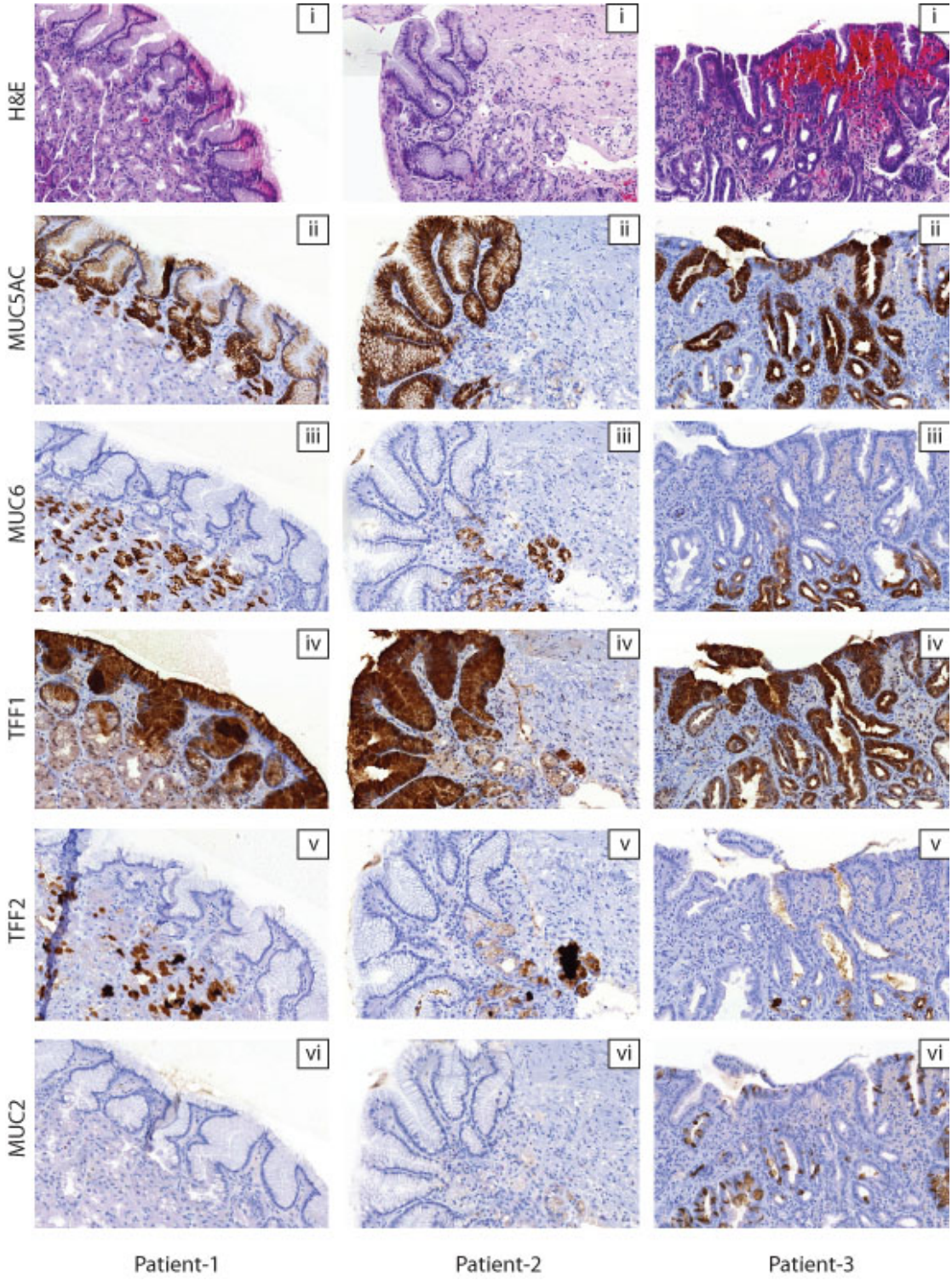

Figure 35: Mucin and trefoil expression in neo-BO (Patients 1, 2 and 3).
Well-oriented glands displaying surface middle and base of the gland were used. (i) H&E staining of neo-BO; (ii) MUC5AC protein was mainly expression in the upper portion of the neo-Barrett's gland; (iii) MUC6 protein expression was mainly seen at the base of neo-Barrett's glands; (iv) TFF1 and (V) TFF2 protein expression in neo-BO were similar to MUC5AC and MUC6 respectively. (vi) MUC2 protein expression was restricted to goblet cells within neo-BO from patient 3 only.

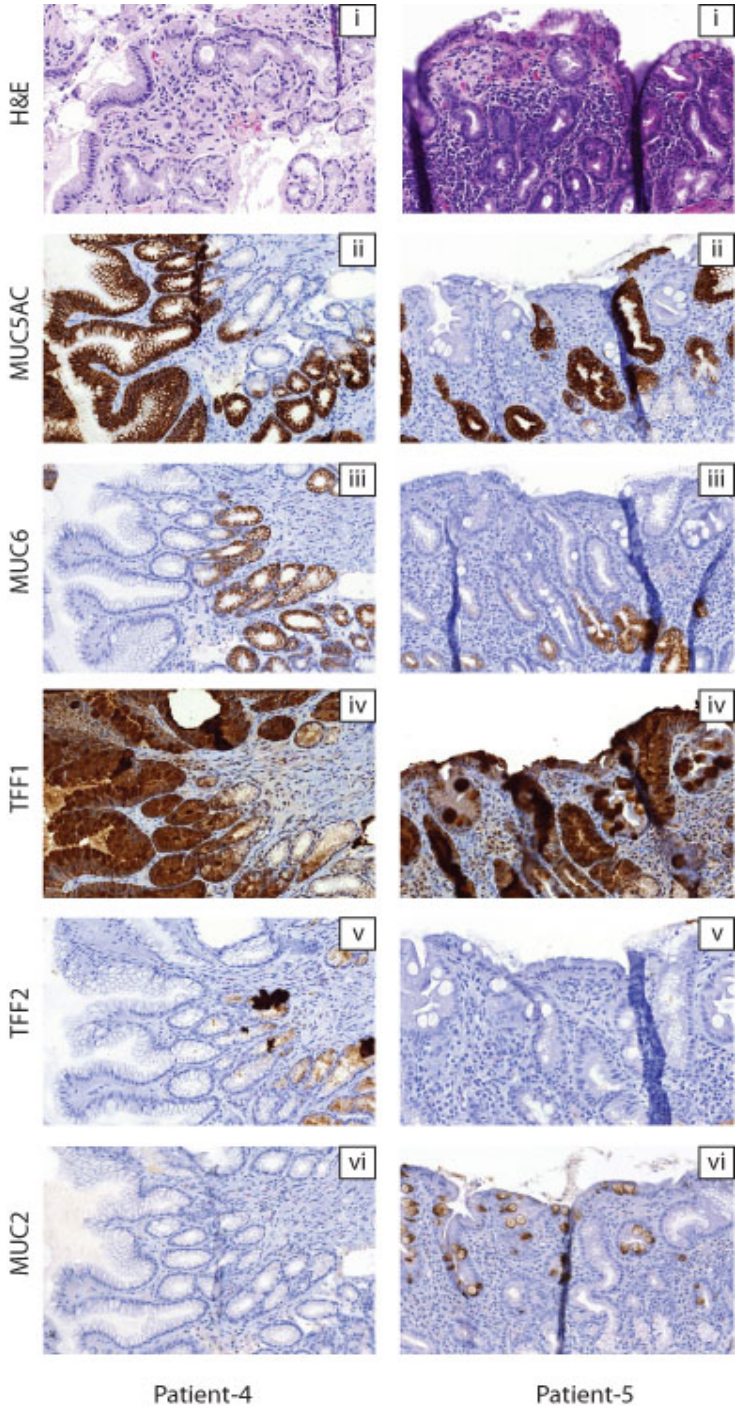

Figure 36: Mucin and trefoil factor expression in neo-BO (Patients 4 and 5). Well-oriented glands displaying surface, middle and base of the gland were used. (i) H&E staining of neo-BO; (ii) MUC5AC protein was mainly expression in the upper portion of neo-Barrett's glands; (iii) MUC6 protein expression was mainly seen at the base of neo-Barrett's glands; (iv) TFF1 (Trefoil family factor) and (V) TFF2 protein expression in neo-BO were similar to MUC5AC and MUC6 respectively; (vi) MUC2 protein expression was mainly restricted to goblet cells and only in patient 5.

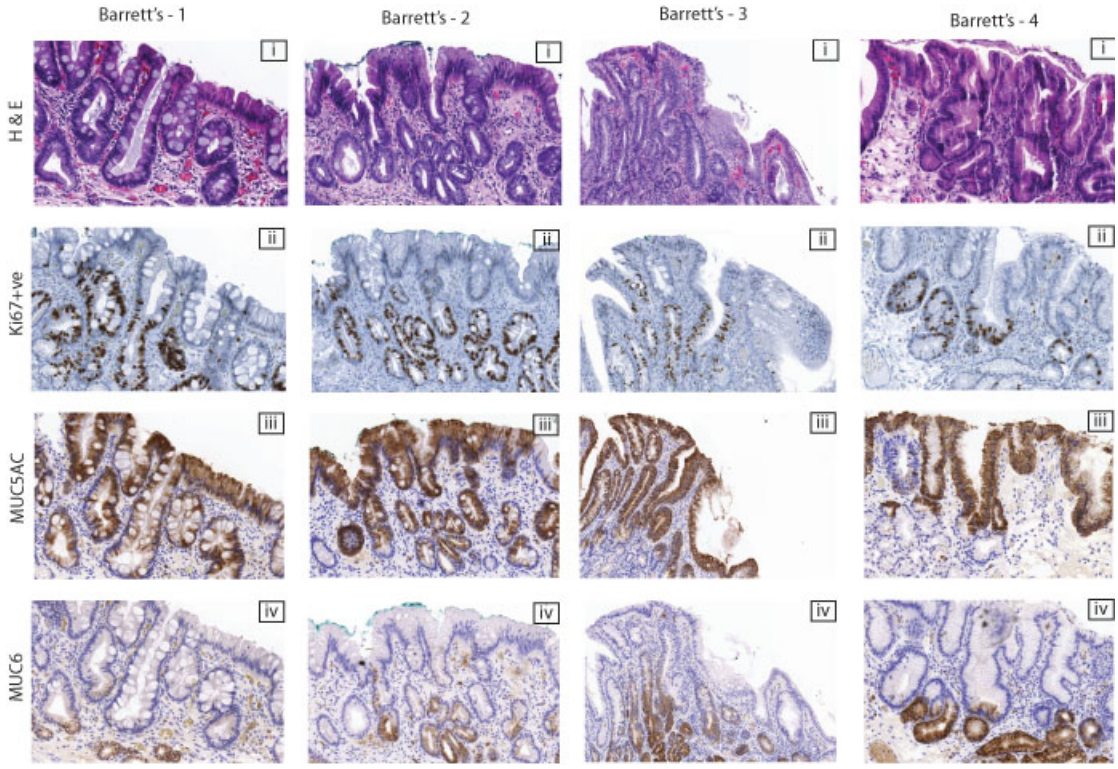

Figure 37: Mucin and trefoil factor expression in Barrett's oesophagus.
Well-oriented glands displaying surface, middle and base of the gland were used. (i) H&E staining of Barrett's; (ii) Showing Ki67 expression within Barrett's glands, Ki67 positive cells are predominantly situated in the central portion of the gland, similar to pyloric glands; (iii) MUC5AC protein was mainly expression in the upper portion of the Barrett's gland; (iv) MUC6 protein expression was mainly seen at the base of Barrett's glands.

5.6 Conclusions:

1) Neo-Barrett's seems to be genuinely a *de novo* Barrett's lesion, and not a recurrence of the clone that gave rise to the OA.

2) Lineage markers within Neo-BO glands appear similar to gastric glands suggesting that Neo-BO evolves from gastric glands from the anastomosis site.

5.7 Discussion:

Barrett's oesophagus represents field cancerisation of the oesophagus. It would be of particular concern if post-oesophagectomy Barrett's oesophagus contained the same founder mutation as the adenocarcinoma and would suggest that Neo-Barrett's has a high risk of reforming OA. However, in the limited number of genes sequenced, no shared mutations were detected. However, data presented here has not shown any mutation evidence of field cancerization in this respect, indicating that neo-Barrett's is genuinely a *de novo* Barrett's lesion and not a recurrence from the original BO. A longitudinal study looking at genotype of initial BO followed by OA and neo-BO from the same patient will give a better understanding of the genetic progression from BO to OA and further to neo-BO. Next generation sequencing of Neo-BO may give a much deeper understanding of the relationship between pre- and post-operative BO.

Recently, Dunn et al., have analysed post-oesophagectomy specimens to establish the phenotypic landscape, the time taken for the appearance of different phenotypes and to assess commonality between BO and neo-BO using

immunohistochemistry. They have shown that 36% of neo-BO showed phenotypic changes of metaplasia, which is 10% less than what has been reported in the past (Oberg et al., 2002, Dresner et al., 2003). Non-goblet cell columnar epithelium was seen earlier than goblet-cell metaplasia (median of 4.8 vs 8.1 years; p=0.025) and 62% of neo-BO specimens expressed cytokeratin 7/20 (marker of Barrett's epithelium). These findings suggest that non-goblet cell columnar metaplasia is commonly seen in post-oesophagectomy BO and goblet-cell columnar metaplasia seems to be a late event (Dunn et al., 2016).

In this study, immunostaining of neo-BO has shown that the gene expression pattern of neo-BO glands is similar to that of gastric-pyloric glands. The upper part of neo-BO gland expresses TFF1 and MUC5AC, whereas, cells at the base express TFF2 and MUC6 similar to gastric-pyloric glands. MUC2 was expressed mainly in goblet cells predominantly in the upper part of the gland. Ki67 + cells were predominantly represented in the middle portion of neo-BO glands, suggesting that the proliferative zone in neo-BO gland is located at the center of the gland which is in the region corresponding to the neck/isthmus of gastric-pyloric glands. This work has shown that gene expression pattern and the proliferative characteristics of neo-BO are similar to gastric glands.

5.7.1 Origins of neo-BO:

How does neo-barrett's develop? The oesophago-gastric junction is always removed during oesophagectomy for oesophageal adenocarcinoma. Hence, the

possibility of residual embryonic cells as the origins of Barrett's can be discounted.

In vivo studies have shown prolonged exposure to gastric acid and bile reflux in patients who had BO (Hoffman et al., 2007) (Marshall et al., 1997). Similarly, studies in patients who underwent oesophagectomy for OA have shown regeneration of columnar epithelium at oesophagogastric anastomosis junction in 12 out of 19 patients who underwent subtotal thoracic oesophagectomy for oesophageal cancer, 9 of which had developed columnar regeneration within four months of surgery (Hamilton and Yardley, 1977). Similar results have been shown in patients who underwent cervical oesophagectomy (Lindahl et al., 1990). These studies also showed significant gastric reflux in patients who underwent oesophagectomy. Dresner et al., demonstrated the development of Barrett's metaplasia in patients who underwent oesophagogastric anastomosis. In their study, the columnar epithelium was seen in 19 out of 40 patients, of which 10 had cardiac-type epithelium and 9 had intestinal metaplasia. Seven patients were followed serially showed initial cardiac-type epithelium followed by intestinal metaplasia. In patients with columnar metaplasia, there was significant acid and bile reflux (Dresner et al., 2003). During oesophagectomy the cardiac/fundic part of stomach is removed, hence the presence of cardiac-type or intestinal type epithelium at the anastomotic junction suggest that proximal migration of gastric glands may not be the source of neo-BO, which is supported by various reports showing development of neo-BO after total gastrectomy (Westhoff et al., 2004) (Nishimaki et al., 1996) (Sandvik and Halvorsen, 1988).

This raises the possibility of the presence of multipotent stem cells within the remnant oesophageal squamous epithelium or oesophageal gland ducts.

The origin of BO has been hotly debated (Quante et al., 2012, Xian et al., 2012). Evidence are more in support of origin of BO from the native oesophageal squamous epithelium (Souza et al., 2008). However, recently, Lavery et al., have suggested that BO may develop from upward movement of cells from the gastric cardiac mucosa. They have shown that BO is a clonal lesion, giving rise to multiple cell lineages, and the stem cell niche is situated in the middle portion of BO glands with bidirectional cellular migration (Lavery et al., 2014b). My work here, also shows similar results and suggests that cells from the gastric cardia may be the source of Neo-BO. Further longitudinal endoscopic surveillance of patients with BO who develop OA and later develop neo-BO and go on to develop recurrent OA will help us to clarify the natural history of this process.

Chapter 6: Examining the rate of clonal expansion and stem cell dynamics in Barrett's oesophagus glands

Chapter 6: Examining the rate of clonal expansion and stem cell dynamics in Barrett's oesophagus glands

6.1 Introduction:

Our understanding of the genetic and epigenetic alterations involved in the development of Barrett's has dramatically improved how we view the evolution of Barrett's. Recently, Stachler et al., (2015), using whole genome sequencing, have constructed phylogenetic trees of Barrett's epithelium from oesophagectomy specimens. They have shown that Barrett's is made up of multiple subclones distributed throughout the tissue. (Stachler et al., 2015). However the dynamics of expansion has not been effectively studied and there is a need to understand the rate at which mutated glands divide through the Barrett's lesion as a potential risk factor for cancer progression. It is established that the size of Barrett's lesions remain static over time (Lim et al., 2010), therefore clones can only expand within a finite space. Recent evidence suggests that clonal expansions within the Barrett's lesion may occur as a result of gland fission (Nicholson et al., 2012), which has also been previously shown in the human stomach (Fellous et al., 2009b) and the colon (Graham et al., 2011a, Greaves et al., 2006). Recently, a large population-based study using fluorescence *in situ* hybridisation by Timmer et al., 2015, have shown that changes in genetic diversity over time as a result of clonal expansion can be used as predictors for progression of BO to OA (Timmer et al., 2015). Furthermore, Li et al., 2014, have used SNP arrays to show that Barrett's patients that do not progress to cancer remain genetically stable and show few changes in genetic diversity whereas progressors show significant increases in the genetic diversity and instability up

to 48 months prior to the development of cancer (Li et al., 2014). These studies suggest that calculating the clonal expansion rate within the Barrett's segment itself may predict cancer risk.

6.1.1 What can methylation patterns tell us about clonal expansion?

To be able to measure the rate of clonal expansion of a gland, we need a marker that changes over time at a small but measurable rate such as methylation of CpG sites in gene promoters (Ahuja et al., 1998, Issa, 2000). It has been shown that methylation increases with age (Kim and Shibata, 2004, Issa et al., 1994, Issa, 2000) and is inherited during mitosis, hence methylation patterns between two cells/glands within a tissue records their ancestry (Holliday, 1987). The divergence caused by random methylation errors that are acquired during mitosis can also be used to record time as they are also inherited by future cell divisions (Kim and Shibata, 2002). Methylation patterns would be similar in recently divided glands that share a recent common ancestry and more diverse in those that are more distantly related (Kim and Shibata, 2004). Methylation patterns can also be used as a proxy to reconstruct stem cell phylogeny, if each stem cell clone is represented by a single methylation pattern then the rate of change of such patterns can inform on the number of stem cells and the rate of niche succession (Graham et al., 2011a, Baker et al., 2014).

Genetic evolution studies have revealed clonal expansions, but have not yet determined their rate of expansion through the Barrett's lesion. Some studies have suggested that Barrett's lesions are clonal and therefore are derived from an

expansion of a single gland (Maley et al., 2004b). More recently, however, it has been shown that Barrett's is polyclonal (exhibiting multiple, independent glands of different ancestries) (Leedham et al., 2008). Regardless of its clonal status, it is logical to hypothesise that rate of progression to cancer may correspond to the clonal expansion rate. When we consider cancer as a disease of evolution then understanding clonal expansion dynamics becomes necessary when attempting to produce adequate cancer risk analysis. Clonal expansions are a known risk factor for oesophageal cancer progression (Maley et al., 2004a) and has been shown to be the case in ulcerative colitis (Salk et al., 2009). An increase in the rate of stem cell divisions and gland fission is the likely mechanism of clonal expansion within the upper gastrointestinal tract (Baker et al., 2014; McDonald et al., 2008). The rate of fission is increased in inflammatory conditions such as inflammatory bowel diseases (Wong et al., 2002). Therefore understanding the rate of stem cell expansion and gland fission rate will infer the clonal expansion rate in Barrett's.

We do not know the expansion dynamics and stem cell dynamics of Barrett's glands and in this chapter, I attempt to investigate these using methylation patterns within the promoter regions of non-expressed genes in *ex vivo* specimens. This study aims to use methylation patterns of CpG islands in the promoters of non-expressed genes such as *CSX* (cardiac-specific homeobox gene otherwise known as NK2 homeobox 5 gene) and *MYOD* (member of the basic-helix-loop-helix family of proteins). Non-expressed genes are used for the study of cell dynamics using methylation because there is no selection bias on clonal

expansion based on gene expression and therefore methylation patterns of these promoters are neutral to the expansion process.

The amount of methylation of CpG islands in non-expressed genes is linked to the cell cycle and therefore is increased with cell division and ageing. Inflammation increases the amount of cell division and therefore the percentage of methylation within CpG islands also increases (Chu et al., 2007). Errors in methylation patterns are acquired stochastically at cell division, therefore the epigenetic distance between cell populations based on their methylation patterns (referred to as 'tags') can be calculated and reflects the time since the most recent cell of common ancestry between cells. We can therefore use methylation patterns as a molecular clock measuring stem cell dynamics (the methylation distance between cells within a gland) and the clonal expansion rate (the methylation distance between glands within a Barrett's lesion). Each Barrett's gland is maintained by a population of stem cells, and therefore the more stem cell divisions that occur within glands, the greater the intragland methylation pattern diversity (Figure 38). Because methylation patterns are inherited at the time of cell division, methylation pattern diversity is therefore a proxy for the number of stem cells in each gland. Barrett's gland stem cell numbers and their behaviour are yet to be characterized. Hence, phylogenetic analysis of cells within Barrett's gland will help to understand the stem cell behaviour and glandular expansion in non-dysplastic Barrett's epithelium.

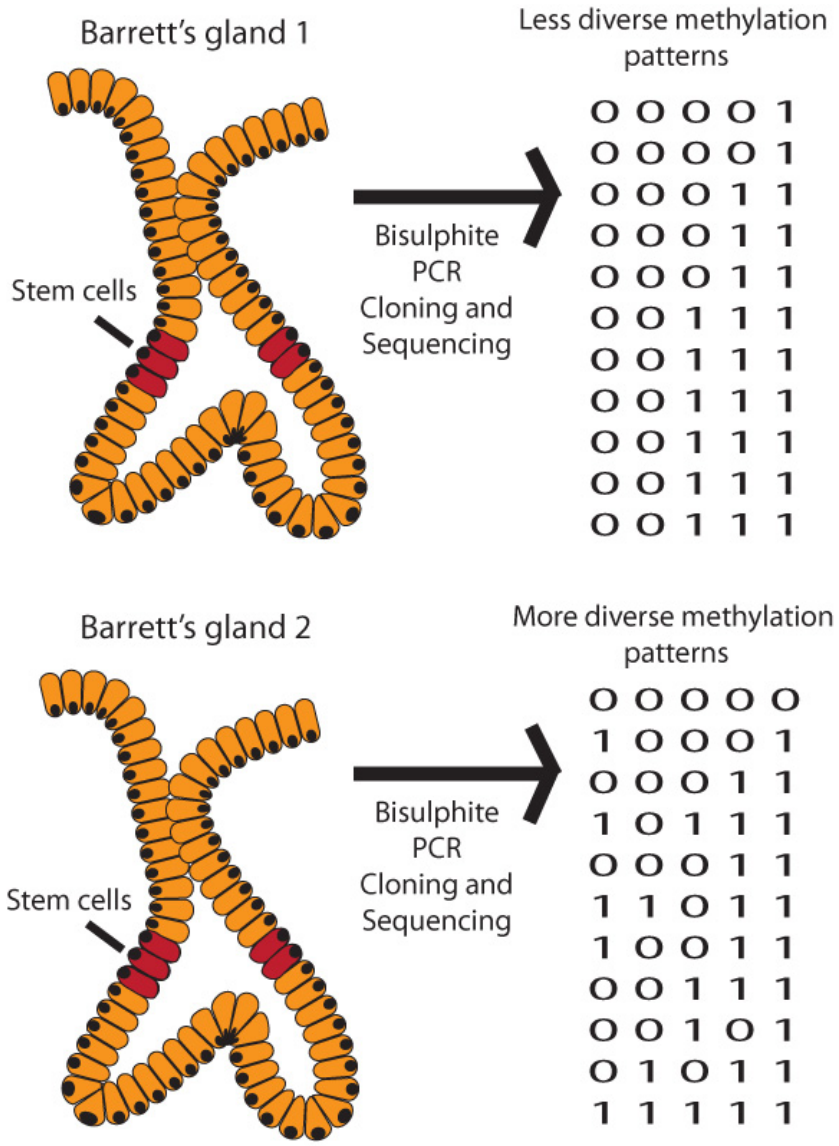

Figure 38: Methylation patterns record the time between gland divisions
Methylation of a CpG island from many cells (represented by the number of rows of binary 'methylated(1)/unmethylated(0)' for each CpG site). Here, tags are sequenced from two different Barrett's glands. It is clear that there is more diversity within the lower gland than the upper gland. Intragland analysis shows increased cell turnover (and therefore stem cell turnover) in the lower gland and intergland analysis demonstrates the time between gland divisions. Modified from (Kim and Shibata, 2002).

The use of methylation patterns as a cellular molecular clock is well established. Yatabe et al., (2001), used methylation patterns to determine the stem cell dynamics of colonic crypts. They showed that the percentage and diversity of

methylation within the promoters of non-expressed genes varied between crypts and also increased with patient age, suggesting that crypt stem cells are sufficiently long-lived to acquire epigenetic diversity (Yatabe et al., 2001). Furthermore, by using a mathematical model assuming 64 stem cells in the niche (and 95% stem cell divisions assumed to be aysmmetric), they have shown niche succession (the process by which the progeny of single stem cell takes over the entire stem cell niches) occurs every 8.2 years (Yatabe et al., 2001). We can be confident that methylation pattern diversity represents stem cell behavious because the majority of non-stem cells die within few days (Potten and Loeffler, 1990, Heath, 1996) and therefore methylation changes within proliferating transit amplifying cells do not contribute to the overall crypt methylation diversity (Kim and Shibata, 2002). Furthermore, Kim et al., have also suggested that methylation patterns within a crypt were consistent with a stem cell niche model (where stem cells undergo random loss and replacement) rather than the presence of multiple immortal stem cell lineages (Yatabe et al., 2001). These data serve to illustrate the potential of understanding clonal expansion dynamics and in this thesis I employ them to investigate Barrett's gland dynamics.

Recently Baker et al., have shown that human colonic crypts consist of five to six stem functional cells that expand in the niche by neutral drift (no stem cell has a selective advantage over its neighbours). They have also shown that each colonic crypt divides approximately every 30-40 years (Baker et al., 2014). In conditions of inflammation, crypt fission is increased (Cheng et al., 1986, Wong et al., 2002) and this would suggest that adjacent crypts would show a much similar methylation pattern as more fission events can occur in the time needed for crypt

methylation patterns to become diverse. Siegmund et al., (2009a) have isolated spatially segregated crypts from across several colonic carcinomas and analysed their methylation patterns. Similar to normal colonic crypts, the epigenetic distance between the glands did not correlate with the spatial distance. Methylation patterns in each gland were consistent with multiple long-lived cancer stem cells. They also suggested that the tumour growth was characterized by rapid initial clonal expansion followed by a growth restriction. These observations suggest that colorectal cancer progression follows a uniform or 'flat' clonal distribution rather than stepwise progression (Siegmund et al., 2009a).

Here, I use these techniques to determine the expansion rate of non-dysplastic Barrett's glands. Calculating this will permit insights to the rate of expansion within a Barrett's lesion, and I will ask if gland fission and Barrett's gland stem cell dynamics are related providing new insights into how clones expand within a lesion of fixed size.

6.2 Hypothesis:

Clonal expansion is characterised by long periods of stasis and large clonal expansions are rare and may contribute to the progression of Barrett's oesophagus to cancer.

6.3 Aims:

1) To use methylation patterns of non-expressed genes to establish the rate of clonal expansion in non-dysplastic Barrett's epithelium.

2) To define the stem cell dynamics and their number within Barrett's glands using methylation patterns.

6.4 Chapter specific methods:

6.4.1 Genomic mutation screening of resection and biopsy samples:

Tissue was macro-dissected from Fresh frozen EMRs and biopsies (for details, refer chapter-2. Methods-2.2) then screened for mutations in the variable regions of p16INK4A, *TP53* and *KRAS* genes. Specimens with an identified mutation were then serially sectioned, and glands were histologically graded and then microdissected using a laser capture microscope. Glands were sequenced for the point mutation identified in the initial screen. 2-dimentional maps indicating the mutation burden of each crypt were constructed.

6.4.2 CCO-staining:

Dual CCO and SDH staining were performed on fresh frozen EMRs to identify wild type (CCO-normal) and mutant (CCO-deficient) glands. Single cells were microdissected and the mtDNA genome was sequenced.

6.4.3 Methylation analysis:

DNA was extracted from laser-captured microdissected glands and subjected to bisulphite treatment (Qiagen, UK). A nested PCR protocol was then used to generate PCR products for cloning. Specific CpG islands within the promoters of *MYOD1* and *CSX* were amplified. The primer was designed using Primer 3 website (MIT, Cambridge, Massachusetts, USA). PCR products were subjected to TA-cloning and individual white bacterial clones were picked for sequencing (approximately 8 per gland). Further, methylation patterns were converted into binary patterns, as shown in Figure 39 and statistical analysis was done.

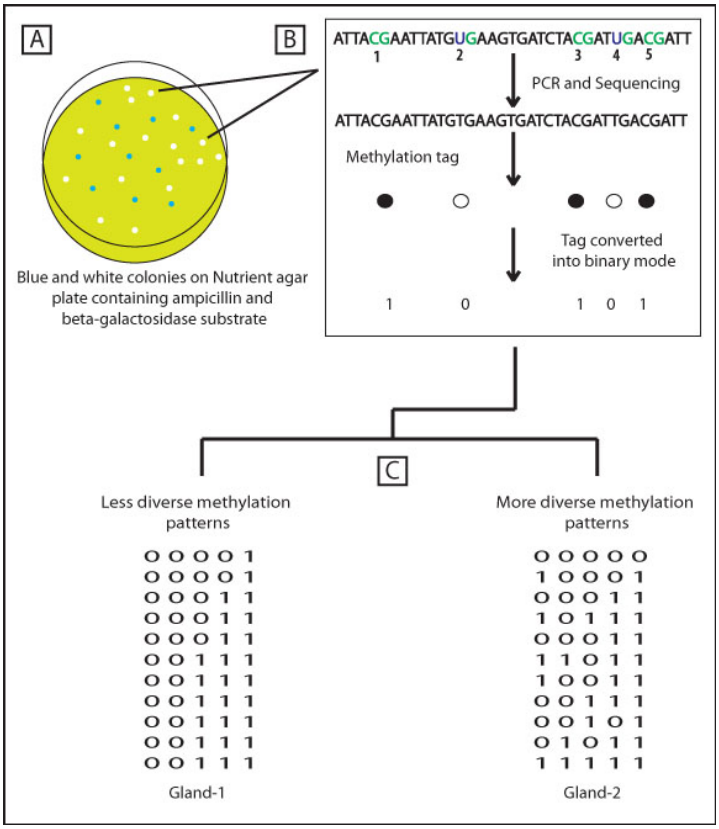

Figure 39: Schematic representation of methylation patterns, following colony PCR and sequencing being converted into binary pattern.
(A) DNA was extracted from 10-12 white colonies and subjected to PCR with M13 universal primers. (B) PCR products were then sequenced. (C) Each row represents methylation tags from individual cloned PCR products derived from bisulfite treated DNA from Barrett's gland. Each column represents CpG site in a CpG island. Gland-1 is less diverse than gland-2 (the methylation patterns are more diverse in gland-2).

6.4.4 Statistical analysis:

Methylation patterns are converted to a binary code. Methylated sites in a CpG island were represented as '1' and unmethylated sites as '0'. Epigenetic diversity was inferred by measuring the difference between methylation patterns (also called as tags) (Kim et al., 2005a).

6.4.4.1 Number of unique patterns:

It is the number of different patterns observed in a gland/clone. The number of unique patterns/tags observed within a gland reflects stem cell numbers and stem cell lineage survival. If the number of stem cells increases then, it will lead to increase diversity within a gland.

6.4.4.2 Percentage methylation:

It is the average number of methylated CpG sites in one CpG island/single locus for colonies picked from single gland/clone. For example, the MYOD tag '10011' is 60% methylated. It reflects the number of divisions since birth (Kim et al., 2005a).

6.4.4.3 Intra-gland or Intra-clone diversity (acd):

It is the average difference between the number of methylation tags within a gland/clone, which measures the epigenetic diversity within a gland/clone. For example, the diversity between MYOD tags 11000 and 00001 is three.

6.4.5.4 Inter-gland or Inter-clone diversity (icd):

It is the average number of pair-wise methylation tag differences between two adjacent and distant glands/clones.

6.4.4.5 Statistical significance test:

Statistics between groups of glands were compared using a Student t test, Mann-Whitney U tests and one-way ANOVA tests as appropriate.

6.5 Results:

6.5.1 Mutation screening of resection specimens:

Fresh frozen resection and biopsy specimens displaying BO were sequenced for mutations in *TP53*, *CDKN2A* and *KRAS*. Only 2 out of 17 specimens revealed mutations; one sample showed a somatic mutation in *CDKN2A* (c.329G>A) and *CDKN2A* LOH. The other revealed an mtDNA mutation (9715G>A). In total six specimens were analysed, and were selected because they displayed well orientated (full length) glands (Table 7). Mapping of the mutation status of each gland onto tissues sections did not reveal multiple clones in the *CDKN2A* mutant patient and all glands were positive for this mutation. The mitochondrial DNA mutated specimen revealed two negative glands amongst multiple CCO-normal glands (the comparison of methylation patterns in this case are shown towards the end of this chapter).

All 6 specimens underwent the same gland selection and bisuplhite protocol (refer Chapter 2, Methodology 2.10). Methylation pattern diversity was compared between glands and within glands. Epigenetically diverse Barrett's glands are likely to represent distant clonal expansions. However, similar methylation patterns within a Barrett's segment indicate a recent clonal expansion.

Patient ID	Age	Sex	Phenotype	Reason for tissue extraction	Targeted mutation screening
1	48	M	Metaplasia	EMR for dysplasia	*CDKN2A* (c.329G>A)
2	51	M	Metaplasia	EMR for dysplasia	mtDNA (9715G>A)
3	55	F	Metaplasia	EMR for dysplasia	None
4	57	M	Metaplasia	EMR for dysplasia	None
5	64	M	Metaplasia	Biopsy for Barrett's surveillance	None
6	72	M	Metaplasia	Biopsy for Barrett's surveillance	None

Table 7: Patient details and histological classification of tissue specimens. M-male, F-female.

6.5.2 Methylation analysis of individual patients:

The DNA from individual laser captured glands were subjected to bisulphite conversion followed by TA-cloning and sequencing to reveal the methylation patterns (8 per gland) in the promoters of CSX and MYOD1 (see Chapter 2, Methodology 2.10 Figure 12). To easily visualize gland methylation patterns I constructed tables displaying methylated CpG sites as black circles and

unmethylated sites as white circles. To illustrate the data generated I show the methylation patterns for patient 1 (Figure 40 and 41), the other patients are shown in the appendices. In patient 1, only gland-1 was wild type for *CDKN2A* and the remaining glands expressed a c.329 G>A mutation. 9 glands were successfully bisuplhite sequenced for CSX (Figure 40) and 14 were bisulphite sequenced for MYOD (figure 41).

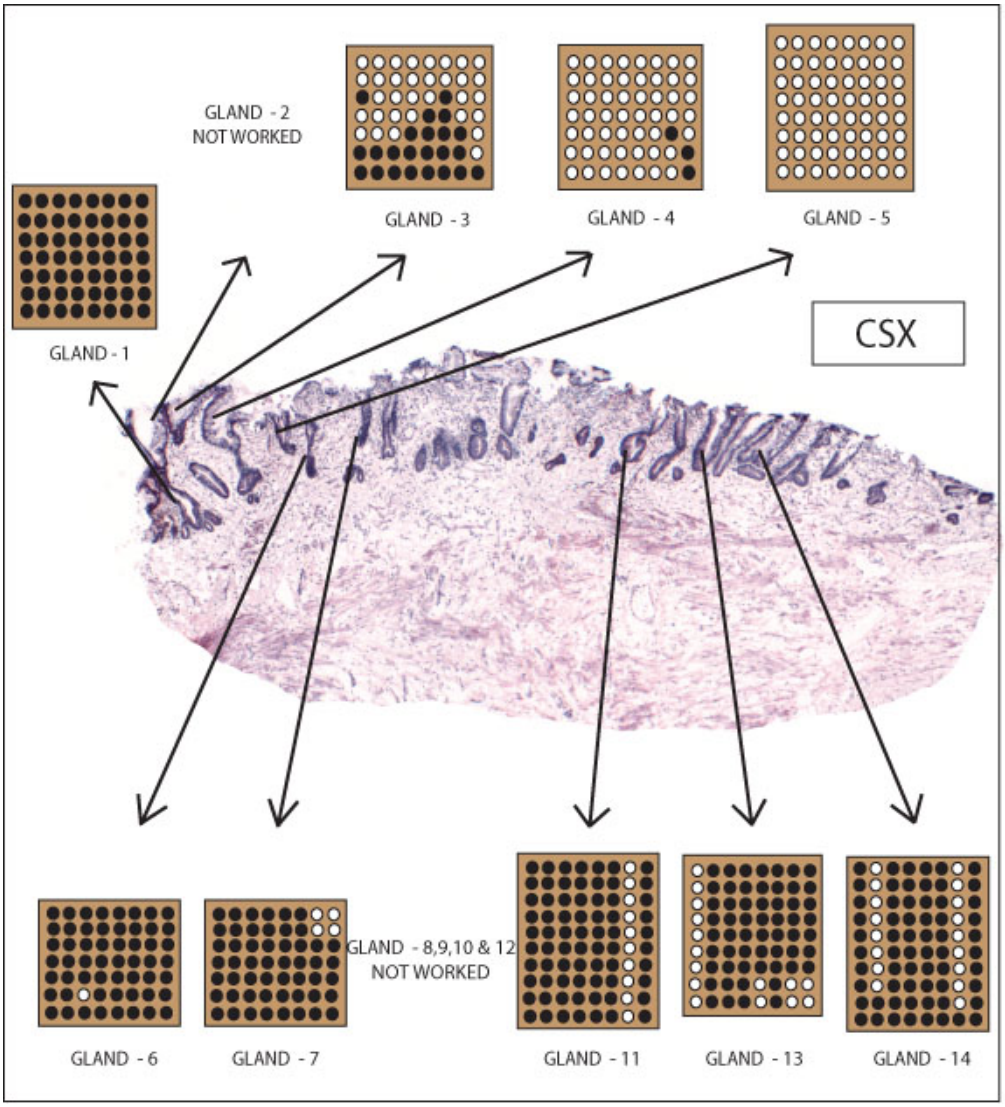

Figure 40: Epigenetic diversity in Barrett's glands (CSX, patient 1).
Each table represents methylation patterns of individual glands; rows represent the methylation status at each CpG locus and columns represents a CpG site. Black circles denote the methylated CpG sites and white circles (unmethylated).

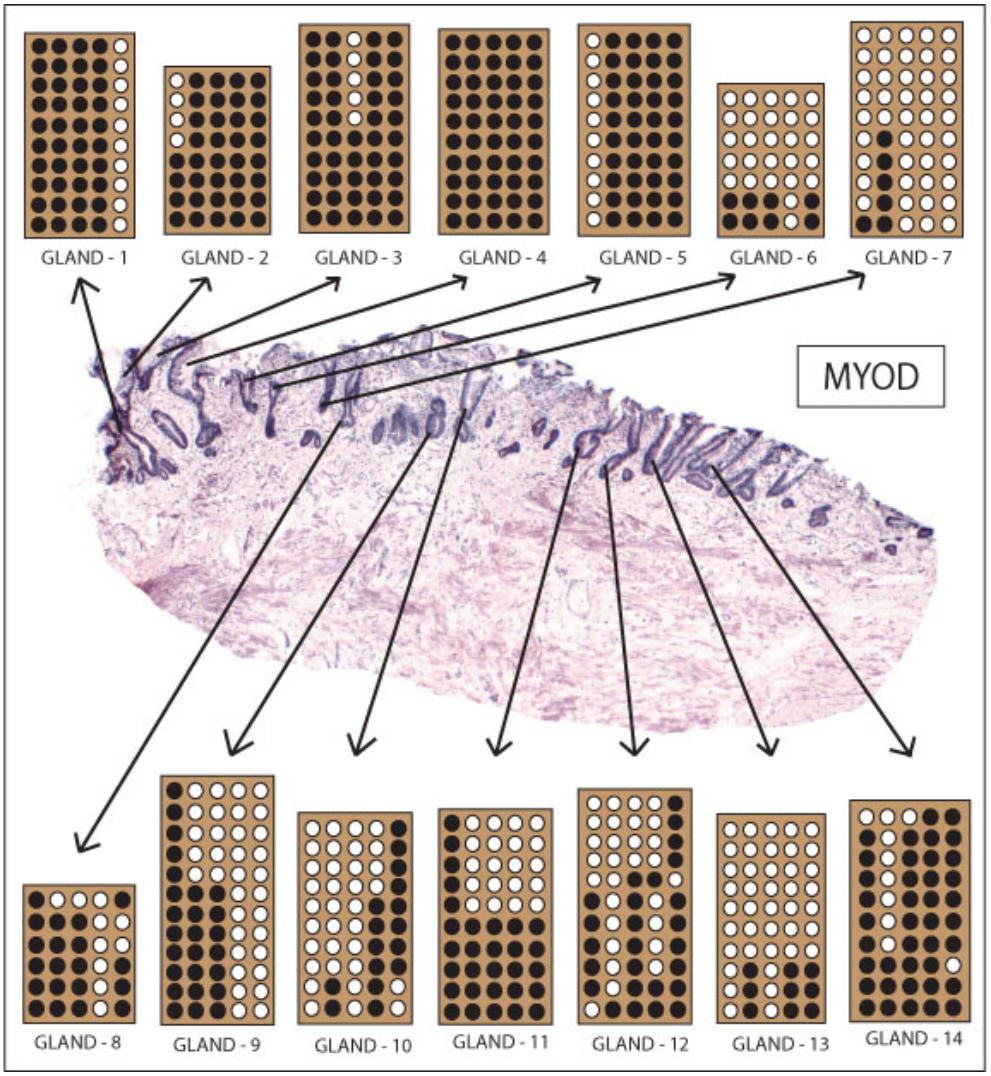

Figure 41: Epigenetic diversity in Barrett's glands (MYOD, patient 1).
MYOD methylation patterns from gland 1-14 (Patient 1), Each box, represent methylation patterns of the individual gland; each row represents a tag and each column represents a CpG site with the MYOD promoter. Black circles denote the methylated CpG sites and white circles (unmethylated).

6.5.3 Individual Barrett's glands are maintained by multiple stem cells:

The number of different methylation patterns (unique tags) observed within each gland were analysed across all 6 patients. Histologically, all glands displayed a non-dysplastic metaplastic phenotype. The number of unique tags within each individual gland demonstrated methylation pattern diversity in both both CSX and MYOD promoters (Figure 42), suggesting that stem cells were long-lived and had enough time to acquire epigenetic diversity. The mean number of unique tags may reflect the average number of stem cells within a gland were 2.9 and 2.8 for CSX and MYOD respectively. These observations suggest stem cell populations in Barrett's glands display random stem cell loss and replacement and that Barrett's glands are maintained by multiple stem cells (at least 3 per gland).

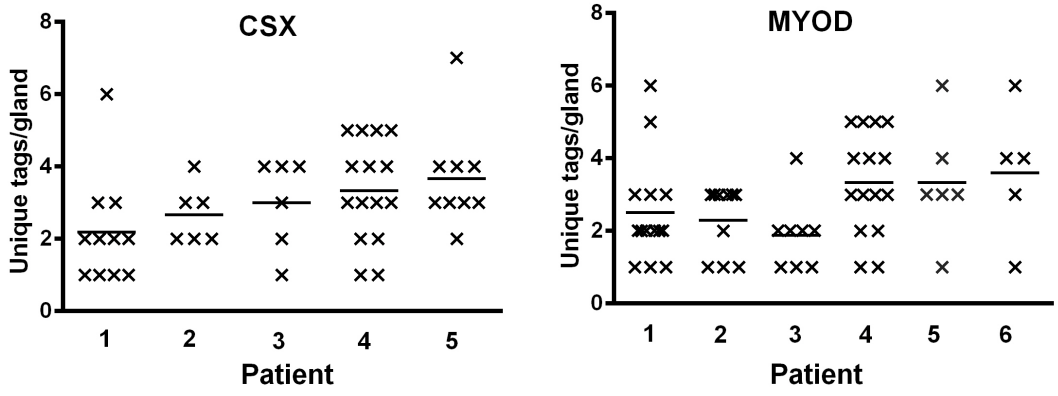

Figure 42: Graph representing number of unique tags for CSX and MYOD in patients with BO.
The number of unique tags in CSX/MYOD reflects stem cell number. There was no significant difference in the number of unique tags between patients in this study (ANOVA p=0.067 and 0.076 for CSX and MYOD respectively).

6.5.4 The relationship between percentage methylation and patient age:

The mean methylation percentage in the youngest patient was 59% (patient 1) when compared to 89% (patient 6) in the oldest individual. The distribution of individual gland methylation patterns within each patient ranged from 10 to 100% in the youngest patient and 80 to 100% in the oldest patient. There was no significant difference of percentage methylation due to age (P=0.78) (Figure 43). Based on limited number of specimens available, the data suggest that glands are of a similar mitotic age relative to patient age.

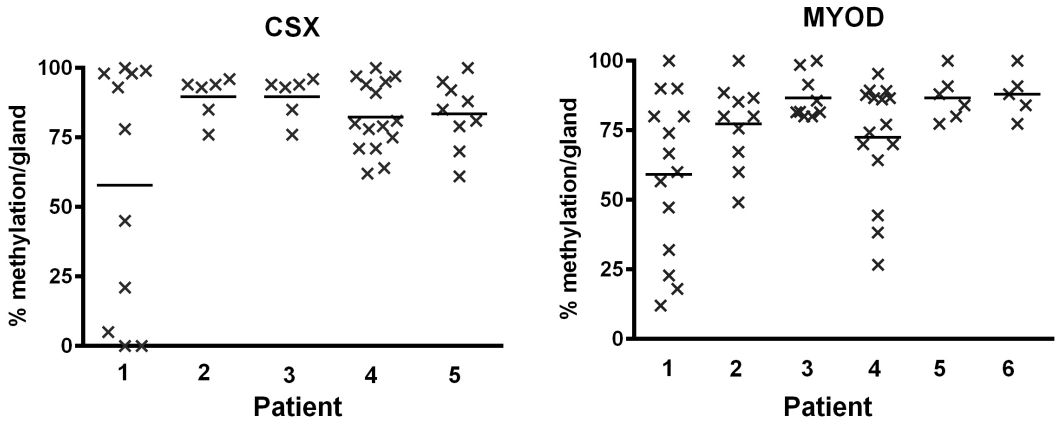

Figure 43: Percentage methylation does not change with age in CSX and MYOD promoters in Barrett's glands.
There was no significant overall difference in percentage methylation between individuals for CSX and MYOD gene.

6.5.5 Epigenetic distance as a measurement of recent clonal ancestry in Barrett's glands

The average epigenetic distance between methylation tags of each cloned PCR product reveals diversity (and therefore the degree to which each cell is related to its neighbours) and the intragland distance (ACD) of each Barrett's gland analysed within all patients for both CSX and MYOD are plotted in Figure 44. The ACD closer to 1 suggest that majority of cells were recently divided, with a quick stem cell turnover and are closely related to their ancestry.

The average epigenetic distance between glands (ICD) was measured in each patient. I compared adjacent glands versus distant glands. Adjacent glands were defined as those glands within one gland width of each other, and distant glands was those glands of greater physical distance. For each patient the ACD and ICD (adjacent and distant) was calculated based on pairwise differences between every gland and was plotted in Figure 45. In both CSX and MYOD, the ACD was lower when compared to both the ICD of adjacent and distant glands suggesting that stem cell turnover time is less than the gland division time. Furthermore, the further glands were away from each other the greater the difference in ICD (Figure 46). These observations suggest that while Barrett's glands show recent local expansions the lesion as a whole does not. The cumulative analysis of methylation distance at a CpG locus within CSX and MYOD promoters in laser captured glands from sections of Barrett's metaplasia from all 6 patients has been shown in Figure 46. Statistically significant diversity was seen when cumulative methylation patterns within a gland were compared with distant

glands (p=2.53E-05 for CSX and 5.28E-10 for MYOD). Once again suggesting, that most cell lineages were created late in progression.

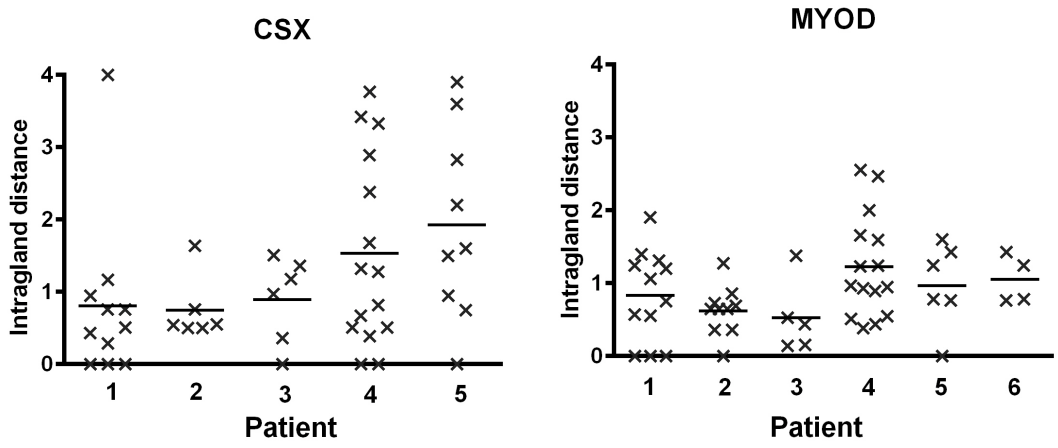

Figure 44: Analysis of ACD within CSX and MYOD promoters in laser captured glands from sections of Barrett's metaplasia.

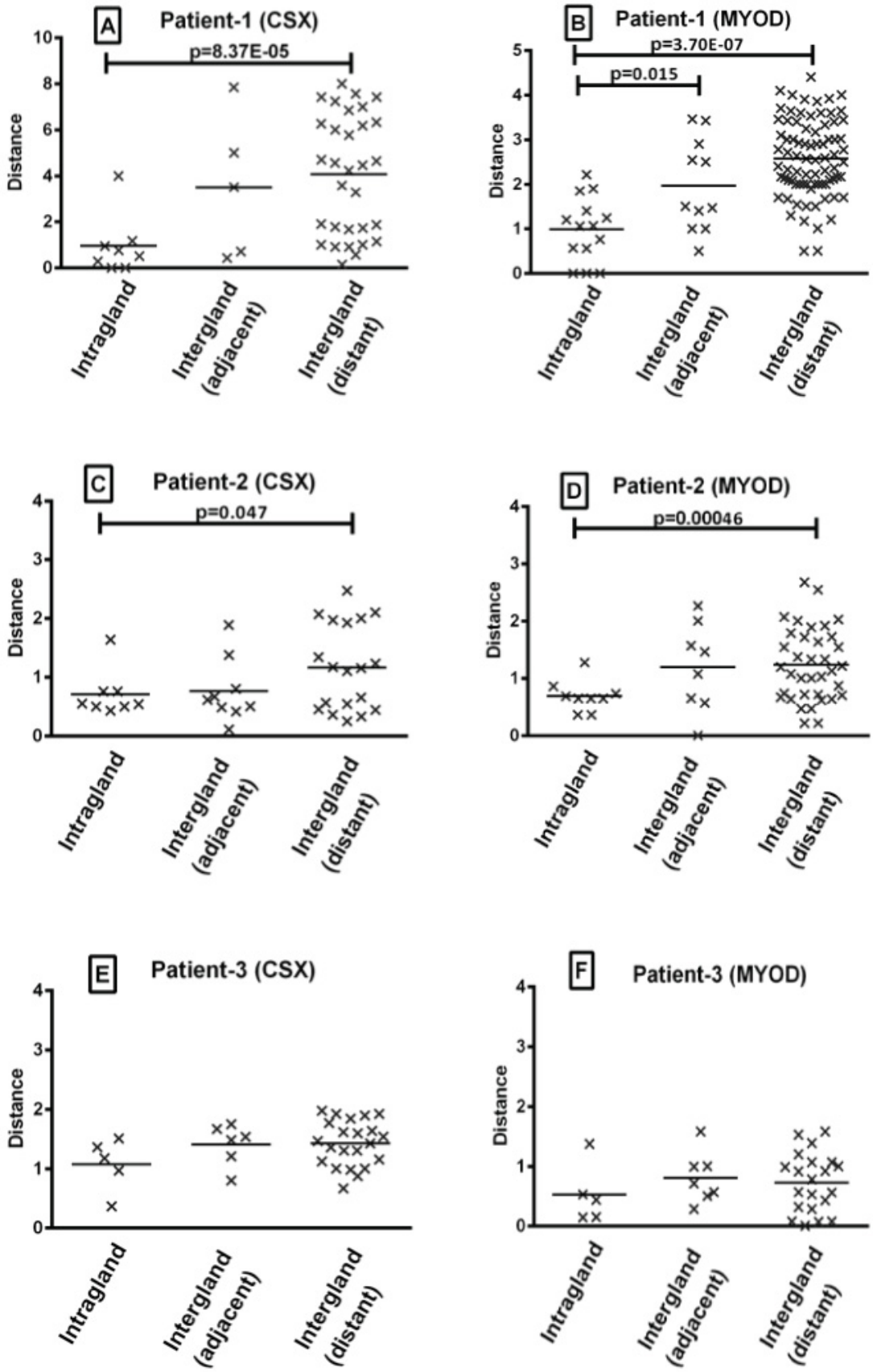
A
Patient-1 (CSX)
p=8.37E-05
Distance
Intragland
Intergland (adjacent)
Intergland (distant)
B
Patient-1 (MYOD)
p=3.70E-07
p=0.015
Distance
Intragland
Intergland (adjacent)
Intergland (distant)
C
Patient-2 (CSX)
p=0.047
Distance
Intragland
Intergland (adjacent)
Intergland (distant)
D
Patient-2 (MYOD)
p=0.00046
Distance
Intragland
Intergland (adjacent)
Intergland (distant)
E
Patient-3 (CSX)
Distance
Intragland
Intergland (adjacent)
Intergland (distant)
F
Patient-3 (MYOD)
Distance
Intragland
Intergland (adjacent)
Intergland (distant)

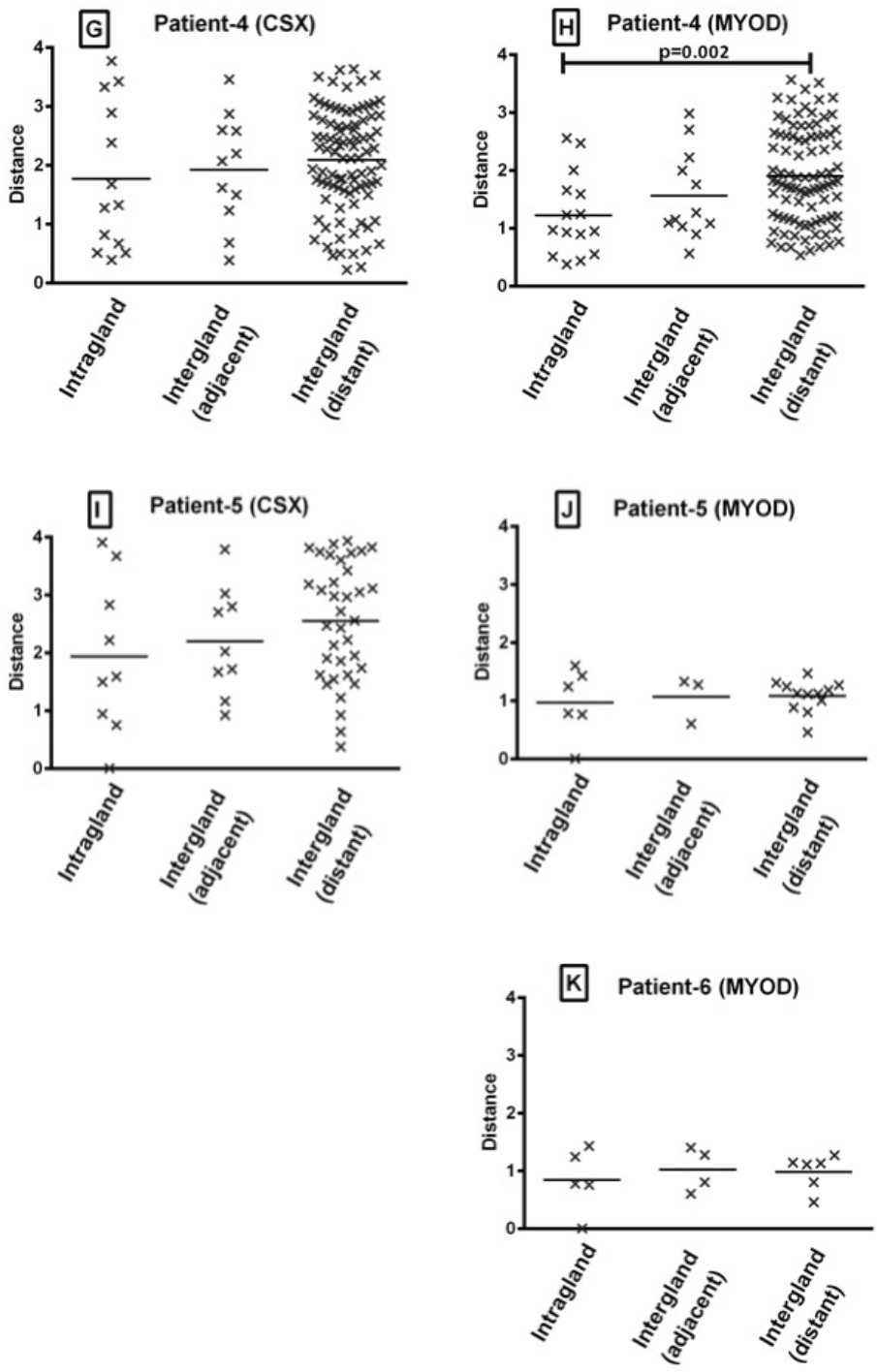

Figure 45: Analysis of methylation distance at a CpG locus within CSX and MYOD promoters in laser captured glands from sections of Barrett's metaplasia (all 6 patients).

The intra-gland methylation distance was lower when compared to comparisons of adjacent and distant glands suggesting that all cells are derived from recent stem cell expansions. The intergland methylation patterns were diverse when compared to adjacent and distant glands. Once again suggesting, that while glands show recent local expansions the lesion as a whole does not. Patient 6 CSX did not work due to lack of DNA.

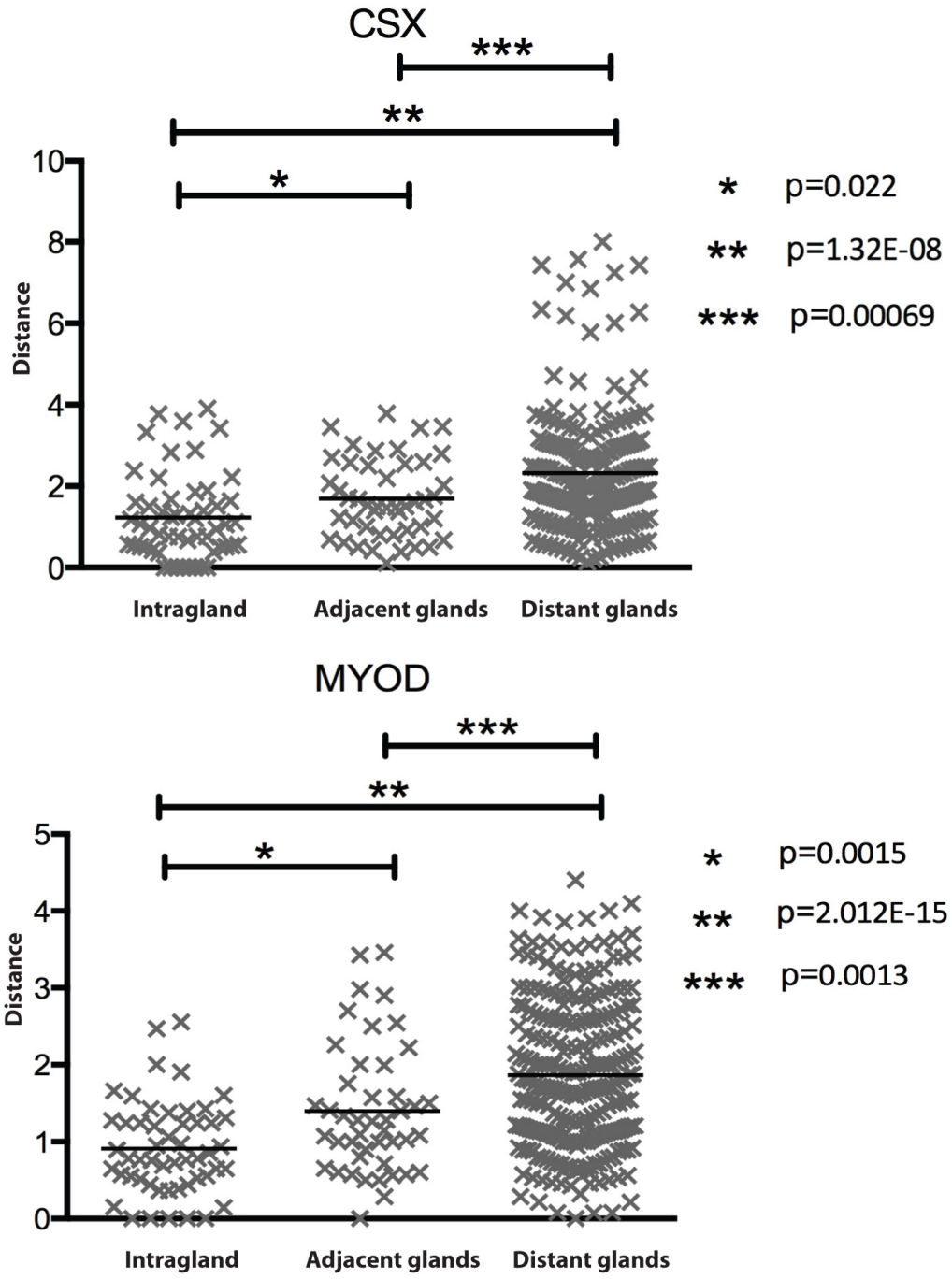

Figure 46: Overall analysis of methylation distance at a CpG locus within CSX and MYOD promoters in laser captured glands from sections of Barrett's metaplasia from all 6 patients.

The overall intra-gland methylation distance (a measure of diversity) was lower when compared to comparisons of adjacent and distant glands suggesting that all cells are derived from recent stem cell expansions. There was statistically significant diversity when cumulative methylation patterns within a gland were compared with adjacent and distant glands. Once again suggesting, that most cell lineages were created early in progression.

The cumulative representation of Percent methylation, intragland diversity (acd) and intergland diversity (icd) has been shown in Appendices, Section 8.5.

6.5.6 Methylation diversity between Adjacent and distant paired glands within Barrett's lesion:

The methylation patterns between paired glands (icd) within individual Barrett's were statistically not significant with p-value of 1.15 and 5.35 for CSX and MYOD respectively (Figure 47), indicating that the adjacent and distant glands within individual Barrett's lesion did not have sufficient time to acquire significant epigenetic diversity. This suggests that Barrett's glands within a segment are closely related, however, selective sweeps where clones expand to fixation within the segment do not occur.

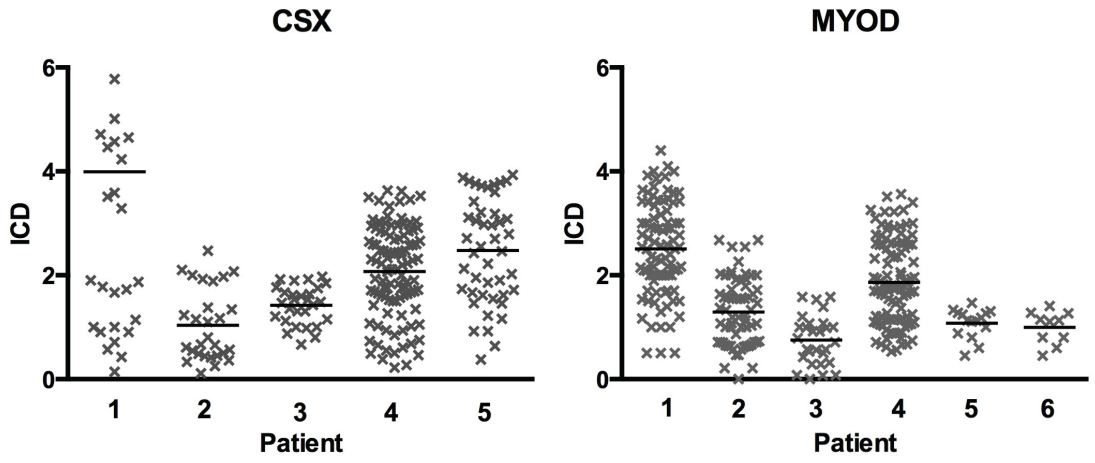

Figure 47: Epigenetic diversity within Barrett's.
Comparison within paired glands (including adjacent and distant gland) showed that methylation patterns between paired glands were statistically not significant ($p>0.05$ for CSX and MYOD using ANOVA). Methylation patterns in some glands were similar and in some they were entirely different from the majority of Barrett's glands, suggesting difference in their evolution.

6.5.7 Validation experiments: Distribution of inter-gland distance within individual Barrett's:

Before statistical analysis the data was checked for normality using Shaphiro-Wilks test. The distribution of inter-gland distance within each Barrett's lesion was plotted to validate as to whether the gland-pairs analysed were sampled from a normal distribution. P value of >0.05 is indicative of normal distribution. The data has been shown in Figure 48 and 49.

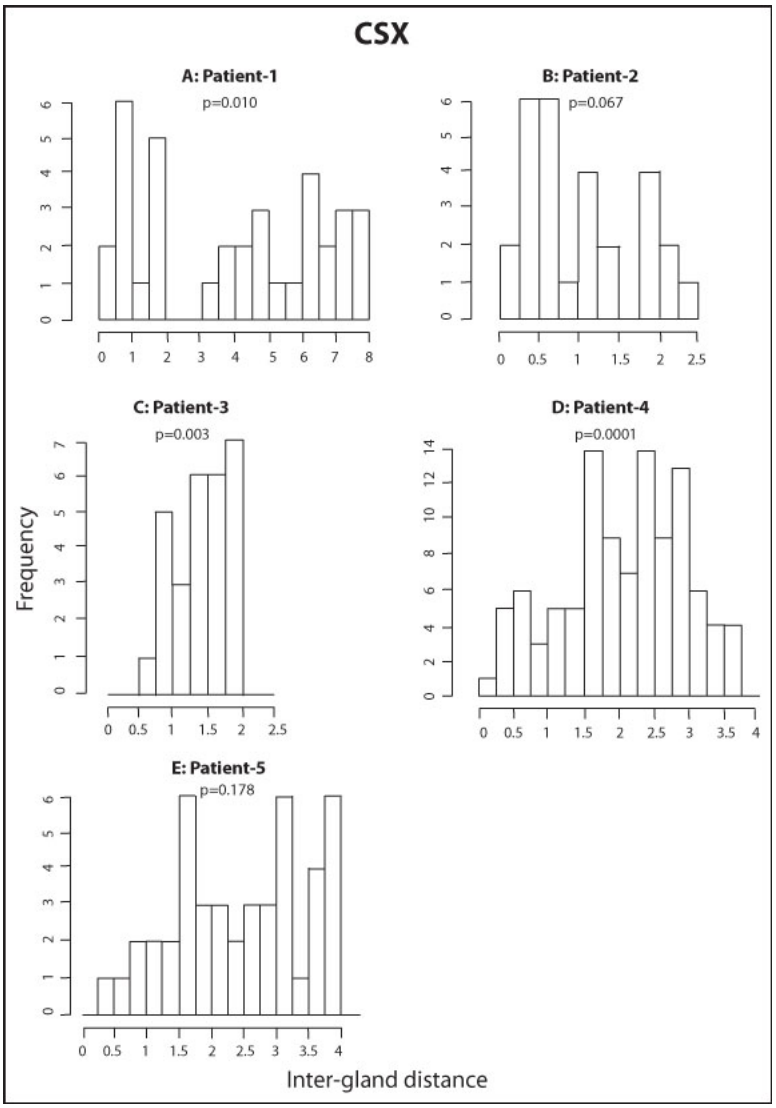

Figure 48: Histograms of ICDs for individual Barrett's (A to E are Patient 1 to Patient 5 respectively).
The distribution of ICDs was not skewed, suggesting that majority of gland-pairs were particularly more or less similar to the bulk (Shapiro–Wilks test of normality was used to check if the data was skewed, P values of >0.05 indicated the data are likely to have been sampled from a normal distribution).

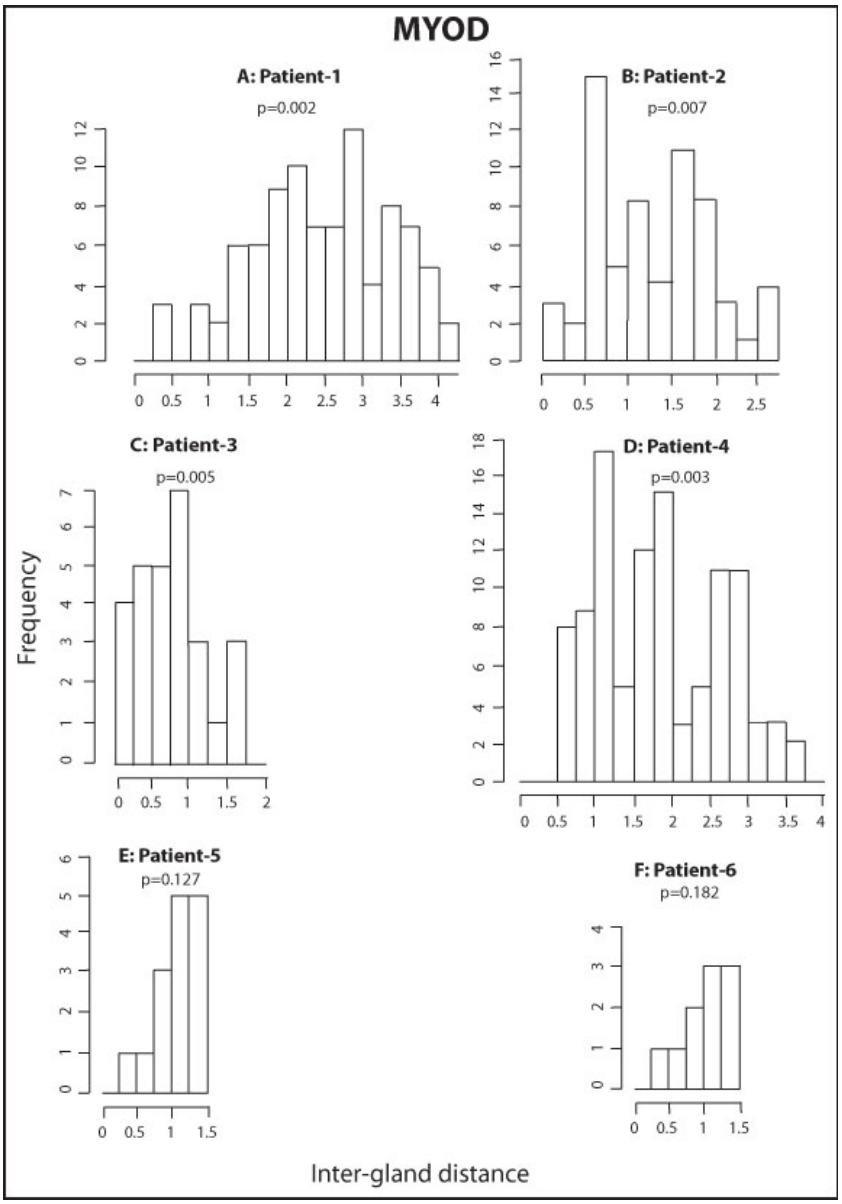

Figure 49: Histograms of ICDs from data obtained from each individual Barrett's patient.

The distribution of ICDs was not skewed, suggesting that majority of gland-pairs were particularly more or less similar to the bulk (Shapiro–Wilks test of normality was used to check if the data was skewed, P values of >0.05 indicated the data are likely to have been sampled from a normal distribution).

6.5.8 Correlation between the percentage methylation and intra-gland distance (acd) for CSX and MYOD:

The percentage methylation was compared against intra-gland diversity to compare, if the percentage methylation would reflect the diversity within a gland. The percentage methylation within a gland was comparatively low if the gland was less diverse (Figure 50), suggesting younger population of cells with lesser methylation.

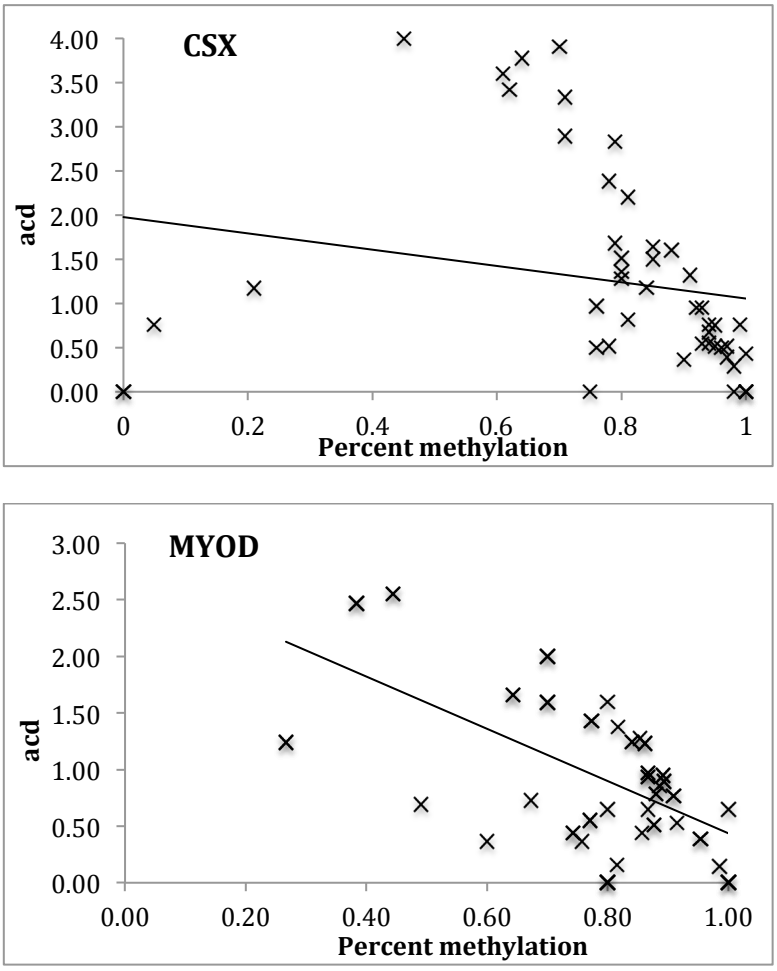

Figure 50: Correlation between percent methylation and inter-gland distance (acd) for CSX and MYOD genes (includes all patients).
There seems to be a negative correlation between the percentage methylation and intragland distance, with a correlation coefficient of -0.199 and -0.607 for CSX and MYOD gene respectively.

There was a positive relationship between percent methylation in CSX and MYOD gene with a correlation coefficient = +0.713 (Figure 51), validating observations seen in both CSX and MYOD data sets. Minor differences can be accounted for because of the number of CpG sites differ between the two promoters.

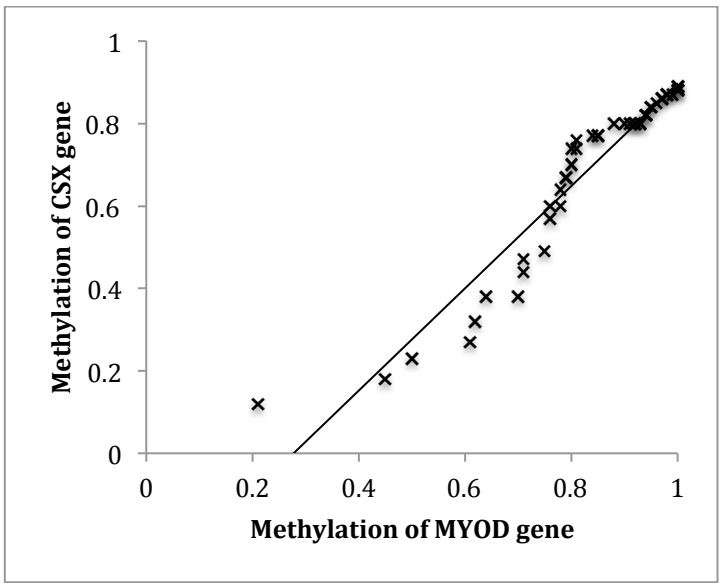

Figure 51: Correlation between average methylation for CSX and MYOD genes (all 6 patients).
There was a positive relationship between percent methylation in CSX and MYOD gene with a correlation coefficient = +0.713

6.5.9 Barrett's lesions show flat clonal expansions:

Comparing methylation patterns between two distant glands may give us the mitotic age (numbers of cell division within glands since fission) of the Barrett's segment and methylation patterns within a gland provides us with the mitotic age of each gland. Depending on the rate Barrett's glands undergo fission the mitotic age of the clone may or may not be similar to the mitotic age of each gland within the clone (Figure 52) (Siegmund et al., 2009a).

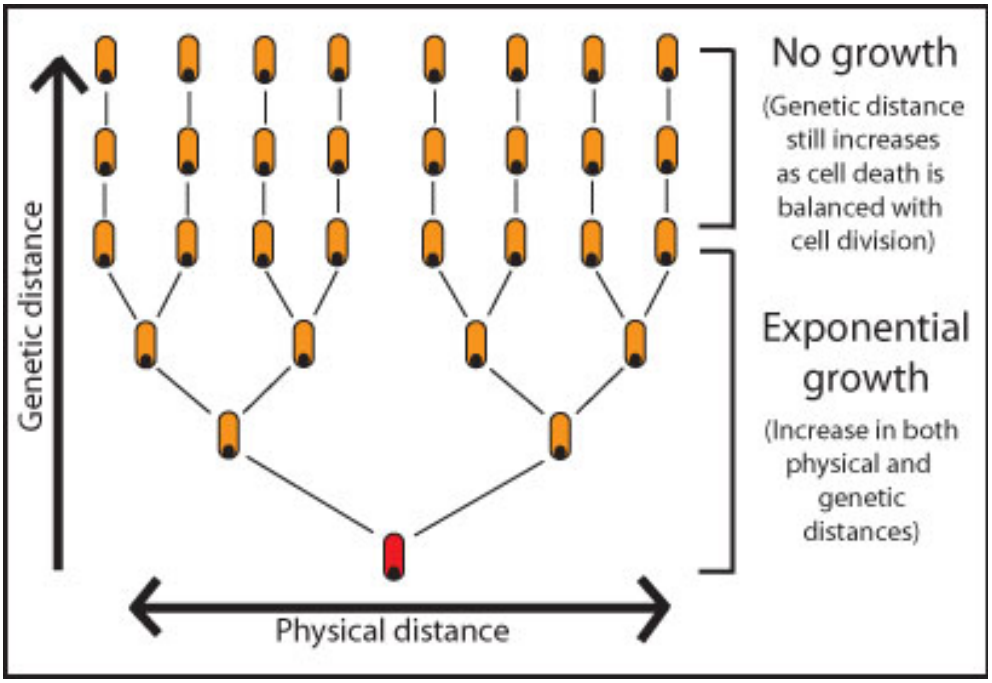

Figure 52: Schematic representation of clonal stasis using a correlation between spatial and epigenetic distance.
As the stem cell (red cell) undergoes clonal expansion, there is an increase in the physical and genetic distance between the progeny. Once the growth slows down, the physical distance does not increase, however, the genetic distance continues to grow as long as the cell death is balanced with cell division. Modified from (Siegmund et al., 2009a).

The methodology used to measure physical distance between glands has been explained in Chapter 2 (2.11.5). To elucidate this relationship, ICD was compared with the spatial distance between Barrett's glands (Figure 53). The epigenetic distance between two cells/glands is the number of pairwise differences between their methylation patterns. Glands located at the either ends of a Barrett's segment are most likely to be distantly related. Hence, by knowing the physical distance between glands, the mitotic age of a Barrett's segment can be inferred by measuring the pairwise differences between methylation patterns of these glands. In both CSX and MYOD, there was no correlation between the epigenetic and spatial distance of glands distributed through the Barrett's lesion.

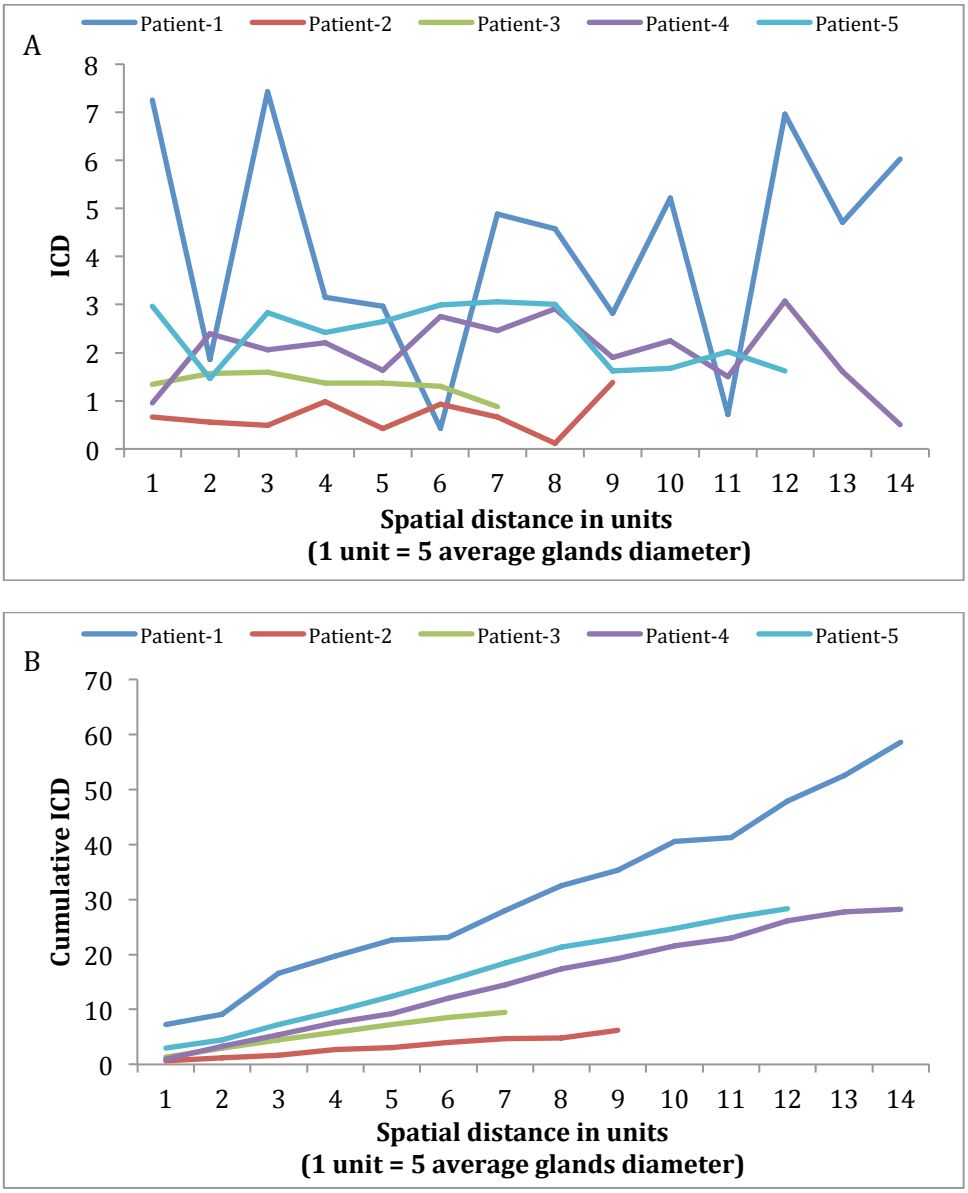

Figure 53: Correlation between spatial and epigenetic distance within Barrett's metaplasia.
(A) The spatial distance was compared against epigenetic distance. Spatial distances between glands were described as a unit, which corresponds to the average gland diameter (in pixels). The average ICD of all pairs of glands within the EMR specimen that fell within the spatial interval was computed. Each coloured line represents individual patient. There was no correlation between spatial and epigenetic distance. (B) The spatial distance was compared against cumulative inter-gland distance. If these two were more closely related, then the line would increase exponentially.

The methylation patterns of all glands from 6 patients were compared with their physical distances. The cumulative correlation has been shown in Figure 53B. There was no correlation between the epigenetic and spatial distance of the glands in CSX and MYOD gene. Methylation patterns in each gland were consistent with multiple (4-1000) long-lived stem cells. Barrett's growth is characterised by rare short-lived clonal expansions. These observations suggest that Barrett's growth progression follows a uniform or 'flat' clonal distribution as seen in colonic cancer cells (Siegmund et al., 2009a) rather than a selective sweep across the lesion.

6.5.10 Epigenetic distance analysis of clonal verus non-clonal glands:

Dual staining of cytochrome *c* oxidase (CCO) and succinate dehydrogenase (SDH, a nuclear-encoded mitochondrial enzyme) histochemistry was performed (see Methods 2.9.1) to identify CCO-deficient glands. Individual cell from each CCO-deficient gland were laser-captured and the mitochondrial genome was sequenced (see Methods 2.11). All blue (CCO-deficient) glands were clonal for a mtDNA mutation (c.9715G>A, see Figure 54. The methylation patterns obtained from both CSX and MYOD clones in both CCO-deficient and CCO-normal Barrett's glands are shown in Figure 55. There was no significant difference between the intra-gland diversity and inter-gland diversity between clonal and non-clonal/unrelated glands ($p=0.55$ and 0.65 for acd and icd respectively), suggesting that mtDNA mutation detected was clonal and did not have any effect on epigenetic diversity (Figure 54, 55, and 56).

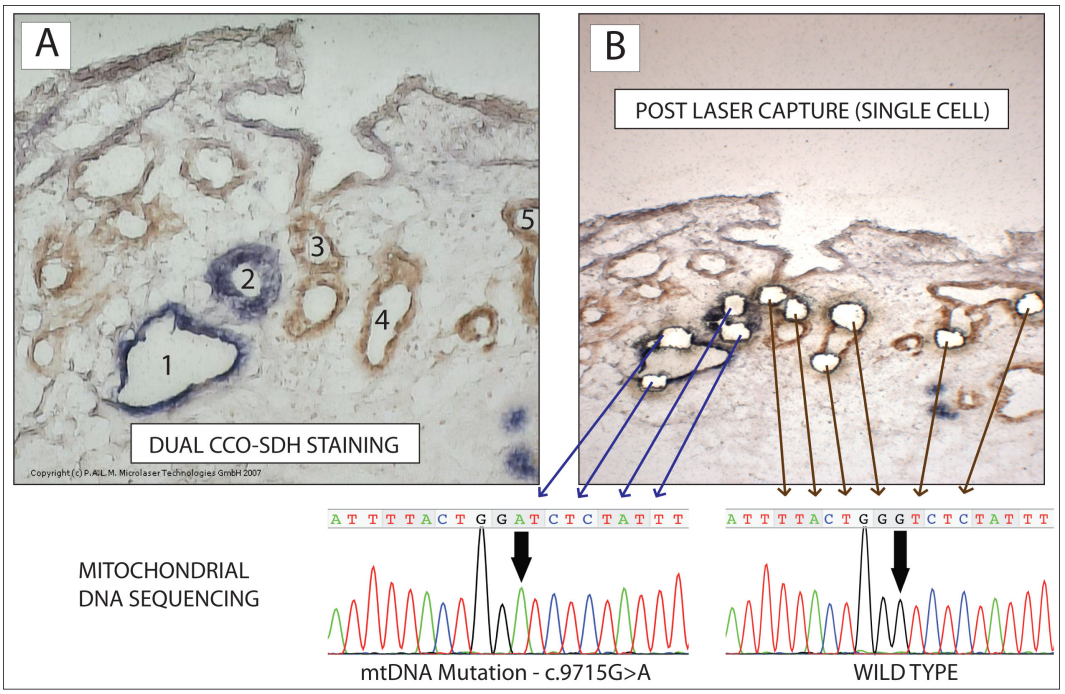

Figure 54: Dual cytochrome C-oxidase and succinate dehydrogenase enzyme histochemistry from patient 2.
(A) Showing clonally related (Blue) and unrelated (Brown) glands, the blue patch consists of 2 CCO deficient glands (gland-1 and 2). (B) Laser capture microdissected small cell areas of the individual gland in serial section. CCO deficient glands contained the same mtDNA mutation (9715G>A) suggesting common ancestry, whereas, brown glands (CCO positive) were wild type for the same mutation.

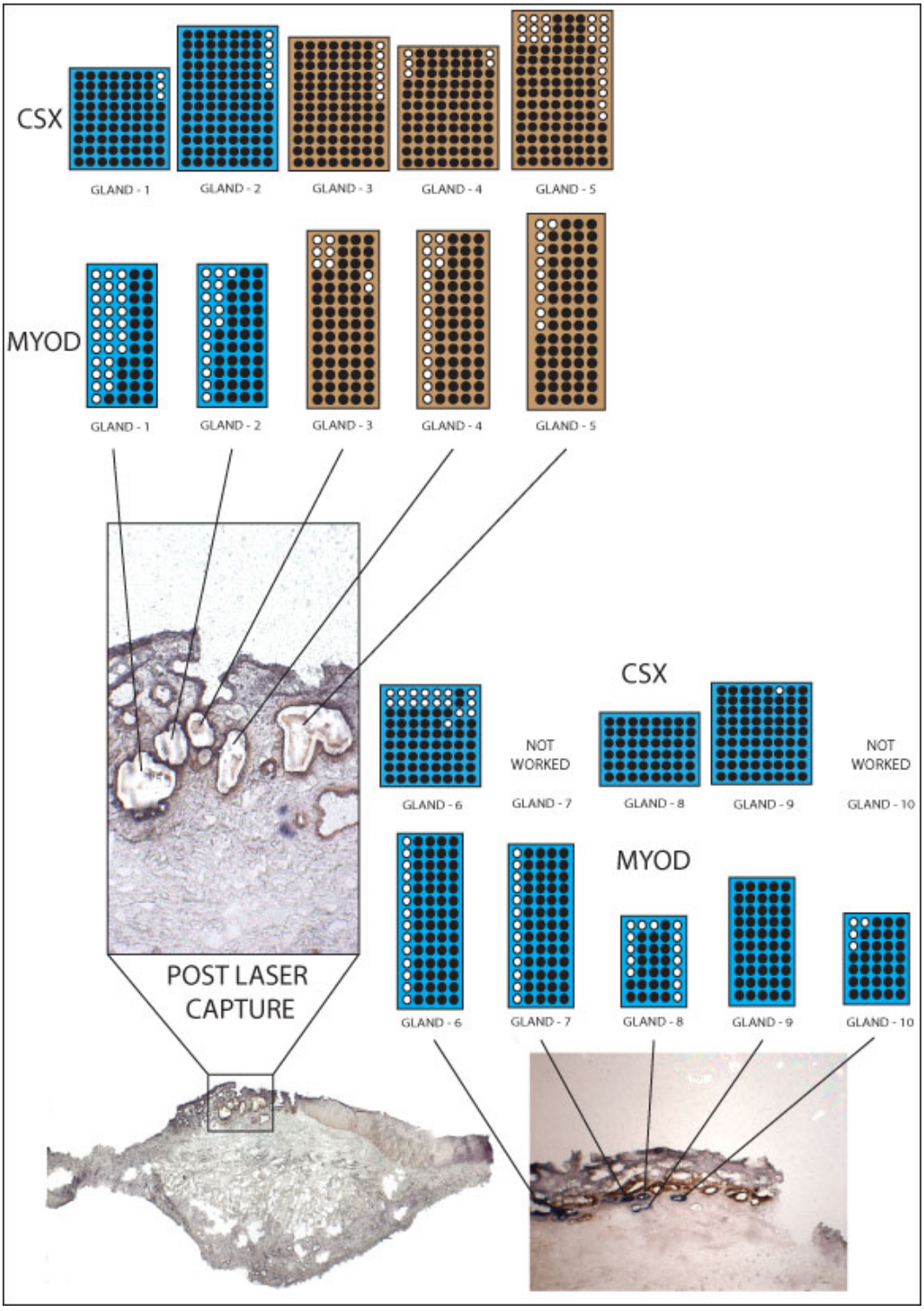

Figure 55: Methylation pattern from an EMR (patient 2) containing clonally related (Blue) and unrelated crypts (Brown) for CSX and MYOD gene.
Filled circle denotes the methylation status of each CpG site (methylated) and unfilled circles (unmethylated). The methylation pattern confirms epigenetic diversity within the gland compared to adjacent and distant glands.

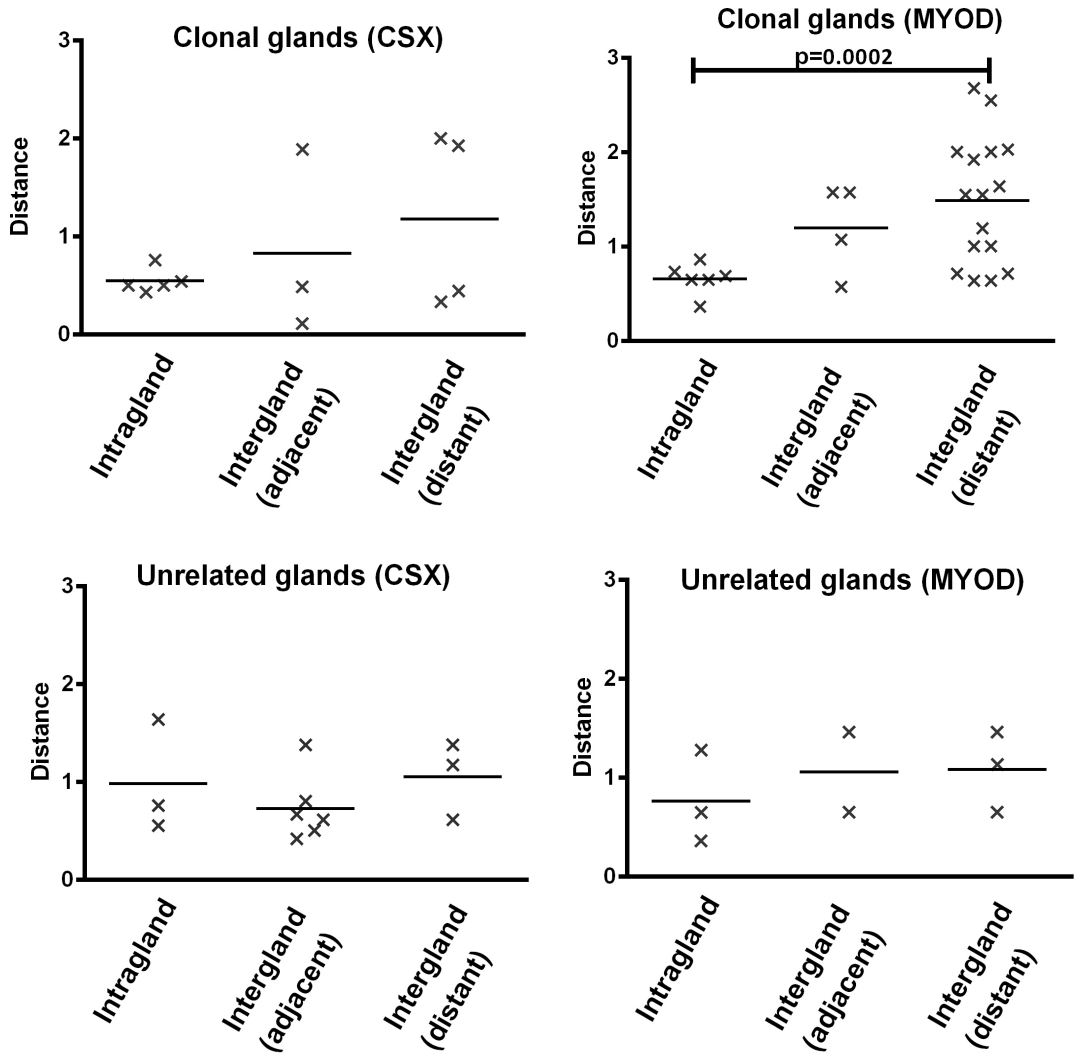

Figure 56: Analysis of methylation distance at a CpG locus within CSX and MYOD promoters in laser captured glands from sections of Barrett's metaplasia (patient 2).

In clonally related CCO-deficient glands; the intragland methylation distance (a measure of diversity) was lower when compared to comparisons of adjacent and distant glands in both CSX and MYOD promoters. In clonally unrelated CCO-positive glands; the Intra-gland methylation distance (a measure of diversity) was lower when compared to comparisons of adjacent and distant glands only in MYOD promoter, suggesting that all cells within the gland are derived from recent stem cell expansions.

6.5.11 Clonal expansion rate of Barrett's glands:

The growth rate of colonic adenomas has been calculated using a mathematical model. Methylation pattern between adenomatous crypts were compared with the same number of colonic crypts using case-resampling bootstrap method (Graham et al., 2011a). After applying a correction for methylation percentage, they found that there was no significant difference between the ICD's of adenoma and normal colonic crypts with $p<0.01$ (Humphries et al., 2013).

The two models constructed for estimating clonal expansion rate in the colon were applied to Barrett's because both the colonic crypt and the Barrett's gland expand by fission. Two assumptions were made (1) the 'Burst' model assumes all clonally-related crypts were formed rapidly with no further crypt division and (2) the 'continual' model assumes steady growth wherein crypts divide every *f* years. Epigenetic diversity seen in colon, fitted the burst model better than the continual model, wherein, sublcones demonstrate a more recent ancestry than the adenoma as a whole (Humphries et al., 2013). This can be directly applied to a Barrett's segment where the bulk methylation distance can reflect the time taken for gland expansion over the segment. Here, I have compared the average inter-gland epigenetic diversity (icd) of Barrett's glands from all five patients and plotted this against both models (indicated by yellow coloured box and whisker plot in Figure 57, with the thick black line representing the median). The furthest distance between the glands in each case was calculated and glands within 50% of the distance were grouped into one (indicated by the brown coloured box and whisker plot below) and glands with >50% of the distance, were grouped together (indicated by the blue coloured box and whisker plot below). The

comparison was made between these two groups and also against bulk glands (yellow coloured box and whisker plot below) in individual Barrett's specimen (Figure 58).

The Inter-gland methylation distance between distant glands was lower when compared to comparisons of adjacent glands. The black line within each yellow box and whisker plot represents the median and crosses the burst model growth line (red line). The diversity observed within Barrett's suggests that the time since Barrett's glands were derived from a single (transformed) ancestral gland was on an average around 14 to 15 years (Figure 59).

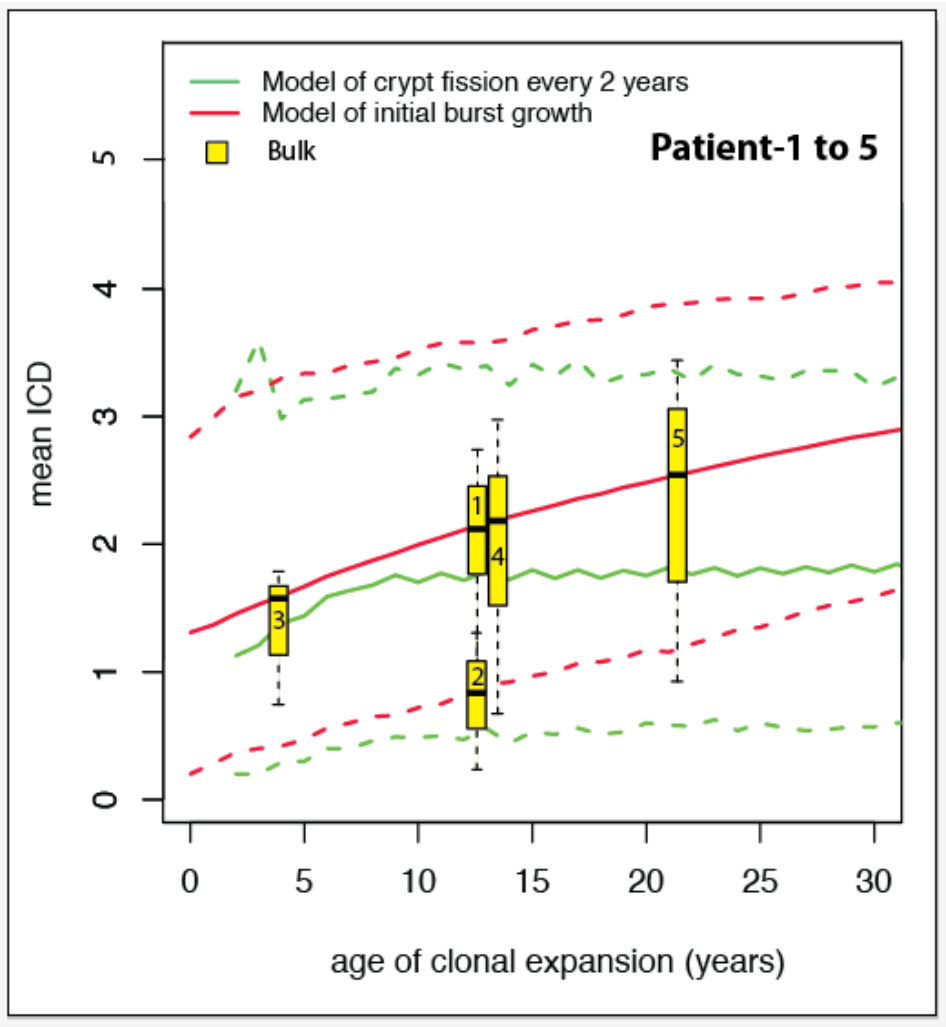

Figure 57: The combined ICDs of individual patients plotted against the colonic model of fission.
The epigenetic diversity in the burst model (red line) and the continual model (green line). The dashed line represents 95% quantiles of the simulated values. ICDs of Barrett's glands combined from each patient are presented here. The overall ICDs from all 5 patients was plotted against the colonic model of fission.

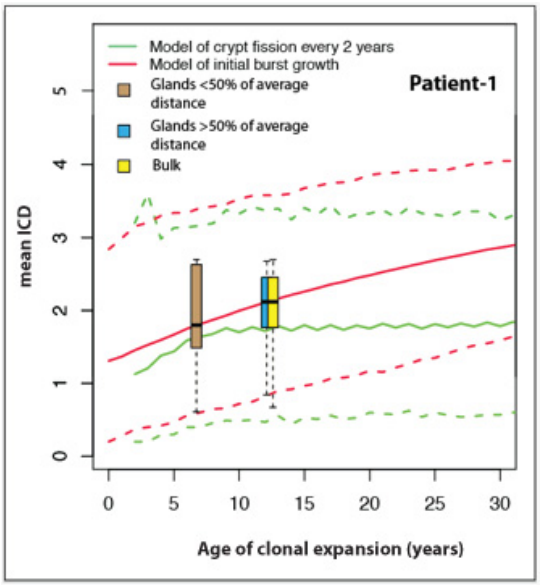
Model of crypt fission every 2 years
Model of initial burst growth
Glands <50% of average distance
Glands >50% of average distance
Bulk
Patient-1
mean ICD
Age of clonal expansion (years)

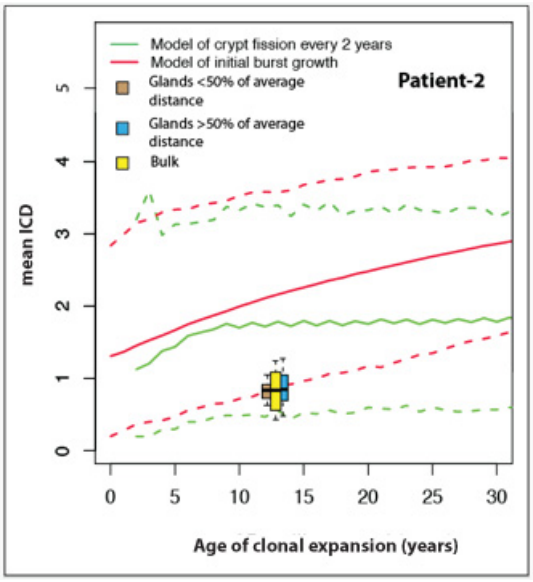
Model of crypt fission every 2 years
Model of initial burst growth
Glands <50% of average distance
Glands >50% of average distance
Bulk
Patient-2
mean ICD
Age of clonal expansion (years)

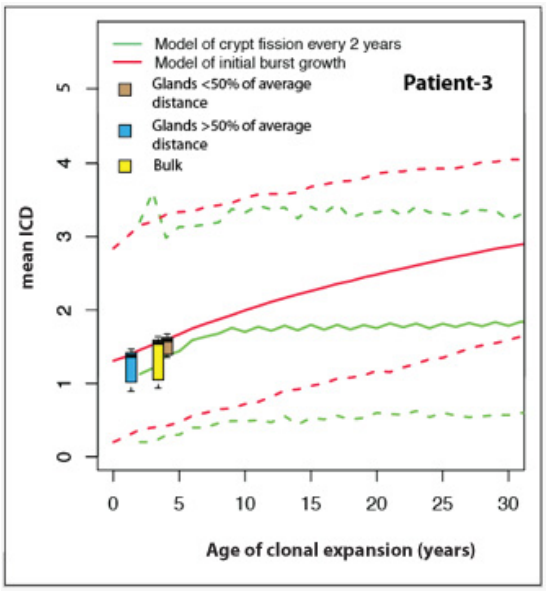
Model of crypt fission every 2 years
Model of initial burst growth
Glands <50% of average distance
Glands >50% of average distance
Bulk
Patient-3
mean ICD
Age of clonal expansion (years)

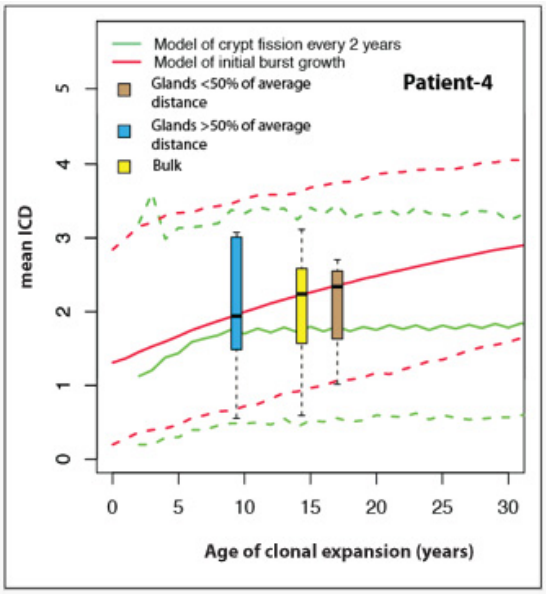
Model of crypt fission every 2 years
Model of initial burst growth
Glands <50% of average distance
Glands >50% of average distance
Bulk
Patient-4
mean ICD
Age of clonal expansion (years)

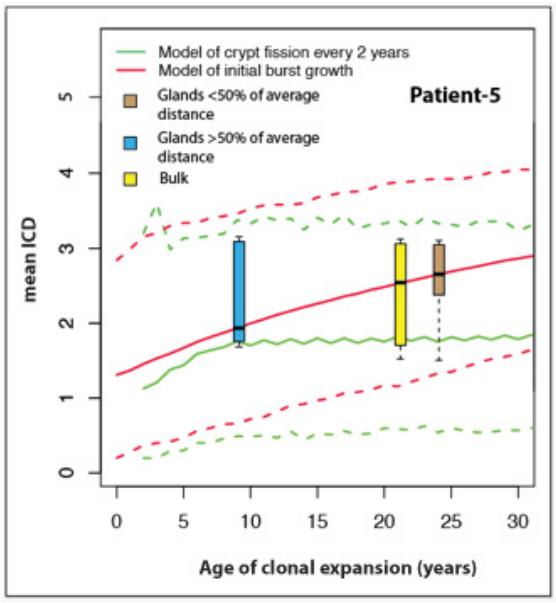

Figure 58: Modeling of the clonal expansion rate in Barrett's from all patients studied.
The median intergland distance between Barrett's glands was simulated with a mathematical model used to estimate colonic adenoma clonal expansion rates. e. The 'burst' model, (red lines) and 'continual fission' model (green lines) are plotted. Interrupted lines represent the 95% quantiles. The ICDs from all Barrett's patients with glands located less the average physical distance between all glands (green box and whiskers) and those greater than 50% of distance (blue) were plotted. The median ICD for all glands was also plotted (as bulk, yellow).

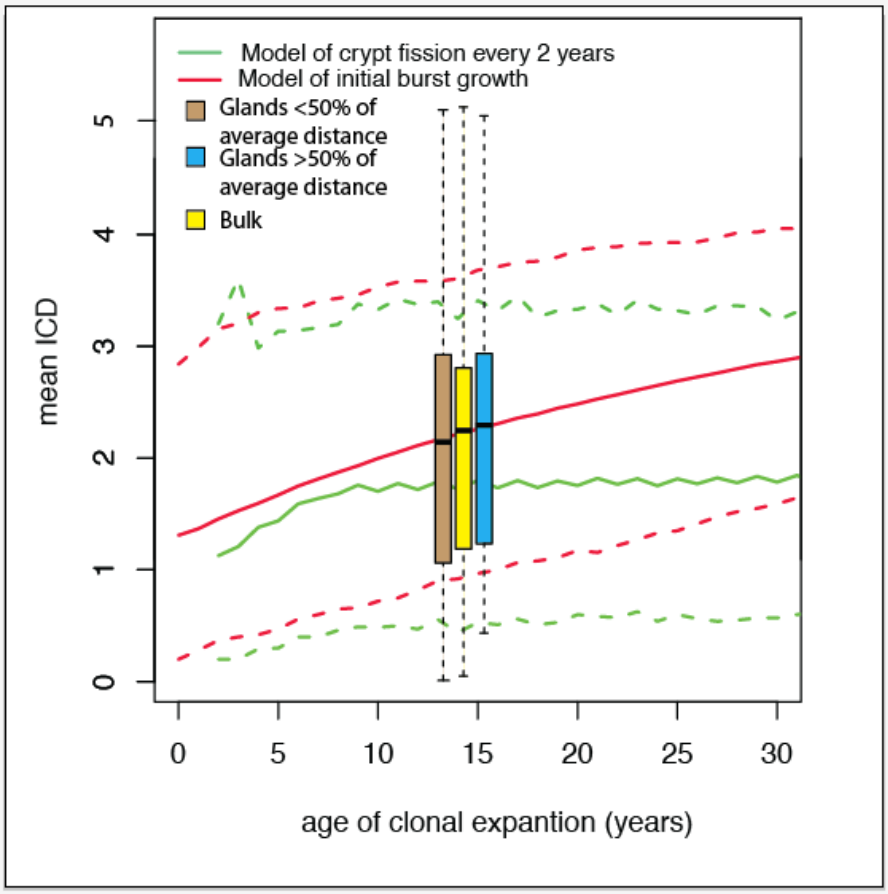

Figure 59: Modelling of Barrett's gland expansion rate (Cumulative).
Epigenetic diversity between Barrett's glands was simulated with a mathematical model used to estimate colonic adenoma growth rate. The epigenetic diversity in the burst model (red line) was higher than the continual model (green line). Interrupted lines represent 95% quantiles. The ICDs from all Barrett's patients with glands present in >50% of the distance, <50% of distance and the bulk, have been represented by brown, blue and yellow Box and Whisker plots with median ICDs of 2.40, 2.28 and 2.34 respectively. The time since Barrett's glands was derived from a single ancestral gland was around 14 to 15 years.

6.5.12 Construction of phylogenetic trees:

Phylogenetic trees were created to understand the evolutionary history of Barrett's glands from single specimens using methylation data to give an insight into the degree of ancestry between glands in this study. Phylogeny was built using a neighbour-joining (nj) method using the analysis of phylogenetics and evolution (ape) package in the R statistical computing programme (Paradis et al., 2004). Each leaf represents an individual Barrett's gland (length of the tip does corresponds to its relative mitotic age) (Figure 60). These observations suggest Barrett's glands do not follow a linear pathway of progression. Widely separated glands similar to a "Y" shaped tree, likely shared a last common ancestor when compared to adjacent glands which shared a more recent common ancestry.

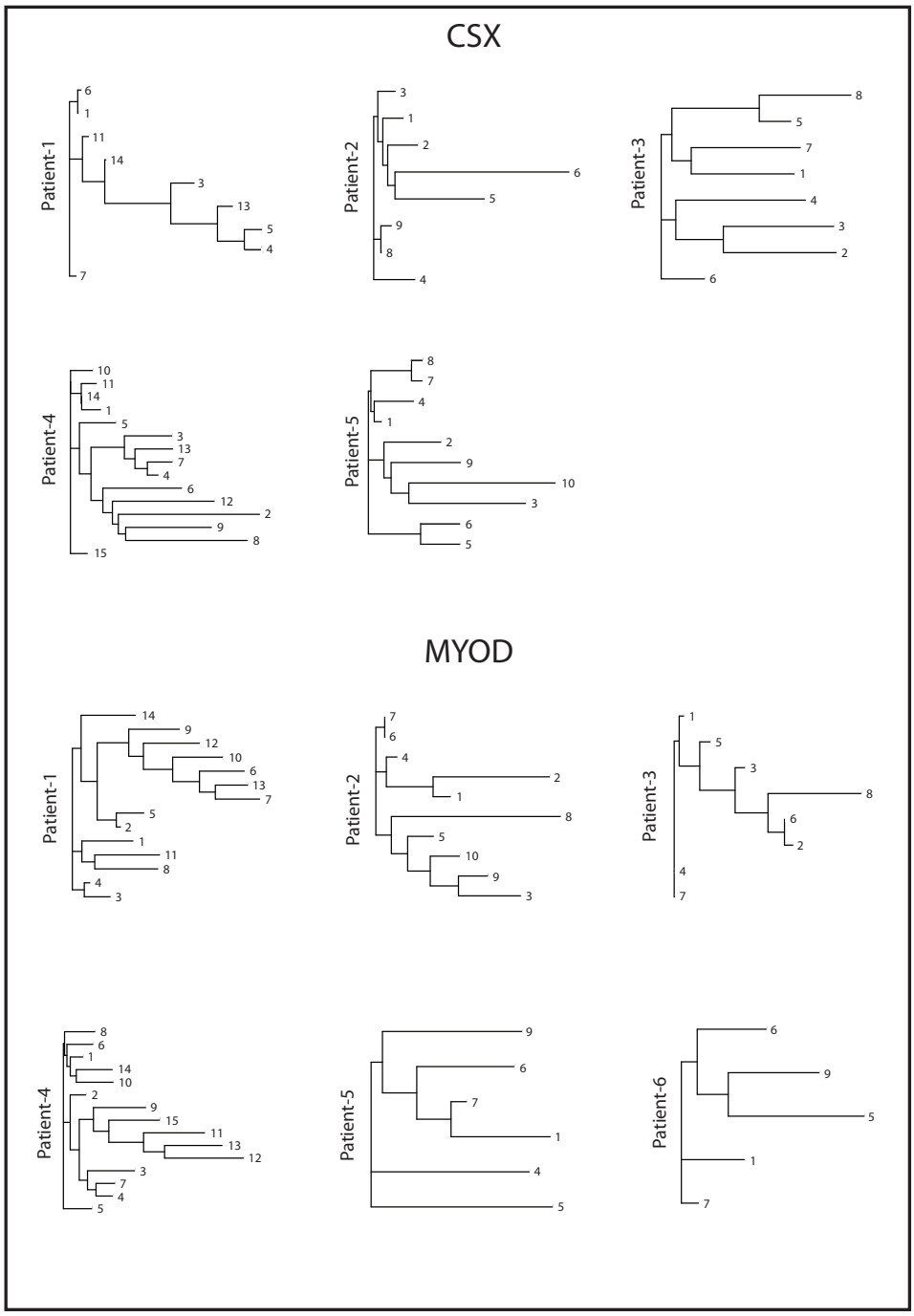

Figure 60: Phylogenetic trees of Barrett's glands relations using their methylation patterns.

Methylation pattern diversity between glands (icd) was used to create a phylogenetic tree for each patient. Analysis of phylogenetics and evolution (ape) package in the R statistical computing programme was used to create neighbour joining (nj)-trees. Each tip represents individual Barrett's gland (length of the tip does correspond to its mitotic age).

6.6 Conclusions:

1) Barrett's gland is maintained by at least 3 long-lived stem cells:

There was a trend towards a rising number of unique tags with age but was statistically not significant. The number of unique patterns/tags observed within a gland reflects stem cell numbers. Methylation patterns within a gland observed in this study were variable and each gland showed at least 3 to 4 different methylation patterns (Figure 61). These stem cells were long-lived and had enough time to acquire epigenetic diversity, suggesting that the Barrett's gland is maintained by at least three stem cells.

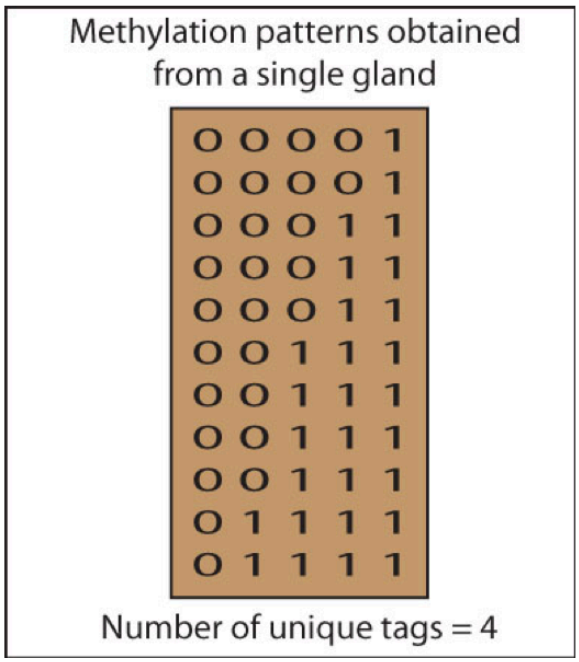

Figure 61: Barrett's gland is maintained by more than one stem cell.
Methylation tags sampled from a Barrett's gland. Each row represents methylation tags from individual cloned PCR products and each column represents CpG site in a CpG island. Methylated site in a CpG island are designated as '1' and unmethylated site as '0'. The number of unique patterns/tags observed within a gland reflects stem cell numbers (4 stem cells in the above figure) and stem cell lineage survival. If the number of stem cells increases then, it will lead to increase diversity within a gland.

2) Barrett's segments as a whole are mitotically older that individual BO glands:

The methylation patterns within a gland (acd) were less diverse when compared to adjacent or distant glands, which in turn were comparatively more diverse (Figure 62). Barrett's stem cells follow niche model with random stem cell loss and replacement leading to niche succession, which counteracts further methylation changes, leading to relatively less diverse methylation patterns within a gland. The populated cells within a Barrett's gland appeared to be mitotically recent compared to the rest of the Barrett's lesion. Our data suggests that the growth of Barrett's metaplasia is slow allowing sufficient time for the adjacent and distant crypt to acquire epigenetic diversity.

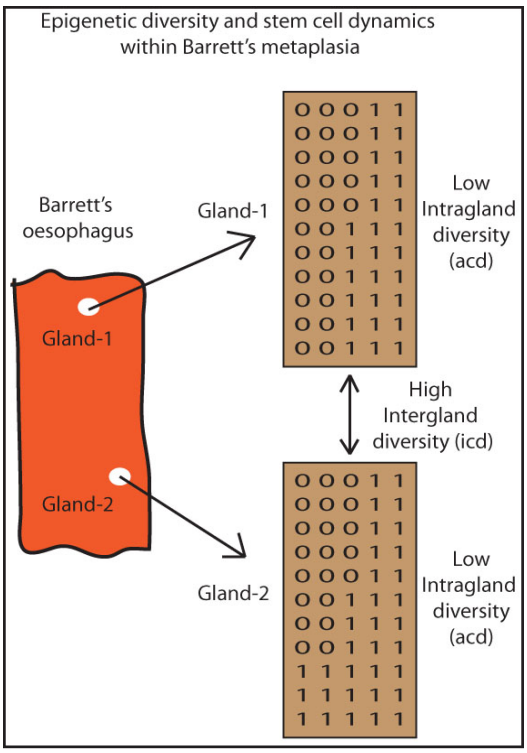

Figure 62: Illustration of epigenetic diversity within Barrett's.
The methylation patterns within individual gland were less diverse when compared against each other, suggesting that distant glands had sufficient time to acquire epigenetic diversity.

3) Correlation between epigenetic diversity and spatial distance:

There was no correlation between the epigenetic and spatial distance of the glands in all six specimens analysed, suggesting that epigenetic diversity is independent of the spatial distance between Barrett's glands (Figure 63). Barrett's follows start-shaped phylogeny wherein the methylation patterns between distant glands remain less diverse (flat distribution) and the cell lineages were created early in progression.

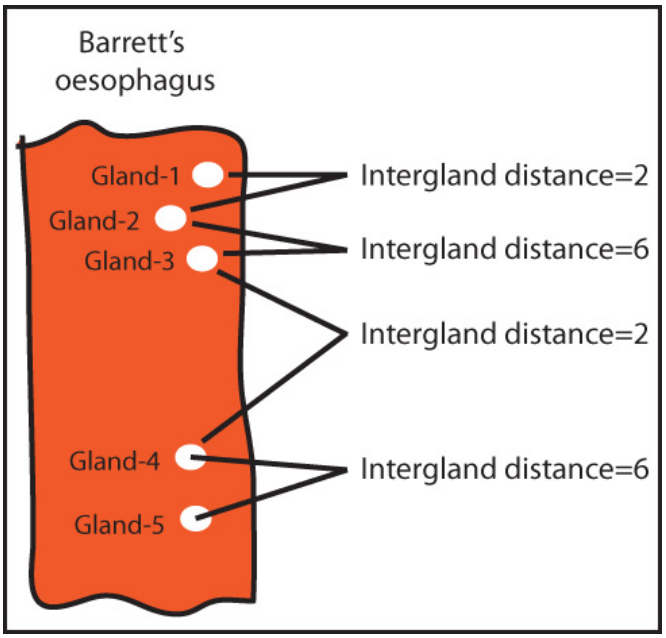

Figure 63: Correlation between epigenetic diversity and spatial distance.
The physical distance between Barrett's glands did not correlate with their intergland epigenetic distance.

4) Barrett's oesophagus shows the flat clonal progression: There was no correlation between the epigenetic and spatial distance of the glands in CSX and MYOD gene. The methylation patterns within adjacent glands were as unrelated as distant glands. These observations suggest, 'burst' model growth with flat clonal distribution.

5) Epigenetic diversity within clonally related glands:

The methylation patterns between adjacent clonal glands with same *CDKN2A* mutation were different and similarity seemed to be independent of clonality (Figure 64).

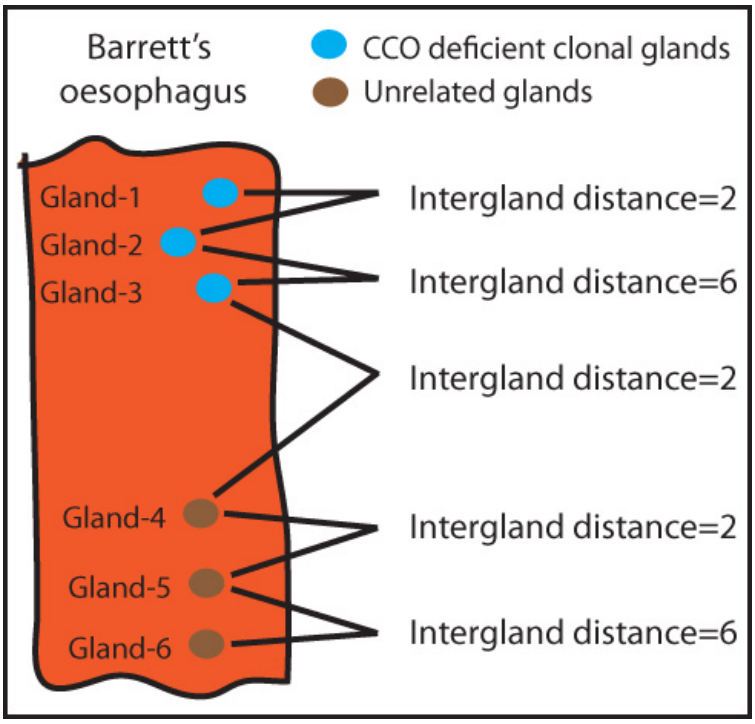

Figure 64: Epigenetic diversity comparing clonal versus unrelated glands
Methylation patterns between clonal glands (Blue circles) were as diverse as unrelated glands. Mitochondrial mutation did not seem to have any impact on the epigenetic diversity within clonally related glands.

6) The time since Barrett's glands were derived from a single (transformed) ancestral gland was on an average around 14 years.

6.7 Discussion:

Our knowledge about Barrett's oesophagus lacks information regarding progression of Barrett's lesion. It is also difficult to predict how and when an individual develops Barrett's lesion. Most human models towards Barrett's progression are based on inferences, as it's hard to observe the growth of Barrett's lesion directly. Since ancestry gets recorded in the cell genomes, it is possible to use random replication error to record cellular ancestry. Interpreting molecular phylogeny requires sophisticated quantitative analysis. It is logical to say that bigger lesions must have started as smaller and localised lesion, and the size of Barrett's lesion should correspond to its age. The 'molecular clock' hypothesis suggests that the greater the number of divisions since a common ancestor, the greater the number of differences (Bromham and Penny, 2003). If Barrett's lesion expands through sequential step-wise clonal expansions, then the newer population of cells should be more diverse than the older population of cells. However, if the lesion develops to it full extent and subsequently becomes stable, then the population of cells/glands should be less diverse and should be of similar age. In this study, it has been shown that Barrett's follows 'burst' model growth causing cell lineages to be created early in progression followed by a stable/flat growth.

Epigenetic alterations such as promoter methylation in non-expressed genes have been used to study stem cell dynamics in the colon, small intestine, endometrium and hair follicles (Yatabe et al., 2001, Kim et al., 2005a, Kim et al., 2005b, Kim et al., 2006b). Yatabe et al., have shown that normal human colonic

crypts are long-lived and contain multiple stem cells. Methylation patterns within a crypt show that these stem cells undergo constant bottlenecks and two continuous counteracting but invisible forces namely drift (difficult to document as mutations in normal human tissue are rare (Martin et al., 1996)) and extinction are involved in shaping crypt diversity (Yatabe et al., 2001). Methylation patterns within a gland or crypt give an opportunity to understand invisible cell fates during somatic evolution. We shall be using this methodology to assess dynamics of BO. Barrett's gland also contains multiple stem cells, which are long-lived and acquire diverse methylation patterns.

Nicholson et al., have shown that CCO-deficient patches consisting of at least 3 to 10 glands are clonal, containing same mtDNA mutation and have suggested that patch increases in size by the process of gland fission (Nicholson et al., 2012). In this study, the methylation patterns between clonally related adjacent glands were different, suggesting that epigenetic diversity is independent of clonality. Adjacent glands were more closely related than a distant gland. Furthermore, the physical distance between Barrett's glands did not correlate with their epigenetic distance. These observations suggest gland fission was a slow process allowing sufficient time for two daughter glands to become epigenetically diverse.

In Colon, it has been shown that CCO-deficient patch increases in size by the process of crypt fission and the patch size increases with age (Taylor et al., 2003, Greaves et al., 2006). The rate of niche succession in colon following radiotherapy has been shown to be around one year (Campbell et al., 1996). In

intestinal crypts, Kozar et al., (2013), have shown that there are at least five to seven functional stem cells in healthy intestinal crypts when compared to nine in adenomas, of which majority are involved in replacing stem cell loss and a minority of stem cells are responsible for tumour growth (Kozar et al., 2013). Recently, to understand the clonal evolution of stem cell populations within the human colon, Baker et al., (2014), have used mtDNA mutation to trace clonal lineage and shown that during a lifetime, normal human colonic crypts undergo fission at least once every 30 to 40 years. They have also shown that there are at least 5 to 6 functional stem cells within a normal colonic crypt. Loss of APC gene seems to increase the crypt fission rate and there was an increase in the functional stem cell number within APC mutated crypts, indicating its importance in tumour growth. However, the data here was insufficient to calculate any patch size. Despite Barrett's glands being clonal for the somatic genomic mutation (patient 1) and mtDNA mutation (paient 2), the Barrett's glands contained multiple unique patterns, suggesting that each gland contained multiple long-lived stem cells (Baker et al., 2014). Methylation patterns within clonal Barrett's glands had various patterns suggesting, niche succession was a slow process, providing sufficient time to acquire de novo methylation. Calculating the rate of niche succession in BO was not possible, as this requires more accurate information about the rate of methylation and stem cell division.

The correlation between methylation patterns in CSX and MYOD gene is due to the difference in the number of CpG sites (CSX has 8 CpG sites compared to MYOD, which has five) and due to the differences in site-specific methylation rates. Increasing the number of CpG sites does not necessarily improve the

accuracy of results as methylation is acquired randomly leading to epigenetic drift, which increases by increasing the number of CpG sites (Yatabe et al., 2001). The average methylation pattern diversity within different clones is a better measure of diversity (Graham et al., 2011a).

The time scale from Barrett's to OA is unclear. In a case report, a long-term follow--up of a patient with Barrett's over a period of 15 years has shown that it took nearly nine years for a patient to progress from short segment BO to long segment BO and further to OA (Iwaya et al., 2016). During its progression through MDC sequence, Barrett's glands are exposed to various evolutionary selective forces. If specific somatic genomic/mtDNA mutations confer a selective advantage to a gland (or clone), then that clone would expand rapidly and methylation patterns would be homogenous due to not enough time having passed for them to have become drivers. The high epigenetic diversity seen within clonally related BO glands suggests only weak selection for that particular clone. Methylation pattern data analysis in BO has suggested, that Barrett's glands comprised of a more recent common ancestor when compared to the whole Barrett's segment. In other words, the Barrett's segment consists of mitotically older population, but BO glands show recent local expansions. The time since Barrett's glands were derived from a single (transformed) ancestral gland was on an average around 14 years. Relative stasis with infrequent rapid regional growth may be the characteristic of BO.

Chapter 7: Discussion

Chapter 7: Discussion

Cancer genomic studies have revealed significant intra-tumour heterogeneity (ITH) with branching phylogenies (Siegmund et al., 2009b, Sottoriva et al., 2013). However, the origins of genetic heterogeneity are unknown. Tumorigenesis is always thought to be secondary to stepwise accumulation of driver alterations (Fearon and Vogelstein, 1990) and is a dynamic process; the ancestral history gets recorded within the cell genomes (Greaves and Maley, 2012, Vogelstein et al., 2013). In the absence of selective sweep, information regarding early growth phase may be recorded within genomes giving rise to genetic heterogeneity, which becomes evident in the final lesion. The heterogeneity could be due to the presence of multiple sub-clonal/private alterations, most of which are said to be non-dominant (passenger mutations/alterations) and can be detected through systematic sampling and genomic profiling of various regions within a lesion (Sottoriva et al., 2015). Hence, a quantitative analysis to understand Barrett's growth dynamics is needed.

It is still debatable as to whether every Barrett's gland arises from a single clone or if there are distinct groups of glands forming multiple clones. The development of oesophageal cancer involves genetic changes and mutations are known to accumulate in Barrett's glands as they go through the metaplasia-dysplasia-carcinoma sequence (MDC). Earlier studies into the genetic evolution of BO have lead to the theory that BO is a genetically clonal lesion from which cancer can arise (Galipeau et al., 1999). However, recent work by Leedham et al.,

has shown that there are multiple independent clones present; therefore, BO is a genetically heterotypic disease. Furthermore, Maley et al., have shown that genetic diversity increases the risk of cancer progression (Maley et al., 2006). Since Barrett's is a premalignant lesion, left in-situ enabling follow-up, it acts as an excellent model to understand the genetic progression from Barrett's to OA. This present study was based on examining Barrett's on a gland-by-gland basis in resected material showing all stages of the MDC sequence to explore the relationship of genetic diversity with progression towards OA.

7.1 Summary of major conclusions from this thesis are;

1) Barrett's dysplasia exhibits genetic heterogeneity.

2) Dysplasia appears to develop independently of *TP53*, *CDKN2A* (p16) and *KRAS* point mutations since wild-type dysplastic glands were observed.

3) The presence of a *TP53*, *CDKN2A* (p16) and *KRAS* mutation in associated cancer suggests that the mutated clone, but not the wild-type dysplastic clone, progressed to cancer.

4) Oesophageal carcinomas are monoclonal outgrowths from polyclonal dysplasia.

5) Dysplastic changes occur in the basal glands but not the upper crypt and surface epithelium in continuity and showing distinct maturational changes were a clonal proliferation. The differentiating upper gland and surface mucosa share the same *CDKN2A* mutation as the basal dysplasia.

6) Heavy mutational burdens in critical tumour suppressor genes can be associated with apparently normal gland organisation and certainly without the appearances of dysplasia.

7) Neo-Barrett's seems to be genuinely a *de novo* Barrett's lesion, and not a recurrence of the clone that gave rise to the OA. However, longitudinal samples from patients who develop new cancer in neo-Barrett's oesophagus will help to confirm these findings.

8a) Barrett's gland is maintained by more than one long-lived stem cell. The number of unique tags in Barrett's glands increased with age and the methylation patterns within individual glands were diverse.

8b) Epigenetic diversity in Barrett's metaplasia: the methylation patterns within a gland (ACD) was less diverse when compared to adjacent or distant glands, which were comparatively more diverse.

8c) Cells within a Barrett's gland appeared to be mitotically recent compared to the rest of the Barrett's lesion. Our data suggests that the growth of Barrett's metaplasia is slow allowing sufficient time for the adjacent and distant glands to acquire epigenetic diversity.

8d) Barrett's oesophagus shows a flat clonal progression: There was no correlation between the epigenetic and spatial distance of the glands in CSX and MYOD gene. The methylation patterns within adjacent glands were as unrelated as distant glands. These observations suggest flat clonal distribution.

8e) Epigenetic diversity within clonally related glands: the methylation patterns between adjacent CCO-deficient clonal glands and glands sharing same *CDKN2A* mutation were different and similarity seemed to be independent of clonality.

8f) There was no correlation between the epigenetic and spatial distance of the glands.

8g) The time since Barrett's glands were derived from a single (transformed) ancestral gland was at least four years and averages around 14 to 15 years.

In Chapter - 3, using targeted somatic genomic mutational status of Barrett's glands, I have shown that Barrett's metaplasia and dysplasia arise from more than one clone suggesting polyclonality, whereas, oesophageal adenocarcinoma seems to be monoclonal. The temporal distribution of clones and their interaction appears to play a vital role in tumorigenesis. Maley et al., using whole biopsy samples, have suggested that BO results from the proliferation of a single progenitor cell (Maley et al., 2004b). However, Leedham et al., used laser capture to analyse on a gland-by-gland basis and have shown that multiple independent clones exist within Barrett's oesophagus (Leedham et al., 2008). Here, I have shown that only one clone progresses to carcinoma and, therefore, Barrett's adenocarcinomas are monoclonal. These observations suggest clonal interaction in premalignant tissue, leading to a bottleneck scenario, wherein the dominant clone progresses to cancer (Gerlinger et al., 2012).

I found that some dysplastic glands to be wild type, indicating that mutations in these targeted genes may not be the only dysplasia-causing event. Here, a change in phenotype could be due to mutations in other genes or other exons of the same genes, which were not considered in the study. It has been shown that biopsies from the tumour only reveals a minority of genetic alterations present

in the entire tumour (Gerlinger et al., 2012), highlighting the importance of deep sequencing and whole genome sequencing.

Clonal expansion via crypt fission is seen in the colon (Greaves et al., 2006), small intestine (Gutierrez-Gonzalez et al., 2009), gastric mucosa (McDonald et al., 2008) and indeed in gastric intestinal metaplasia (Gutierrez-Gonzalez et al., 2009) patches of clonally-identical crypts are seen, strongly suggesting that crypt or gland fission is the process underlying this expansion. Recently, Barrett's glands have been shown to be clonal populations and Barrett's mucosa contains large groups of clonally-identical glands (Nicholson et al., 2011), and it appears probable that mutant clones involved in the development of Barrett's dysplasia also clonally expand via gland fission, probably with a growth advantage conferred by the p16 or *TP53* mutation. On the other hand, immediately adjacent glands may not be derived from the same clone (Rhiner and Moreno, 2009). There is no evidence that Barrett's segments increase in length with time (Gatenby et al., 2007). Martens and colleagues have drawn attention to the fact that many pre-cancerous tissues have a distinct spatial structure, which will impinge in the manner in which clones expand (Martens and Hallatschek, 2011, Martens et al., 2011). Such spatial structure, coupled with the possibility that clones can interfere or compete, can lead to lower adaptation speeds in comparison to non-structured or well-mixed populations, and this will increase the time to acquire a given number of driver mutations: this may well explain the long prodromal period seen before invasion occurs in pre-invasive lesions such as Barrett's (Spechler, 2003), inflammatory bowel disease (Jess et al., 2006) and most colorectal adenomas (Hofstad et al., 1996). The existence, as

indicated by the present work, of multiple contiguous but genotypically different clones which do reach the size predicted by Martens et al., (Martens et al., 2011) for clonal interference to occur, would appear to underline the potential for clonal competition in BE, with a 'winning' clone eventually acquiring sufficient growth advantage to become carcinoma.

In Chapter - 4, it has been shown that BO with glands containing basal dysplasia-like atypia (BCDA) is associated with either synchronous or metachronous dysplasia or OA elsewhere in the oesophagus (Lomo et al., 2006, Coco et al., 2011). It has been shown that these pre-tumour clones can often grow and occupy vast areas of up to 17cm of non-dysplastic Barrett's segment (Barrett et al., 1999, Maley et al., 2004a, Wong et al., 2001). Recently, Galandiuk et al., have shown that non-dysplastic epithelium in the colon can carry a mutation in *KRAS* and *CDKN2A* (Galandiuk et al., 2012). It has been shown that dysplasia can occur as a result of a single APC mutation in FAP adenomas (Lamlum et al., 2000); conversely, non-dysplastic tissue can also carry substantial mutational burden (Leedham et al., 2009). These observations suggest that mutation on its own or in association with other mutations are not sufficient to change the epithelial phenotype to dysplasia. This raises the question of the acceptability of dysplasia as a marker for cancer risk prediction, and morphologically non-dysplastic cells can also carry carcinogenic mutations. Hence, genetic profiling of pre-dysplastic epithelium may be a more suitable marker to identify patients who belong to the high-risk group of developing OA. Saadi et al., have shown that different phenotypes, such as metaplasia, dysplasia and OA can be distinguish based on a group of gene expression profile signatures from microdissected Barrett's

stromal tissue. Overexpression of any of five genes (TMEPAI, FAP, JMY, BCL6 and TSP1) indicated a poor prognosis in patients with OA (Saadi et al., 2010). However, the exact mechanism involved in stromal interaction is unclear.

In Chapter - 5, work on neo-Barrett's performed here did not show any evidence of field cancerization, indicating that neo-Barrett's is genuinely a de novo Barrett's lesion and not a recurrence from the original BO. Mutations found in OA were not found in neo-Barrett from same patient suggesting that the new lesion is an acquired condition and is not due to the effect of field cancerization. Longitudinal studies looking at the genotype of original Barrett's followed by OA and neo-BO from the same patient will give a better understanding of the genetic progression from BO to OA and further to neo-BO. The origin of BO has always been debated (Quante et al., 2012, Xian et al., 2012). The evidence is more in support of origin of Barrett's from the native oesophageal squamous epithelium (Souza et al., 2008). However, recently, Lavery et al., have suggested that BO may develop from upward movement of cells from the gastric cardiac mucosa. They have shown that Barret's glands are clonal, giving rise to multiple cell lineages and the stem cell niche is situated in the middle portion of BO glands with bidirectional cellular migration (Lavery et al., 2014a). My work here also shows similar findings in neo-BO, suggesting that gastric-cardiac mucosa cells may give rise to Neo-BO. The significant outcome of this study may be that neo-BO glands developed from gastric glands, which had expressed TFF1+/MUC5AC+ and TFF2+/MUC6+ cell lineages. Further longitudinal endoscopic surveillance of patients with BO who develop OA and later develop neo-BO and go on to develop recurrent OA will help us to clarify the natural history of this process.

In Chapter - 6, I have shown that methylation patterns within individual Barrett's glands show a mosaic pattern and patterns between two morphologically similar glands were not same, suggesting epigenetic diversity within Barrett's oesophagus, similar to methylation patterns in the colon (Graham et al., 2011a, Yatabe et al., 2001). It has been shown that neonatal intestinal crypts are polyclonal to start with and by day 14 these crypts undergo monoclonal conversion (Schmidt et al., 1988). Methylation patterns are acquired as somatic inheritance and act like a molecular clock (Tsao et al., 2000, Holliday and Pugh, 1975). During adult life, methylation patterns undergo drift to become more diverse and polymorphic. This diversity has been shown in normal tissue (Zhu et al., 1999) and tumours such as colonic carcinomas (Sakurazawa et al., 2000), leiomyoma (Silva et al., 1993) and breast carcinoma (Graff et al., 2000). In this study, it has been shown that an individual Barrett's gland consists of various methylation patterns suggesting the presence of multiple stem cells, which may undergo bottleneck competition. Stem cell plasticity may be responsible for differences in methylation patterns between Barrett's glands. The methylation tags within Barrett's glands increased with age and so did the percentage methylation, similar to the colon (Yatabe et al., 2001). Nicholson et al., have shown that Barrett's glands are maintained by multiple stem cells (Nicholson et al., 2011). Methylation patterns within clonal Barrett's glands (clonal mutation in patient 1 and patient 2) were not similar, suggesting a quasi-clonal Barrett's gland, long-lived stem cells and plasticity. The exact number of stem cells in the niche is unclear; it may vary within individual glands. Currently, it is not possible to predict the exact number of stem cells in each gland. Methylation tags seem to

record the gland history and give us an approximate estimate of stem cell numbers in individual glands.

This study provides evidence that Barrett's glands are quasi-clonal and that stem cells within glands are long-lived, undergoing constant bottleneck competition to acquire diverse methylation patterns. These changes can be explained by two dynamic processes, which are working against each other towards building the gland architecture, such as, stem cell extinction and drift. In the specimens examined, the mutation rate in Barrett's metaplasia was very low and it was difficult to show clonal drift. These dynamics reflect complex processes involved in tumorigenesis before the monoclonal conversion occurs.

7.2 Limitations of this study:

Only genetic alterations in commonly mutated genes such as *TP53* and *CDKN2A* (p16) have been primarily studied here. Not all DNA extractions yield DNA of sufficient quality to perform nested PCR sequencing, limiting the number of informative clones fully investigated. Limited tissue available for EMRs raises a possibility that other clones reside in distant regions away from the EMR site. Conclusions from chapter-4 are based on limited number of specimens.

7.3 Application of this study:

- This work will help to understand the clonal structure of BO and OA.
- It could help in the development of the biomarkers for the prediction of patients who are at a higher risk of developing carcinoma and determining the timing of intervention.

7.4 Future work and direction:

Further work involving methylation analysis and comparing methylation patterns in different phenotypes such as metaplasia alone (Barrett's biopsies), metaplasia with associated dysplasia (EMRs/oesophagectomy) and dysplasia alone (EMRs/oesophagectomy) would help to understand the dynamics of individual phenotypes and will help to gain insight into the timeline of MDC. Comparing methylation patterns in clonal (somatic/mtDNA mutated) Vs unrelated glands would help to understand the impact of mutations on the dynamics of BO. By comparing methylation patterns of glands in fission by using EDTA gland isolation technique would help to understand niche succession in BO.

The clonal relationship shared between different phenotypes within Barrett's oesophagus can be used to understand the dynamics of various clones, which progress to oesophageal adenocarcinoma. It may further help to understand the genetic events, which lead onto distant metastasis. Recent work in Genome-wide study will guide us to identify various subclones and also help to understanding the genetic diversity involved at different stages of MDC.

With the wider use of advance technologies such as whole genome sequencing, more data is available which was not present at the beginning of this study. These studies, increases the chances of identifying various unbias target genes and will help to compare various genetic event in specimens from Barrett's patients who progressed to OA against Barrett's patients who have not progressed to OA. This will further help in the development of the biomarkers

for the prediction of patients who are at a higher risk of developing carcinoma and determining the timing of intervention, such as, surveillance endoscopy, endoscopic or surgical treatment.

REFERENCES:

AGRAWAL, N., JIAO, Y., BETTEGOWDA, C., HUTFLESS, S. M., WANG, Y., DAVID, S., CHENG, Y., TWADDELL, W. S., LATT, N. L., SHIN, E. J., WANG, L. D., WANG, L., YANG, W., VELCULESCU, V. E., VOGELSTEIN, B., PAPADOPOULOS, N., KINZLER, K. W. & MELTZER, S. J. 2012. Comparative genomic analysis of esophageal adenocarcinoma and squamous cell carcinoma. *Cancer Discov,* 2**,** 899-905.

AHNEN, D. J., POULSOM, R., STAMP, G. W., ELIA, G., PIKE, C., JEFFERY, R., LONGCROFT, J., RIO, M. C., CHAMBON, P. & WRIGHT, N. A. 1994. The ulceration-associated cell lineage (UACL) reiterates the Brunner's gland differentiation programme but acquires the proliferative organization of the gastric gland. *J Pathol,* 173**,** 317-26.

AHUJA, N., LI, Q., MOHAN, A. L., BAYLIN, S. B. & ISSA, J. P. 1998. Aging and DNA methylation in colorectal mucosa and cancer. *Cancer Res,* 58**,** 5489-94.

AL YASSIN, T. M. & TONER, P. G. 1977. Fine structure of squamous epitheilum and submucosal glands of human oesophagus. *J Anat,* 123**,** 705-21.

ANDOR, N., GRAHAM, T. A., JANSEN, M., XIA, L. C., AKTIPIS, C. A., PETRITSCH, C., JI, H. P. & MALEY, C. C. 2016. Pan-cancer analysis of the extent and consequences of intratumor heterogeneity. *Nat Med,* 22**,** 105-13.

BADREDDINE, R. J. & WANG, K. K. 2010. Barrett esophagus: an update. *Nat Rev Gastroenterol Hepatol,* 7**,** 369-78.

BAKER, A. M., CERESER, B., MELTON, S., FLETCHER, A. G., RODRIGUEZ-JUSTO, M., TADROUS, P. J., HUMPHRIES, A., ELIA, G., MCDONALD, S. A., WRIGHT, N. A., SIMONS, B. D., JANSEN, M. & GRAHAM, T. A. 2014. Quantification of crypt and stem cell evolution in the normal and neoplastic human colon. *Cell Rep,* 8**,** 940-7.

BARKER, N., BARTFELD, S. & CLEVERS, H. 2010. Tissue-resident adult stem cell populations of rapidly self-renewing organs. *Cell Stem Cell,* 7**,** 656-70.

BARKER, N., RIDGWAY, R. A., VAN ES, J. H., VAN DE WETERING, M., BEGTHEL, H., VAN DEN BORN, M., DANENBERG, E., CLARKE, A. R., SANSOM, O. J. & CLEVERS, H. 2009. Crypt stem cells as the cells-of-origin of intestinal cancer. *Nature,* 457**,** 608-11.

BARKER, N., VAN ES, J. H., KUIPERS, J., KUJALA, P., VAN DEN BORN, M., COZIJNSEN, M., HAEGEBARTH, A., KORVING, J., BEGTHEL, H., PETERS, P. J. & CLEVERS, H. 2007. Identification of stem cells in small intestine and colon by marker gene Lgr5. *Nature,* 449**,** 1003-7.

BARR, H., SHEPHERD, N. A., DIX, A., ROBERTS, D. J., TAN, W. C. & KRASNER, N. 1996. Eradication of high-grade dysplasia in columnar-lined (Barrett's) oesophagus by photodynamic therapy with endogenously generated protoporphyrin IX. *Lancet,* 348**,** 584-5.

BARRETT, M. T., SANCHEZ, C. A., PREVO, L. J., WONG, D. J., GALIPEAU, P. C., PAULSON, T. G., RABINOVITCH, P. S. & REID, B. J. 1999. Evolution of neoplastic cell lineages in Barrett oesophagus. *Nat Genet,* 22**,** 106-9.

BARRETT, N. R. 1950. Chronic peptic ulcer of the oesophagus and 'oesophagitis'. *Br J Surg,* 38**,** 175-82.

BERENSON, M. M., JOHNSON, T. D., MARKOWITZ, N. R., BUCHI, K. N. & SAMOWITZ, W. S. 1993. Restoration of squamous mucosa after ablation of Barrett's esophageal epithelium. *Gastroenterology,* 104**,** 1686-91.

BHAT, S., COLEMAN, H. G., YOUSEF, F., JOHNSTON, B. T., MCMANUS, D. T., GAVIN, A. T. & MURRAY, L. J. 2011. Risk of malignant progression in Barrett's esophagus patients: results from a large population-based study. *J Natl Cancer Inst,* 103**,** 1049-57.

BIDDLESTONE, L. R., BARHAM, C. P., WILKINSON, S. P., BARR, H. & SHEPHERD, N. A. 1998. The histopathology of treated Barrett's esophagus: squamous reepithelialization after acid suppression and laser and photodynamic therapy. *Am J Surg Pathol,* 22**,** 239-45.

BIDICHANDANI, S. I., ASHIZAWA, T. & PATEL, P. I. 1998. The GAA triplet-repeat expansion in Friedreich ataxia interferes with transcription and may be associated with an unusual DNA structure. *Am J Hum Genet,* 62**,** 111-21.

BIGNOLD, L. P. 2003. Pathogenetic mechanisms of nuclear pleomorphism of tumour cells based on the mutator phenotype theory of carcinogenesis. *Histol Histopathol,* 18**,** 657-64.

BINATO, M., GURSKI, R. R., FAGUNDES, R. B., MEURER, L. & EDELWEISS, M. I. 2009. P53 and Ki-67 overexpression in gastroesophageal reflux disease--Barrett's esophagus and adenocarcinoma sequence. *Dis Esophagus,* 22**,** 588-95.

BIRD, A. 2002. DNA methylation patterns and epigenetic memory. *Genes Dev,* 16**,** 6-21.

BLANPAIN, C. & FUCHS, E. 2009. Epidermal homeostasis: a balancing act of stem cells in the skin. *Nat Rev Mol Cell Biol,* 10**,** 207-17.

BRAAKHUIS, B. J., TABOR, M. P., KUMMER, J. A., LEEMANS, C. R. & BRAKENHOFF, R. H. 2003. A genetic explanation of Slaughter's concept of field cancerization: evidence and clinical implications. *Cancer Res,* 63**,** 1727-30.

BREMNER, C. G., LYNCH, V. P. & ELLIS, F. H., JR. 1970. Barrett's esophagus: congenital or acquired? An experimental study of esophageal mucosal regeneration in the dog. *Surgery,* 68**,** 209-16.

BROMHAM, L. & PENNY, D. 2003. The modern molecular clock. *Nat Rev Genet,* 4**,** 216-24.

CAMERON, A. J. 2002. Epidemiology of Barrett's esophagus and adenocarcinoma. *Dis Esophagus,* 15**,** 106-8.

CAMPBELL, F., WILLIAMS, G. T., APPLETON, M. A., DIXON, M. F., HARRIS, M. & WILLIAMS, E. D. 1996. Post-irradiation somatic mutation and clonal stabilisation time in the human colon. *Gut,* 39**,** 569-73.

CHANDRASOMA, P., WIJETUNGE, S., DEMEESTER, S., MA, Y., HAGEN, J., ZAMIS, L. & DEMEESTER, T. 2012. Columnar-lined esophagus without intestinal metaplasia has no proven risk of adenocarcinoma. *Am J Surg Pathol,* 36**,** 1-7.

CHANDRASOMA, P. T., DER, R., MA, Y., DALTON, P. & TAIRA, M. 2000. Histology of the gastroesophageal junction: an autopsy study. *Am J Surg Pathol,* 24**,** 402-9.

CHANDRASOMA, P. T., DER, R., MA, Y., PETERS, J. & DEMEESTER, T. 2003. Histologic classification of patients based on mapping biopsies of the gastroesophageal junction. *Am J Surg Pathol,* 27**,** 929-36.

CHAVES, P., CRESPO, M., RIBEIRO, C., LARANJEIRA, C., PEREIRA, A. D., SUSPIRO, A., CARDOSO, P., LEITAO, C. N. & SOARES, J. 2007. Chromosomal analysis of Barrett's cells: demonstration of instability and detection of the metaplastic lineage involved. *Mod Pathol,* 20**,** 788-96.

CHENG, H., BJERKNES, M., AMAR, J. & GARDINER, G. 1986. Crypt production in normal and diseased human colonic epithelium. *Anat Rec,* 216**,** 44-8.
CHONG, I. Y., CUNNINGHAM, D., BARBER, L. J., CAMPBELL, J., CHEN, L., KOZAREWA, I., FENWICK, K., ASSIOTIS, I., GUETTLER, S., GARCIA-MURILLAS, I., AWAN, S., LAMBROS, M., STARLING, N., WOTHERSPOON, A., STAMP, G., GONZALEZ-DE-CASTRO, D., BENSON, M., CHAU, I., HULKKI, S., NOHADANI, M., ELTAHIR, Z., LEMNRAU, A., ORR, N., RAO, S., LORD, C. J. & ASHWORTH, A. 2013. The genomic landscape of oesophagogastric junctional adenocarcinoma. *J Pathol,* 231**,** 301-10.
CHU, M. W., SIEGMUND, K. D., ECKSTAM, C. L., KIM, J. Y., YANG, A. S., KANEL, G. C., TAVARE, S. & SHIBATA, D. 2007. Lack of increases in methylation at three CpG-rich genomic loci in non-mitotic adult tissues during aging. *BMC Med Genet,* 8**,** 50.
CLAYTON, R. N., PFEIFER, M., ATKINSON, A. B., BELCHETZ, P., WASS, J. A., KYRODIMOU, E., VANDERPUMP, M., SIMPSON, D., BICKNELL, J. & FARRELL, W. E. 2000. Different patterns of allelic loss (loss of heterozygosity) in recurrent human pituitary tumors provide evidence for multiclonal origins. *Clin Cancer Res,* 6**,** 3973-82.
COAD, R. A., WOODMAN, A. C., WARNER, P. J., BARR, H., WRIGHT, N. A. & SHEPHERD, N. A. 2005. On the histogenesis of Barrett's oesophagus and its associated squamous islands: a three-dimensional study of their morphological relationship with native oesophageal gland ducts. *J Pathol,* 206**,** 388-94.
COCO, D. P., GOLDBLUM, J. R., HORNICK, J. L., LAUWERS, G. Y., MONTGOMERY, E., SRIVASTAVA, A., WANG, H. & ODZE, R. D. 2011. Interobserver variability in the diagnosis of crypt dysplasia in Barrett esophagus. *Am J Surg Pathol,* 35**,** 45-54.
DANIELY, Y., LIAO, G., DIXON, D., LINNOILA, R. I., LORI, A., RANDELL, S. H., OREN, M. & JETTEN, A. M. 2004. Critical role of p63 in the development of a normal esophageal and tracheobronchial epithelium. *Am J Physiol Cell Physiol,* 287**,** C171-81.
DEMEESTER, S. R. & DEMEESTER, T. R. 2000. Columnar mucosa and intestinal metaplasia of the esophagus: fifty years of controversy. *Ann Surg,* 231**,** 303-21.
DENG, G., LU, Y., ZLOTNIKOV, G., THOR, A. D. & SMITH, H. S. 1996. Loss of heterozygosity in normal tissue adjacent to breast carcinomas. *Science,* 274**,** 2057-9.
DESAI, T. K., KRISHNAN, K., SAMALA, N., SINGH, J., CLULEY, J., PERLA, S. & HOWDEN, C. W. 2012. The incidence of oesophageal adenocarcinoma in non-dysplastic Barrett's oesophagus: a meta-analysis. *Gut,* 61**,** 970-6.
DEXTER, S. P., SUE-LING, H., MCMAHON, M. J., QUIRKE, P., MAPSTONE, N. & MARTIN, I. G. 2001. Circumferential resection margin involvement: an independent predictor of survival following surgery for oesophageal cancer. *Gut,* 48**,** 667-70.
DRESNER, S. M., GRIFFIN, S. M., WAYMAN, J., BENNETT, M. K., HAYES, N. & RAIMES, S. A. 2003. Human model of duodenogastro-oesophageal reflux in the development of Barrett's metaplasia. *Br J Surg,* 90**,** 1120-8.
DULAK, A. M., STOJANOV, P., PENG, S., LAWRENCE, M. S., FOX, C., STEWART, C., BANDLA, S., IMAMURA, Y., SCHUMACHER, S. E., SHEFLER, E., MCKENNA,

A., CARTER, S. L., CIBULSKIS, K., SIVACHENKO, A., SAKSENA, G., VOET, D., RAMOS, A. H., AUCLAIR, D., THOMPSON, K., SOUGNEZ, C., ONOFRIO, R. C., GUIDUCCI, C., BEROUKHIM, R., ZHOU, Z., LIN, L., LIN, J., REDDY, R., CHANG, A., LANDRENAU, R., PENNATHUR, A., OGINO, S., LUKETICH, J. D., GOLUB, T. R., GABRIEL, S. B., LANDER, E. S., BEER, D. G., GODFREY, T. E., GETZ, G. & BASS, A. J. 2013. Exome and whole-genome sequencing of esophageal adenocarcinoma identifies recurrent driver events and mutational complexity. *Nat Genet,* 45**,** 478-86.

DUNN, L. J., BURT, A. D., HAYES, N. & GRIFFIN, S. M. 2016. Columnar Metaplasia in the Esophageal Remnant After Esophagectomy: A Common Occurrence and a Valuable Insight Into the Development of Barrett Esophagus. *Ann Surg*.

EK, W. E., LEVINE, D. M., D'AMATO, M., PEDERSEN, N. L., MAGNUSSON, P. K., BRESSO, F., ONSTAD, L. E., SCHMIDT, P. T., TORNBLOM, H., NORDENSTEDT, H., ROMERO, Y., MAYO CLINIC ESOPHAGEAL, A., BARRETT'S ESOPHAGUS REGISTRY, C., CHOW, W. H., MURRAY, L. J., GAMMON, M. D., LIU, G., BERNSTEIN, L., CASSON, A. G., RISCH, H. A., SHAHEEN, N. J., BIRD, N. C., REID, B. J., CORLEY, D. A., HARDIE, L. J., YE, W., WU, A. H., ZUCCHELLI, M., SPECTOR, T. D., HYSI, P., VAUGHAN, T. L., WHITEMAN, D. C., MACGREGOR, S. & INVESTIGATORS, B. S. 2013. Germline genetic contributions to risk for esophageal adenocarcinoma, Barrett's esophagus, and gastroesophageal reflux. *J Natl Cancer Inst,* 105**,** 1711-8.

ENDOH, Y., MIYAWAKI, M., TAMURA, G., WATANABE, H. & MOTOYAMA, T. 1999. Esophageal adenocarcinoma that probably originated in the esophageal gland duct: a case report. *Pathol Int,* 49**,** 156-9.

FEARON, E. R. & VOGELSTEIN, B. 1990. A genetic model for colorectal tumorigenesis. *Cell,* 61**,** 759-67.

FELLOUS, T. G., ISLAM, S., TADROUS, P. J., ELIA, G., KOCHER, H. M., BHATTACHARYA, S., MEARS, L., TURNBULL, D. M., TAYLOR, R. W., GREAVES, L. C., CHINNERY, P. F., TAYLOR, G., MCDONALD, S. A., WRIGHT, N. A. & ALISON, M. R. 2009a. Locating the stem cell niche and tracing hepatocyte lineages in human liver. *Hepatology,* 49**,** 1655-63.

FELLOUS, T. G., MCDONALD, S. A., BURKERT, J., HUMPHRIES, A., ISLAM, S., DE-ALWIS, N. M., GUTIERREZ-GONZALEZ, L., TADROUS, P. J., ELIA, G., KOCHER, H. M., BHATTACHARYA, S., MEARS, L., EL-BAHRAWY, M., TURNBULL, D. M., TAYLOR, R. W., GREAVES, L. C., CHINNERY, P. F., DAY, C. P., WRIGHT, N. A. & ALISON, M. R. 2009b. A methodological approach to tracing cell lineage in human epithelial tissues. *Stem Cells,* 27**,** 1410-20.

FRANKLIN, W. A., GAZDAR, A. F., HANEY, J., WISTUBA, II, LA ROSA, F. G., KENNEDY, T., RITCHEY, D. M. & MILLER, Y. E. 1997. Widely dispersed p53 mutation in respiratory epithelium. A novel mechanism for field carcinogenesis. *J Clin Invest,* 100**,** 2133-7.

GALANDIUK, S., RODRIGUEZ-JUSTO, M., JEFFERY, R., NICHOLSON, A. M., CHENG, Y., OUKRIF, D., ELIA, G., LEEDHAM, S. J., MCDONALD, S. A., WRIGHT, N. A. & GRAHAM, T. A. 2012. Field cancerization in the intestinal epithelium of patients with Crohn's ileocolitis. *Gastroenterology,* 142**,** 855-864 e8.

GALIPEAU, P. C., PREVO, L. J., SANCHEZ, C. A., LONGTON, G. M. & REID, B. J. 1999. Clonal expansion and loss of heterozygosity at chromosomes 9p and 17p

in premalignant esophageal (Barrett's) tissue. *J Natl Cancer Inst,* 91**,** 2087-95.
GATENBY, P. A., RAMUS, J. R., CAYGILL, C. P., SHEPHERD, N. A. & WATSON, A. 2008. Relevance of the detection of intestinal metaplasia in non-dysplastic columnar-lined oesophagus. *Scand J Gastroenterol,* 43**,** 524-30.
GATENBY, P. A., RAMUS, J. R., CAYGILL, C. P. & WATSON, A. 2007. Does the length of the columnar-lined esophagus change with time? *Dis Esophagus,* 20**,** 497-503.
GERLINGER, M., ROWAN, A. J., HORSWELL, S., LARKIN, J., ENDESFELDER, D., GRONROOS, E., MARTINEZ, P., MATTHEWS, N., STEWART, A., TARPEY, P., VARELA, I., PHILLIMORE, B., BEGUM, S., MCDONALD, N. Q., BUTLER, A., JONES, D., RAINE, K., LATIMER, C., SANTOS, C. R., NOHADANI, M., EKLUND, A. C., SPENCER-DENE, B., CLARK, G., PICKERING, L., STAMP, G., GORE, M., SZALLASI, Z., DOWNWARD, J., FUTREAL, P. A. & SWANTON, C. 2012. Intratumor heterogeneity and branched evolution revealed by multiregion sequencing. *N Engl J Med,* 366**,** 883-92.
GLICKMAN, J. N., BLOUNT, P. L., SANCHEZ, C. A., COWAN, D. S., WONGSURAWAT, V. J., REID, B. J. & ODZE, R. D. 2006. Mucin core polypeptide expression in the progression of neoplasia in Barrett's esophagus. *Hum Pathol,* 37**,** 1304-15.
GLICKMAN, J. N., SPECHLER, S. J., SOUZA, R. F., LUNSFORD, T., LEE, E. & ODZE, R. D. 2009. Multilayered epithelium in mucosal biopsy specimens from the gastroesophageal junction region is a histologic marker of gastroesophageal reflux disease. *Am J Surg Pathol,* 33**,** 818-25.
GOING, J. J., FLETCHER-MONAGHAN, A. J., NEILSON, L., WISMAN, B. A., VAN DER ZEE, A., STUART, R. C. & KEITH, W. N. 2004. Zoning of mucosal phenotype, dysplasia, and telomerase activity measured by telomerase repeat assay protocol in Barrett's esophagus. *Neoplasia,* 6**,** 85-92.
GORE, S., HEALEY, C. J., SUTTON, R., EYRE-BROOK, I. A., GEAR, M. W., SHEPHERD, N. A. & WILKINSON, S. P. 1993. Regression of columnar lined (Barrett's) oesophagus with continuous omeprazole therapy. *Aliment Pharmacol Ther,* 7**,** 623-8.
GRAFF, J. R., GABRIELSON, E., FUJII, H., BAYLIN, S. B. & HERMAN, J. G. 2000. Methylation patterns of the E-cadherin 5' CpG island are unstable and reflect the dynamic, heterogeneous loss of E-cadherin expression during metastatic progression. *J Biol Chem,* 275**,** 2727-32.
GRAHAM, T. A., HUMPHRIES, A., SANDERS, T., RODRIGUEZ-JUSTO, M., TADROUS, P. J., PRESTON, S. L., NOVELLI, M. R., LEEDHAM, S. J., MCDONALD, S. A. & WRIGHT, N. A. 2011a. Use of methylation patterns to determine expansion of stem cell clones in human colon tissue. *Gastroenterology,* 140**,** 1241-1250 e1-9.
GRAHAM, T. A., MCDONALD, S. A. & WRIGHT, N. A. 2011b. Field cancerization in the GI tract. *Future Oncol,* 7**,** 981-93.
GREAVES, L. C., PRESTON, S. L., TADROUS, P. J., TAYLOR, R. W., BARRON, M. J., OUKRIF, D., LEEDHAM, S. J., DEHERAGODA, M., SASIENI, P., NOVELLI, M. R., JANKOWSKI, J. A., TURNBULL, D. M., WRIGHT, N. A. & MCDONALD, S. A. 2006. Mitochondrial DNA mutations are established in human colonic stem cells, and mutated clones expand by crypt fission. *Proc Natl Acad Sci U S A,* 103**,** 714-9.

GREAVES, M. & MALEY, C. C. 2012. Clonal evolution in cancer. *Nature,* 481**,** 306-13.
GREPMEIER, U., DIETMAIER, W., MERK, J., WILD, P. J., OBERMANN, E. C., PFEIFER, M., HOFSTAEDTER, F., HARTMANN, A. & WOENCKHAUS, M. 2005. Deletions at chromosome 2q and 12p are early and frequent molecular alterations in bronchial epithelium and NSCLC of long-term smokers. *Int J Oncol,* 27**,** 481-8.
GUTIERREZ-GONZALEZ, L., DEHERAGODA, M., ELIA, G., LEEDHAM, S. J., SHANKAR, A., IMBER, C., JANKOWSKI, J. A., TURNBULL, D. M., NOVELLI, M., WRIGHT, N. A. & MCDONALD, S. A. 2009. Analysis of the clonal architecture of the human small intestinal epithelium establishes a common stem cell for all lineages and reveals a mechanism for the fixation and spread of mutations. *J Pathol,* 217**,** 489-96.
HAFNER, C., TOLL, A., FERNANDEZ-CASADO, A., EARL, J., MARQUES, M., ACQUADRO, F., MENDEZ-PERTUZ, M., URIOSTE, M., MALATS, N., BURNS, J. E., KNOWLES, M. A., CIGUDOSA, J. C., HARTMANN, A., VOGT, T., LANDTHALER, M., PUJOL, R. M. & REAL, F. X. 2010. Multiple oncogenic mutations and clonal relationship in spatially distinct benign human epidermal tumors. *Proc Natl Acad Sci U S A,* 107**,** 20780-5.
HAMELIN, R., FLEJOU, J. F., MUZEAU, F., POTET, F., LAURENT-PUIG, P., FEKETE, F. & THOMAS, G. 1994. TP53 gene mutations and p53 protein immunoreactivity in malignant and premalignant Barrett's esophagus. *Gastroenterology,* 107**,** 1012-8.
HAMILTON, S. R. & YARDLEY, J. H. 1977. Regnerative of cardiac type mucosa and acquisition of Barrett mucosa after esophagogastrostomy. *Gastroenterology,* 72**,** 669-75.
HARTMANN, A., ROSNER, U., SCHLAKE, G., DIETMAIER, W., ZAAK, D., HOFSTAEDTER, F. & KNUECHEL, R. 2000. Clonality and genetic divergence in multifocal low-grade superficial urothelial carcinoma as determined by chromosome 9 and p53 deletion analysis. *Lab Invest,* 80**,** 709-18.
HEATH, J. P. 1996. Epithelial cell migration in the intestine. *Cell Biol Int,* 20**,** 139-46.
HEPPNER, G. H. 1984. Tumor heterogeneity. *Cancer Res,* 44**,** 2259-65.
HOFSTAD, B., VATN, M. H., ANDERSEN, S. N., HUITFELDT, H. S., ROGNUM, T., LARSEN, S. & OSNES, M. 1996. Growth of colorectal polyps: redetection and evaluation of unresected polyps for a period of three years. *Gut,* 39**,** 449-56.
HOLLIDAY, R. 1987. The inheritance of epigenetic defects. *Science,* 238**,** 163-70.
HOLLIDAY, R. & PUGH, J. E. 1975. DNA modification mechanisms and gene activity during development. *Science,* 187**,** 226-32.
HRITZ, I., GYORFFY, H., MOLNAR, B., LAKATOS, G., SIPOS, F., PREGUN, I., JUHASZ, M., PRONAI, L., SCHAFF, Z., TULASSAY, Z. & HERSZENYI, L. 2009. Increased p53 expression in the malignant transformation of Barrett's esophagus is accompanied by an upward shift of the proliferative compartment. *Pathol Oncol Res,* 15**,** 183-92.
HUMPHRIES, A., CERESER, B., GAY, L. J., MILLER, D. S., DAS, B., GUTTERIDGE, A., ELIA, G., NYE, E., JEFFERY, R., POULSOM, R., NOVELLI, M. R., RODRIGUEZ-JUSTO, M., MCDONALD, S. A., WRIGHT, N. A. & GRAHAM, T. A. 2013.

Lineage tracing reveals multipotent stem cells maintain human adenomas and the pattern of clonal expansion in tumor evolution. *Proc Natl Acad Sci U S A,* 110**,** E2490-9.
ISSA, J. P. 2000. CpG-island methylation in aging and cancer. *Curr Top Microbiol Immunol,* 249**,** 101-18.
ISSA, J. P., OTTAVIANO, Y. L., CELANO, P., HAMILTON, S. R., DAVIDSON, N. E. & BAYLIN, S. B. 1994. Methylation of the oestrogen receptor CpG island links ageing and neoplasia in human colon. *Nat Genet,* 7**,** 536-40.
IWAYA, Y., YAMAZAKI, T., WATANABE, T., SEKI, A., OCHI, Y., HARA, E., ARAKURA, N., TANAKA, E. & HASEBE, O. 2016. A case of Barrett's adenocarcinoma with marked endoscopic morphological changes in Barrett's esophagus over a long follow-up period of 15 years. *Dig Endosc*.
JANKOWSKI, J. A., WRIGHT, N. A., MELTZER, S. J., TRIADAFILOPOULOS, G., GEBOES, K., CASSON, A. G., KERR, D. & YOUNG, L. S. 1999. Molecular evolution of the metaplasia-dysplasia-adenocarcinoma sequence in the esophagus. *Am J Pathol,* 154**,** 965-73.
JESS, T., LOFTUS, E. V., JR., VELAYOS, F. S., HARMSEN, W. S., ZINSMEISTER, A. R., SMYRK, T. C., TREMAINE, W. J., MELTON, L. J., 3RD, MUNKHOLM, P. & SANDBORN, W. J. 2006. Incidence and prognosis of colorectal dysplasia in inflammatory bowel disease: a population-based study from Olmsted County, Minnesota. *Inflamm Bowel Dis,* 12**,** 669-76.
JOHNS, B. A. 1952. Developmental changes in the oesophageal epithelium in man. *J Anat,* 86**,** 431-42.
KARAM, S. M., STRAITON, T., HASSAN, W. M. & LEBLOND, C. P. 2003. Defining epithelial cell progenitors in the human oxyntic mucosa. *Stem Cells,* 21**,** 322-36.
KASTELEIN, F., BIERMANN, K., STEYERBERG, E. W., VERHEIJ, J., KALISVAART, M., LOOIJENGA, L. H., STOOP, H. A., WALTER, L., KUIPERS, E. J., SPAANDER, M. C., BRUNO, M. J. & PROBAR-STUDY, G. 2013. Aberrant p53 protein expression is associated with an increased risk of neoplastic progression in patients with Barrett's oesophagus. *Gut,* 62**,** 1676-83.
KESTENS, C., LEENDERS, M., OFFERHAUS, G. J., VAN BAAL, J. W. & SIERSEMA, P. D. 2014. Risk of neoplastic progression in Barrett's esophagus diagnosed as indefinite for dysplasia: a nationwide cohort study. *Endoscopy*.
KIM, J., REBER, H. A., DRY, S. M., ELASHOFF, D., CHEN, S. L., UMETANI, N., KITAGO, M., HINES, O. J., KAZANJIAN, K. K., HIRAMATSU, S., BILCHIK, A. J., YONG, S., SHOUP, M. & HOON, D. S. 2006a. Unfavourable prognosis associated with K-ras gene mutation in pancreatic cancer surgical margins. *Gut,* 55**,** 1598-605.
KIM, J. Y., SIEGMUND, K. D., TAVARE, S. & SHIBATA, D. 2005a. Age-related human small intestine methylation: evidence for stem cell niches. *BMC Med,* 3**,** 10.
KIM, J. Y., TAVARE, S. & SHIBATA, D. 2005b. Counting human somatic cell replications: methylation mirrors endometrial stem cell divisions. *Proc Natl Acad Sci U S A,* 102**,** 17739-44.
KIM, J. Y., TAVARE, S. & SHIBATA, D. 2006b. Human hair genealogies and stem cell latency. *BMC Biol,* 4**,** 2.
KIM, K. M. & SHIBATA, D. 2002. Methylation reveals a niche: stem cell succession in human colon crypts. *Oncogene,* 21**,** 5441-9.

KIM, K. M. & SHIBATA, D. 2004. Tracing ancestry with methylation patterns: most crypts appear distantly related in normal adult human colon. *BMC Gastroenterol,* 4**,** 8.

KIRCHES, E., MAWRIN, C., SCHNEIDER-STOCK, R., KRAUSE, G., SCHERLACH, C. & DIETZMANN, K. 2003. Mitochondrial DNA as a clonal tumor cell marker: gliomatosis cerebri. *J Neurooncol,* 61**,** 1-5.

KITAGO, M., UEDA, M., AIURA, K., SUZUKI, K., HOSHIMOTO, S., TAKAHASHI, S., MUKAI, M. & KITAJIMA, M. 2004. Comparison of K-ras point mutation distributions in intraductal papillary-mucinous tumors and ductal adenocarcinoma of the pancreas. *Int J Cancer,* 110**,** 177-82.

KOZAR, S., MORRISSEY, E., NICHOLSON, A. M., VAN DER HEIJDEN, M., ZECCHINI, H. I., KEMP, R., TAVARE, S., VERMEULEN, L. & WINTON, D. J. 2013. Continuous clonal labeling reveals small numbers of functional stem cells in intestinal crypts and adenomas. *Cell Stem Cell,* 13**,** 626-33.

LAMLUM, H., PAPADOPOULOU, A., ILYAS, M., ROWAN, A., GILLET, C., HANBY, A., TALBOT, I., BODMER, W. & TOMLINSON, I. 2000. APC mutations are sufficient for the growth of early colorectal adenomas. *Proc Natl Acad Sci U S A,* 97**,** 2225-8.

LANGNER, C., WOLF, E. M., PLIESCHNEGGER, W., GEPPERT, M., WIGGINGHAUS, B., HOSS, G. M., EHERER, A., SCHNEIDER, N. I., REHAK, P. & VIETH, M. 2014. Multilayered epithelium at the gastroesophageal junction is a marker of gastroesophageal reflux disease: data from a prospective Central European multicenter study (histoGERD trial). *Virchows Arch,* 464**,** 409-17.

LAVERY, D. L., MARTINEZ, P., GAY, L. J., CERESER, B., NOVELLI, M. R., RODRIGUEZ-JUSTO, M., MEIJER, S. L., GRAHAM, T. A., MCDONALD, S. A., WRIGHT, N. A. & JANSEN, M. 2015. Evolution of oesophageal adenocarcinoma from metaplastic columnar epithelium without goblet cells in Barrett's oesophagus. *Gut*.

LAVERY, D. L., NICHOLSON, A. M., POULSOM, R., JEFFERY, R., HUSSAIN, A., GAY, L. J., JANKOWSKI, J. A., ZEKI, S. S., BARR, H., HARRISON, R., GOING, J., KADIRKAMANATHAN, S., DAVIS, P., UNDERWOOD, T., NOVELLI, M. R., RODRIGUEZ-JUSTO, M., SHEPHERD, N., JANSEN, M., WRIGHT, N. A. & MCDONALD, S. A. 2014b. The stem cell organisation, and the proliferative and gene expression profile of Barrett's epithelium, replicates pyloric-type gastric glands. *Gut,* 63**,** 1854-63.

LEEDHAM, S. J., GRAHAM, T. A., OUKRIF, D., MCDONALD, S. A., RODRIGUEZ-JUSTO, M., HARRISON, R. F., SHEPHERD, N. A., NOVELLI, M. R., JANKOWSKI, J. A. & WRIGHT, N. A. 2009. Clonality, founder mutations, and field cancerization in human ulcerative colitis-associated neoplasia. *Gastroenterology,* 136**,** 542-50 e6.

LEEDHAM, S. J., PRESTON, S. L., MCDONALD, S. A., ELIA, G., BHANDARI, P., POLLER, D., HARRISON, R., NOVELLI, M. R., JANKOWSKI, J. A. & WRIGHT, N. A. 2008. Individual crypt genetic heterogeneity and the origin of metaplastic glandular epithelium in human Barrett's oesophagus. *Gut,* 57**,** 1041-8.

LI, X., GALIPEAU, P. C., PAULSON, T. G., SANCHEZ, C. A., ARNAUDO, J., LIU, K., SATHER, C. L., KOSTADINOV, R. L., ODZE, R. D., KUHNER, M. K., MALEY, C. C., SELF, S. G., VAUGHAN, T. L., BLOUNT, P. L. & REID, B. J. 2014. Temporal

and spatial evolution of somatic chromosomal alterations: a case-cohort study of Barrett's esophagus. *Cancer Prev Res (Phila),* 7**,** 114-27.
LIM, Y. J., SON, H. J., LEE, J. S., BYUN, Y. H., SUH, H. J., RHEE, P. L., KIM, J. J. & RHEE, J. C. 2010. Clinical course of subepithelial lesions detected on upper gastrointestinal endoscopy. *World J Gastroenterol,* 16**,** 439-44.
LIN, Y. W., LEE, H. S., CHEN, C. H., HUANG, G. T., LEE, P. H. & SHEU, J. C. 2005. Clonality analysis of multiple hepatocellular carcinomas by loss of heterozygosity pattern determined by chromosomes 16q and 13q. *J Gastroenterol Hepatol,* 20**,** 536-46.
LOMO, L. C., BLOUNT, P. L., SANCHEZ, C. A., LI, X., GALIPEAU, P. C., COWAN, D. S., AYUB, K., RABINOVITCH, P. S., REID, B. J. & ODZE, R. D. 2006. Crypt dysplasia with surface maturation: a clinical, pathologic, and molecular study of a Barrett's esophagus cohort. *Am J Surg Pathol,* 30**,** 423-35.
LORD, R. V., WICKRAMASINGHE, K., JOHANSSON, J. J., DEMEESTER, S. R., BRABENDER, J. & DEMEESTER, T. R. 2004. Cardiac mucosa in the remnant esophagus after esophagectomy is an acquired epithelium with Barrett's-like features. *Surgery,* 136**,** 633-40.
LORINC, E. & OBERG, S. 2012. Submucosal glands in the columnar-lined oesophagus: evidence of an association with metaplasia and neosquamous epithelium. *Histopathology,* 61**,** 53-8.
MALEY, C. C., GALIPEAU, P. C., FINLEY, J. C., WONGSURAWAT, V. J., LI, X., SANCHEZ, C. A., PAULSON, T. G., BLOUNT, P. L., RISQUES, R. A., RABINOVITCH, P. S. & REID, B. J. 2006. Genetic clonal diversity predicts progression to esophageal adenocarcinoma. *Nat Genet,* 38**,** 468-73.
MALEY, C. C., GALIPEAU, P. C., LI, X., SANCHEZ, C. A., PAULSON, T. G., BLOUNT, P. L. & REID, B. J. 2004a. The combination of genetic instability and clonal expansion predicts progression to esophageal adenocarcinoma. *Cancer Res,* 64**,** 7629-33.
MALEY, C. C., GALIPEAU, P. C., LI, X., SANCHEZ, C. A., PAULSON, T. G. & REID, B. J. 2004b. Selectively advantageous mutations and hitchhikers in neoplasms: p16 lesions are selected in Barrett's esophagus. *Cancer Res,* 64**,** 3414-27.
MARRANO, D., VITI, G., GRIGIONI, W. & MARRA, A. 1987. Synchronous and metachronous cancer of the stomach. *Eur J Surg Oncol,* 13**,** 493-8.
MARTENS, E. A. & HALLATSCHEK, O. 2011. Interfering waves of adaptation promote spatial mixing. *Genetics,* 189**,** 1045-60.
MARTENS, E. A., KOSTADINOV, R., MALEY, C. C. & HALLATSCHEK, O. 2011. Spatial structure increases the waiting time for cancer. *New J Phys,* 13.
MARTIN, G. M., OGBURN, C. E., COLGIN, L. M., GOWN, A. M., EDLAND, S. D. & MONNAT, R. J., JR. 1996. Somatic mutations are frequent and increase with age in human kidney epithelial cells. *Hum Mol Genet,* 5**,** 215-21.
MARUSYK, A., ALMENDRO, V. & POLYAK, K. 2012. Intra-tumour heterogeneity: a looking glass for cancer? *Nat Rev Cancer,* 12**,** 323-34.
MCDONALD, S. A., GREAVES, L. C., GUTIERREZ-GONZALEZ, L., RODRIGUEZ-JUSTO, M., DEHERAGODA, M., LEEDHAM, S. J., TAYLOR, R. W., LEE, C. Y., PRESTON, S. L., LOVELL, M., HUNT, T., ELIA, G., OUKRIF, D., HARRISON, R., NOVELLI, M. R., MITCHELL, I., STOKER, D. L., TURNBULL, D. M., JANKOWSKI, J. A. & WRIGHT, N. A. 2008. Mechanisms of field cancerization in the human stomach: the expansion and spread of mutated gastric stem cells. *Gastroenterology,* 134**,** 500-10.

MCDONALD, S. A., LAVERY, D., WRIGHT, N. A. & JANSEN, M. 2015. Barrett oesophagus: lessons on its origins from the lesion itself. *Nat Rev Gastroenterol Hepatol,* 12**,** 50-60.
MERLO, L. M., PEPPER, J. W., REID, B. J. & MALEY, C. C. 2006. Cancer as an evolutionary and ecological process. *Nat Rev Cancer,* 6**,** 924-35.
MEYER, W., VOLLMAR, F. & BAR, W. 1979. Barrett-esophagus following total gastrectomy. A contribution to it's pathogenesis. *Endoscopy,* 11**,** 121-6.
MILLER, B. E., MILLER, F. R., LEITH, J. & HEPPNER, G. H. 1980. Growth interaction in vivo between tumor subpopulations derived from a single mouse mammary tumor. *Cancer Res,* 40**,** 3977-81.
MUTTER, G. L., INCE, T. A., BAAK, J. P., KUST, G. A., ZHOU, X. P. & ENG, C. 2001. Molecular identification of latent precancers in histologically normal endometrium. *Cancer Res,* 61**,** 4311-4.
NESHAT, K., SANCHEZ, C. A., GALIPEAU, P. C., BLOUNT, P. L., LEVINE, D. S., JOSLYN, G. & REID, B. J. 1994. p53 mutations in Barrett's adenocarcinoma and high-grade dysplasia. *Gastroenterology,* 106**,** 1589-95.
NG, I. O., GUAN, X. Y., POON, R. T., FAN, S. T. & LEE, J. M. 2003. Determination of the molecular relationship between multiple tumour nodules in hepatocellular carcinoma differentiates multicentric origin from intrahepatic metastasis. *J Pathol,* 199**,** 345-53.
NICHOLSON, A. M., GRAHAM, T. A., SIMPSON, A., HUMPHRIES, A., BURCH, N., RODRIGUEZ-JUSTO, M., NOVELLI, M., HARRISON, R., WRIGHT, N. A., MCDONALD, S. A. & JANKOWSKI, J. A. 2012. Barrett's metaplasia glands are clonal, contain multiple stem cells and share a common squamous progenitor. *Gut,* 61**,** 1380-9.
NORDLING, C. O. 1953. A new theory on cancer-inducing mechanism. *Br J Cancer,* 7**,** 68-72.
NOWELL, P. C. 1976. The clonal evolution of tumor cell populations. *Science,* 194**,** 23-8.
O'RIORDAN, J. M., BYRNE, P. J., RAVI, N., KEELING, P. W. & REYNOLDS, J. V. 2004a. Long-term clinical and pathologic response of Barrett's esophagus after antireflux surgery. *Am J Surg,* 188**,** 27-33.
O'RIORDAN, J. M., TUCKER, O. N., BYRNE, P. J., MCDONALD, G. S., RAVI, N., KEELING, P. W. & REYNOLDS, J. V. 2004b. Factors influencing the development of Barrett's epithelium in the esophageal remnant postesophagectomy. *Am J Gastroenterol,* 99**,** 205-11.
OBERG, S., JOHANSSON, J., WENNER, J. & WALTHER, B. 2002. Metaplastic columnar mucosa in the cervical esophagus after esophagectomy. *Ann Surg,* 235**,** 338-45.
OBERG, S., PETERS, J. H., DEMEESTER, T. R., LORD, R. V., JOHANSSON, J., DEMEESTER, S. R. & HAGEN, J. A. 2000. Determinants of intestinal metaplasia within the columnar-lined esophagus. *Arch Surg,* 135**,** 651-5; discussion 655-6.
ODZE, R. D. & MALEY, C. C. 2010. Neoplasia without dysplasia: lessons from Barrett esophagus and other tubal gut neoplasms. *Arch Pathol Lab Med,* 134**,** 896-906.
ORMSBY, A. H., GOLDBLUM, J. R., RICE, T. W., RICHTER, J. E., FALK, G. W., VAEZI, M. F. & GRAMLICH, T. L. 1999. Cytokeratin subsets can reliably distinguish

Barrett's esophagus from intestinal metaplasia of the stomach. *Hum Pathol,* 30**,** 288-94.
PAULL, A., TRIER, J. S., DALTON, M. D., CAMP, R. C., LOEB, P. & GOYAL, R. K. 1976. The histologic spectrum of Barrett's esophagus. *N Engl J Med,* 295**,** 476-80.
POHL, H. & WELCH, H. G. 2005. The role of overdiagnosis and reclassification in the marked increase of esophageal adenocarcinoma incidence. *J Natl Cancer Inst,* 97**,** 142-6.
POTTEN, C. S. & LOEFFLER, M. 1990. Stem cells: attributes, cycles, spirals, pitfalls and uncertainties. Lessons for and from the crypt. *Development,* 110**,** 1001-20.
POWELL, J. & MCCONKEY, C. C. 1992. The rising trend in oesophageal adenocarcinoma and gastric cardia. *Eur J Cancer Prev,* 1**,** 265-9.
QUANTE, M., BHAGAT, G., ABRAMS, J. A., MARACHE, F., GOOD, P., LEE, M. D., LEE, Y., FRIEDMAN, R., ASFAHA, S., DUBEYKOVSKAYA, Z., MAHMOOD, U., FIGUEIREDO, J. L., KITAJEWSKI, J., SHAWBER, C., LIGHTDALE, C. J., RUSTGI, A. K. & WANG, T. C. 2012. Bile acid and inflammation activate gastric cardia stem cells in a mouse model of Barrett-like metaplasia. *Cancer Cell,* 21**,** 36-51.
REID, B. J., HAGGITT, R. C., RUBIN, C. E., ROTH, G., SURAWICZ, C. M., VAN BELLE, G., LEWIN, K., WEINSTEIN, W. M., ANTONIOLI, D. A., GOLDMAN, H. & ET AL. 1988. Observer variation in the diagnosis of dysplasia in Barrett's esophagus. *Hum Pathol,* 19**,** 166-78.
REID, B. J., PAULSON, T. G. & LI, X. 2015. Genetic Insights in Barrett's Esophagus and Esophageal Adenocarcinoma. *Gastroenterology,* 149**,** 1142-1152 e3.
REIS, C. A., DAVID, L., CORREA, P., CARNEIRO, F., DE BOLOS, C., GARCIA, E., MANDEL, U., CLAUSEN, H. & SOBRINHO-SIMOES, M. 1999. Intestinal metaplasia of human stomach displays distinct patterns of mucin (MUC1, MUC2, MUC5AC, and MUC6) expression. *Cancer Res,* 59**,** 1003-7.
RHINER, C. & MORENO, E. 2009. Super competition as a possible mechanism to pioneer precancerous fields. *Carcinogenesis,* 30**,** 723-8.
RIDDELL, R. H. 2005. The genesis of Barrett esophagus: has a histologic transition from gastroesophageal reflux disease-damaged epithelium to columnar metaplasia ever been seen in humans? *Arch Pathol Lab Med,* 129**,** 164-9.
RIDDELL, R. H., GOLDMAN, H., RANSOHOFF, D. F., APPELMAN, H. D., FENOGLIO, C. M., HAGGITT, R. C., AHREN, C., CORREA, P., HAMILTON, S. R., MORSON, B. C. & ET AL. 1983. Dysplasia in inflammatory bowel disease: standardized classification with provisional clinical applications. *Hum Pathol,* 14**,** 931-68.
RIDDELL, R. H. & ODZE, R. D. 2009. Definition of Barrett's esophagus: time for a rethink--is intestinal metaplasia dead? *Am J Gastroenterol,* 104**,** 2588-94.
RONKAINEN, J., ARO, P., STORSKRUBB, T., JOHANSSON, S. E., LIND, T., BOLLING-STERNEVALD, E., VIETH, M., STOLTE, M., TALLEY, N. J. & AGREUS, L. 2005. Prevalence of Barrett's esophagus in the general population: an endoscopic study. *Gastroenterology,* 129**,** 1825-31.
ROSS-INNES, C. S., BECQ, J., WARREN, A., CHEETHAM, R. K., NORTHEN, H., O'DONOVAN, M., MALHOTRA, S., DI PIETRO, M., IVAKHNO, S., HE, M., WEAVER, J. M., LYNCH, A. G., KINGSBURY, Z., ROSS, M., HUMPHRAY, S., BENTLEY, D., FITZGERALD, R. C., OESOPHAGEAL CANCER, C.,

MOLECULAR STRATIFICATION STUDY, G., OESOPHAGEAL CANCER, C. & MOLECULAR STRATIFICATION, O. S. G. 2015. Whole-genome sequencing provides new insights into the clonal architecture of Barrett's esophagus and esophageal adenocarcinoma. *Nat Genet,* 47**,** 1038-46.

ROUSE, R. V., SOETIKNO, R. M., BAKER, R. J., BARNARD, I. C., TRIADAFILOPOULOS, G. & LONGACRE, T. A. 1995. Esophageal submucosal gland duct adenoma. *Am J Surg Pathol,* 19**,** 1191-6.

SAADI, A., SHANNON, N. B., LAO-SIRIEIX, P., O'DONOVAN, M., WALKER, E., CLEMONS, N. J., HARDWICK, J. S., ZHANG, C., DAS, M., SAVE, V., NOVELLI, M., BALKWILL, F. & FITZGERALD, R. C. 2010. Stromal genes discriminate preinvasive from invasive disease, predict outcome, and highlight inflammatory pathways in digestive cancers. *Proc Natl Acad Sci U S A,* 107**,** 2177-82.

SAKURAZAWA, N., TANAKA, N., ONDA, M. & ESUMI, H. 2000. Instability of X chromosome methylation in aberrant crypt foci of the human colon. *Cancer Res,* 60**,** 3165-9.

SALK, J. J., SALIPANTE, S. J., RISQUES, R. A., CRISPIN, D. A., LI, L., BRONNER, M. P., BRENTNALL, T. A., RABINOVITCH, P. S., HORWITZ, M. S. & LOEB, L. A. 2009. Clonal expansions in ulcerative colitis identify patients with neoplasia. *Proc Natl Acad Sci U S A,* 106**,** 20871-6.

SAMPLINER, R. E., FENNERTY, B. & GAREWAL, H. S. 1996. Reversal of Barrett's esophagus with acid suppression and multipolar electrocoagulation: preliminary results. *Gastrointest Endosc,* 44**,** 532-5.

SAMPLINER, R. E., STEINBRONN, K., GAREWAL, H. S. & RIDDELL, R. H. 1988. Squamous mucosa overlying columnar epithelium in Barrett's esophagus in the absence of anti-reflux surgery. *Am J Gastroenterol,* 83**,** 510-2.

SCHMIDT, G. H., WINTON, D. J. & PONDER, B. A. 1988. Development of the pattern of cell renewal in the crypt-villus unit of chimaeric mouse small intestine. *Development,* 103**,** 785-90.

SEERY, J. P. 2002. Stem cells of the oesophageal epithelium. *J Cell Sci,* 115**,** 1783-9.

SENOO, M., PINTO, F., CRUM, C. P. & MCKEON, F. 2007. p63 Is essential for the proliferative potential of stem cells in stratified epithelia. *Cell,* 129**,** 523-36.

SHEPHERD, N. A. 2000. Barrett's oesophagus and proton pump inhibitors: a pathological perspective. *Gut,* 46**,** 147-9.

SHIBATA, D. 2009. Inferring human stem cell behaviour from epigenetic drift. *J Pathol,* 217**,** 199-205.

SHIELDS, H. M., ROSENBERG, S. J., ZWAS, F. R., RANSIL, B. J., LEMBO, A. J. & ODZE, R. 2001. Prospective evaluation of multilayered epithelium in Barrett's esophagus. *Am J Gastroenterol,* 96**,** 3268-73.

SIEGMUND, K. D., MARJORAM, P., TAVARE, S. & SHIBATA, D. 2009a. Many colorectal cancers are "flat" clonal expansions. *Cell Cycle,* 8**,** 2187-93.

SIEGMUND, K. D., MARJORAM, P., WOO, Y. J., TAVARE, S. & SHIBATA, D. 2009b. Inferring clonal expansion and cancer stem cell dynamics from DNA methylation patterns in colorectal cancers. *Proc Natl Acad Sci U S A,* 106**,** 4828-33.

SILVA, A. J., WARD, K. & WHITE, R. 1993. Mosaic methylation in clonal tissue. *Dev Biol,* 156**,** 391-8.

SKINNER, D. B., WALTHER, B. C., RIDDELL, R. H., SCHMIDT, H., IASCONE, C. & DEMEESTER, T. R. 1983. Barrett's esophagus. Comparison of benign and malignant cases. *Ann Surg,* 198**,** 554-65.
SLAUGHTER, D. P., SOUTHWICK, H. W. & SMEJKAL, W. 1953. Field cancerization in oral stratified squamous epithelium; clinical implications of multicentric origin. *Cancer,* 6**,** 963-8.
SOSLOW, R. A., ALTORKI, N. K., YANG, G., XIE, D. & YANG, C. S. 1999. mdm-2 expression correlates with wild-type p53 status in esophageal adenocarcinoma. *Mod Pathol,* 12**,** 580-6.
SOTTORIVA, A., KANG, H., MA, Z., GRAHAM, T. A., SALOMON, M. P., ZHAO, J., MARJORAM, P., SIEGMUND, K., PRESS, M. F., SHIBATA, D. & CURTIS, C. 2015. A Big Bang model of human colorectal tumor growth. *Nat Genet,* 47**,** 209-16.
SOTTORIVA, A., SPITERI, I., SHIBATA, D., CURTIS, C. & TAVARE, S. 2013. Single-molecule genomic data delineate patient-specific tumor profiles and cancer stem cell organization. *Cancer Res,* 73**,** 41-9.
SOUZA, R. F., KRISHNAN, K. & SPECHLER, S. J. 2008. Acid, bile, and CDX: the ABCs of making Barrett's metaplasia. *Am J Physiol Gastrointest Liver Physiol,* 295**,** G211-8.
SPECHLER, S. J. 2002. Barrett's Esophagus. *New England Journal of Medicine,* 346**,** 836-842.
SPECHLER, S. J. 2003. The natural history of dysplasia and cancer in esophagitis and Barrett esophagus. *J Clin Gastroenterol,* 36**,** S2-5; discussion S26-8.
STACHLER, M. D., TAYLOR-WEINER, A., PENG, S., MCKENNA, A., AGOSTON, A. T., ODZE, R. D., DAVISON, J. M., NASON, K. S., LODA, M., LESHCHINER, I., STEWART, C., STOJANOV, P., SEEPO, S., LAWRENCE, M. S., FERRER-TORRES, D., LIN, J., CHANG, A. C., GABRIEL, S. B., LANDER, E. S., BEER, D. G., GETZ, G., CARTER, S. L. & BASS, A. J. 2015. Paired exome analysis of Barrett's esophagus and adenocarcinoma. *Nat Genet,* 47**,** 1047-55.
STEIN, H. J., FEITH, M., VON RAHDEN, B. H. & SIEWERT, J. R. 2003. Approach to early Barrett's cancer. *World J Surg,* 27**,** 1040-6.
TAANMAN, J. W. 1999. The mitochondrial genome: structure, transcription, translation and replication. *Biochim Biophys Acta,* 1410**,** 103-23.
TAKUBO, K., ESAKI, Y., WATANABE, A., UMEHARA, M. & SASAJIMA, K. 1993. Adenoma accompanied by superficial squamous cell carcinoma of the esophagus. *Cancer,* 71**,** 2435-8.
TAYLOR, R. W., BARRON, M. J., BORTHWICK, G. M., GOSPEL, A., CHINNERY, P. F., SAMUELS, D. C., TAYLOR, G. A., PLUSA, S. M., NEEDHAM, S. J., GREAVES, L. C., KIRKWOOD, T. B. & TURNBULL, D. M. 2003. Mitochondrial DNA mutations in human colonic crypt stem cells. *J Clin Invest,* 112**,** 1351-60.
TAYLOR, R. W. & TURNBULL, D. M. 2005. Mitochondrial DNA mutations in human disease. *Nat Rev Genet,* 6**,** 389-402.
THEODOROU, D., AYAZI, S., DEMEESTER, S. R., ZEHETNER, J., PEYRE, C. G., GRANT, K. S., AUGUSTIN, F., OH, D. S., LIPHAM, J. C., CHANDRASOMA, P. T., HAGEN, J. A. & DEMEESTER, T. R. 2012. Intraluminal pH and goblet cell density in Barrett's esophagus. *J Gastrointest Surg,* 16**,** 469-74.
TIMMER, M. R., MARTINEZ, P., LAU, C. T., WESTRA, W. M., CALPE, S., RYGIEL, A. M., ROSMOLEN, W. D., MEIJER, S. L., TEN KATE, F. J., DIJKGRAAF, M. G., MALLANT-HENT, R. C., NABER, A. H., VAN OIJEN, A. H., BAAK, L. C.,

SCHOLTEN, P., BOHMER, C. J., FOCKENS, P., MALEY, C. C., GRAHAM, T. A., BERGMAN, J. J. & KRISHNADATH, K. K. 2015. Derivation of genetic biomarkers for cancer risk stratification in Barrett's oesophagus: a prospective cohort study. *Gut*.

TSAO, J. L., YATABE, Y., SALOVAARA, R., JARVINEN, H. J., MECKLIN, J. P., AALTONEN, L. A., TAVARE, S. & SHIBATA, D. 2000. Genetic reconstruction of individual colorectal tumor histories. *Proc Natl Acad Sci U S A,* 97**,** 1236-41.

TSIOURIS, A., HAMMOUD, Z. & VELANOVICH, V. 2011. Barrett's esophagus after resection of the gastroesophageal junction: effects of concomitant fundoplication. *World J Surg,* 35**,** 1867-72.

UPTON, M. P., NISHIOKA, N. S., RANSIL, B. J., ROSENBERG, S. J., PURICELLI, W. P., ZWAS, F. R. & SHIELDS, H. M. 2006. Multilayered epithelium may be found in patients with Barrett's epithelium and dysplasia or adenocarcinoma. *Dig Dis Sci,* 51**,** 1783-90.

VAEZI, M. F. & RICHTER, J. E. 1996. Role of acid and duodenogastroesophageal reflux in gastroesophageal reflux disease. *Gastroenterology,* 111**,** 1192-9.

VELICESCU, M., WEISENBERGER, D. J., GONZALES, F. A., TSAI, Y. C., NGUYEN, C. T. & JONES, P. A. 2002. Cell division is required for de novo methylation of CpG islands in bladder cancer cells. *Cancer Res,* 62**,** 2378-84.

VOGELSTEIN, B., PAPADOPOULOS, N., VELCULESCU, V. E., ZHOU, S., DIAZ, L. A., JR. & KINZLER, K. W. 2013. Cancer genome landscapes. *Science,* 339**,** 1546-58.

VOUTILAINEN, M., SIPPONEN, P., MECKLIN, J. P., JUHOLA, M. & FARKKILA, M. 2000. Gastroesophageal reflux disease: prevalence, clinical, endoscopic and histopathological findings in 1,128 consecutive patients referred for endoscopy due to dyspeptic and reflux symptoms. *Digestion,* 61**,** 6-13.

WANG, K. K., SAMPLINER, R. E. & PRACTICE PARAMETERS COMMITTEE OF THE AMERICAN COLLEGE OF, G. 2008. Updated guidelines 2008 for the diagnosis, surveillance and therapy of Barrett's esophagus. *Am J Gastroenterol,* 103**,** 788-97.

WANG, X., OUYANG, H., YAMAMOTO, Y., KUMAR, P. A., WEI, T. S., DAGHER, R., VINCENT, M., LU, X., BELLIZZI, A. M., HO, K. Y., CRUM, C. P., XIAN, W. & MCKEON, F. 2011. Residual embryonic cells as precursors of a Barrett's-like metaplasia. *Cell,* 145**,** 1023-35.

WASAN, H. S., PARK, H. S., LIU, K. C., MANDIR, N. K., WINNETT, A., SASIENI, P., BODMER, W. F., GOODLAD, R. A. & WRIGHT, N. A. 1998. APC in the regulation of intestinal crypt fission. *J Pathol,* 185**,** 246-55.

WEAVER, J. M., ROSS-INNES, C. S., SHANNON, N., LYNCH, A. G., FORSHEW, T., BARBERA, M., MURTAZA, M., ONG, C. A., LAO-SIRIEIX, P., DUNNING, M. J., SMITH, L., SMITH, M. L., ANDERSON, C. L., CARVALHO, B., O'DONOVAN, M., UNDERWOOD, T. J., MAY, A. P., GREHAN, N., HARDWICK, R., DAVIES, J., OLOUMI, A., APARICIO, S., CALDAS, C., ELDRIDGE, M. D., EDWARDS, P. A., ROSENFELD, N., TAVARE, S., FITZGERALD, R. C. & CONSORTIUM, O. 2014. Ordering of mutations in preinvasive disease stages of esophageal carcinogenesis. *Nat Genet,* 46**,** 837-43.

WESTHOFF, B., BROTZE, S., WESTON, A., MCELHINNEY, C., CHERIAN, R., MAYO, M. S., SMITH, H. J. & SHARMA, P. 2005. The frequency of Barrett's esophagus in high-risk patients with chronic GERD. *Gastrointest Endosc,* 61**,** 226-31.

WONG, A. & FITZGERALD, R. C. 2005. Epidemiologic risk factors for Barrett's esophagus and associated adenocarcinoma. *Clin Gastroenterol Hepatol,* 3**,** 1-10.

WONG, D. J., PAULSON, T. G., PREVO, L. J., GALIPEAU, P. C., LONGTON, G., BLOUNT, P. L. & REID, B. J. 2001. p16(INK4a) lesions are common, early abnormalities that undergo clonal expansion in Barrett's metaplastic epithelium. *Cancer Res,* 61**,** 8284-9.

WONG, W. M., MANDIR, N., GOODLAD, R. A., WONG, B. C., GARCIA, S. B., LAM, S. K. & WRIGHT, N. A. 2002. Histogenesis of human colorectal adenomas and hyperplastic polyps: the role of cell proliferation and crypt fission. *Gut,* 50**,** 212-7.

WU, M., PASTOR-PAREJA, J. C. & XU, T. 2010. Interaction between Ras(V12) and scribbled clones induces tumour growth and invasion. *Nature,* 463**,** 545-8.

XIAN, W., HO, K. Y., CRUM, C. P. & MCKEON, F. 2012. Cellular origin of Barrett's esophagus: controversy and therapeutic implications. *Gastroenterology,* 142**,** 1424-30.

YANG, A., KAGHAD, M., WANG, Y., GILLETT, E., FLEMING, M. D., DOTSCH, V., ANDREWS, N. C., CAPUT, D. & MCKEON, F. 1998. p63, a p53 homolog at 3q27-29, encodes multiple products with transactivating, death-inducing, and dominant-negative activities. *Mol Cell,* 2**,** 305-16.

YANG, A., SCHWEITZER, R., SUN, D., KAGHAD, M., WALKER, N., BRONSON, R. T., TABIN, C., SHARPE, A., CAPUT, D., CRUM, C. & MCKEON, F. 1999. p63 is essential for regenerative proliferation in limb, craniofacial and epithelial development. *Nature,* 398**,** 714-8.

YATABE, Y., TAVARE, S. & SHIBATA, D. 2001. Investigating stem cells in human colon by using methylation patterns. *Proc Natl Acad Sci U S A,* 98**,** 10839-44.

YOUNES, M., LEBOVITZ, R. M., LECHAGO, L. V. & LECHAGO, J. 1993. p53 protein accumulation in Barrett's metaplasia, dysplasia, and carcinoma: a follow-up study. *Gastroenterology,* 105**,** 1637-42.

YOUSEF, F., CARDWELL, C., CANTWELL, M. M., GALWAY, K., JOHNSTON, B. T. & MURRAY, L. 2008. The incidence of esophageal cancer and high-grade dysplasia in Barrett's esophagus: a systematic review and meta-analysis. *Am J Epidemiol,* 168**,** 237-49.

ZAGARI, R. M., FUCCIO, L., WALLANDER, M. A., JOHANSSON, S., FIOCCA, R., CASANOVA, S., FARAHMAND, B. Y., WINCHESTER, C. C., RODA, E. & BAZZOLI, F. 2008. Gastro-oesophageal reflux symptoms, oesophagitis and Barrett's oesophagus in the general population: the Loiano-Monghidoro study. *Gut,* 57**,** 1354-9.

ZHU, X., DENG, C., KUICK, R., YUNG, R., LAMB, B., NEEL, J. V., RICHARDSON, B. & HANASH, S. 1999. Analysis of human peripheral blood T cells and single-cell-derived T cell clones uncovers extensive clonal CpG island methylation heterogeneity throughout the genome. *Proc Natl Acad Sci U S A,* 96**,** 8058-63.

Appendices:

8.1 Primers and PCR reaction conditions:

Table 8 highlights primers with their sequences used in this study and also gives the reaction conditions for the PCR reaction.

Primers	**Sequence 5' to 3' (include modification codes if applicable)**	**Reaction conditions (Annealing temp / MgCl2 / Q-solution)**
p16-2A 1st F	GCTTCCTTTCCGTCATGC	60 / 2 / 5
p16-2A 1st R	CAGGTACCGTGCGACATC	
p16-2B 1st F	CTGTTCTCTCTGGCAGGTCA	60 / 2 / 5
p16-2B 1st R	TGTGCTGGAAAATGAATGCT	
p16-2A 2nd F	CCTGGCTCTGACCATTCTGT	60 / 2 / 5
p16-2A 2ndR	CAGCTCCTCAGCCAGGTC	
p16-2B 2nd F	CTTCCTGGACACGCTGGT	60 / 2 / 5
p16-2B 2nd R	TGGAAGCTCTCAGGGTACAAA	
KRAS 1st F	GAGTTTGTATTAAAAGGTACTGGTGGA	60 / 2 / 5
KRAS 1st R	ATCAAAGAATGGTCCTGCAC	
KRAS 2nd F	TTTGATAGTGTATTAACCTTAT	55 / 2 / 5
KRAS 2nd R	TATTAAAACAAGATTTACCTC	
p53-5 1st F	CACTTGTGCCCTGACTTTCA	55 / 1 / 5
p53-5 1st R	GAGCAATCAGTGAGGAATCAGA	
p53-6 1st F	AGAGACGACAGGGCTGGTT	60 / 2 / 5
p53-6 1st R	TGGAGGGCCACTGACAAC	
p53-7 1st F	TGCTTGCCACAGGTCTCC	60 / 1 / 5
p53-7 1st R	GGTCAGAGGCAAGCAGAGG	
p53-8 1st F	TTTTTAAATGGGACAGGTAGGA	60 / 2 / 5
p53-8 1st R	CACCCTTGGTCTCCTCCAC	
p53-5 2nd F	TCTGTCTCCTTCCTCTTCCTACA	60 / 1 / 5
p53-5 2nd R	AACCAGCCCTGTCGTCTCT	
p53-6 2nd F	CAGGCCTCTGATTCCTCACT	60 / 1 / 0

p53-6 2nd R	CTTAACCCCTCCTCCCAGAG	
p53-7 2nd F	CTTGGGCCTGTGTTATCTCC	60 / 1 / 5
p53-7 2nd R	GTGTGCAGGGTGGCAAGT	
p53-8 2nd F	GCCTCTTGCTTCTCTTTTCC	60 / 2 / 0
p53-8 2nd R	GCTTCTTGTCCTGCTTGCTT	

Table 8: List of primers, primer sequence and reaction conditions. F-forward and R-reverse.

Table 9 and Table 10 highlights the number of cycles done, various stages involved and conditions required for the PCR and the sequencing reaction respectively.

Number of cycles	Steps	Temperature (^{o}C)	Time (minutes)
1	Initial denaturing	95	4
37	Denaturing Primer annealing Extension	94 55 or 60 72	1 1 1
1	Final extension	72	10

Table 9: PCR reaction conditions.

Number of cycles	Steps	Temperature (^{o}C)	Time (minutes)
1	Initial denaturing	96	5
34	Denaturing Primer annealing Extension	96 50 60	0.5 0.75 4
1	Final extension	60	7

Table 10: Sequencing reaction conditions.

Table 11 highlights primers with their sequences used in this study and also gives the PCR reaction conditions for the LOH reaction.

Primers	**Sequence 5' to 3'**	**Reaction conditions (Annealing temp / Q-solution)**
Multiplex 1		57 / 0
D18S58 F	GCTCCCGGCTGGTTTT	
D18S58 R	GCAGGAAATCGCAGGAACTT	
D5S346 F	ACTCACTCTAGTGATAAATCGGG	
D5S346 R	AGCAGATAAGACAGTATTACTAGTT	
D9S932 F	CTCCCTTTGTATTTCTGTTCTATT	
D9S932 R	AAGCTATGATGGTGCCACC	
D3S1300 F	ACAAAGGAACGTCATGTGGTAGG	
D3S1300 R	GCTGTTTATTCTTCGTGGAATGCC	
Multiplex 2		57 / 0
D17S250 F	GGAAGAATCAAATAGACAAT	
D17S250 R	GCTGGCCATATATATATTTAAACC	
D18S474 F	CTCCACCCACTAGATGTCAG	
D18S474 R	ACTTGCTTAAGCCTTGGACT	
D17S1832 F	ACGCCTTGACATAGTTGC	
D17S1832 R	TGTGTGACTGTTCAGCCTC	
D3S1313 F	TACTTTCCTTCAGATCCTTGG	
D3S1313 R	AACTAGGGGCCATGAATAAG	
Multiplex 3		57 / 0
D17S1176 F	ACTTCATATACATATCACGTGC	
D17S1176 R	TCAATGGAGAATTACGATAGTG	
D17S1678 F	TTTGGGTCTTTGAACCCTTG	
D17S1678 R	CCACAACAAAACACCAGTGC	
D17S1881 F	CCCAGTTTAAGGAGTTTGGC	
D17S1881 R	TAGGGCAGTCAGCCTTGTG	
Multiplex 4		57 / 5
D9S942 F	GCAAGATTCCAAACAGTA	
D9S942 R	CTCATCCTGCGGAAACCATT	
D5S2001 F	GCCAAGATGGTCTCGATCTC	
D5S2001 R	TCTGAACAGGTGATGGCAAC	
D17S1506 F	TGTGGGATGGGGTGAGATTTC	

D17S1506 R	CTGTTGGTCGGTGGGTTG	
D5S489 F	GGGCTTTTGTGTTGTTTCTA	
D5S489 R	GAAAACCCATAACCAGACTTG	

Table 11: Microsatellite loss of heterozygosity analysis. Primers, sequence and conditions. F-forward and R-reverse.

Table 12, table 13 and table 14 highlights the number of cycles done, various stages involved and conditions required for the first and the second round PCR and sequencing reaction respectively for the mitochondrial DNA sequencing.

Number of cycles	Steps	Temperature (^oC)	Time (minutes)
1	Initial denaturing	95	10
38	Denaturing Primer annealing Extension	94 55 or 60 72	0.75 0.75 2
1	Final extension	72	8

Table 12: First round PCR reaction conditions for mitochondrial DNA sequencing.

Number of cycles	Steps	Temperature (^oC)	Time (minutes)
1	Initial denaturing	95	10
30	Denaturing Primer annealing Extension	94 55 or 60 72	0.75 0.75 1
1	Final extension	72	8

Table 13: Second round PCR reaction conditions for mitochondrial DNA sequencing.

Number of cycles	Steps	Temperature (^oC)	Time
1	Initial denaturing	96	1 minute
25	Denaturing Primer annealing Extension	96 50 60	10 seconds 5 seconds 4 minute
1	Final extension	60	

Table 14: Sequencing reaction conditions for mitochondrial DNA sequencing.

Table 15 and 16 highlights reference sequence and PCR conditions for CSX and MYOD gene.

Primers	**Sequence 5' to 3'**	**Reaction conditions (Annealing temp / Q-solution)**
CSX 1F	GAGTTTGGTAGGGAAGGGATT	55/0
CSX 1R	AAAACACTCCTAAAAAAACAACTA	
CSX 2F	GGAGATTTAGGAATTTTTTTTGTTTT	60/0
CSX 2R	CACCAAACTACAAAATCACTCATTACA	
MYOD 1F	GGGTTTTTTTTTTAGTTGAAGAGGT	60/5
MYOD 1R	ACCTAAAAATTACTCAACAAAT	
MYOD 2F	TGGAGGGGATTTTTAATTTGG	55/5
MYOD 2R	AACCCAATCCTTCTTCCCTAA	
M13 F	GTAAAACGACGGCCAGT	55/0
M13 R	CAGGAAACAGCTATGAC	

Table 15: Methylation primer details. Primer sequence and conditions. F-forward and R-reverse.

LOCUS	SEQUENCE
CSX (8CpGs)	**G**gagaTTtaggaaTtttttTtgtTTTa**CGCGCG**tttgttTttg**CG**Ta**CG**ggagagtttgtg g**CG**g**CG**attatgTag**CG**tgTaatgagtgatTTtgTagTTtggtg
MYOD (5CpGs)	tggaggggattTTtaaTTtgggTaggatT**CG**agtttggagagattgg**CGCG**aagTtttagT agTaatTtT**CG**attTTtgtaTaaTTatagTtgggtttTtaag**CG**tTtagggaagaaggaTt gggTT

Table 16: Reference post-bisulphite treatment sequence for CSX and MYOD. In the above sequence; T represent a tymine base produce by post bisulphite converstion of a cytosine base. CpG sites are presumed methylated and are represented in bold. Second round primer binding sites are underlined.

Table 17 highlights 1st round PCR mitochondrial primers with their sequences used in this study.

Primer	Primer sequence	Primer position
AF	GCTCACATCACCCCATAAAC	627-646
AR	GATTACTCCGGTCTGAACTC	3087-3068
BF	ACCAACAAGTCATTATTACCC	2395-2415
BR	TGAGGAAATACTTGATGGCAG	4653-4633
CF	CCGTCATCTACTCTACCATC	4489-4508
CR	GGACGGATCAGACGAAGAG	6468-6450
DF	AATACCCATCATAATCGGAGG	6113-6133
DR	GGTGATGAGGAATAGTGTAAG	8437-8417
EF	AACCACTTTCACCGCTACAC	8128-8147
ER	AGTGAGATGGTAAATGCTAG	10516-10487
FF	ACTTCACGTCATTATTGGCTC	9821-9841
FR	ATAGGAGGAGAATGGGGGATAG	12101-12080
GF	ACCCCCCACTATTAACCTACTG	11866-11887
GR	GGTAGAATCCGAGTATGTTGG	13924-13904
HF	TATTCGCAGGATTTCTCATTAC	13721-13742
HR	AGCTTTGGGTGCTAATGGTG	15997-15978
IF	CCCATCCTCCATATATCCAAAC	15659-15680
IR	GGTTAGTATAGCTTAGTTAAAC	868-847

Table 17: Mitochondrial primer sequences for 1st round PCR. F-forward and R-reverse.

Table 18 highlights 2nd round PCR primers with their sequences used in this study.

Primer	Primer sequence	Primer position
1F	TGTAAAACGACGGCCAGTTCACCCTCTAAATCACCAG	721-740
1R	CAGGAAACAGCTATGACCGATGGCGGTATATAGGCTGAG	1268-1248
2F	TGTAAAACGACGGCCAGTTTAAAACTCAAAGGACCTGGC	1157-1177
2R	CAGGAAACAGCTATGACCCTGGTAGTAAGGTGGAGTGGG	1709-1689
3F	TGTAAAACGACGGCCAGTAACTTAACTTGACCGCTCTGAG	1650-1671
3R	TGTAAAACGACGGCCAGTAACTTAACTTGACCGCTCTGAG	2193-2175
4F	TGTAAAACGACGGCCAGTACTGTTAGTCCAAAGAGGAAC	2091-2111

4R	CAGGAAACAGCTATGACCTCGTGGAGCCATTCATACAG	2644-2625
5F	TGTAAAACGACGGCCAGTCAGTGACACATGTTTAACGGC	2549-2569
5R	CAGGAAACAGCTATGACCGATTACTCCGGTCTGAACTC	3087-3068
6F	TGTAAAACGACGGCCAGTCAGCCGCTATTAAAGGTTCG	3017-3036
6R	CAGGAAACAGCTATGACCGGAGGGGGGTTCATAGTAG	3374- 3356
7F	TGTAAAACGACGGCCAGTCCTTAGCTCTCACCATCGC	3533-3351
7R	CAGGAAACAGCTATGACCAGAGTGCGTCATATGTTGTTC	4057-4037
8F	TGTAAAACGACGGCCAGTAATAAACACCCTCACCACTAC	4005-4025
8R	CAGGAAACAGCTATGACCGTTTATTTCTAGGCCTACTCAG	4577-4556
9F	TGTAAAACGACGGCCAGTACACTCATCACAGCGCTAAG	4518-4537
9R	CAGGAAACAGCTATGACCGATTTTGCGTAGCTGGGTTTG	5003-4983
10F	TGTAAAACGACGGCCAGTTCCATCATAGCAGGCAGTTG	4950-4969
10R	CAGGAAACAGCTATGACCTGTAGGAGTAGCGTGGTAAGG	5481-5462
11F	TGTAAAACGACGGCCAGTACCTCAATCACACTACTCCC	5367-5386
11R	CAGGAAACAGCTATGACCTAGTCAACGGTCGGCGAAC	5924-5906
12F	TGTAAAACGACGGCCAGTCACTCAGCCATTTTACCTCAC	5875-5895
12R	CAGGAAACAGCTATGACCATGGCAGGGGGTTTTATATTG	6430-6410
13F	TGTAAAACGACGGCCAGTTTAGGGGCCATCAATTTCATC	6378-6398
13R	CAGGAAACAGCTATGACCAAGAAAGATGAATCCTAGGGC	6944-6924
14F	TGTAAAACGACGGCCAGTATTTAGCTGACTCGCCACAC	6863-6882
14R	CAGGAAACAGCTATGACCCATCCATATAGTCACTCCAGG	7396-7376
15F	TGTAAAACGACGGCCAGTGGCTCATTCATTTCTCTAACAG	7272-7293
15R	CAGGAAACAGCTATGACCGGCAGGATAGTTCAGACGG	7791-7773
16F	TGTAAAACGACGGCCAGTTAACATCTCAGACGCTCAGG	7744-7763
16R	CAGGAAACAGCTATGACCTACAGTGGGCTCTAGAGGG	8301-8283
17F	TGTAAAACGACGGCCAGTACAGTTTCATGCCCATCGTC	8196-8215
17R	CAGGAAACAGCTATGACCGTATAAGAGATCAGGTTCGTC	8740-8720
18F	TGTAAAACGACGGCCAGTACCACCCAACAATGACTAATC	8656-8676
18R	CAGGAAACAGCTATGACCGTTGTCGTGCAGGTAGAGG	9201-9183
19F	TGTAAAACGACGGCCAGTATCCTAGAAATCGCTGTCGC	9127-9146
19R	CAGGAAACAGCTATGACCATTAGACTATGGTGAGCTCAG	9661-9641
20F	TGTAAAACGACGGCCAGTCATCCGTATTACTCGCATCAG	9607-9627
20R	CAGGAAACAGCTATGACCTAGCCGTTGAGTTGTGGTAG	10147-10128
21F	TGTAAAACGACGGCCAGTCAACACCCTCCTAGCCTTAC	10085-10104
21R	CAGGAAACAGCTATGACCAGGCACAATATTGGCTAAGAG	10649-10629
22F	TGTAAAACGACGGCCAGTATCGCTCACACCTCATATCC	10534-10553
22R	CAGGAAACAGCTATGACCATGATTAGTTCTGTGGCTGTG	11109-11089
23F	TGTAAAACGACGGCCAGTCTAATCTCCCTACAAATCTCC	11054-11074

23R	CAGGAAACAGCTATGACCTAGGTCTGTTTGTCGTAGGC	11605-11586
24F	TGTAAAACGACGGCCAGTTCCTTGTACTATCCCTATGAG	11541-11561
24R	CAGGAAACAGCTATGACCCGTGTGAATGAGGGTTTTATG	12054-12034
25F	TGTAAAACGACGGCCAGTACAATGGGGCTCACTCACC	12001-12019
25R	CAGGAAACAGCTATGACCGTGGCTCAGTGTCAGTTCG	12545-12527
26F	TGTAAAACGACGGCCAGTCATGTGCCTAGACCAAGAAG	12498-12517
26R	CAGGAAACAGCTATGACCCTGATTTGCCTGCTGCTGC	13009-12991
27F	TGTAAAACGACGGCCAGTGCCCTTCTAAACGCTAATCC	12940-12959
27R	CAGGAAACAGCTATGACCGGGAGGTTGAAGTGAGAGG	13453-13435
28F	TGTAAAACGACGGCCAGTCGGGTCCATCATCCACAAC	13365-13383
28R	CAGGAAACAGCTATGACCGTTAGGTAGTTGAGGTCTAGG	13859-13839
29F	TGTAAAACGACGGCCAGTACCTAAAACTCACAGCCCTC	13790-13809
29R	CAGGAAACAGCTATGACCAGGATTGGTGCTGTGGGTG	14374-14356
30F	TGTAAAACGACGGCCAGTCAACCACCACCCCATCATAC	14331-14350
30R	CAGGAAACAGCTATGACCAAGGAGTGAGCCGAAGTTTC	14857-14838
31F	TGTAAAACGACGGCCAGTATTCATCGACCTCCCCACC	14797-14815
31R	CAGGAAACAGCTATGACCGGTTGTTTGATCCCGTTTCG	15368-15349
32F	TGTAAAACGACGGCCAGTAGCCCTAGCAACACTCCAC	15316-15334
32R	CAGGAAACAGCTATGACCTACAAGGACAGGCCCATTTG	15896-15877
33F	TGTAAAACGACGGCCAGTATCGGAGGACAACCAGTAAG	15758-15777
33R	CAGGAAACAGCTATGACCGTGGGTAGGTTTGTTGGTATC	16294-16274
34F	TGTAAAACGACGGCCAGTCTCAACTATCACACATCAACTG	16223-16244
34R	CAGGAAACAGCTATGACCAGATACTGCGACATAGGGTG	129-110
35F	TGTAAAACGACGGCCAGTCACCCTATTAACCACTCACG	15-34
35R	CAGGAAACAGCTATGACCCTGGTTAGGCTGGTGTTAGG	389-370
36F	TGTAAAACGACGGCCAGTGCCACAGCACTTAAACACATC	323-343
36R	CAGGAAACAGCTATGACCTGCTGCGTGCTTGATGCTTG	771-752

Table 18: Mitochondrial primer sequences for 2nd round PCR. F-forward and R-reverse.

Table 19 highlights the number of cycles done, various stages involved and conditions required for the bisulphite reaction for methylation analysis.

Step	**Temperature**	**Time**
Denaturation	95°C	5 minutes
Incubation	60°C	25 minutes
Denaturation	95°C	5 minutes
Incubation	60°C	85 minutes
Denaturation	95°C	5 minutes
Incubation	60°C	175 minutes
Hold	20°C	Indefinite

Table 19: Bisulphite reaction conditions for methylation analysis.

8.2 EMRs from patient 2, patient 3, patient 6, patient 7 and patient 8 (Chapter-3):

An additional EMR specimen from patient 2 has been shown in Figure 65.

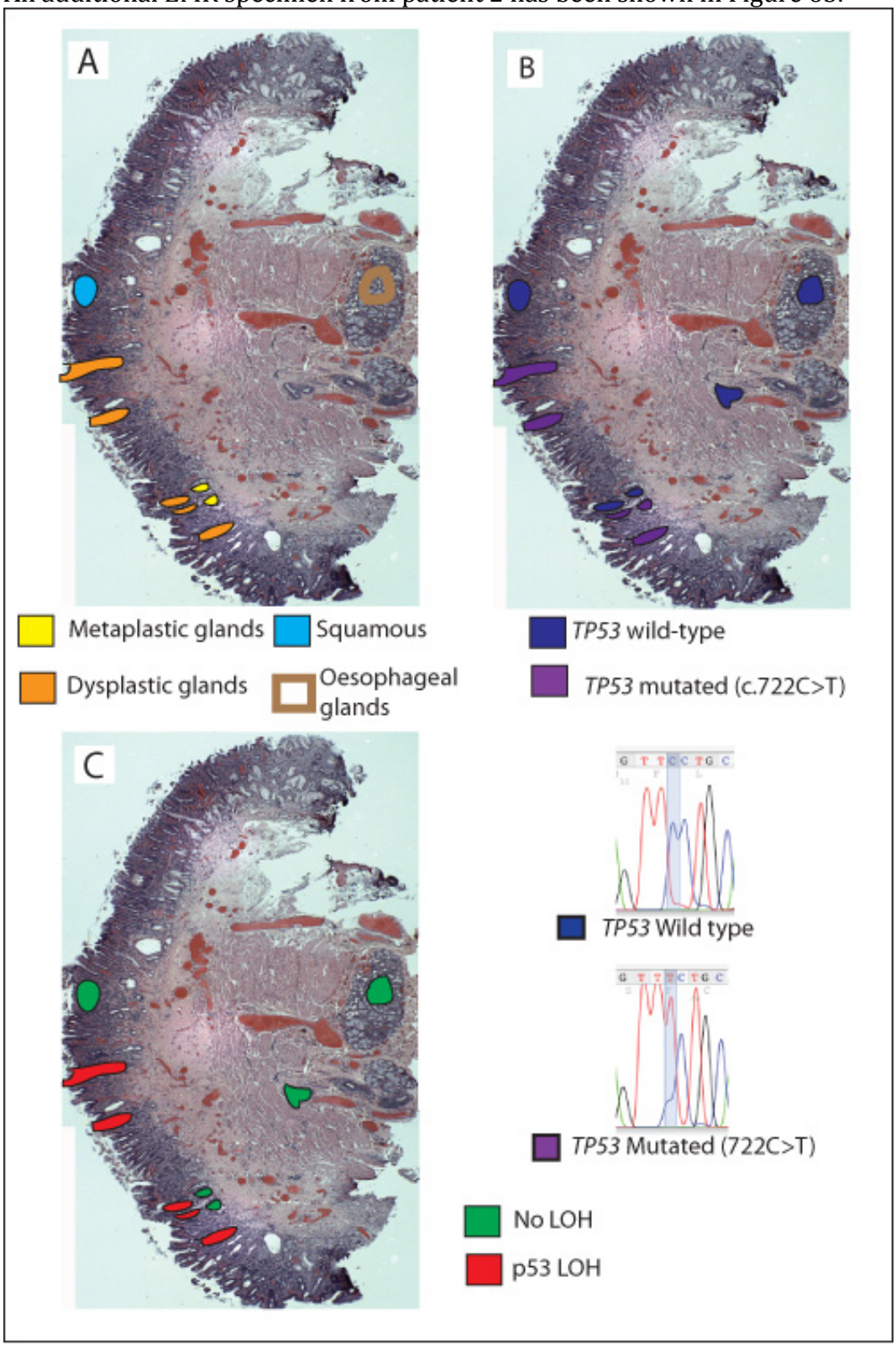

Figure 65: 2_dimentional map illustrating spatial distribution of different phenotype and genotype with their LOH status from patient 2 in Table 3 (Tissue-C) with Barrett's high grade dysplasia.
H&E photograph with the phenotype of each microdissected gland (A) with spatial distribution of clones that are wild type (Blue) or mutated (Purple) for *TP53* (722C>T) (B). Microdissected individual glands with *TP53* LOH at two microsatellite markers (D17S1176 and D17S1881) are coloured red and glands without LOH are coloured green (C).

Patient 3: EMR specimen from patient 3 mainly consists of metaplastic glands. 18 different glands were laser captured from the specimen. 17 out of 18 glands were mutated for *CDKN2A* (c.329G>A) and also showed *CDKN2A* LOH (Appendix, Table 21), but one gland was wild type for the same mutation (Figure 66), suggesting at least two clones in Barrett's metaplasia. Although only a single gland did not display the *CDKN2A* mutation, it was repeatedly verified and demonstrates the evolvability of Barrett's metaplasia.

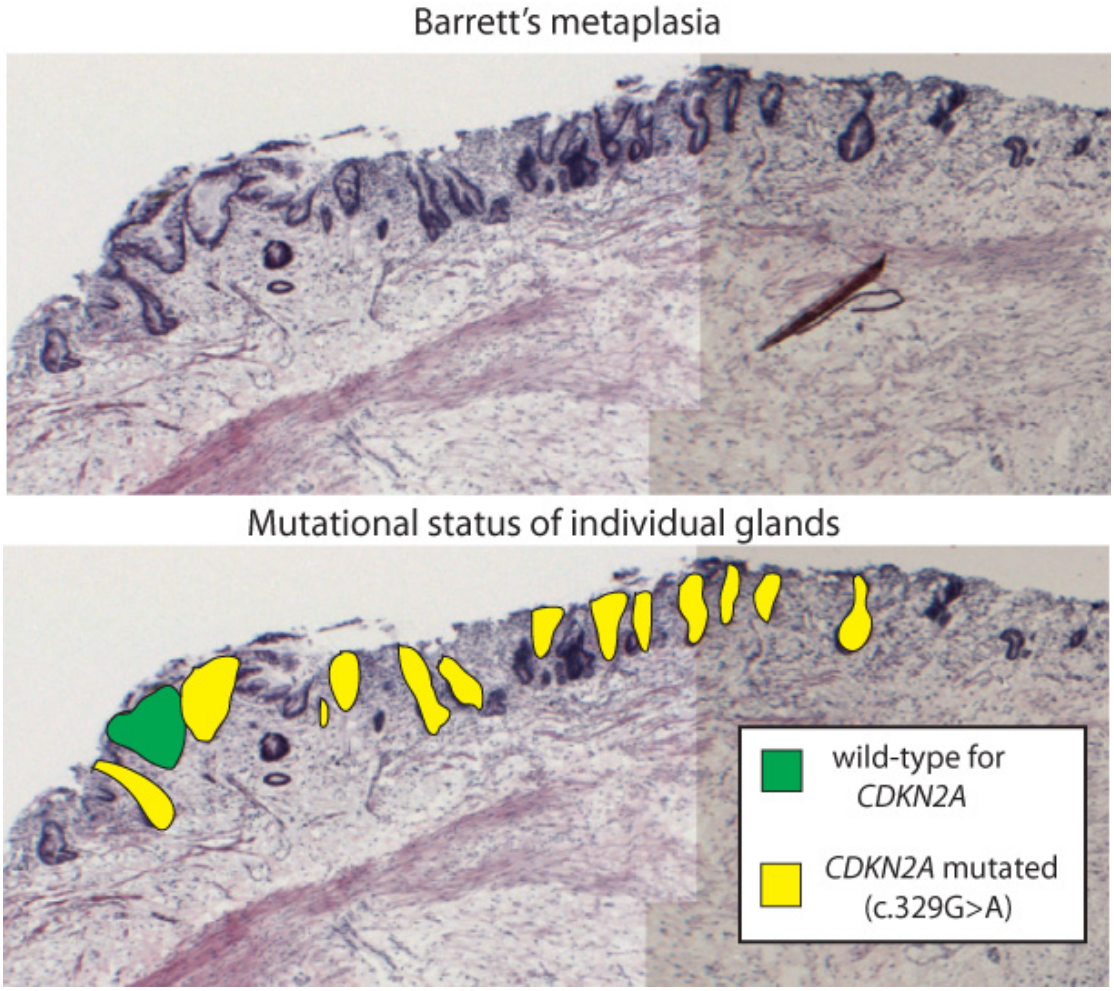

Figure 66: Heterogeneity in non-dysplastic Barrett's.
H&E of an EMR from patient 3 (Top half). Two-dimensional map of an EMR showing the mutational status of individual laser captured glands with cellular genotypes (Bottom half). Most metaplastic glands were mutated for *CDKN2A* (c.329G>A) mutation except one wild-type gland. These figures are composites of multiple images.

Patient 6: This EMR only had metaplastic glands along with cancer area. Seven individual metaplastic glands laser captured were all WT for *TP53*. 4 cancer areas laser-captured were mutated for *TP53* (c.743G>A) (Table 3).

Patient 7: Seven individual glands were laser-captured from the dysplastic area. All glands were mutated for *TP53* (c.451C>T). Two squamous areas laser-captured were WT for *TP53* (Table 3).

Patient 8: There were only dysplastic glands present in both pieces of tissue from patient 8 (Table 3) along with normal squamous areas. 29 individual glands were laser captured from those two specimens. 3 out of 29 glands were WT and 26 out of 29 glands were mutated for *TP53* (c.814G>A, see Figure 67) and 10 out of 13 glands showed *TP53* LOH (Figure 68), once again suggesting at least more than two clones in dysplasia. These observations suggest Barrett's dysplasia is polyclonal.

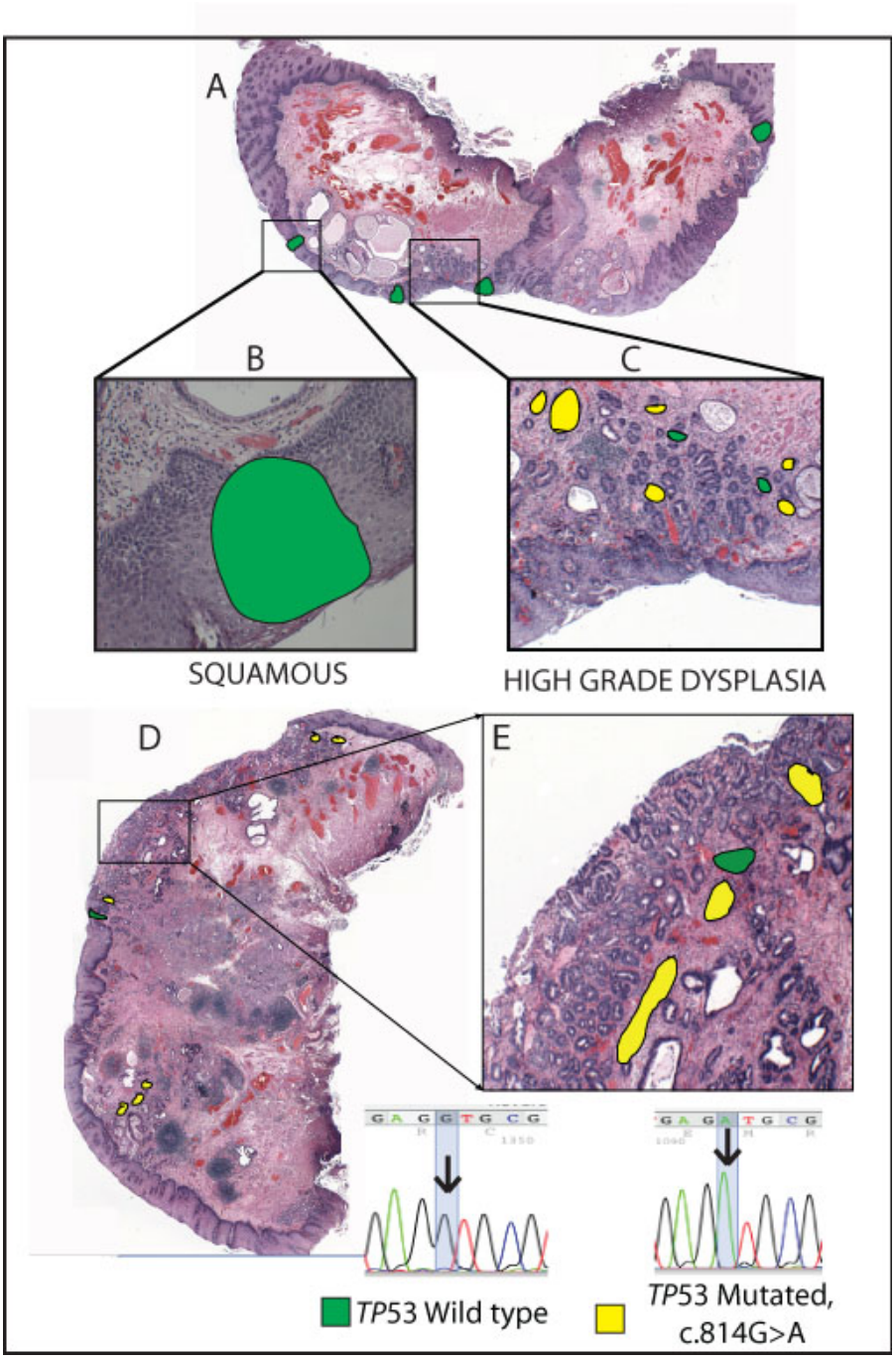

Figure 67: Genetic heterogeneity in Barrett's dysplasia from patient 8 in Table 3.
H&E photograph with the spatial distribution of clones in an EMR was taken from a patient with Barrett's high-grade dysplasia (A & D). The genotype of microdissected squamous area and individual Barrett's gland (B, C & E). Wild-type glands are coloured green and mutated (*TP53* c.814G>A) glands are coloured yellow.

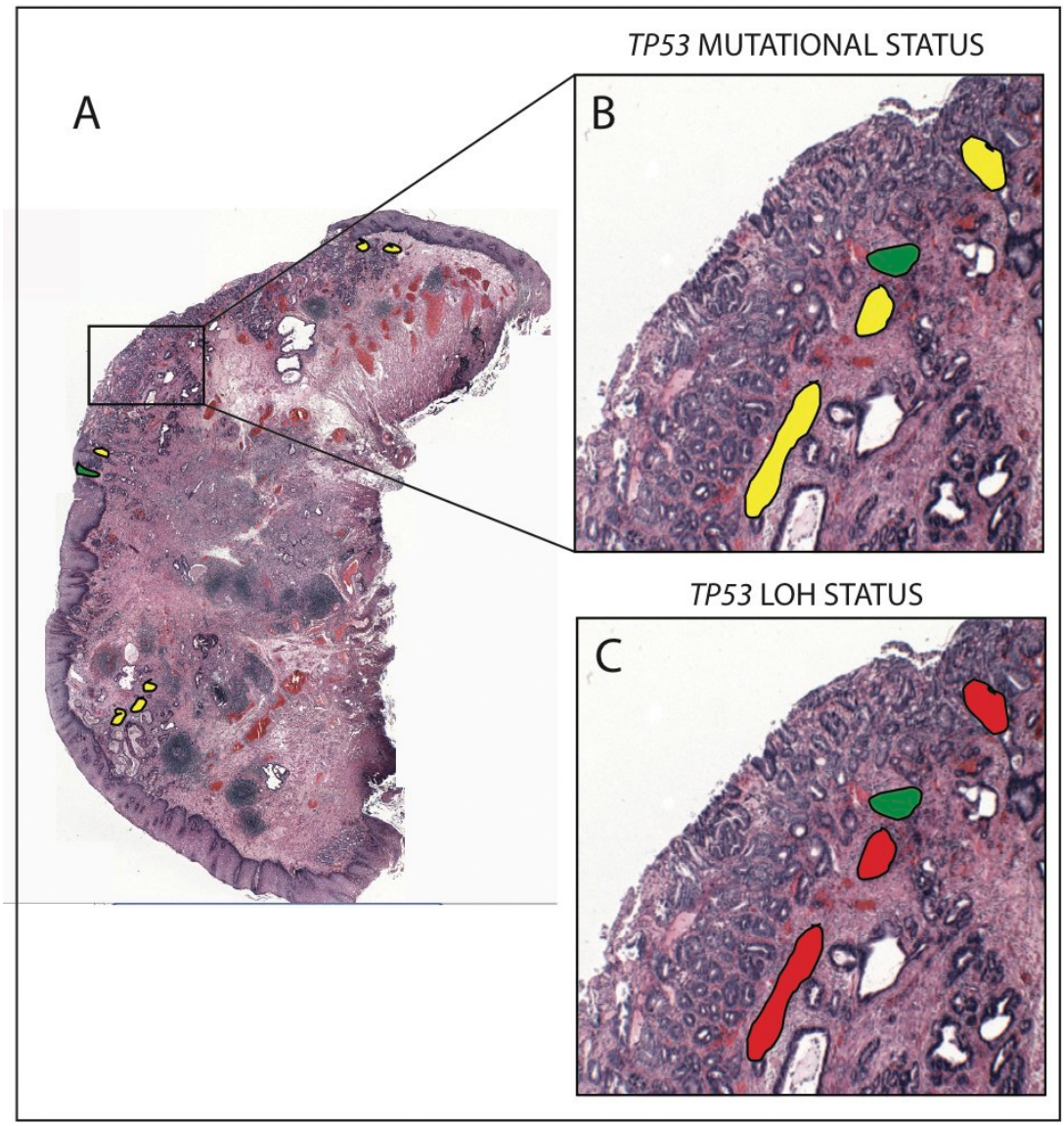

Figure 68: LOH status of *TP53* in EMR from patient 8 in Table 3.
H&E photograph with the spatial distribution of clones in an EMR was taken from patient 4 with Barrett's high-grade dysplasia (A). High-grade dysplastic glands mutated for *TP53* (c.814G>A) (Yellow colour in figure-B) also showed LOH for *TP53* at two microsatellite markers (D17S1176 and D17S1881) (Red colour in figure-C). *TP53* wild type gland coloured green did not have *TP53* LOH.

8.3 LOH analysis:

8.3.1 LOH analysis of specimen from patient 2 (Table 3):

The constitutional DNA was informative for one of the microsatellite marker for *TP53* (D17S1832). The results have been shown in the Table 20 below. LOH and mutational status of individual crypts from patient 2 in Table 3 have been summarized in Table 18. The spatial distribution of different phenotype and genotype with their LOH status from patient 2 in Table 3 have been shown in Figure 65 earlier. Some metaplastic and dysplastic crypts, which are wild type for *TP53*, also had LOH for *TP53*, suggesting that the clone with *TP53* LOH must have appeared first followed by the clone mutated for *TP53* with LOH. WT=wild type.

EMR glands	Phenotype	Mutational status for *TP53* (c.722C>T)	*TP53* LOH (D17S1832)
1	Metaplasia	WT	No LOH
2	Metaplasia	WT	No LOH
3	Metaplasia	WT	No LOH
4	Metaplasia	WT	No LOH
5	Metaplasia	WT	No LOH
6	Metaplasia	WT	LOH
7	Metaplasia	WT	LOH
8	Metaplasia	WT	LOH
9	Metaplasia	WT	No LOH
10	Metaplasia	Mutated	LOH
11	Metaplasia	Mutated	LOH
12	Dysplasia	WT	No LOH
13	Dysplasia	WT	No LOH
14	Dysplasia	WT	LOH
15	Dysplasia	WT	LOH
16	Dysplasia	Mutated	LOH
17	Dysplasia	Mutated	LOH

EMR glands	Phenotype	Mutational status for *TP53* (c.722C>T)	*TP53* LOH (D17S1832)
18	Dysplasia	Mutated	LOH
19	Dysplasia	Mutated	LOH
20	Dysplasia	Mutated	LOH
21	Dysplasia	Mutated	LOH
22	Dysplasia	Mutated	LOH
23	Dysplasia	Mutated	LOH
24	Dysplasia	Mutated	LOH
25	Dysplasia	Mutated	Not worked
26	Dysplasia	Mutated	Not worked
27	Dysplasia	Mutated	LOH
28	Dysplasia	Mutated	LOH
29	Oesophageal duct	WT	No LOH
30	Carcinoma x 4 areas	Mutated	LOH

Table 20: Correlation between phenotype and genotype results for patient 2.

Multiplex PCR was performed with a panel of microsatellite markers located within *TP53* (17q) SMAD4 (18q) and *CDKN2A* gene. For each marker, loss of heterozygosity was considered to be present if the area under one allelic peak was less than 0.5 times or more than two times the area of the corresponding allele in the constitutional DNA. Mutational status of individual glands did not correlate with their LOH status.

8.3.2 LOH analysis of specimen from patient 3 (Table 3):

The constitutional DNA was only informative for *CDKN2A*. These glands were then screened for LOH at *CDKN2A* using a panel of microsatellite markers (shown in Table 21). All glands, which were mutated for *CDKN2A* showed LOH on four microsatellite markers for *CDKN2A*. The LOH analysis of one gland, which was WT for *CDKN2A* mutation, did not work. Summary of LOH status is shown in Table 21.

EMR crypts	Mutational status (*CDKN2A*)	*CDKN2A* (D9S1752)	*CDKN2A* (D9S171)	*CDKN2A* (D9S942)	*CDKN2A* (D9S932)
1	WT	N/W	N/W	N/W	N/W
2	Mutated	N/W	LOH	LOH	LOH
3	Mutated	LOH	LOH	LOH	LOH
4	Mutated	LOH	LOH	LOH	LOH
5	Mutated	LOH	LOH	LOH	LOH
6	Mutated	LOH	LOH	LOH	LOH
7	Mutated	LOH	LOH	LOH	LOH
8	Mutated	LOH	LOH	LOH	LOH
9	Mutated	LOH	No LOH	No LOH	LOH
10	Mutated	LOH	LOH	LOH	LOH
11	Mutated	LOH	No LOH	No LOH	LOH
12	Mutated	LOH	LOH	LOH	LOH
13	Mutated	LOH	No LOH	No LOH	LOH
14	Mutated	LOH	LOH	LOH	LOH
15	Mutated	LOH	LOH	LOH	LOH
16	Mutated	LOH	LOH	LOH	LOH
17	Mutated	LOH	LOH	LOH	LOH
18	Mutated	LOH	LOH	No LOH	LOH

Table 21: Summary of LOH results for patient 3.
Multiplex PCR was performed with a panel of microsatellite markers located within *TP53* (17q), SMAD4 (18q) and *CDKN2A* gene. For each marker, loss of heterozygosity was considered to be present if the area under one allelic peak was less than 0.5 times or more than two times the area of the corresponding allele in the constitutional DNA. All glands which were mutated for *CDKN2A* also had LOH.

8.3.3 LOH analysis of specimen from patient 5 (Table 3):

The constitutional DNA was only informative for two microsatellite markers of *TP53* (D17S250 and D17S1832). Laser captured glands were then screened for LOH at *TP53* using a panel of microsatellite markers. Two out of 9 metaplastic glands showed LOH for *TP53* microsatellite marker (D17S1832). All 8 dysplastic glands which were mutated for *TP53* (c.256 G>A), also showed LOH for *TP53* of at least one microsatellite marker and all eight areas of cancer had LOH for *TP53*. Summary of LOH status is given in table 22. Here, *TP53* mutated clone with *TP53* LOH must have occurred first followed by the *TP53-KRAS* double mutated clone. The table also shows that the clone mutated for *TP53* and *KRAS* progressed to carcinoma (Table 22).

GLAND	PHENOTYPE	*TP53* LOH STATUS (D17S1832)	*TP53* MUTATION	*KRAS* MUTATION
1	Metaplasia	-	WT	WT
2	Metaplasia	-	WT	WT
3	Metaplasia	-	WT	WT
4	Metaplasia	-	WT	WT
5	Metaplasia	-	WT	WT
6	Metaplasia	-	WT	WT
7	Metaplasia	-	WT	WT
8	Metaplasia	+	WT	WT
9	Metaplasia	+	Mutated	WT
10	Dysplasia	+	Mutated	WT
11	Dysplasia	+	Mutated	WT
12	Dysplasia	+	Mutated	WT
13	Dysplasia	+	Mutated	WT
14	Dysplasia	+	Mutated	Mutated
15	Dysplasia	+	Mutated	Mutated
16	Dysplasia	+	Mutated	Mutated
17	Dysplasia	+	Mutated	Mutated
18	Carcinoma (8 different areas)	+	Mutated	Mutated

Table 22: Clonal ordering from patient 5 in Table 3.

The clone mutated for *TP53* with LOH must have appeared first followed by the *TP53-KRAS* double mutated clone. The clone mutated for *TP53* and *KRAS* with *TP53* LOH progressed to carcinoma. WT=wild type.

8.3.4 LOH analysis of specimen from patient 8 (Table 2):

Standard DNA (muscle area) was laser capture for LOH analysis. DNA was informative for two microsatellite markers for *TP53* (D17S1176 and D17S1881). Due to lack of DNA, only 13 glands out of 29 were analysed. The results have been shown in the table 23 below. The spatial distribution of different phenotype and genotype with their LOH status from patient 8 in Table 3 have been shown in Figure 68 earlier.

EMR glands	Mutational status for *TP53* (c.814G>A)	*TP53* LOH	
		(D17S1176)	(D17S1881)
1	N/W	No LOH	No LOH
2	WT	No LOH	No LOH
3	WT	Not amplified	LOH
4	WT	Not amplified	LOH
5	Mutated	LOH	LOH
6	Mutated	Not amplified	LOH
7	Mutated	Not amplified	LOH
8	Mutated	LOH	LOH
9	Mutated	LOH	LOH
10	Mutated	Not amplified	LOH
11	Mutated	LOH	LOH
12	Mutated	Not amplified	LOH
13	Mutated	LOH	LOH

Table 23: Summary of LOH results for patient 8.
Multiplex PCR was performed for a panel of microsatellite markers located within *TP53* (17q), SMAD4 (18q) and *CDKN2A* gene. For each marker, loss of heterozygosity was considered to be present if the area under one allelic peak

was less than 0.5 times or more than two times the area of the corresponding allele in the constitutional DNA. Mutational status of individual glands did not correlate with their LOH status.

8.4 Methylation analysis:

8.4.1 Methylation patterns in patient 3:

Multiple glands from patient 3 specimen were laser-captured microdissected and underwent methylation analysis for CSX and MYOD gene. The results have been plotted below (Figure 69).

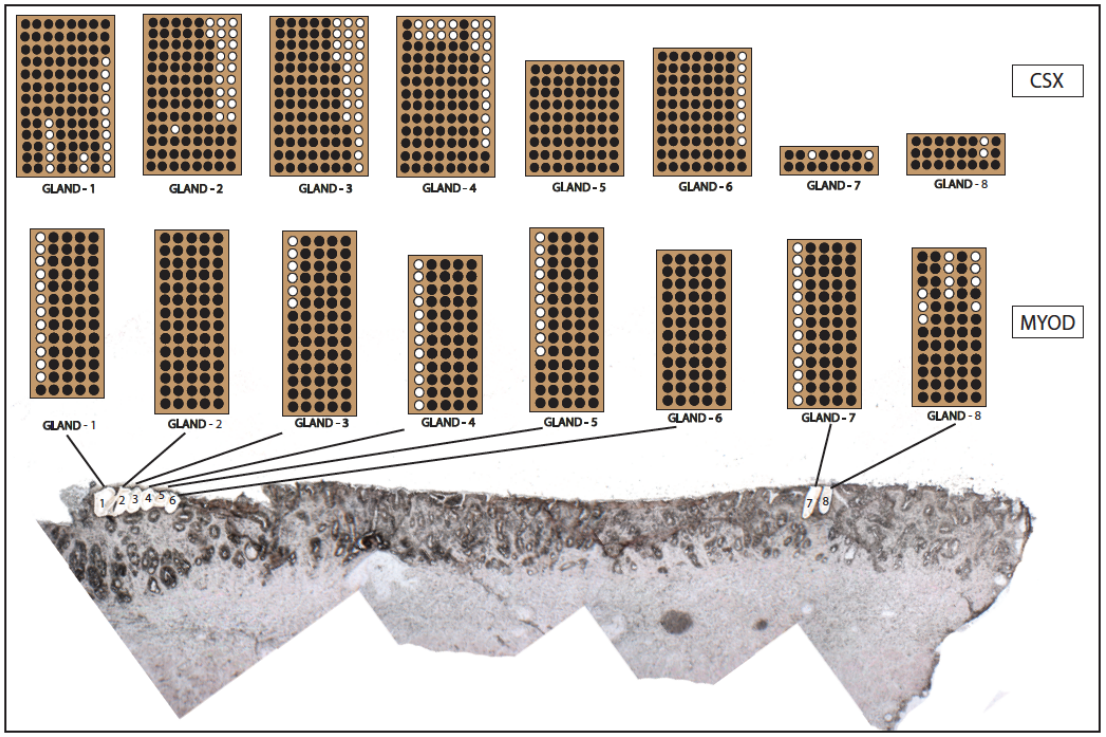

Figure 69: Epigenetic diversity in Barrett's glands (patient 3).
MYOD methylation patterns from gland 1-14 (Patient 1), Each box, represent methylation patterns of the individual gland; each row represents a tag (molecule) and each column represents a CpG site. Filled circle denotes the methylation status of each CpG site (methylated) and unfilled circles (unmethylated). The methylation pattern confirms epigenetic diversity within the gland is less when compared to the adjacent and distant glands.

8.4.2 Methylation patterns in patient 4:

Multiple glands from patient 4 specimen were laser-captured microdissected and underwent methylation analysis for CSX and MYOD gene. The results have been plotted below (Figure 70 and 71).

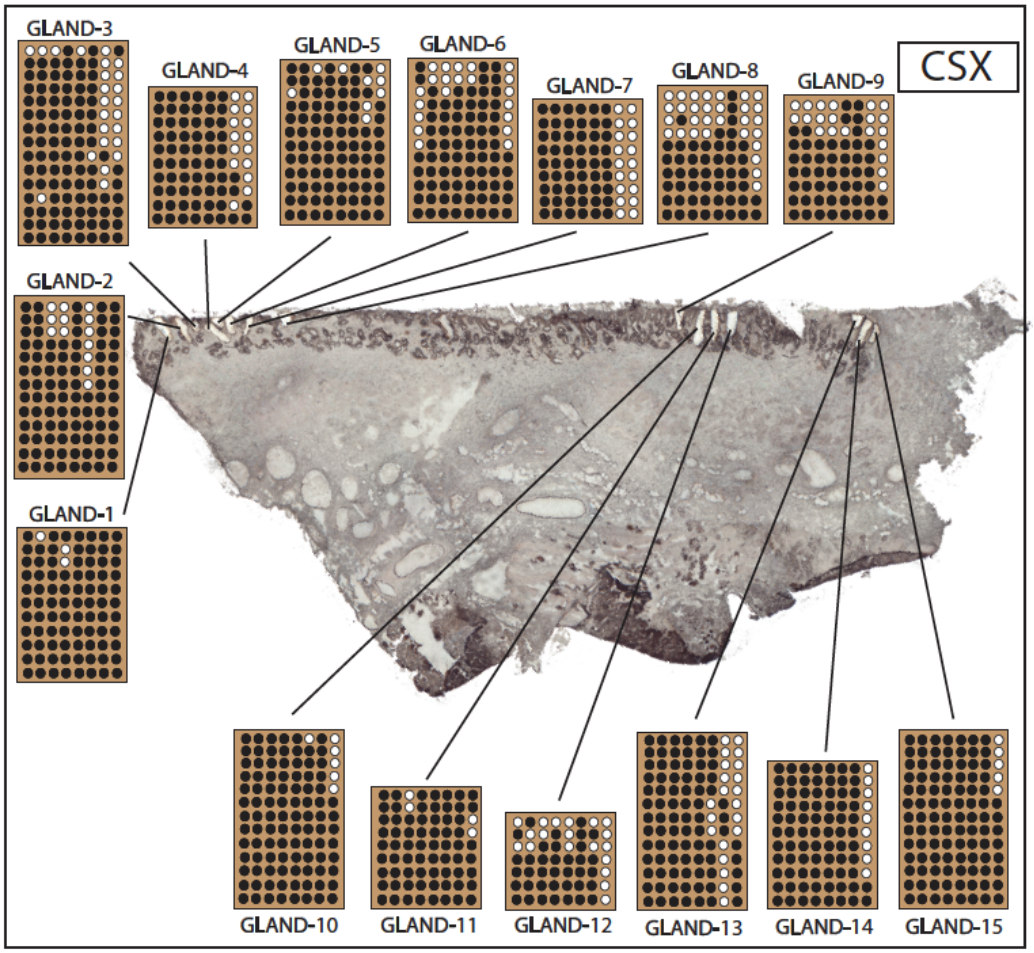

Figure 70: Epigenetic diversity in Barrett's glands (patient 4):
Methylation patterns from gland 1-15 in CSX promoters. Each box represents methylation patterns of individual gland; each row represents a tag (molecule) and each column represents a CpG site. The methylation status of each CpG is represented by circle, filled circle denotes methylated CpG site and unfilled circle represents unmethylated site. The methylation pattern confirms epigenetic diversity within the gland compared to adjacent and distant glands.

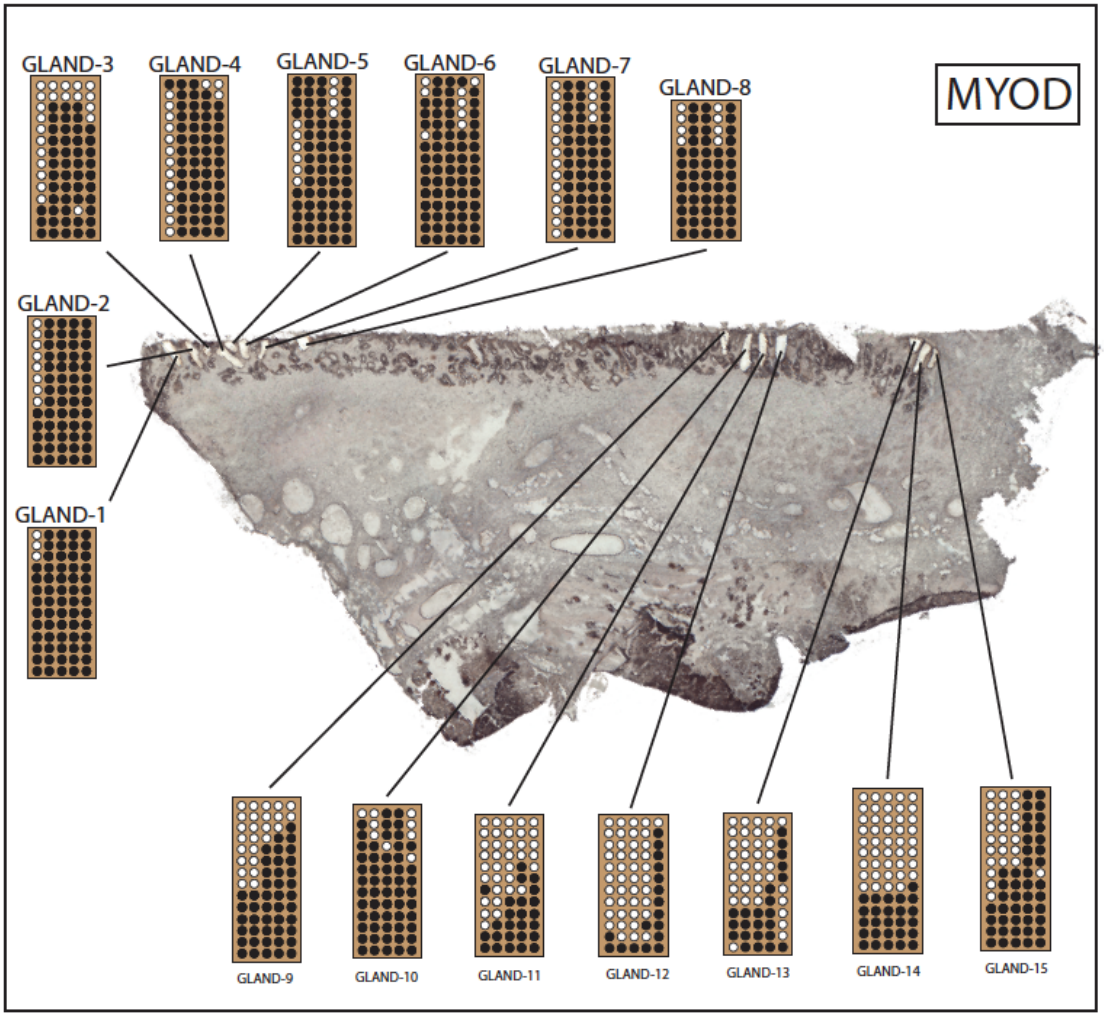

Figure 71: Epigenetic diversity in Barrett's glands (patient 4):
Methylation patterns from gland 1-15 in MYOD promoters. Each box represents methylation patterns of individual gland; each row represents a tag (molecule) and each column represents a CpG site. The methylation status of each CpG is represented by circle, filled circle denotes methylated CpG site and unfilled circle represents unmethylated site. The methylation pattern confirms epigenetic diversity within the gland compared to adjacent and distant glands.

8.4.3 Methylation patterns in patient 5:

Multiple glands from patient 5 specimen were laser-captured microdissected and underwent methylation analysis for CSX and MYOD gene. The results have been plotted below (Figure 72).

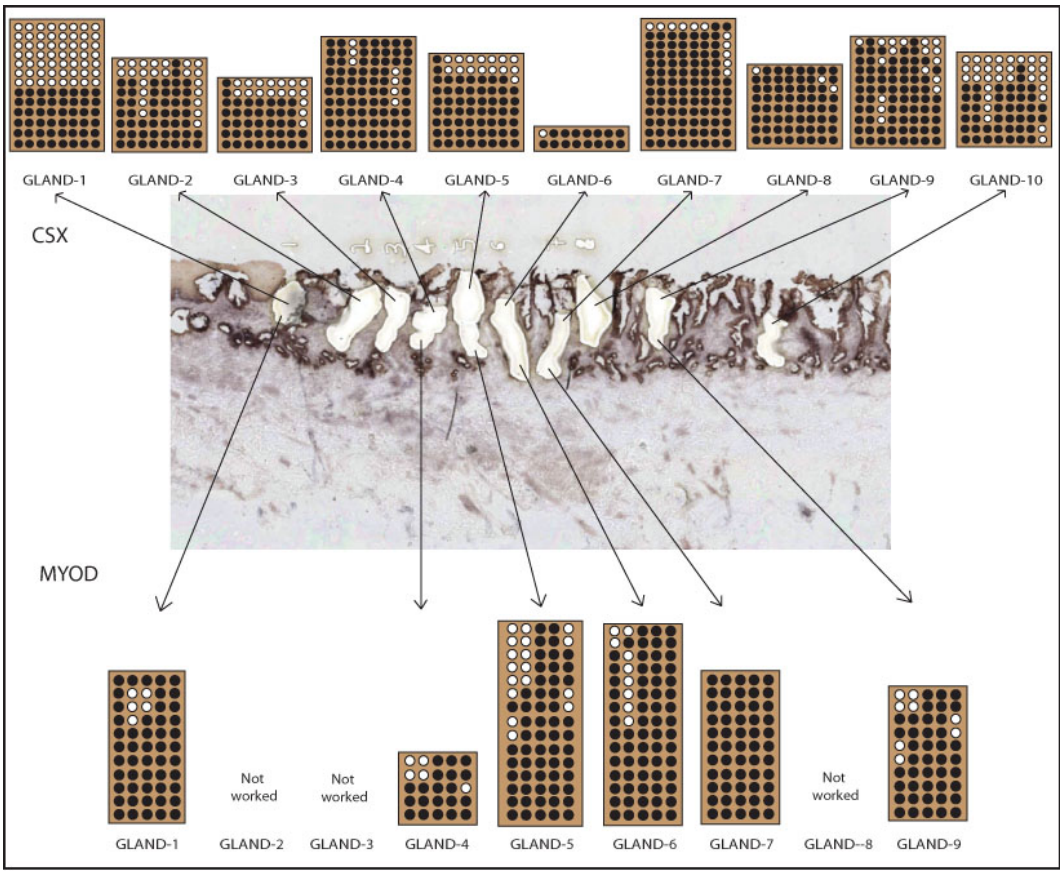

Figure 72: Epigenetic diversity in Barrett's glands (patient 5):
Methylation patterns from gland 1-10 in CSX and MYOD promoters. Each box represents methylation patterns of individual gland; each row represents a tag (molecule) and each column represents a CpG site. The methylation status of each CpG is represented by circle, filled circle denotes methylated CpG site and unfilled circle represents unmethylated site. The methylation pattern confirms epigenetic diversity within the gland compared to adjacent and distant glands.

8.4.4 Methylation patterns in patient 6:

Multiple glands from patient 6 specimen were laser-captured microdissected and underwent methylation analysis for CSX and MYOD gene. The results have been plotted below (Figure 73).

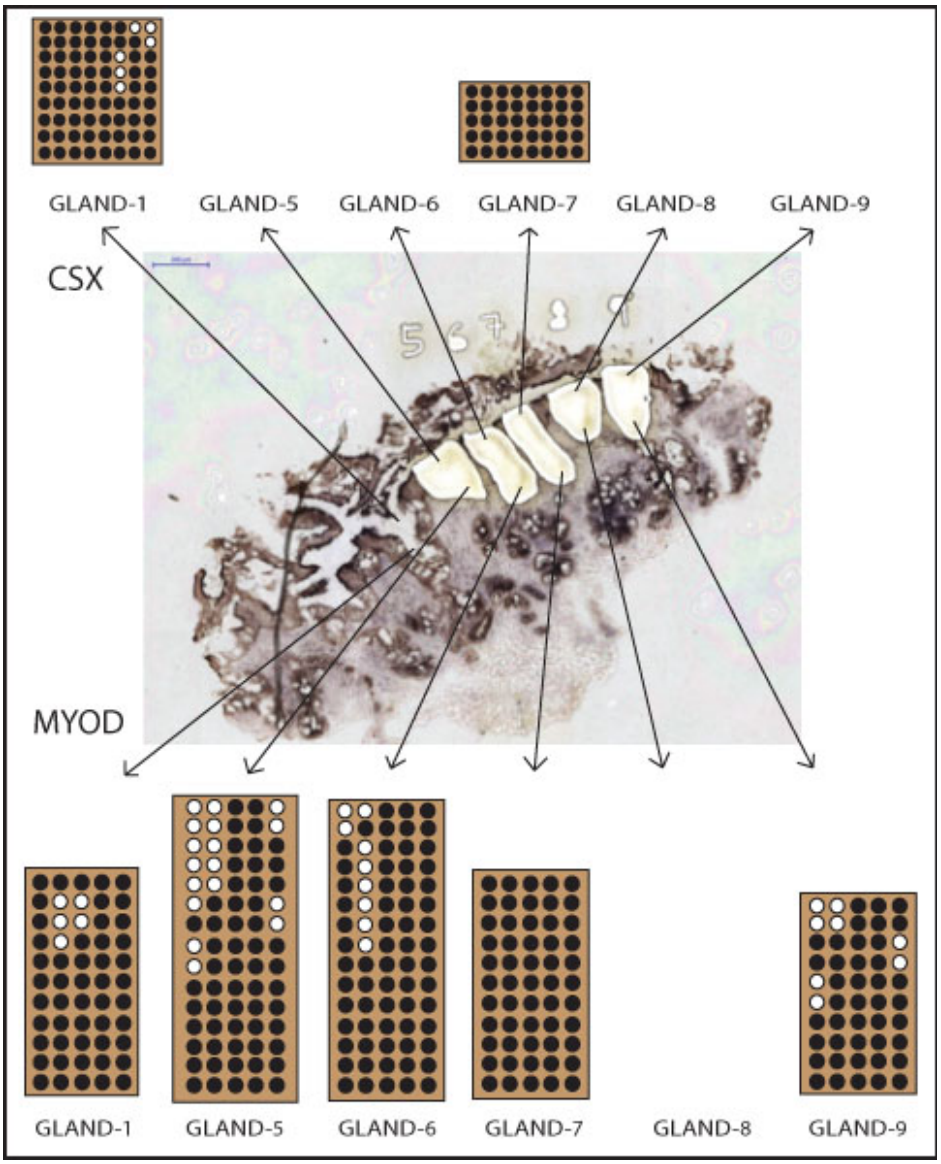

Figure 73: Epigenetic diversity in Barrett's glands (patient 6):
Methylation patterns from gland 1-9 in CSX and MYOD promoters. Each box represents methylation patterns of individual gland; each row represents a tag (molecule) and each column represents a CpG site. The methylation status of each CpG is represented by circle, filled circle denotes methylated CpG site and unfilled circle represents unmethylated site. The methylation pattern confirms epigenetic diversity within the gland compared to adjacent and distant glands.

8.5 Cummulative representation of percent methylation, intragland diversity and intergland diversity

Cumulative representation of above parameters has been shown in Figure 74.

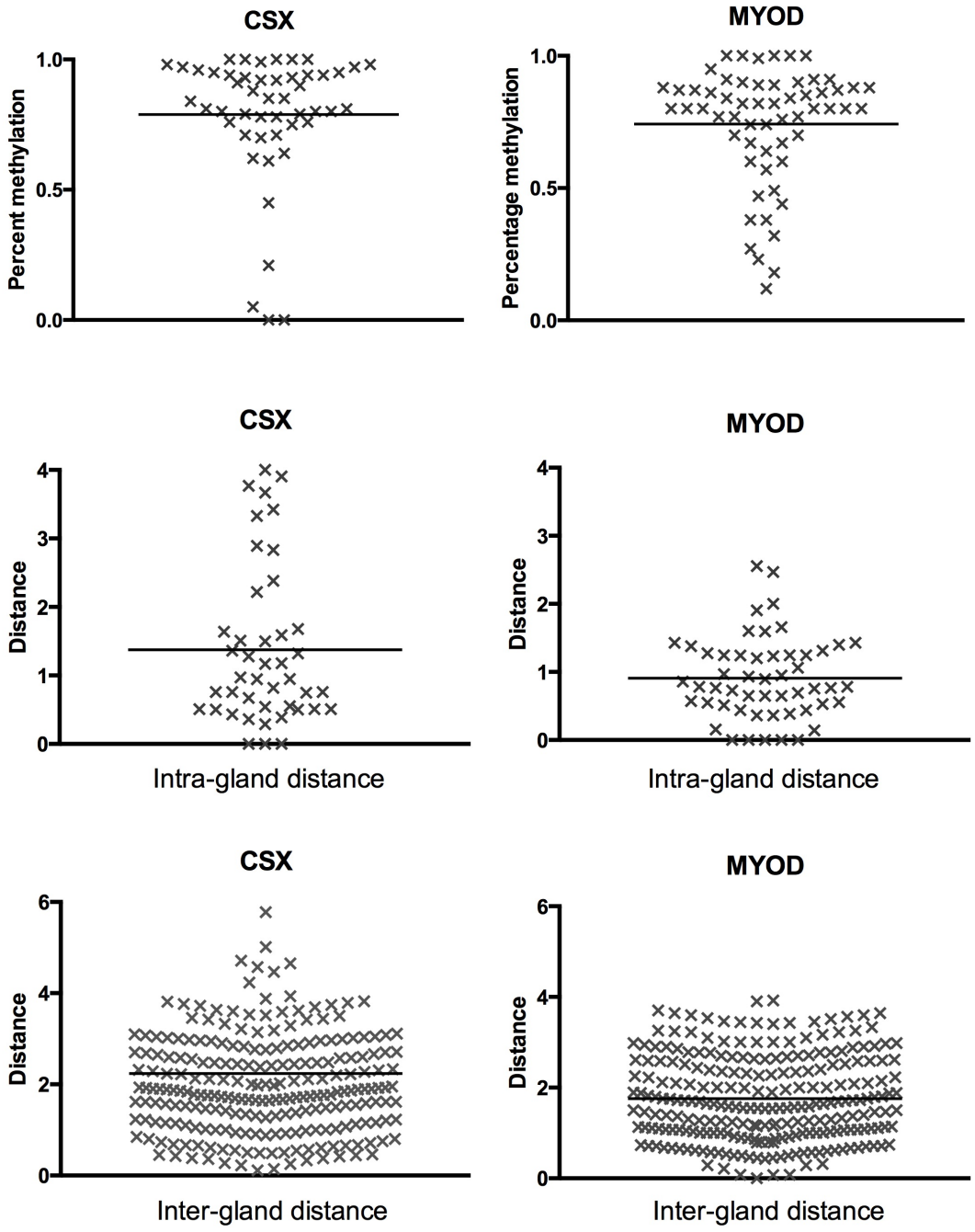

Figure 74: Cummulative representation of percent methylation, intragland diversity and intergland diversity.
The percentage methylation between CSX and MYOD was not significantly different (p=0.3157). The diversity within a Barrett's gland (acd) was less when compared to between the glands (icd), suggesting that cells within a Barrett's

gland were closely related, i.e., recent ancestry when compared to the adjacent or distant glands.

8.6 Correlation between epigenetic diversity and spatial distance for CSX and MYOD gene (individual patient):

The spatial distances between glands were described as a unit, which corresponds to the average gland diameter (in pixels) was plotted against their intergland epigenetic distance and found that there was no correlation between these two parameters (Figure 75).

CSX gene MYOD gene

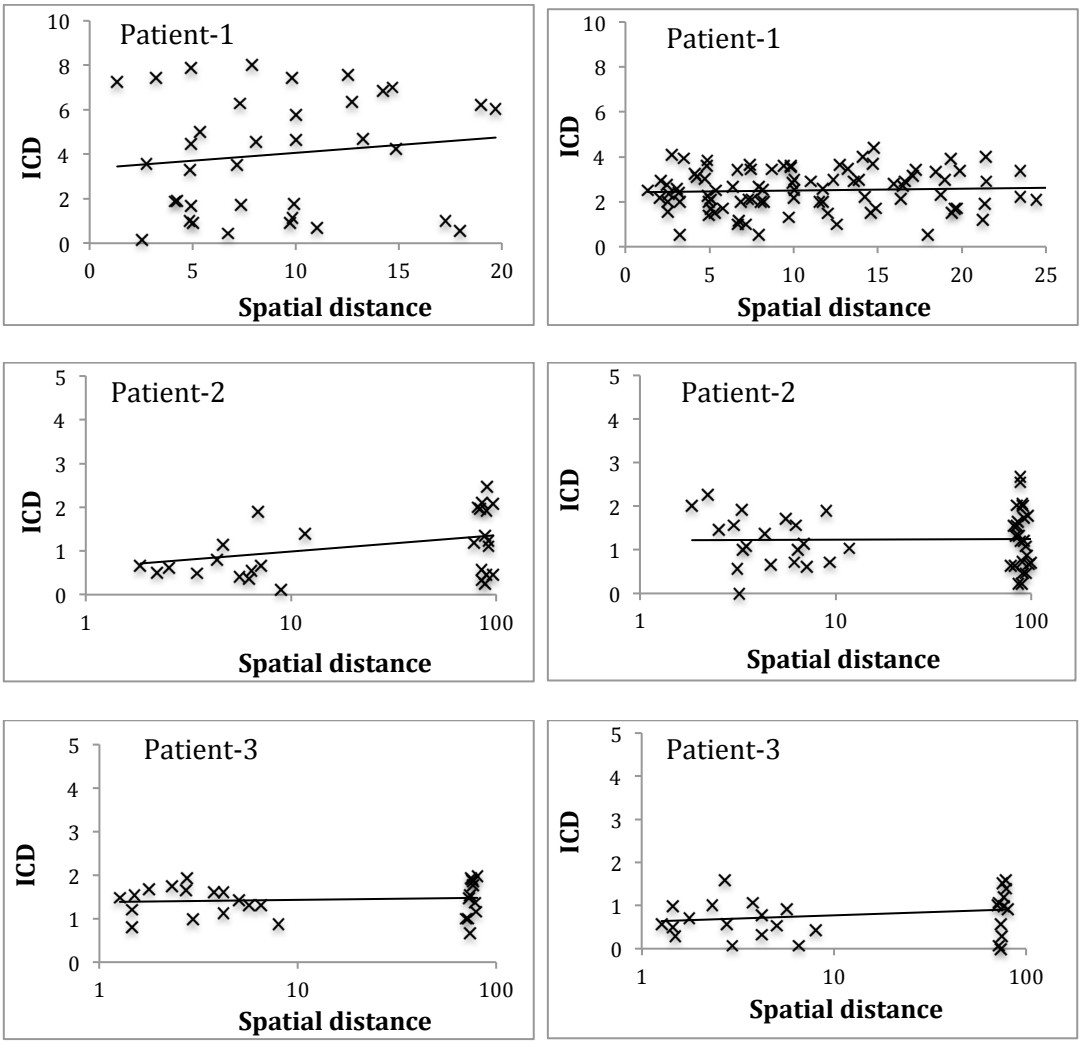

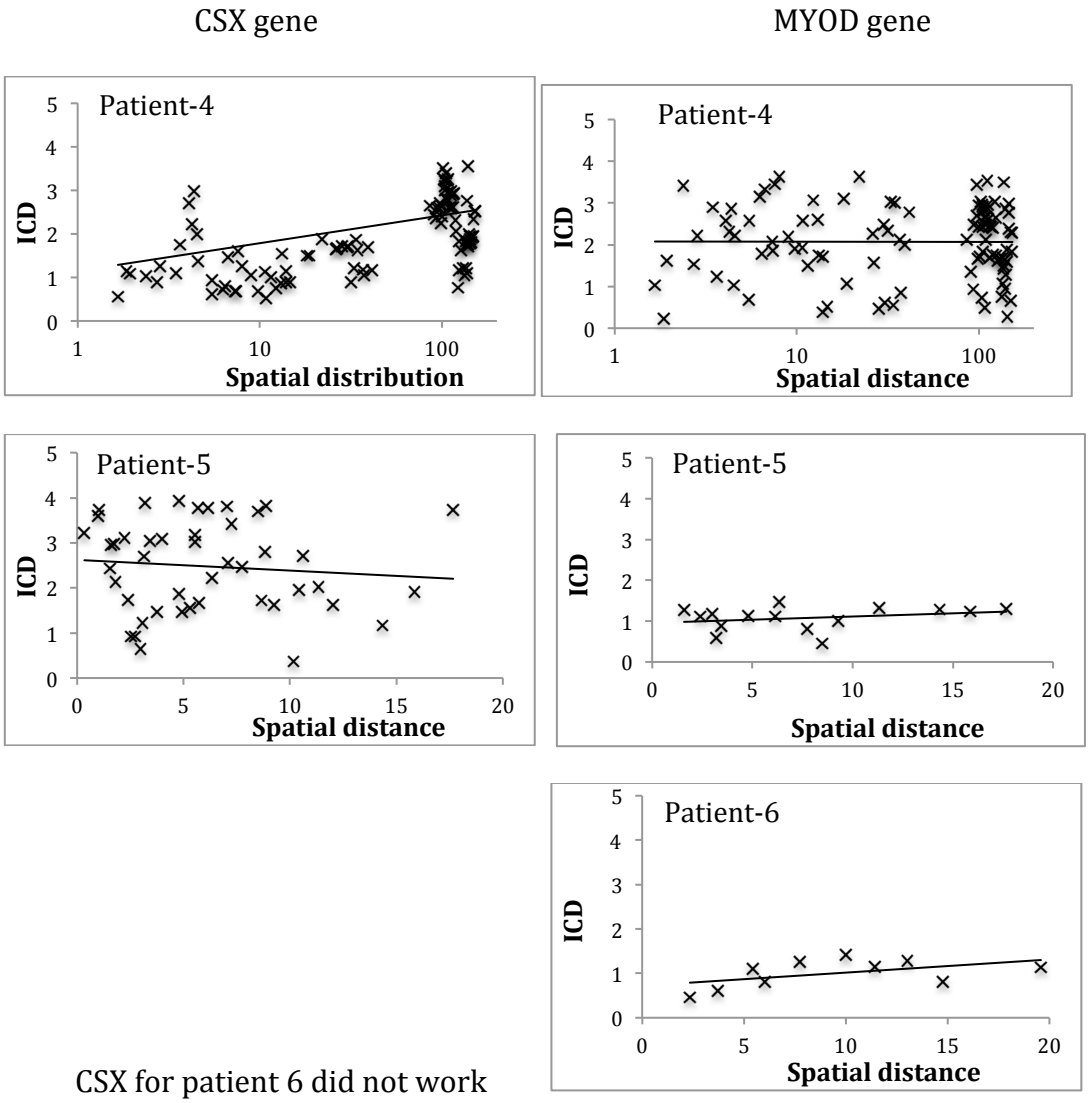

Figure 75: Correlation between spatial and epigenetic distance in Barrett's metaplasia.

Spatial distances between glands were described as a unit, which corresponds to the average gland diameter (in pixels). The average ICD of all pairs of glands within the EMR specimen that fell within the spatial interval was computed. In CSX and MYOD promoters, there was no correlation between spatial distance and epigenetic distance. The straight line indicates that spatially closely related glands are epigenetically no more similar than distant pairs of glands. If these two were more closely related then the line would increase exponentially.